Cranfield University

School of Mechanical Engineering

Department of Turbomachinery and Engineering Mechanics

PhD Thesis

Academic year 1997/98

Vincenzo Botte

A robust and accurate Navier-Stokes algorithm for three-dimensional applications adopting arbitrary modelling of the Reynolds stresses

Cranfield University

School of Mechanical Engineering

Department of Turbomachinery and Engineering Mechanics

PhD Thesis

Academic year 1997/98

Vincenzo Botte

A robust and accurate Navier-Stokes algorithm for three-dimensional applications adopting arbitrary modelling of the Reynolds stresses

Supervisor: Dr. A. Tourlidakis

September 1999

This thesis is submitted in partial fulfilment of the requirements for the Degree of PhD in Turbomachinery and Engineering Mechanics.

Cranfield University

School of Mechanical Engineering

Department of Turbomachinery and Engineering Mechanics

PhD Thesis

Vincenzo Botte

A robust and accurate Navier-Stokes algorithm for three-dimensional applications adopting arbitrary modelling of the Reynolds stresses

Abstract

In this thesis a new Navier-Stokes solver for complex three-dimensional geometries, adopting arbitrary modelling of the Reynolds stresses, is presented. A $k-\varepsilon$ model, adopting a modelling of the turbulent transport not based on the eddy viscosity, has been written in generalised coordinates and solved with a finite volume approach, using both a GMRES solver and a direct solver for the solution of the linear systems of equations. The results presented show that the modification adopted for the modelling of the turbulent transport also provides a more accurate value of the physical diffusion and, as a consequence, improves the increase in accuracy when using higher-order convection schemes.

A simple non-linear modelling of the Reynolds stresses has been designed introducing an additional term, quadratic in the main strain rate, to the basic Boussinesq's form; the corresponding constant has been evaluated through comparison with experimental data. The computational procedure is implemented for the flow analysis in a 90° square section bend and the obtained results show that with the non-linear modelling a much better agreement with the measured data is obtained, both for the velocity and the pressure. The importance of the convection scheme is also discussed, showing how the effect of the non-linear correction added to the Reynolds stresses is effectively hidden by the additional numerical diffusion introduced by a low-order convection scheme as the first-order Upwind, thus making necessary the use of higher-order schemes.

Some results for centrifugal turbo machinery are also presented, giving some initial indications on the effects of the proposed modification in the modelling of the turbulent diffusion on the prediction of the flow in rotating passages.

List of contents

Nomenclature

a = coefficient of the generic discretised transport equation; also: function of the grid spacing (when deriving the convection schemes)

A = surface of the cell face; also: generic matrix

B, C, D = coefficients appearing in the derivation of the pressure correction equation

$const$ = generic constant

C_p = pressure coefficient

$C_\mu, C_1, C_2, C_S, C_\varepsilon, C_{\varepsilon 1}, C_{\varepsilon 2}, C$ = turbulence modelling constants

$C_1, C_2, \ldots, C_6$ = coefficients of the generic quadratic function in two dimensions

d = diagonal coefficient

D = diagonal block

D_{ij} = twice the mean strain rate tensor

DWF = downwind weighting factor

E = function of the wall roughness

F_i = external force in the i-th momentum equation; also: $F_i = \rho A_i U_i$ (when deriving the pressure correction equation)

FNE = value of the variable at the middle of the north-east edge of the cell

FNW = value of the variable at the middle of the north-west edge of the cell

g^{rs} = metric coefficients = $\dfrac{\partial \xi_r}{\partial x_i} \dfrac{\partial \xi_s}{\partial x_i}$

G = production of k

i = index varying in the ξ direction; also: generic index for summations

$influx$ = convective influx for unit volume

I = rothalpy; also: surface integral

$\underline{\underline{I}}$ = unit tensor

j = index varying in the η direction; also: generic index for summations

J = Jacobian

$\underline{J}$ = flux

k = turbulent kinetic energy

$\underline{k}$ = direction of the z axis

l = length of scale of turbulence

m = index varying in the ζ direction; also: generic index for summations

mp= mass unbalance (or mass source)

n = dimension of the systems of equations

$\underline{n}$ = direction normal to the wall

np = number of unknowns on a transversal plane

nx, ny, nz = number of points in the ξ, η and ζ directions

nza = number of non-zero coefficients

p = static pressure

P = node at the centre of the control volume

Pr = Prandtl number

r, s, t = local coordinates (when deriving the two and three-dimensional QUICK); also: r,s = generic indices for summations

r^* = normalised distance from the outer wall of the bend

rs = restart number (GMRES)

ξ,ς = tangential directions at the wall (evaluation of the wall function formulae)

R = gas constant for air = 287 J/kg K

Re = Reynolds number

S = source term of the generic discretised transport equation

t = time

T = static temperature (in K)

T_b = blend parameter

u_i, u, v, w = mean Cartesian velocity components

U_i, U, V, W = Contravariant velocity components, $U_i = J\frac{\partial \xi_i}{\partial x_j} u_j$;

also: U = streamwise velocity, V = gapwise velocity

U_b = bulk velocity

U_P = velocity component parallel to the wall

$\underline{V}$ = mean Cartesian velocity vector

x_i, x, y, z = Cartesian coordinates

y^+ = non dimensional distance from the wall

z^* = normalised distance from the plane of symmetry of the bend

Greek

α = under-relaxation coefficient

Γ = turbulent exchange coefficient

δ_{ij} = Kronecker's delta

δ_n = normal distance from the wall

$\Delta\Theta$ = volume of the cell

$\Delta\xi$ = distance between grid points in the ξ direction

$\Delta\eta,\Delta\zeta$ = cell dimension in the η and ζ directions

ε = dissipation rate of k

ε_{ijk} = alternating tensor

ϕ = generic scalar variable

K = von Karman's constant = 0.41

λ = second viscosity coefficient

Λ = function of y^+

μ = molecular viscosity (or first viscosity coefficient)
μ_t = eddy viscosity
ν = kinematic viscosity = μ / ρ
ρ = density
$\underline{\sigma}$ = internal stress tensor
σ = turbulent Prandtl number
Σ_C = convective stability
$\underline{\tau}, \tau_{ij}$ = shear stress
Ω_i = Cartesian components of the rotational speed vector
$\underline{\Omega}$ = rotational speed vector
ξ_i, ξ, η, ζ = curvilinear (or generalised) coordinates

Subscripts:
C = node upstream of the cell face
D = node downstream of the node C
f = generic cell face
i, j, l, m, r, s = generic indices for summations
I = corresponding to the entalpy equation
k = corresponding to the k equation
K = generic node
l, r = left and right cell faces (one-dimensional case)
L, R = left and right nodes (one-dimensional case)
LL = node at the left of the node L (one-dimensional case)
ps = pressure side
P = node at the centre of the control volume
ref = reference value
ss = suction side
u_i = corresponding to the i-th momentum equation
U = node upstream of the node C
W, E, S, N, B, F = nodes preceding and following the node P in the ξ, η and ζ directions
w = value at the wall
w, e, s, n, b, f = faces on the cell facing, respectively, the nodes W, E, S, N, B, F e.g.: w = west face of the control volume, e = east face of the control volume, etc.
x_i = derivative in respect to the x_i coordinate; e.g.: $\phi_x = \partial\phi / \partial x$
ϕ = corresponding to the generic variable ϕ
ε = corresponding to the ε equation
ξ_i = derivative in respect to the ξ_i coordinate

Superscripts
n = iteration level

u_i = corresponding to the i-th momentum equation
p = corresponding to the pressure correction equation
R = turbulent component
R,B = turbulent component evaluated with the Boussinesq's approximation
V = viscous component
~ = normalised using the upstream and downstream values

$\bar{}$ = mean value
' = fluctuation
} when deriving the equations for turbulent flows

~= density - weighted average
'' = fluctuation from the average
} additional def. for compressible turb. flows

* = approximated
' = correction
} when deriving the pressure correction equation

' = constant
'' = multiplies the variable
} when linearising the source term

Chapter 1
Introduction

The tremendous progress in computer science that has happened in the last few decades has directly influenced the development of several scientific fields and it is undeniable that fluid dynamics has been benefited most from the fast increase in computational resources available and its rapidly declining cost. In the space of not more than thirty years we have seen the rapid evolution from the simple linear methods, massively adopted for the design of the first passenger jets, to the solution of three-dimensional turbulent Navier-Stokes equations at all speeds and for all possible geometries.

Applications with direct industrial use have been from large economic investment in the development of flow prediction techniques; in particular, in the last decades a large effort has been directed towards the development of prediction techniques for turbomachinery flows, in the attempt to increase the efficiency whilst reducing the costs linked to experimental testing.

Turbomachinery flows are among the most complex flows encountered in fluid dynamic practice; they usually are three-dimensional, with laminar, transitional and turbulent flow; the prediction of such flows undoubtedly represents one of the most challenging fields of Computational Fluid Dynamics and a large volume of research on this subject has recently appeared in the literature. Particular effort has been directed towards the development of turbulence models that could accurately describe the features of turbulent flow affected by curvature and rotation.

The first turbulence models that have been adopted in turbomachinery applications are simple algebraic models. As widely reported in the literature, Lakshminarayana 1985 and 1991, these models are adequate for two-dimensional compressible flows with mild pressure gradients, and are definitely not suitable for flows with curvature and rotation, being of little value in three-dimensional complex flows. Although the use of algebraic models should be restricted to two-dimensional flows with mild pressure gradients and mild curvature, they are still widely adopted in industrial applications; this is particularly true in the prediction of the flow in centrifugal compressors and pumps, where the complexity of the flow, with strong adverse pressure gradients in the streamwise direction, could make the use of more advanced techniques quite problematic, especially in respect to the numerical stability of the procedure.

The paper of Hirsch et al. (1996) on the numerical investigation of the flow in centrifugal impellers, is a typical example of this kind of approach: the accuracy of the prediction is mostly dependent on the choice of the grid (about 370,000 grid points, with the use of a multiblock technique for an accurate geometrical modelling of the edges of the blades), while a relative low order scheme (second order) is used for the treatment of the convection and, most importantly, the algebraic model of Baldwin-Lomax (1978) is adopted for the turbulence. Hirsch et al. claim in the conclusions that, although the influence of rotation and curvature on the turbulent flow cannot be accurately described by such a simple turbulence model, the level of validation obtained seems to indicate that such effects are not predominant in the establishment of the main properties.

A more accurate description of the turbulent flow can be obtained using two equations models, that generally produce reasonable results without an excessive computational cost; by far the most widely used two equation model is the k-ε, generally used in the form originally proposed by Jones and Launder (1972), that can now be considered almost as a 'standard choice' for the modelling of turbulence. One of the major limitations of the model, especially in relation to the prediction of flows affected by curvature and rotation, is the adoption of a linear relation between stress and strain for the modelling of the eddy viscosity, as originally proposed by Boussinesq (1877).

It is well known that a linear relation between stress and strain in the modelling of the Reynolds stresses, as in Boussinesq's formulation, fails to resolve turbulence anisotropy and to represent correctly the interaction between curvature strain and the normal stresses (Bradshaw, 1973). It is now generally accepted that the strong variability in the strength of interaction between different strain types and the turbulent stresses can only be resolved fundamentally through the use of second-moment closure, in which separate transport equations are solved for all Reynolds stress components (Lien and Leschziner, 1994a). However, this type of closure is complex, poses particular challenges in respect to its stable integration into general computational schemes and is costly to apply in practice, while, at the same time, still presents some weaknesses and defects (Lien and Leschziner, 1994b).

Most researchers prefer to keep the simple formulation of the $k-\varepsilon$ model while trying to increase the accuracy introducing additional terms and/or modifying the value of the modelling constants in order to take into account the influence of effects such as curvature or rotation, often using empirical observations or simplified analysis of the Reynolds stresses equations (see, for example, the review on turbulence models for

complex flows from Lakshminarayana 1985), or modifying the definition of the eddy-viscosity.

k-ε models adopting a non-linear eddy-viscosity formulation have recently been used in the flow prediction of axial turbomachinery flows, such as, for example, the use of a cubic eddy-viscosity model for the study of a compressor cascade blade operating at off-design conditions (Chen et al., 1996) and the flow around a turbine blade (Craft et al., 1997); in this case, a standard k-ε model is adopted, but the definition of the eddy-viscosity is modified in order to take into account the anisotropy in the turbulence introduced by curvature and rotation (Craft et al., 1996). Chen et al. (1996) have shown that in the flow prediction of cascades operating at off-design conditions it is particularly important to adopt advanced turbulence models, as linear eddy-viscosity models return excessive levels of turbulence around the leading edge, and thus prevent laminar leading-edge separation and associated transition, while the use of cubic eddy-viscosity models results in a much improved description of the phenomena.

Another example of inclusion of anisotropic effects in the k-ε model for turbomachinery flows is the work of Luo and Lakshminarayana (1995), who have computed the three-dimensional flow through the turbine nozzle passage of a single stage turbine using a zonal k-ε/Algebraic Reynolds stress model (ARSM), in which the formulation of the components of the Reynolds stress is modified in the endwall region to represent the anisotropy of turbulence. In this case only the production term in the k-ε equations is modified when using the ARSM. The results show that the predictions with the anisotropic ARSM model are close to those with the isotropic k-ε model for the mean flow properties, and only a slight improvement in the prediction of some secondary flow quantities has been obtained by the ARSM. Luo and Lakshminarayana conclude that the turbine secondary flows are primarily driven by pressure gradients and that the effects of the anisotropy of turbulence appear to be insignificant in this case.

It has to be noted that most, if not all, of the applications of advanced turbulence models to turbomachinery flows which have appeared in the literature are relative to axial flow machines. It is indeed true that while quite advanced numerical techniques constitute now a central part in the design of axial flow machines, the design of centrifugal machines is still based on empirical methods using simple one-dimensional correlations or inviscid methods, and CFD computations are performed mostly using algebraic turbulence models, as in Hirsch et al. (1996).

It is important to notice that in most of the cases the $k-\varepsilon$ model is used in the form proposed originally by Jones and Launder (1972), where the turbulent transport

diffusion term of k and ε is assumed (arbitrarily, for analogy between turbulent and molecular mixing) to be proportional to the gradient of the variable, through the eddy viscosity divided by a turbulent Prandtl number.

A much more accurate modelling of the turbulent transport diffusion term in the $k-\varepsilon$ equations, not depending on such a strong assumption, was proposed by Hanjalic and Launder (1972); the use of such a modelling of the diffusion term leads to a $k-\varepsilon$ formulation not dependent any more on the eddy-viscosity but capable of adopting arbitrary modelling of the Reynolds stresses. Both Baker and Orzechowki (1983) and Speziale (1987) used a $k-\varepsilon$ formulation based on Hanjalic and Launder's formulae to introduce non-linear modelling of the Reynolds stresses, but tested their models in very simple and specific cases.

In the existing literature there has been a very limited use of these formulae, generally in very simplified cases, and never in general non-orthogonal coordinates, to model complex three-dimensional flows using a Navier-Stokes solver; furthermore, this kind of formulation has never been tested for rotating passages and, in particular, for turbomachinery flows. The $k-\varepsilon$ formulation so obtained, in effect allows a much more natural introduction of a non-linear modelling of the Reynolds stresses than the formulation based on the eddy-viscosity, while providing a more accurate definition of the diffusion term, in respect to the standard formulation that appears to over-predict the value of the physical diffusion (as will be shown in this thesis). At the same time, this formulation is more complex and less stable than the one based on the eddy viscosity.

The main objective of this thesis is to study the effects of introducing the Hanjalic and Launder formulae for the turbulent diffusion into a three-dimensional Navier Stokes procedure, specifically oriented towards the prediction of turbomachinery flows.

A new Navier-Stokes algorithm, that adopts for the turbulence modelling a $k-\varepsilon$ model based on Hanjalic and Launder's formulae for the turbulent diffusion transport terms, has been designed. The algorithm is based on a finite-volume procedure for a collocated grid in curvilinear coordinates, using a pressure correction procedure obtained extending the classical SIMPLE method of Patankar and Spalding (1980) to the case of generalised coordinates and non-staggered grid (as in Rhie and Chow, 1983). The proposed algorithm has been explicitly designed to overcome the problems of stability that are generally associated with the prediction of the flow in centrifugal machines, through the accurate solution of the governing equations, and in particular of the pressure correction equation.

The first attempt to simulate the flow in a centrifugal compressor using the pressure correction solution of the time-averaged Navier-Stokes equations was performed by Moore and Moore (1980a), who used a partially parabolic pressure correction procedure for the incompressible flow prediction in a low speed shrouded impeller. Although the turbulence, compressibility and tip leakage effects were neglected, this simulation represented a major step towards the application of Navier-Stokes analysis in centrifugal compressor impellers. Moore and Moore (1980b) extended their method to compute the turbulent, compressible flow in a high speed impeller passage. Hah et al. (1988) developed a fully elliptic viscous flow analysis method using a pressure correction relaxation procedure and Hah and Krain (1990) implemented the above method to simulate the flow in a high pressure backswept impeller. Dawes (1987) presented the results obtained for the flow inside a backswept impeller using a time-marching process for the solution of the three-dimensional system of equations expressed in a finite volume form. Tourlidakis and Elder (1993) presented numerical investigations of a radial and two backswept impeller flows with tip leakage using a fully elliptic pressure correction method.

The algorithm that will be presented in this thesis differs from the ones adopted in the above studies not only in the modelling of turbulence, but also in the adoption of high-order convection schemes with a flux limiter and the accurate solution of the three-dimensional system of equations.

The numerical discretisation of the convection terms in the Navier-Stokes equations is of fundamental importance for the accuracy of the procedure; the use of low-order schemes, such as the first-order Upwind scheme, causes the introduction of a large amount of additional numerical diffusion, with disastrous effects on the accuracy of the solution. At the same time, the introduction of such an artificial damping has a very stabilising effect on the convergence of the numerical procedure; this explains the reason why the use of low-order schemes is still widespread, constituting the most frequent choice in many applications of CFD, as noted by Leonard and Drummond in a recent review (1995).

High-order schemes, such as the third-order QUICK developed by Leonard (1979 and 1988), that will be the main convection scheme adopted in this thesis, while dramatically increasing the accuracy of the solution and drastically reducing the number of grid points required for the description of the flow phenomena, can generate unphysical overshoots or undershoots during the numerical transition, causing unphysically negative values for the turbulence quantities and the computational

divergence of the algorithm. A flux limiter, based on the boundedness criterion of Gaskell and Lau (1988), in the formulation with normalised variables of Leonard and Mokhtari (1990), will be adopted in this thesis in conjunction with high-order schemes, to eliminate any possible unphysical calculated value of the convected variable.

The use of high-order schemes can also cause a sharp deterioration in the stability of the numerical procedure, as compared to low-order schemes. Particular care has to be given to the accurate solution of the systems of linear equations obtained from the discretisation of the transport equations in order to avoid the production of large numerical error which, with limited numerical damping, can provoke the divergence of the procedure. For this reason, part of this thesis will be dedicated to the study of the linear solver, in particular for the solution of the pressure correction equation, that appears to be ill-conditioned and extremely sensitive both to the use of high-order schemes and to the boundary conditions adopted for the pressure field.

These problems of stability caused by the use of high-order convection schemes are the reason why many researchers prefer to use lower-order schemes, and therefore are able to adopt more approximate and less computationally expensive linear solvers, while using a very large number of grid points to achieve a reasonable level of accuracy. This option, that can probably sometimes produce an increase in the overall efficiency of the code, is not usable in this particular study of turbulence modelling: the modifications that in this study will be introduced in the modelling of the $k-\varepsilon$ equations will affect only the diffusion terms in the transport equations, so that excessive numerical diffusion introduced by the convection scheme would eliminate any possible benefits of the new formulation, as will be shown in this thesis. It is therefore essential to adopt a high-order convection scheme; for this reason, an extensive part of this thesis will be dedicated to the study of high-order schemes and the search of an accurate linear solver, to obtain an accurate and robust algorithm.

In the second chapter of this thesis, the governing equations in curvilinear coordinates of the standard eddy-viscosity formulation, the finite volume discretisation procedure and the pressure correction method will be introduced.

In the third chapter the solution method of the discretised equation, with particular emphasis on the solution of the systems of linear equations, is presented.

The fourth chapter is dedicated to the study of high-order convection schemes, with theoretical indications on the formal accuracy and convective stability of the several convection schemes presented, and to the development of a flux limiter.

An initial validation of the code is presented in the fifth chapter, with an extensive study on the performance of the linear solver for the pressure correction equation and some interesting and original results on the effect of the use of high-order schemes and of the flux limiter on the performance of the linear solver.

The sixth chapter is dedicated to the turbulence modelling, with a detailed presentation of the proposed new formulation of the $k-\varepsilon$ model in curvilinear coordinates; a simple quadratic modelling of the Reynolds stresses, that will then be used in the following chapter to show the capability of the algorithm to handle non-linear modelling of the Reynolds stresses, is also presented.

A validation of the turbulence modelling is then performed in the seventh chapter, using a simple three-dimensional test case, with a detailed investigation on the effects of the proposed modification of the $k-\varepsilon$ equations.

In the eighth chapter the results obtained from the numerical study of a rotating diffuser are presented, giving initial useful information on the consequence of the new modelling of the turbulent diffusion term in the prediction of the flow field in rotating passages.

Some initial results obtained for turbulent flows in centrifugal machines are then presented in the ninth chapter. Due to the limitations on computer resources available and to the high memory requirements of the proposed algorithm, relatively coarse grids have been adopted in these last cases, quite far from the level of grid refinement that is now considered to be the 'state of the art' in the field, and the results presented in this chapter are intended more as an additional validation of the proposed algorithm than a complete study of these particular turbomachinery flows.

Finally, in the two appendices the interpolation procedure adopted to obtain the values of the variables in specific points, and the description of the wall function adopted for the boundary conditions, are presented.

Chapter 2
Theoretical formulation and method of computation

2.1 - Introduction.

In this section the basic equations in generalised coordinates, the finite volume dicretisation procedure and thc pressure correction method will be presented.

The method presented in this section is commonly adopted in the prediction of the flow field for problems of engineering interest and represents just the starting point of this study. The exposition is therefore limited to the basic concepts, while the derivation of the governing equations will be presented in detail in the sixth chapter of this thesis, where the proposed formulation of the turbulence modelling is introduced.

2.2 - Governing equations.

The Navier Stokes equations for a turbulent flow will be considered, with the following assumptions:

- steady mean flow;
- perfect gas ($p = \rho RT$);
- use of a relative frame of reference rotating with the passage; the energy equation is formulated in terms of the conservation of the rothalpy (i.e. the total enthalpy in a rotating frame of reference);
- the source term in the rothalpy equation is neglected;
- the dependent variables are replaced with their time-averages plus their fluctuations (Reynolds decomposition) and then the entire equation is time-averaged [1];
- isotropic turbulent viscosity; the Boussinesq eddy viscosity concept is adopted: the Reynolds stresses and the turbulent scalar fluxes follow the same type of stress-strain relation as in laminar flow;
- a standard two-equation k-ε model is used for the modelling of the turbulence; the wall function approach has been adopted in the near-wall regions where the viscous phenomena are dominant;

In a Cartesian tensor form these equations are written:

---

[1] *In all the equations the variables are intended as time-averaged, following the definition of the Reynolds mean:* $\bar{\phi} = \frac{1}{\Delta t}\int_t^{t+\Delta t} \phi\, dt$ *, where* Δt *is required to be large compared to the period of random turbuence.*

• Continuity:

$$\frac{\partial}{\partial x_j}\left(\rho u_j\right)=0 \tag{2.2.1}$$

• Momentum: (i = 1,2,3)

$$\frac{\partial}{\partial x_j}\left(\rho u_j u_i\right)=-\frac{\partial p}{\partial x_i}+\frac{\partial}{\partial x_j}\left[(\mu+\mu_t)\left(\frac{\partial u_i}{\partial x_j}+\frac{\partial u_j}{\partial x_i}-\frac{2}{3}\delta_{ij}\frac{\partial u_m}{\partial x_m}\right)\right]+F_i \tag{2.2.2}$$

where F_i is the component of the centrifugal plus the Coriolis forces vector in the i direction:

$$F_i=-2\rho\varepsilon_{ijm}\Omega_j u_m-\rho\left(\Omega_n x_n\right)\Omega_i+\rho\left(\Omega_n\Omega_n\right)x_i\ ,$$

ε_{ijm} is the alternating tensor, which assumes the value 1 if ijm are in cyclic order (i.e. 123, 231, 312), -1 if ijm are in anti-cyclic order (i.e. 321, 132, 213) and 0 otherwise, and Ω_j is the component of the rotational speed vector in the j direction.

The turbulent equation obtained has the same form as the laminar one with the molecular viscosity μ replaced by an effective viscosity $\left(\mu+\mu_t\right)$, having included in the pressure the term: $-\frac{2}{3}\delta_{ij}\overline{u'_m u'_m}$.

• Rothalpy:

$$\frac{\partial}{\partial x_j}\left(\rho u_j I\right)=\frac{\partial}{\partial x_j}\left[\left(\frac{\mu}{\mathrm{Pr}}+\frac{\mu_t}{\mathrm{Pr}_t}\right)\frac{\partial I}{\partial x_j}\right] \tag{2.2.3}$$

where Pr is the Prandtl number of the fluid.

• Eddy viscosity:

$$\mu_t=C_\mu\rho\frac{k^2}{\varepsilon} \tag{2.2.4}$$

• Turbulent energy:

$$\frac{\partial}{\partial x_j}\left(\rho u_j k\right)=\frac{\partial}{\partial x_j}\left(\frac{\mu_t}{\mathrm{Pr}_k}\cdot\frac{\partial k}{\partial x_j}\right)+G-\rho\varepsilon \tag{2.2.5}$$

• Turbulence energy dissipation:

$$\frac{\partial}{\partial x_j}\left(\rho u_j \varepsilon\right)=\frac{\partial}{\partial x_j}\left(\frac{\mu_t}{\mathrm{Pr}_\varepsilon}\cdot\frac{\partial \varepsilon}{\partial x_j}\right)+\frac{\varepsilon}{k}\left(C_1 G-C_2\rho\varepsilon\right) \tag{2.2.6}$$

where G is the generation rate of turbulence defined by:

$$G=\mu_t\left(\frac{\partial u_i}{\partial x_m}+\frac{\partial u_m}{\partial x_i}\right)\frac{\partial u_i}{\partial x_m} \tag{2.2.7}$$

The constants C_1, C_2 and C_μ are equal to 0.09, 1.44 and 1.92 and the turbulent Prandtl numbers Pr_t, Pr_k and Pr_ε are 1.0, 1.0 and 1.3.

The boundary conditions for the k-ε method are given with a wall function, as defined in Appendix B.

To overcome the problem of the discretisation of irregularly shaped flow domains, a general system of Boundary Fitted Coordinates (BCF) is employed: the equations are transformed from the physical space (described by Cartesian coordinates) to a computational space, in which the boundaries of the domain coincide with lines of a structured mesh, described by generalised coordinates ξ, η and ζ (as in the example presented in fig.2.1 and 2.2). The strong conservation form of the transformed equations will be adopted (all the terms arising from the divergence operator are under differential operator); the unknown quantities in the momentum equations are still the Cartesian velocity components (semi-Cartesian form).

For the expression of the general transport law a transformation:

$$\xi=\xi(x,y,z):\ \eta=\eta(x,y,z);\ \zeta=\zeta(x,y,z) \tag{2.2.8}$$

has to be implemented; the partial derivatives arising from a divergence operator are transformed in a fully conservative form according to:

$$\frac{\partial \phi}{\partial x_i} = \frac{1}{J}\frac{\partial}{\partial \xi_r}\left(J\phi \frac{\partial \xi_r}{\partial x_i} \right) \tag{2.2.9}$$

where J is the Jacobian of the transformation given by:

$$J = x_\xi \left(y_\eta z_\zeta - z_\eta y_\zeta \right) - y_\xi \left(x_\eta z_\zeta - z_\eta x_\zeta \right) + z_\xi \left(x_\eta y_\zeta - y_\eta x_\zeta \right) \tag{2.2.10}$$

while the other partial derivatives are transformed according to:

$$\frac{\partial \phi}{\partial x_i} = \frac{\partial \phi}{\partial \xi_r}\frac{\partial \xi_r}{\partial x_i} \tag{2.2.11}$$

The velocity components U, V and W which are used in the generalised system when transforming the flow conservation equations, are related to the Cartesian ones, u, v and w, by [2]:

$$U_i = J \frac{\partial \xi_i}{\partial x_j} u_j \tag{2.2.12}$$

At the same time the Cartesian velocity components may be expressed by the inverse relations:

$$u_i = \frac{1}{J} \cdot \frac{\partial x_i}{\partial \xi_j} U_j \tag{2.2.13}$$

The application of these transformation relations to the general transport equation for the scalar quantity ϕ provides the transport equation in the generalised coordinate system.

---

[2]*The Jacobian in the definition of the velocities (2.2.12) has been introduced arbitrarily. U, V, and W are therefore the contravariant velocity components scaled by the Jacobian of the transformation. Some of the Jacobian terms appearing in the following equations are due to the definition (2.2.12).*

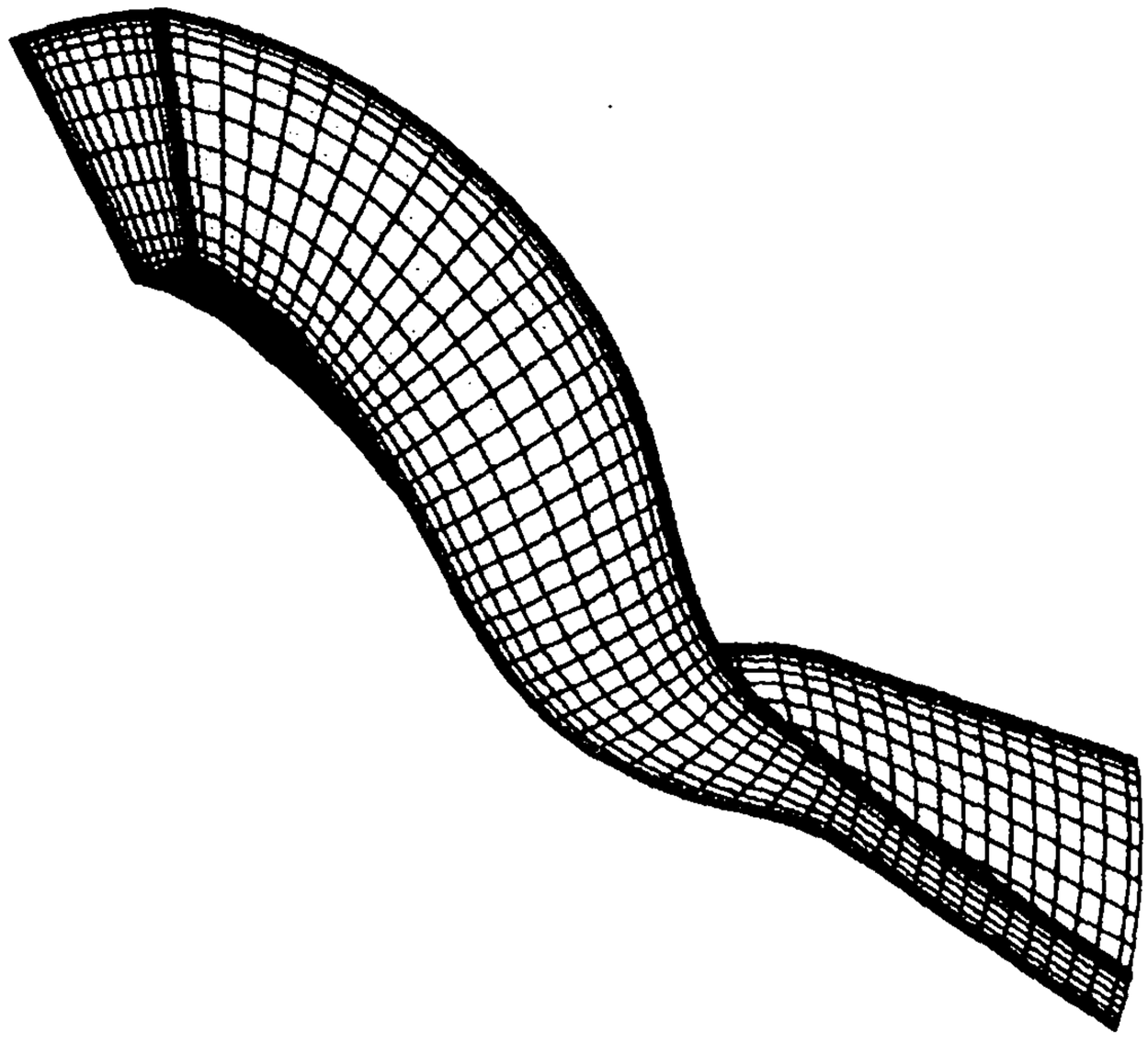

Figure 2.1 - Example of grid in the physical space.

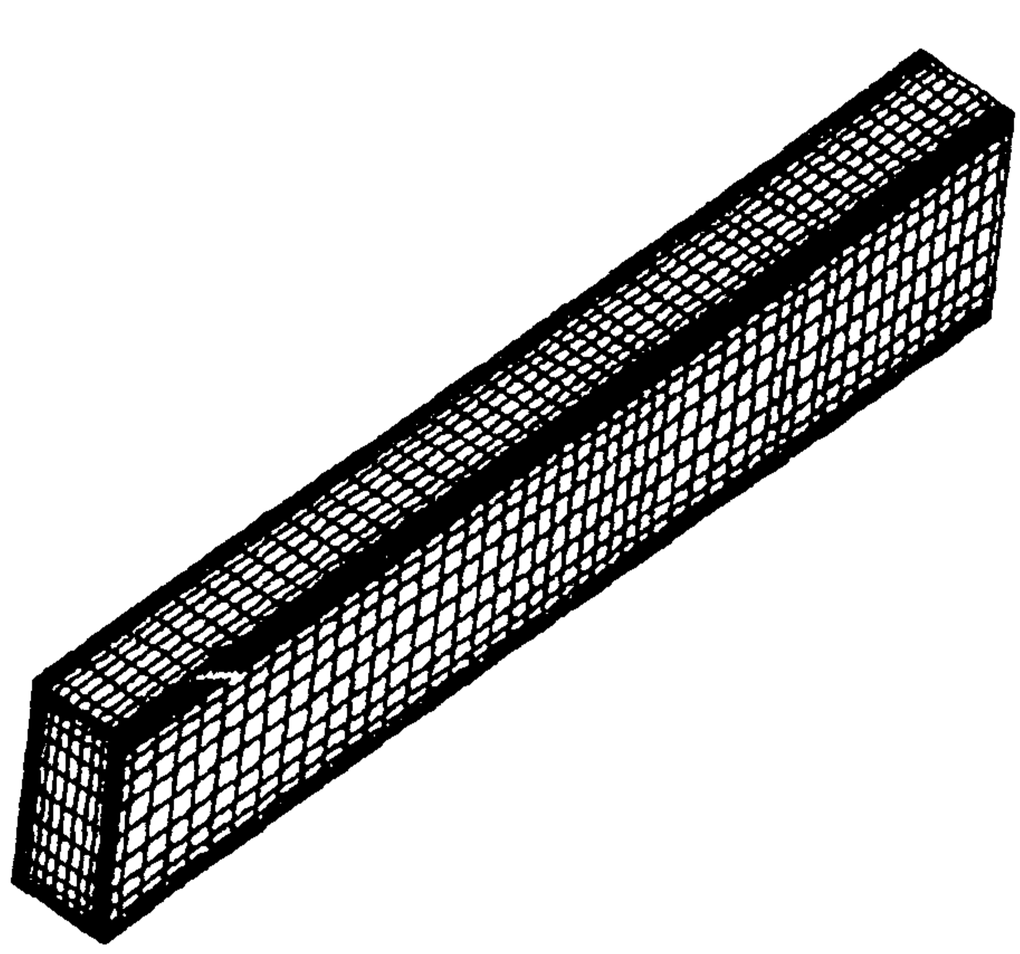

Figure 2.2 - Grid in the computational space.

• Convection term:

$$\frac{\partial}{\partial x_j}\left(\rho u_j \phi\right) = \frac{1}{J} \cdot \frac{\partial\left(\rho U_j \phi\right)}{\partial \xi_j} \tag{2.2.14}$$

• Diffusion term:

$$\frac{\partial}{\partial x_j}\left(\mu \frac{\partial \phi}{\partial x_j}\right) = \frac{1}{J} \cdot \frac{\partial}{\partial \xi_j}\left(\mu J g^{jm} \frac{\partial \phi}{\partial \xi_m}\right) \tag{2.2.15}$$

where the metric components are given by the relation:

$$g^{jm} = \frac{\partial \xi_j}{\partial x_i} \cdot \frac{\partial \xi_m}{\partial x_i} \tag{2.2.16}$$

The governing equations, in semi-Cartesian form, can be rewritten as follows:

• Continuity:

$$\frac{\partial}{\partial \xi_j}\left(\rho U_j\right) = 0 \tag{2.2.17}$$

• Momentum:

$$\frac{1}{J} \cdot \frac{\partial}{\partial \xi_j}\left[\rho U_j u_i - J(\mu + \mu_t) g^{jm} \frac{\partial u_i}{\partial \xi_m}\right] = S_{u_i} \quad i = 1,2,3 \tag{2.2.18}$$

where the pressure term:

$$-\left(\frac{\partial p}{\partial \xi} \cdot \frac{\partial \xi}{\partial x_i} + \frac{\partial p}{\partial \eta} \cdot \frac{\partial \eta}{\partial x_i} + \frac{\partial p}{\partial \zeta} \cdot \frac{\partial \zeta}{\partial x_i}\right) \tag{2.2.19}$$

has been incorporated in the source term.

• Scalar equation:

$$\frac{1}{J}\cdot\frac{\partial}{\partial\xi_j}\left(\rho U_j\phi - J\frac{\mu+\mu_t}{\mathrm{Pr}_\phi}g^{jm}\frac{\partial\phi}{\partial\xi_m}\right) = S_\phi \qquad (2.2.20)$$

where the terms S_{u_i} and S_ϕ are the transformed source terms obtained by applying the rules for the transformation of the Cartesian derivatives appearing in the corresponding source terms (i.e. using the relation (2.2.9)).

2.3 - Discretisation procedure.

A finite volume method for the numerical solution of the partial differential equations will be adopted. The flow properties are defined only at the nodes (non-staggered grid).

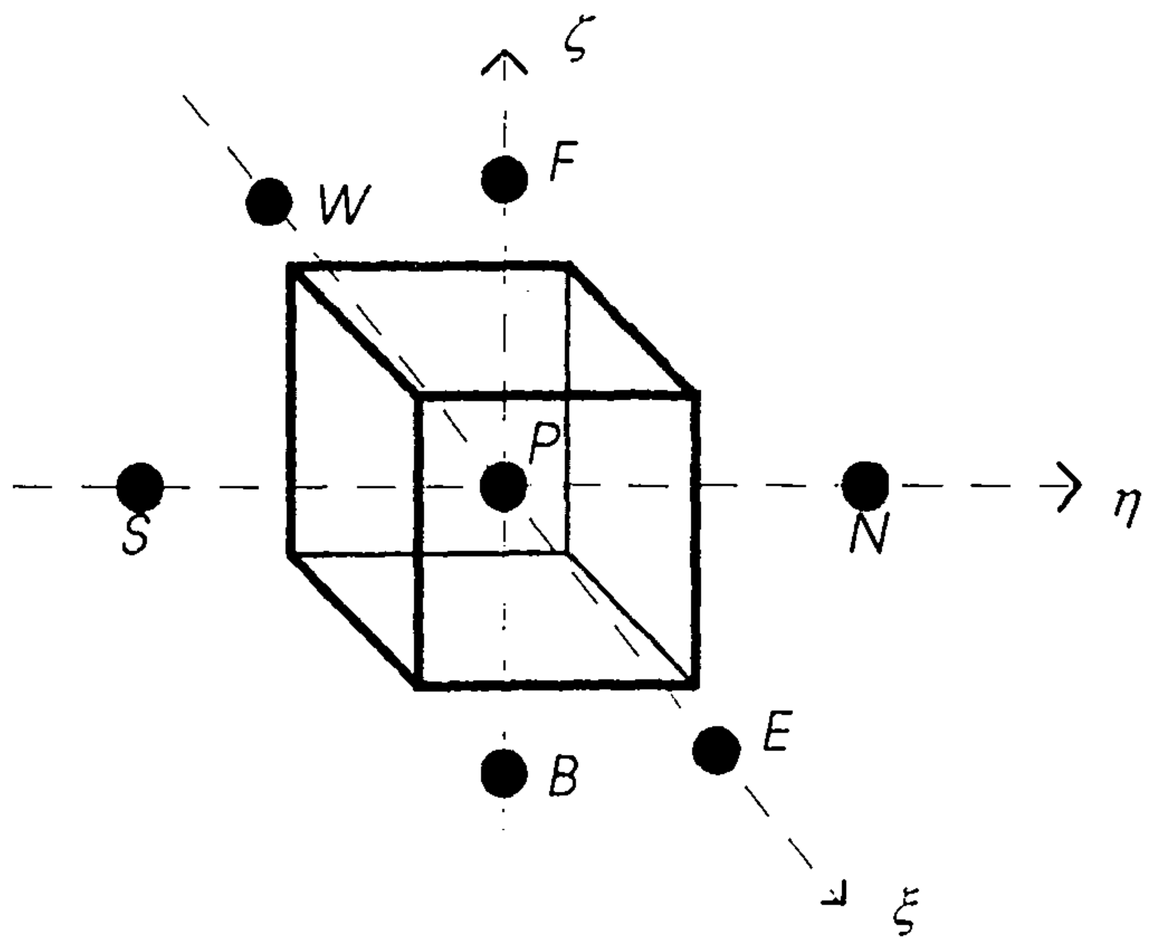

Figure 2.3 - Typical control volume.

Figure 2.3 shows a typical control volume surrounding the grid point P and the conventional names for the neighbouring points. The faces of the cell will be indicated with *e,w,n,s,f,b* (for, respectively, the *east* face, the *west* face, the *nord* face, etc.). The cell faces are supposed to be positioned exactly in the middle of the distance between two adjacent points; this particular arrangement is chosen to facilitate the evaluation of the variables at the cell faces, as a simple average of the values of a variable at the two adjacent nodes is a second-order accurate description of the corresponding value at the cell face. At the same time the grid point does not necessarily correspond to the

geometrical centre of the cell, and for highly distorted and non-uniform grid this factor could lead to loss of accuracy, although this phenomenon is expected to be small.

In this section the discretisation of the transport equation for the following variables: u,v,w (eq. (2.2.2)), I (eq. (2.2.3)), k (eq. (2.2.5)) and ε (eq. (2.2.6)) will be described, where the equations have been transformed in the form (2.2.18) or (2.2.20).

The set of equations is written for every grid point of the domain and integrated over the corresponding control volume or computational cell. With the use of Gauss's theorem the volume integrals on the left hand side of the transport equation can be expressed as surface integrals over the six faces of each control volume.

The integration of the transport equations over the control volume which encloses the grid node P can be therefore expressed in the following form:

$$I_e - I_w + I_n - I_s + I_f - I_b = \int_{\Delta\Theta_P} S_\phi \cdot d\Theta \qquad (2.3.1)$$

where I_i are surface integrals of the terms under the divergence operator on the left hand side of the transport equations and $\Delta\Theta_P$ is the volume of the cell. Each of these terms consists of a convective term and of a diffusive term; the last one can be split in two parts: the orthogonal diffusive term, containing the derivatives normal to the cell faces, and the cross diffusive term, which includes the rest of the diffusion terms.

• Metric coefficients.

The derivatives of the Cartesian coordinates x,y,z with respect to the generalised coordinates ξ, η, ζ appearing in the definition of the metric coefficients are evaluated through finite difference formulae in the computational space, while the others can be obtained through a series of relationships between the coordinate transformation components. E.g. from the transformation (2.2.8) can be obtained:

$$\xi_x = \frac{1}{J}\left(y_\eta z_\zeta - z_\eta y_\zeta\right) \qquad (2.3.2)$$

and the derivatives on the right hand side in the point P can be evaluated with a central difference (second order accurate assuming a constant spacing between the grid points), e.g.:

$$\left(\frac{\partial y}{\partial \eta}\right)_P = \frac{y_N - y_S}{\eta_N - \eta_S} \qquad (2.3.3)$$

• Convective term.

For the discretisation of the convective terms of the general transport equation the mean value theorem is utilised; for one of the faces, e.g. the *e* one:

$$\phi_e = \frac{\int_{A_e} \rho U \phi \, dA}{\int_{A_e} \rho U \, dA} \tag{2.3.4}$$

The convective term at the *e* face involves the mass flux through this face; supposing the values of ρ and U constant on the cell face, this can be estimated by employing the expression:

$$(\rho_e U_e A_e)\phi_e \tag{2.3.5}$$

The value of the density and of the convecting velocity on the cell face are obtained by linear interpolation between the values on the nodes surrounding the face (e.g. for the *e* face, the nodes *P* and *E*)

Also the value of the variable ϕ on the cell face has to be estimated using the corresponding values stored at the surrounding grid nodes. The interpolation technique used to obtain this value is chosen on the basis of considerations about the numerical stability and the accuracy of the procedure and will be extensively described in the fourth chapter of this thesis.

The basic approach uses an Upwind technique for the evaluation of ϕ_e: the value of ϕ on the cell face is approximated with the value upstream, where the upstream direction is based on the value of the convecting velocity on the cell face. The limitations of this approach will be extensively described in this thesis.

• Diffusion term.

The diffusion term of the transport equation consists of two parts: the normal diffusion term, which incorporates the first derivative of ϕ in the direction normal to the cell faces (e.g. for the *n* face):

$$\int_{A_n} J\left(\frac{\mu + \mu_t}{\mathrm{Pr}_\phi}\right) \cdot \left(g^{22} \frac{\partial \phi}{\partial \eta}\right) dA \tag{2.3.6}$$

and the cross diffusion term which contains first derivatives of ϕ in directions crossing the cell face:

$$\int_{A_n} J\left(\frac{\mu+\mu_t}{\mathrm{Pr}_\phi}\right)\left(g^{21}\frac{\partial\phi}{\partial\xi}+g^{23}\frac{\partial\phi}{\partial\zeta}\right)dA \qquad (2.3.7)$$

The calculation of the first derivative in the equation (2.3.6) is performed by using a simple central difference scheme:

$$\left(\frac{\partial\phi}{\partial\eta}\right)_n = \frac{\phi_N-\phi_P}{\eta_N-\eta_P} \qquad (2.3.8)$$

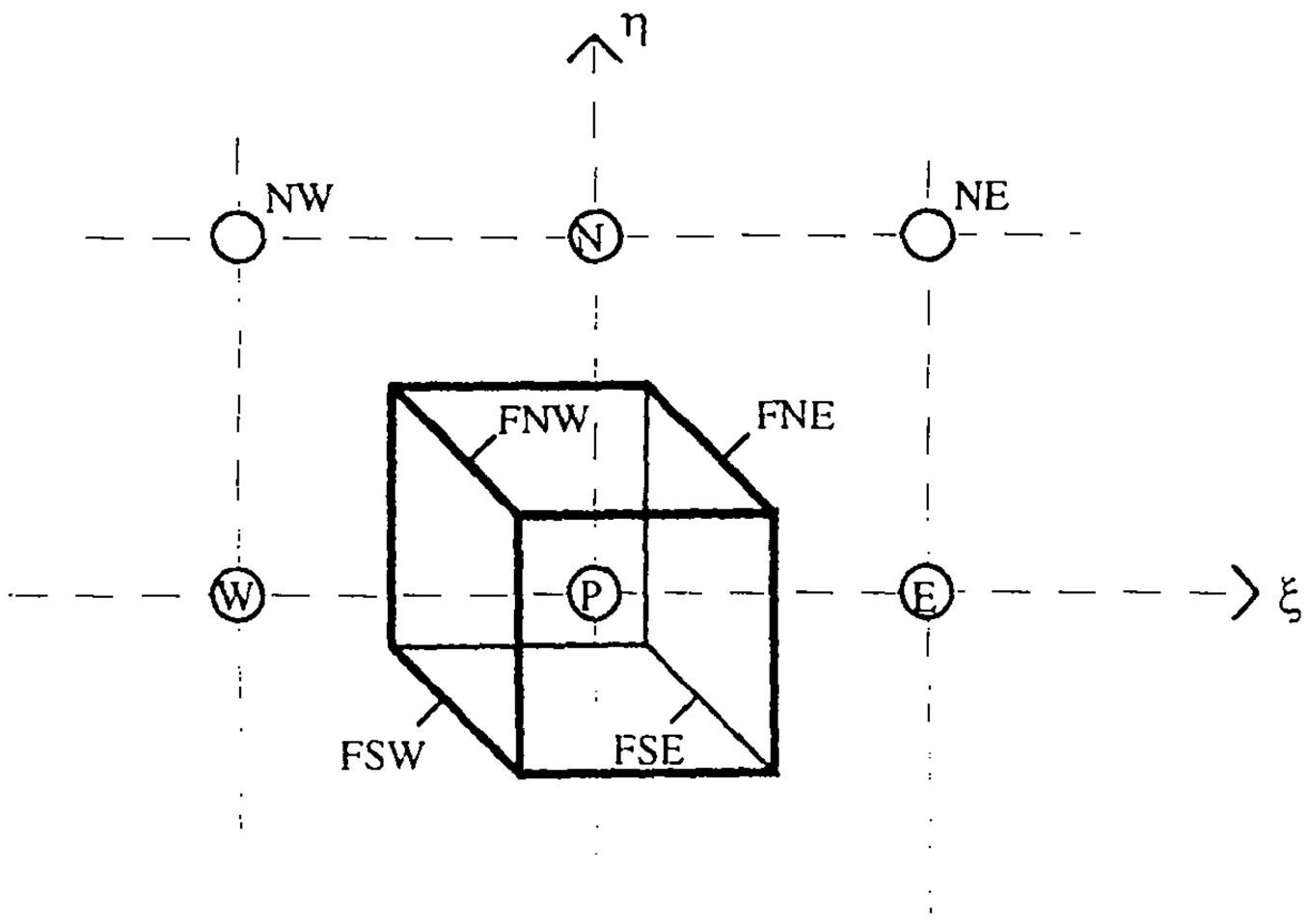

Figure 2.4 - Nodes involved in the calculation of the values at the middle of the NE and NW cell edges.

For the calculation of the cross derivatives in equation (2.3.7) the values of ϕ at the middle of the cell edges have to be employed. E.g., referring to figure 2.4, for the calculation of $(\partial\phi/\partial\xi)_n$ the values of *FNE* and *FNW* are needed; these can be evaluated from the nodal values of the neighbouring nodes, e.g.:

$$FNE = \frac{1}{4}\left(\phi_P+\phi_E+\phi_N+\phi_{NE}\right) \qquad (2.3.9)$$

• Source term.

The rest of the terms in the transport equations, which are not included in the convective and diffusive term, are assumed to constitute the source terms. The volume integral of the source term is approximated by the product of the value of the source term at the node P by the volume of the control cell. If the source term is a function of the dependent variable ϕ, then the source term is linearised into two distinct parts:

$$\int S_\phi \, d\Theta = \left(S'_{\phi P} + S''_{\phi P} \cdot \phi_P\right) \Delta\Theta_P \qquad (2.3.10)$$

$\Delta\Theta_P$

where the sign of $S''_{\phi P}$ should be always negative to enhance diagonal dominance in the coefficient matrix.

The pressure derivatives at the node P appearing in the source terms (cf. eq. (2.2.19)) are evaluated with a central difference scheme, e.g.:

$$\left(p_\xi\right)_P = \frac{p_E - p_W}{\xi_E - \xi_W} \qquad (2.3.11)$$

• General form of the equations.

For each variable ϕ the result of the discretisation of the transport equation for a control volume around the generic grid node P is a discrete equation which has the typical form:

$$a_P \phi_P = a_E \phi_E + a_W \phi_W + a_N \phi_N + a_S \phi_S + a_F \phi_F + a_B \phi_B + S_P =$$
$$= \sum_{K=E,W,N,S,F,B} a_K \phi_K + S_P \qquad (2.3.12)$$

Writing equation (2.3.12) for all the N grid points of the domain, a linear system of N equations is obtained for each variable ϕ. The procedure adopted is semi-implicit: in order to obtain an independent system of equations for each variable, when writing the equation for the generic variable ϕ, the values of the other variables are supposed to be known. Furthermore, in some of the calculations the variable ϕ itself is supposed known, such as in the evaluation of the cross diffusion terms, the generation rate of turbulence, etc. With this approach the coefficients a_K consist of contributions only from the convective and normal diffusive terms, while all the other contributions appear in the source term. The coefficient a_P consists of the same contributions plus the $S''_{\phi P}$ term. These approximations introduce the need for an iterative solution of the problem:

for every step, all the approximate systems are solved and the values obtained for the variables are used to calculate a new value of the coefficients and the source terms. To evaluate the flow field, an equation for the pressure field is still required.

2.4 - The pressure correction method.

The continuity equation will be used as a basis for the calculation of the correct pressure field through the iterative numerical procedure; the pressure correction scheme employed will be based on the classical SIMPLE method of Patankar and Spalding (1980), extended to a generalised coordinate system and collocated (non-staggered) grid arrangement of the variables, as suggested by Rhie and Chow (1983).

The general equation (2.3.12) is modified in the case of the momentum equations by explicitly expressing the pressure term:

$$a_P^{u_i}\left(u_i\right)_P = \sum_{K=E,W,N,S,F,B} a_K^{u_i}\left(u_i\right)_K + S_P^{u_i} - \Delta\Theta_P\left(\frac{\partial \xi_j}{\partial x_i}\cdot\frac{\partial p}{\partial \xi_j}\right)_P \qquad i=1,2,3 \tag{2.4.1}$$

where $\Delta\Theta_P$ is the volume of the cell centered at the point P.

Assuming a pressure field p^*, which is obtained either from an initial guess or from the previous iteration, the solution of the momentum equation (2.4.1) will provide values for the velocity field u^*, v^*, w^*. From these values the curvilinear velocity components U^*, V^* and W^* are calculated. These velocity components will not satisfy the discretised continuity equation but a mass source will be produced:

$$mp = F^*_{1e} - F^*_{1w} + F^*_{2n} - F^*_{2s} + F^*_{3f} - F^*_{3b} \tag{2.4.2}$$

where $F^*_i = \rho A_i U^*_i$.

In order to eliminate this mass source both the pressure field and the velocity fields have to be appropriately corrected. For this purpose, corrections u', v', w' and p' are added to the u^*, v^*, w^* and p^* respectively:

$$u_i = u^*_i + u'_i \quad i=1,2,3; \qquad p = p^* + p' \tag{2.4.3}$$

Both the set of values u, v, w, p and u^*, v^*, w^*, p^* satisfy the momentum equations; therefore substituting the definition (2.4.3) in the equations (2.4.1) the equations that relate each Cartesian velocity correction to the pressure correction are obtained:

$$a_P^{u_i}\left(u'_i\right)_P = \sum_{K=E,W,N,S,F,B} a_K^{u_i}\left(u'_i\right)_K + S_P^{u_i} - \Delta\Theta_P\left(\frac{\partial \xi_j}{\partial x_i}\cdot\frac{\partial p'}{\partial \xi_j}\right)_P \quad i=1,2,3 \tag{2.4.4}$$

The final solution is not affected if the first term of the right hand side of equations (2.4.4) is neglected, since the corrections u', v' and w' become equal to zero in the converged solution. Consequently the following expressions for the corrected u, v and w can be written:

$$u_i = u^*_i + \left(B^{u_i} p'_\xi + C^{u_i} p'_\eta + D^{u_i} p'_\zeta\right) \quad i=1,2,3 \tag{2.4.5}$$

where:

$$B^{u_i} = -\xi_{x_i}\frac{\Delta\Theta_P}{a_P^{u_i}};\quad C^{u_i} = -\eta_{x_i}\frac{\Delta\Theta_P}{a_P^{u_i}};\quad D^{u_i} = -\zeta_{x_i}\frac{\Delta\Theta_P}{a_P^{u_i}} \tag{2.4.6}$$

The corresponding curvilinear U, V and W values are obtained by substituting the relation (2.4.5) into the expressions (2.2.12); e.g. for the first component:

$$\begin{aligned} U &= U^* + J\left(B^u\xi_x + B^v\xi_y + B^w\xi_z\right)p'_\xi + \\ &\underline{+J\left(C^u\xi_x + C^v\xi_y + C^w\xi_z\right)p'_\eta} + \underline{J\left(D^u\xi_x + D^v\xi_y + D^w\xi_z\right)p'_\zeta} \end{aligned} \tag{2.4.7}$$

The terms with the underbar are the cross-pressure terms which appear due to the non-orthogonality of the grid system; these terms are neglected, without affecting the converged solution when the pressure correction p' becomes equal to zero. Consequently, simplified formulae for U, V and W can be derived:

$$U = U^* + Bp'_\xi;\quad V = V^* + Cp'_\eta;\quad W = W^* + Dp'_\zeta \tag{2.4.8}$$

where:

$$B = J\left(B^{u_i}\xi_{x_i}\right)\quad C = J\left(C^{u_i}\eta_{x_i}\right)\quad D = J\left(D^{u_i}\zeta_{x_i}\right) \tag{2.4.9}$$

The substitution of the corrected curvilinear velocity components U, V and W into the discretised continuity equation results in a discrete equation for the pressure correction p':

$$a_P^p p'(P) = \sum_{K=E,W,N,S,F,B} a_K^p p'(K) - mp \qquad (2.4.10)$$

where mp is given by the relation (2.4.2) and the coefficients a_K^p involve the value of the density and of B, C and D on the cell faces and the cell dimensions.

The solution of the equation (2.4.10) (with the appropriate boundary conditions) provides values for the pressure correction p' which is used to correct the pressure with the last of the (2.4.3) and the curvilinear velocities U, V and W with the relations (2.4.8). The Cartesian velocity components u, v and w are then calculated through the transformation relations (2.2.12).

The entire solution algorithm can be outlined as follows:

1 - For a given pressure field p^* the momentum equations are solved yelding values for the Cartesian components u^*, v^* and w^* and from the transformation relations the values of U^*, V^* and W^* are obtained.

2 - The continuity equation is enforced by solving the pressure correction equation. The pressure and the velocities are updated accordingly.

3 - The equations for k and ε are solved and the turbulence viscosity is updated.

4 - The energy equation is solved and the static temperature field is obtained through the rothalpy values. The density is then calculated through the perfect gas law.

The steps 1 to 4 are repeated until a convergent solution is reached.

For the stability of this iterative algorithm under-relaxation has to be used to update the variables: u^*, v^* and w^* (with respect to the previous iteration values of u, v and w) are under-relaxed while solving the momentum equations; furthermore only a fraction of p' is added to p^*: $p=p^*+\alpha_p \cdot p'$, with $\alpha_p<1$. For the scalar quantities:

$$\phi^{n+1} = \phi^n + \alpha_\phi \left(\phi^{n+1} - \phi^n\right) \quad \alpha_\phi < 1 \qquad (2.4.11)$$

2.5 - Use of the momentum interpolation.

The use of a collocated grid and of a central difference approximation of the pressure gradient can generate an oscillatory pressure field: this scheme cannot sense pressure oscillation between two adjacent grid points. To eliminate the oscillations with

the present ordinary grid arrangement, when evaluating the curvilinear velocities U, V and W on the cell boundaries the pressure term based on the central difference is replaced by a forward difference on the cell boundary (Rhie and Chow scheme or Momentum Interpolation scheme, 1983). E.g., for the velocity U on the *east* face, referring to figure 2.5:

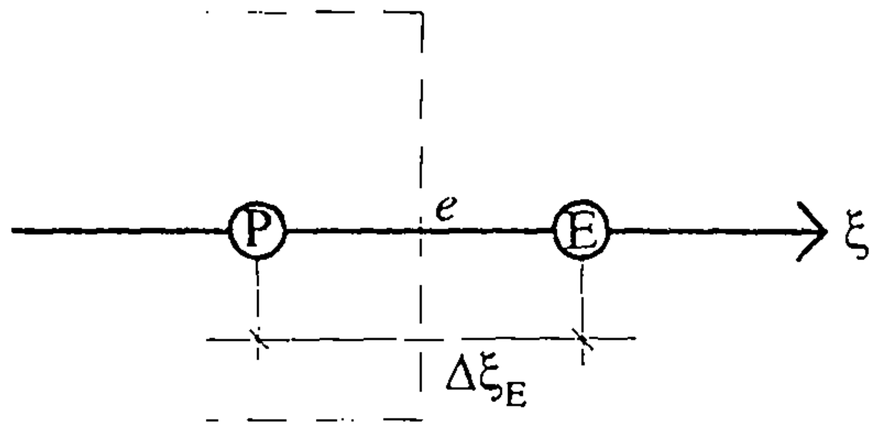

Figure 2.5

$$U_e = \frac{1}{2}\left[U(P)+U(E)\right] + B_e\left\{\frac{p(P)-p(E)}{\Delta\xi_E} - \frac{1}{2}\left[\frac{\partial p}{\partial \xi}(P)+\frac{\partial p}{\partial \xi}(E)\right]\right\} \qquad (2.5.1)$$

where:

$$B_e = \frac{1}{2}\left[B(P)+B(E)\right] \qquad (2.5.2)$$

Notice that the cell face is positioned exactly in the middle of the distance between the points P and E, so that the use of the average for the evaluation of the quantities on the cell face, as in expression (2.5.2), provides accurate results.

This procedure ensures the required coupling between the velocity field and the pressure but, unfortunately, when under-relaxation is used, produces a solution that is dependent on the value of under-relaxation α, with this scheme becoming less effective with the decrease of the value of α.

In what follows the derivation of the basic scheme (2.5.1) and the effect of the under-relaxation α will be described. The transport equation for the Cartesian velocity u can be written as (for a two-dimensional flow field):

$$u(P) = H(P) - \frac{\Delta\Theta_P}{a_P^u(P)}\frac{\partial \xi}{\partial x}(P)\frac{\partial p}{\partial \xi}(P) \qquad (2.5.3)$$

where H includes all the terms on the right-hand side of the transport equation except the pressure gradient in the direction normal to the cell face:

$$H(P) = \frac{1}{a_P^u(P)}\left[\sum_{K=E,W,N,S} a_K^u(P)u(P) + S(P) - \Delta\Theta_P \frac{\partial p}{\partial \eta}(P)\frac{\partial \eta}{\partial x}(P)\right] \qquad (2.5.4)$$

The under-relaxation α can be introduced as follows:

$$u(P) = \alpha H(P) + (1-\alpha)u^{n-1}(P) - \alpha\frac{\Delta\Theta_P}{a_P^u(P)}\frac{\partial \xi}{\partial x}(P)\frac{\partial p}{\partial \xi}(P) \qquad (2.5.5)$$

where u^{n-1} is the value of u at the previous iteration; a similar expression can be obtained for point E:

$$u(E) = \alpha H(E) + (1-\alpha)u^{n-1}(E) - \alpha\frac{\Delta\Theta_E}{a_P^u(E)}\frac{\partial \xi}{\partial x}(E)\frac{\partial p}{\partial \xi}(E) \qquad (2.5.6)$$

In the standard procedure of the momentum interpolation, the value of u on the *east* face is obtained by averaging the terms on the right-hand side of equations (2.5.5) and (2.5.6), except the last term, that is replaced with a corresponding term containing a forward difference on the cell boundary:

$$u_e = \alpha\left\{\frac{1}{2}[H(P)+H(E)] - \left(\frac{\Delta\Theta}{a_p^u}\frac{\partial \xi}{\partial x}\right)_e \frac{p(E)-p(P)}{\Delta\xi_E}\right\} + \\ +(1-\alpha)\frac{1}{2}\left[u^{n-1}(P)+u^{n-1}(E)\right] \qquad (2.5.7)$$

where

$$\left(\frac{\Delta\Theta}{a_p^u}\frac{\partial \xi}{\partial x}\right)_e = \frac{1}{2}\left[\frac{\Delta\Theta_P}{a_p^u(P)}\frac{\partial \xi}{\partial x}(P) + \frac{\Delta\Theta_E}{a_p^u(E)}\frac{\partial \xi}{\partial x}(E)\right] \qquad (2.5.8)$$

This procedure, as will become evident later, provides equation (2.5.1) for the value of the transformed velocity U. Following the idea of S. Majumdar (1988), an

interpolating procedure producing a result not depending on the value of α can be obtained if the under-relaxation is introduced directly in the evaluation of the cell face:

$$u_e = \alpha\left\{\frac{1}{2}[H(P)+H(E)]-\left(\frac{\Delta\Theta}{a_p^u}\frac{\partial\xi}{\partial x}\right)_e \frac{p(E)-p(P)}{\Delta\xi_E}\right\}+(1-\alpha)u_e^{n-1} \qquad (2.5.9)$$

corresponding to:

$$u_e = \alpha\left\{\begin{array}{l}\text{interpolated value on the cell face}\\ \text{with the pressure gradient replaced}\end{array}\right\}+$$
$$+(1-\alpha)\left\{\begin{array}{l}\text{value of the face evaluated}\\ \text{at the previous iteration}\end{array}\right\}$$

which, as the iterative procedure converges, tends towards the required interpolated value. Obtaining *H(P)* and *H(E)* from equations (2.5.5) and (2.5.6):

$$u_e = \frac{1}{2}[u(P)+u(E)]+(1-\alpha)\left\{u_e^{n-1}-\frac{1}{2}\left[u^{n-1}(P)+u^{n-1}(E)\right]\right\}+$$
$$+\alpha\left\{-\left(\frac{\Delta\Theta}{a_p^u}\frac{\partial\xi}{\partial x}\right)_e \frac{p(E)-p(P)}{\Delta\xi_E}+\right.$$
$$\left.+\frac{1}{2}\left[\frac{\Delta\Theta_P}{a_p^u(P)}\frac{\partial\xi}{\partial x}(P)\frac{\partial p}{\partial\xi}(P)+\frac{\Delta\Theta_E}{a_p^u(E)}\frac{\partial\xi}{\partial x}(E)\frac{\partial p}{\partial\xi}(E)\right]\right\} \qquad (2.5.10)$$

A similar expression can be obtained for the other components of the Cartesian velocity (assuming that the same value of under-relaxation is used):

$$v_e = \frac{1}{2}[v(P)+v(E)]+(1-\alpha)\left\{v_e^{n-1}-\frac{1}{2}\left[v^{n-1}(P)+v^{n-1}(E)\right]\right\}+$$
$$+\alpha\left\{-\left(\frac{\Delta\Theta}{a_p^v}\frac{\partial\xi}{\partial y}\right)_e \frac{p(E)-p(P)}{\Delta\xi_E}+\right.$$
$$\left.+\frac{1}{2}\left[\frac{\Delta\Theta_P}{a_p^v(P)}\frac{\partial\xi}{\partial y}(P)\frac{\partial p}{\partial\xi}(P)+\frac{\Delta\Theta_E}{a_p^v(E)}\frac{\partial\xi}{\partial y}(E)\frac{\partial p}{\partial\xi}(E)\right]\right\} \qquad (2.5.11)$$

The required value of the transformed velocity on the *east* face is then obtained from the combination of the values (2.5.10) and (2.5.11):

$$U_e = J_e\left[\left(\frac{\partial\xi}{\partial x}\right)_e u_e + \left(\frac{\partial\xi}{\partial y}\right)_e v_e\right] \tag{2.5.12}$$

where:

$$J_e = \frac{1}{2}[J(P) + J(E)] \;\; ; \;\; \left(\frac{\partial\xi}{\partial x_i}\right)_e = \frac{1}{2}\left[\frac{\partial\xi}{\partial x_i}(P) + \frac{\partial\xi}{\partial x_i}(E)\right] \tag{2.5.13}$$

Inserting the expressions (2.5.10) and (2.5.11) in equation (2.5.12) the following expression is obtained:

$$\begin{aligned}
U_e = {} & J_e\left\{\left(\frac{\partial\xi}{\partial x}\right)_e\left[\frac{u(P)+u(E)}{2}\right] + \left(\frac{\partial\xi}{\partial y}\right)_e\left[\frac{v(P)+v(E)}{2}\right]\right\} + (1-\alpha)U_e^{n-1} + \\
& -(1-\alpha)J_e\left\{\left(\frac{\partial\xi}{\partial x}\right)_e\left[\frac{u^{n-1}(P)+u^{n-1}(E)}{2}\right] + \left(\frac{\partial\xi}{\partial y}\right)_e\left[\frac{v^{n-1}(P)+v^{n-1}(E)}{2}\right]\right\} + \\
& + \alpha B_e \frac{p(E)-p(P)}{\Delta\xi_E} + \\
& -\alpha\left\{\left(\frac{\partial\xi}{\partial x}\right)_e \frac{1}{2}\left[\frac{\Delta\Theta_P}{a_p^u(P)}\frac{\partial\xi}{\partial x}(P)\frac{\partial p}{\partial\xi}(P) + \frac{\Delta\Theta_E}{a_p^u(E)}\frac{\partial\xi}{\partial x}(E)\frac{\partial p}{\partial\xi}(E)\right] + \right. \\
& \left. + \left(\frac{\partial\xi}{\partial y}\right)_e \frac{1}{2}\left[\frac{\Delta\Theta_P}{a_p^v(P)}\frac{\partial\xi}{\partial y}(P)\frac{\partial p}{\partial\xi}(P) + \frac{\Delta\Theta_E}{a_p^v(E)}\frac{\partial\xi}{\partial y}(E)\frac{\partial p}{\partial\xi}(E)\right]\right\}
\end{aligned} \tag{2.5.14}$$

Neglecting the variation of the coefficients in respect to the averaged values on the cell faces, an expression similar to the (2.5.1) is obtained:

$$\begin{aligned}
U_e = {} & \frac{1}{2}[U(P)+U(E)] + \alpha B_e\left\{\frac{p(P)-p(E)}{\Delta\xi_E} - \frac{1}{2}\left[\frac{\partial p}{\partial\xi}(P) + \frac{\partial p}{\partial\xi}(E)\right]\right\} + \\
& + (1-\alpha)\left\{U_e^{n-1} - \frac{1}{2}\left[U^{n-1}(P) + U^{n-1}(E)\right]\right\}
\end{aligned} \tag{2.5.15}$$

Notice that the presence of the last term is due to the introduction of the under-relaxation coefficient directly on the cell face; using equation (2.5.7) instead of equation (2.5.9), the Rhie and Chow scheme (2.5.1) is obtained.

It is important to observe that the values of the components of the transformed velocity on the cell faces have to be evaluated twice for every step of the iterative procedure: the first interpolation is carried out soon after the solution of the momentum equations, being in this case $p=p^*$ (value of the pressure field before the correction) and $U_i = U_i^*$ the corresponding velocity; the values on the cell faces have to be evaluated again after the solution of the continuity equation, using the updated values of pressure and velocity. For this second interpolation, the expression (2.5.15) can be used as well, assuming that the updated values of pressure and velocity satisfy the momentum equations. It is easy to notice that both interpolation schemes converge towards the same value as the iterative procedure progresses.

In this study the original Rhie and Chow scheme has been adopted, and has proven to be a reliable method for the complete elimination of pressure oscillation if relatively high values of the under-relaxation factors are used in the solution of the momentum equations, thus avoiding the use of the additional memory that would be required by the use of the modified scheme (2.5.15).

Furthermore, in preliminary numerical tests the scheme (2.5.15) appears to have a negative effect on the stability of the procedure, in particular when using a turbulence model not based on the eddy viscosity (that will be presented in the sixth chapter of this thesis), probably due to the introduction of a larger correction in the evaluated values of the velocities on the cell faces. More tests have to be carried out on this particular subject.

2.6 - The boundary conditions.

The systems of equations obtained from the numerical approach described in the previous sections have to be closed by an appropriate set of boundary conditions.

Not all the variables can be assigned arbitrarily on the boundaries: the pressure and the velocity are linked through the momentum equations, therefore only one of the two can be freely assigned on the boundaries.

For example, in a three-dimensional centrifugal compressor, defining the generalised coordinates as follows:

- ξ from blade to blade;
- η from hub to shroud;
- ζ following the main flow direction;

the boundary conditions in the absolute frame of reference for the velocity components and the scalar quantities (**except the pressure**) can be assigned as follows (see also figure 2.6, where the boundary conditions in the computational space are rassumed):

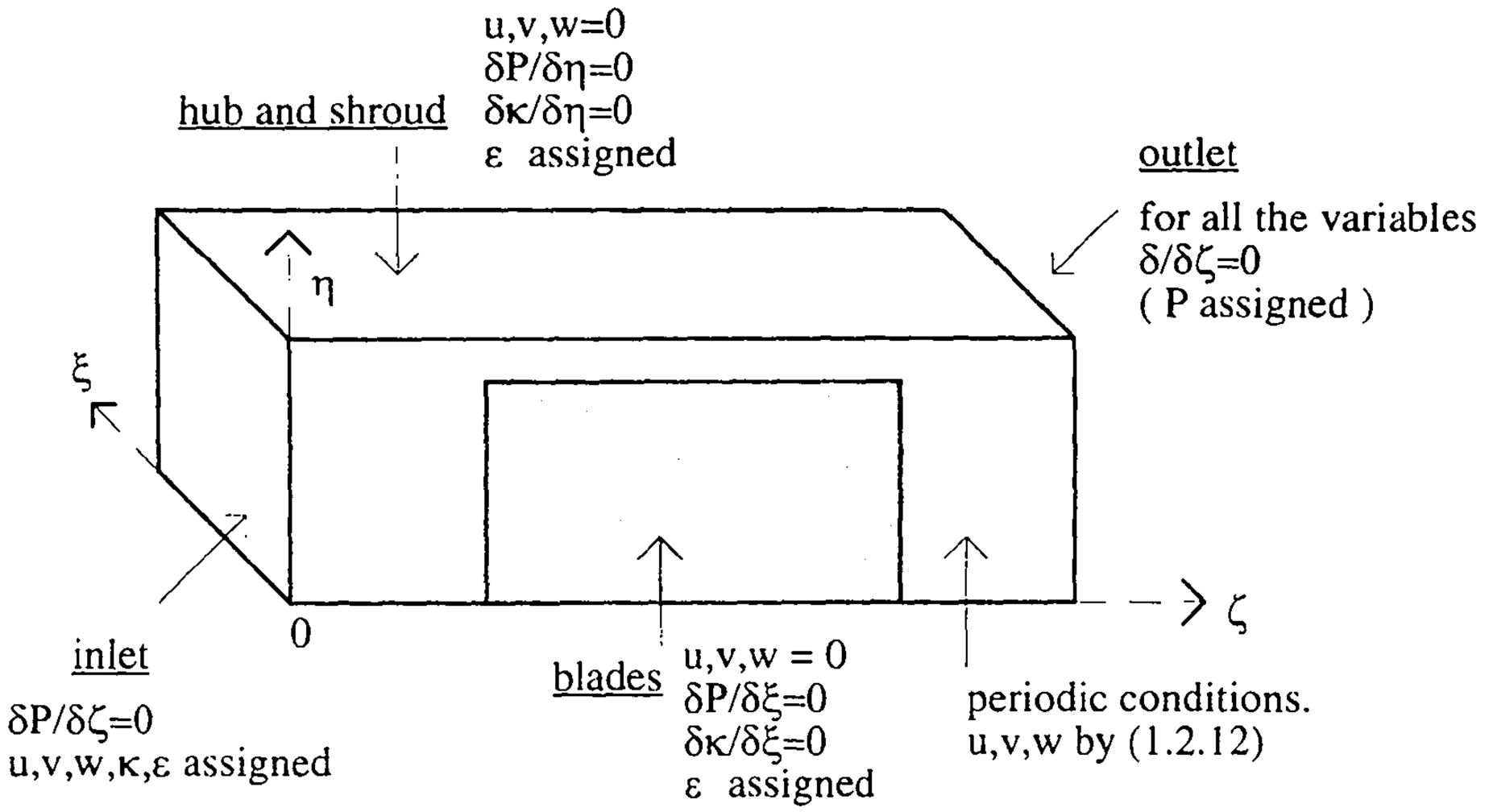

Figure 2.6 - Boundary conditions in the computational space for the absolute system of reference.

• Inlet ($\zeta = 0$): all the variables are assigned;

• Solid walls (blades, hub and shroud):

- the velocity is zero (no slip condition);

- the normal derivative of the turbulent kinetic energy, k, is zero;

- the value of the turbulence energy dissipation, ε, is assigned. This condition, like the previous one, comes from the wall function theory; furthermore, the diffusion term in all the transport equations is modified to take into account the diffusive contribution due to the wall shear stress evaluated with the wall function theory;

• Periodic boundaries on the sides ($\xi = 0$ and $\xi = \xi_{max}$, excluding the blades): periodic conditions are implemented in the computational space: for the generic variable ϕ the following condition is imposed:

$$\phi(0, \eta, \zeta) = \phi(\xi_{max}, \eta, \zeta) \quad \text{(not for the blades)} \tag{2.6.1}$$

this is because only one representative flow passage between two adjacent blades is considered, with the assumption of repeating flow conditions, in order to reduce the computational effort required to handle the whole cascade. This condition can be applied for all the scalar variables ($I, k, \varepsilon, p, \rho$) and the velocity components in the

computational space (U, V, W) ; the Cartesian velocity components (u,v,w) are instead obtained with the relations (2.2.12).

• Outlet ($\zeta = \zeta_{max}$): the diffusion is supposed to be negligible and the flow convection dominated. The values on the outlet boundaries, in this hypothesis, can be determined by extrapolation from upstream. A common assumption for all the variables in the outlet is:

$$\partial\phi/\partial\zeta = 0 \qquad (2.6.2)$$

The corresponding boundary conditions for the **pressure** in the transformed space are:

• Inlet: the value of the pressure cannot be assigned, The boundary condition for the pressure at the inlet, therefore, has to be a Neumann one, as the only information available is that the upstream flow is uniform in the stream direction:

$$\frac{\partial p}{\partial \zeta} = 0 \quad \text{for} \quad \zeta = 0 \qquad (2.6.3)$$

• Solid walls (blades, hub and shroud): the derivative of the pressure in the direction normal to the walls can be assumed to be zero for the hypothesis of constant pressure in the boundary layer in the normal direction, where the normal direction to the walls corresponds to the ξ or the η directions for the chosen set of generalised coordinates:

$$\frac{\partial p}{\partial \xi} = 0 \quad \text{on the blades;} \qquad (2.6.4)$$

$$\frac{\partial p}{\partial \eta} = 0 \quad \text{on the hub and the shroud.} \qquad (2.6.5)$$

Notice that the ξ (or the η) direction corresponds to the direction normal to the wall only if the grid is orthogonal at the wall; if the grid is locally skewed, the expressions (2.6.4) and (2.6.5) could not be correct. In this study they are used in all the cases, and the error eventually introduced is neglected.

• Outlet ($\zeta = \zeta_{max}$): in this case the velocity distribution is not explicitly assigned; the pressure can therefore be freely assigned (e.g. imposing a zero value to the pressure

correction, corresponding to a constant distribution of the pressure at the outlet) or given with the relation (2.6.2).

The boundary conditions used for the pressure are imposed also for the energy equation (and consequently for the density);

To obtain the boundary conditions for the rotating frame of reference the relative velocity components have to be considered.

Chapter 3
The solution procedure

3.1 - Introduction.

One of the reasons for the development of a completely new procedure is to overcome some of the limits of a previous code, aimed at the calculation of the flow field inside rotating passages of centrifugal compressor configurations and based on the background exposed in the previous chapter, developed at Cranfield University by A. Tourlidakis, named TURBO3D (Tourlidakis, 1992; Tourlidakis and Elder, 1993). The solution procedure that was adopted in TURBO3D is typical of many numerical codes commonly used in engineering applications of CFD.

The new code, that will be referred to as TURBO3D_2, has been designed to take full advantage of the features of the Cray J916/4-512 currently available at Cranfield University; in effect most of the limits of the previous code are due to the restriction of RAM memory and CPU time on the computers available in the past.

In TURBO3D the systems of equations are solved on a plane-by-plane basis: for each $\xi - \eta$ plane an ADI line solver is used to obtain a solution, using the values on the previous plane just evaluated and the ones of the next plane from the previous iteration. This procedure, that has been very popular in the past for problems with a predominant main flow direction, introduces further approximations in the solution of the problem:

- The variations and/or the derivatives in the ζ direction (main flow direction) are the most affected from this kind of approach. The pressure solver is almost insensitive to pressure variations in this direction and a one-dimensional pressure correction in the ζ direction has to be introduced. The nature of this correction makes it impossible to impose correctly the Neumann condition for the pressure at the inlet or to assign a constant value of the pressure at the outlet. Furthermore the Rhie and Chow scheme can be correctly applied only for the velocities in the other two directions.

- The line solver can be practically used only for Dirichlet conditions; the line solver starts from the side with $\xi = 0$ and solves the system advancing in the ξ direction, then starts from the side with $\eta = 0$ and solves again in the η direction. In TURBO3D the values of the variables of the previous iterations are used on the boundary, so the boundary conditions of figure 2.6 are transformed in Dirichlet conditions.

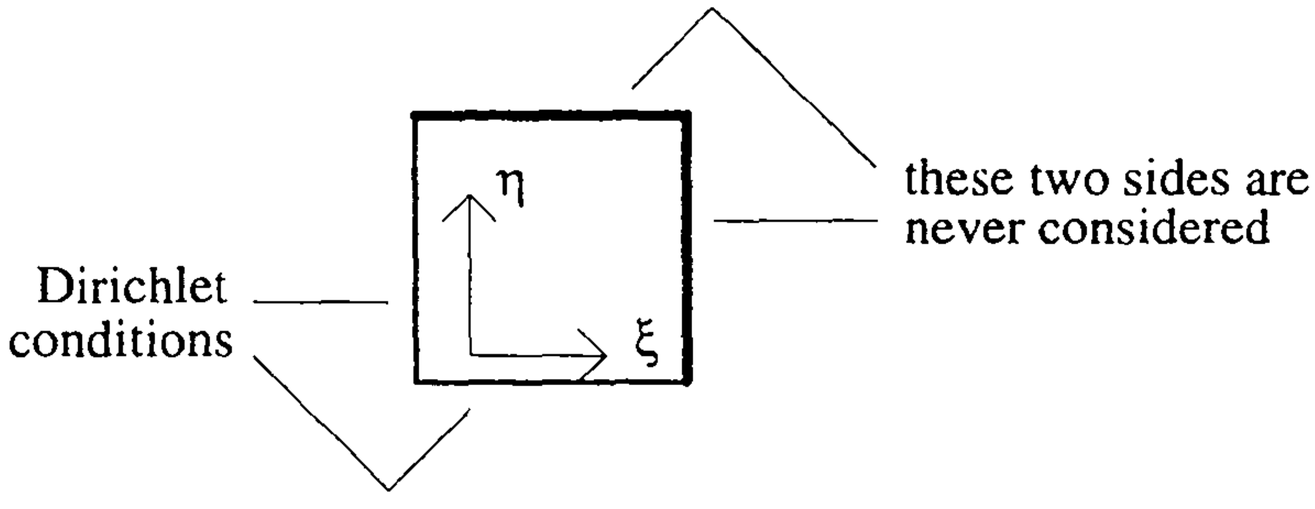

Figure 3.1 - ADI solver as used in TURBO3D.

• Storing the variables on a line or on a plane, as in TURBO3D, causes a decrease in the efficiency of the code, as often the same quantities have to be evaluated more than once. E.g., when the values of the variables on the six cell faces are needed, only the values on three faces have to be evaluated (e, n, f) as the others can be obtained from the previous cells for conservation reasons: the values on the w face are equal to the values on the e face of the previous cell in the ξ direction, the same for the other two directions and the faces s and b. This kind of approach, that is impossible in TURBO3D for all the directions, also ensures that the numerical scheme is conservative.

• Most of the geometric quantities, as the metric coefficients, that are constant in the whole procedure, are evaluated for each iteration, having been stored in a one dimensional basis.

TURBO3D_2, on the other hand, uses a fully three-dimensional approach, solving the systems in the whole field at each iteration, imposing the correct boundary conditions as expressed in the first chapter. The choice of the linear solver is of great importance for the efficiency of the code and will be extensively discussed in this chapter and in the following ones.

In the next sections it will be shown how all the problems mentioned before have been overcome in the new code and, at the same time, a high efficiency on the Cray has been achieved.

The code has been designed not only to provide a more efficient and more accurate computational tool, but also as a research tool to test the effect of the linear solver on the procedure and the effect of the boundary conditions on the solution, the scheme adopted for the convection term, turbulence modelling, etc.

3.2 - Geometrical quantities, derivatives, etc.

• The conservative property has been used for all the quantities to be evaluated on the cell faces: only the values on the *e*, *n* and *f* faces are evaluated and stored. When the values on the middle of the cell edges are needed, only three of the twelve values are evaluated and stored: referring to figure 2.4, once evaluated the value of *FNE* for all the cells *FNW*, *FSE* and *FSW* can be obtained as the values of *FNE* for the previous cells in the ξ and η directions.

• All the geometrical quantities are evaluated and stored before the beginning of the iterative procedure. This approach requires a considerable amount of memory but improves dramatically the efficiency of the code.

• Every quantity that is used more than once and requires complex calculations is evaluated only once and then stored. To reduce the amount of memory required the same area of memory is used for quantities that are used in different sections of the code (through EQUIVALENCE statements [3]).

• All the derivatives, appearing both in the geometrical quantities or in the source terms, have been evaluated with second-order formulae for non-uniform mesh. The choice of the mesh in the computational space (ξ, η, ζ) is completely arbitrary, so a uniform mesh could be used and simpler formulae as the (2.3.11) would be second-order accurate. But, as the grid in the physical space (x,y,z) is generally highly non-uniform (e.g.: clustering near the blades or the walls), the choice of a uniform grid in the computational space may cause very large or very small numbers for the metric coefficients, with the risk of generating higher truncation errors in the operations. For these reasons the grid in the computational space is chosen with the same volume distribution of the original one (i.e. metric coefficients close to 1) and formulae for non uniform grid are used. E.g. the formula (2.3.11) becomes (fig. 3.2):

$$\left(p_{\xi}\right)_P = \frac{1}{\Delta\xi_P + \Delta\xi_E}\left[\frac{\Delta\xi_P}{\Delta\xi_E}\left(p_E - p_P\right) + \frac{\Delta\xi_E}{\Delta\xi_P}\left(p_P - p_W\right)\right] \qquad (3.2.1)$$

---

[3] *The standard FORTRAN 77 has been used, with few extensions, and compiled with the "no declare" option (all the variables have been explicitly declared).*

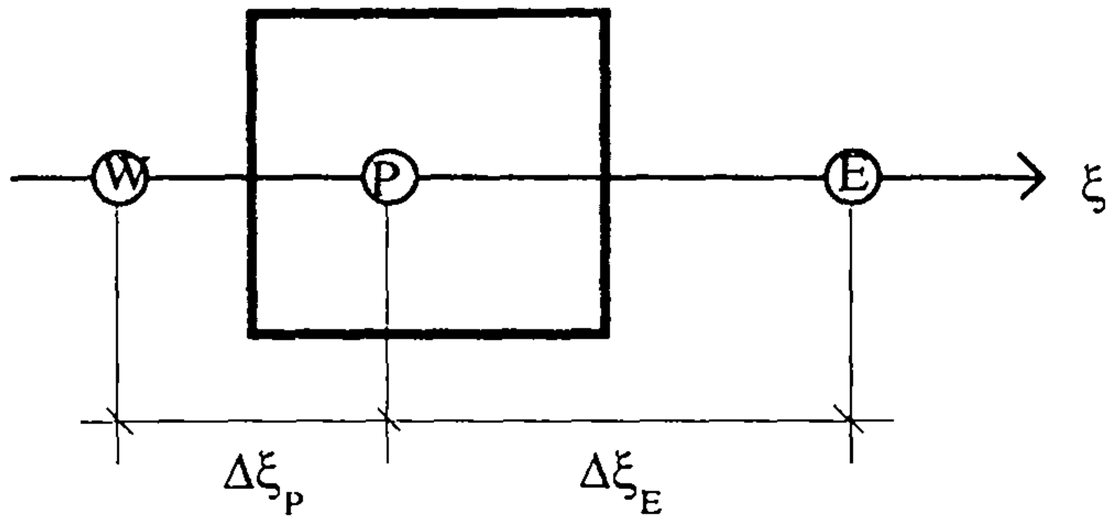

Figure 3.2 - Non uniform grid.

3.3 - Boundary conditions.

In the rest of this thesis, i, j and m will be used to indicate three indices varying in the ξ, η and ζ directions respectively and with nx, ny and nz the number of grid nodes in the same directions.

For each direction the first and the last grid nodes are on the boundary and the corresponding control volume reduces to a surface (zero volume). The control volume boundaries are assumed to be located in the middle of the distance between adjacent grid nodes; this rule is used for all the internal nodes except for the cells near the boundaries: the second and the $(nx_i - 1)th$ cells have one of the faces on the boundaries. In figure 3.3 the case of the ξ direction is represented.

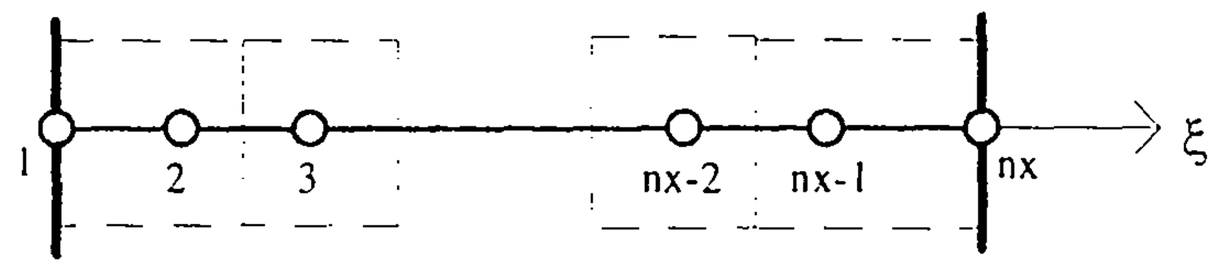

Figure 3.3 - Numbering of the grid nodes near the boundaries.

• Periodic conditions - for the transport equations of ε, k, I, p, and the evaluation of ρ, μ, U, V, W on the cell faces.

The periodic conditions (2.5.1) could be easily discretized with:

$$\phi(1, j, m) = \phi(nx, j, m) \tag{3.3.1}$$

This kind of approach is not convenient as the nodes for i=1 and i=nx are unknown and is not possible to write for these grid points the general equation (2.3.12) as the corresponding cells have zero volume.

The approach used is instead based on the following assumptions [4]:

1) when writing the equations for the cell i=nx-1 the first control volume, corresponding to the grid point i=2, will be considered as the E cell (see figure 3.4). Equation (2.3.12) becomes:

$$a_P\phi(nx-1,j,m) = a_E\phi(2,j,m) + a_W\phi(nx-2,j,m) + \ldots \qquad (3.3.2)$$

where $a_K = a_K(nx-1,j,m)$.

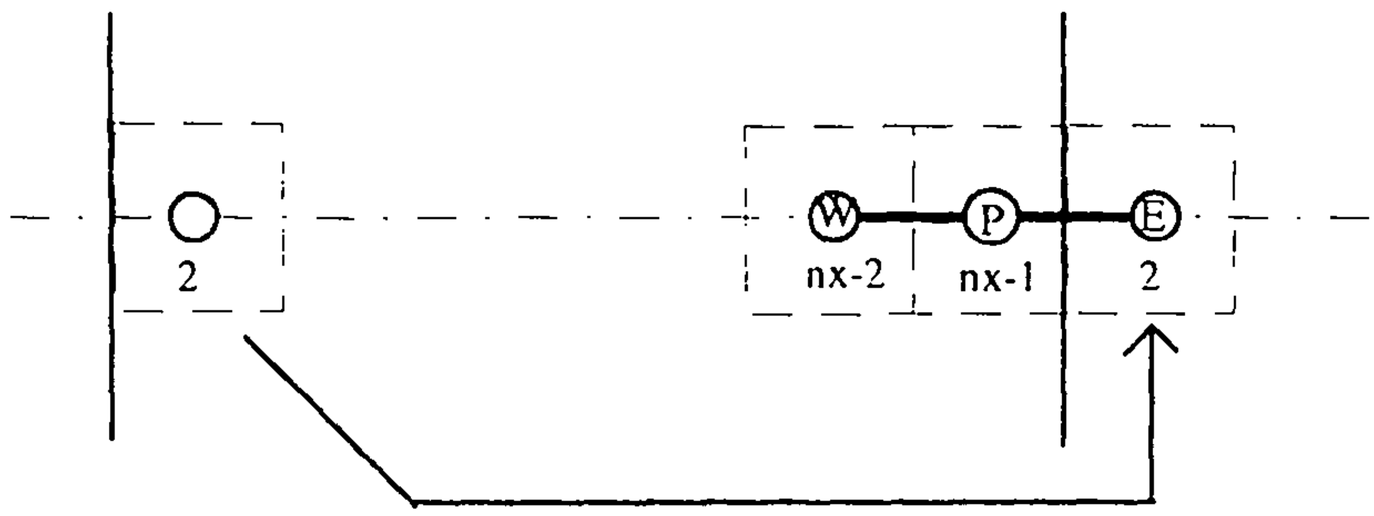

Figure 3.4: Nodes involved in the ξ direction in the equation for i=nx-1.

At the same time, writing the equations for the cell i=2 the last control volume, corresponding to the grid point i=nx-1, will be considered as the W cell. The equation becomes:

$$a_P\phi(2,j,m) = a_E\phi(3,j,m) + a_W\phi(nx-1,j,m) + \ldots \qquad (3.3.3)$$

where $a_K = a_K(2,j,m)$.

The same rule is used every time the E node for i=nx-1 (or the W node for i=2) is needed. E.g., referring to figure 3.5, the formula (3.2.1) becomes:

$$\left(p_\xi\right)_{nx-1} = \frac{1}{\Delta\xi_{nx-1} + \left(\Delta\xi_{nx} + \Delta\xi_2\right)} \cdot \left[\frac{\Delta\xi_{nx-1}}{\left(\Delta\xi_{nx} + \Delta\xi_2\right)}\left(p_2 - p_{nx-1}\right) + \frac{\left(\Delta\xi_{nx} + \Delta\xi_2\right)}{\Delta\xi_{nx-1}}\left(p_{nx-1} - p_{nx-2}\right)\right] \qquad (3.3.4)$$

---

[4] *What follows is not applied on the blades, where Neumann or Dirichlet conditions are imposed.*

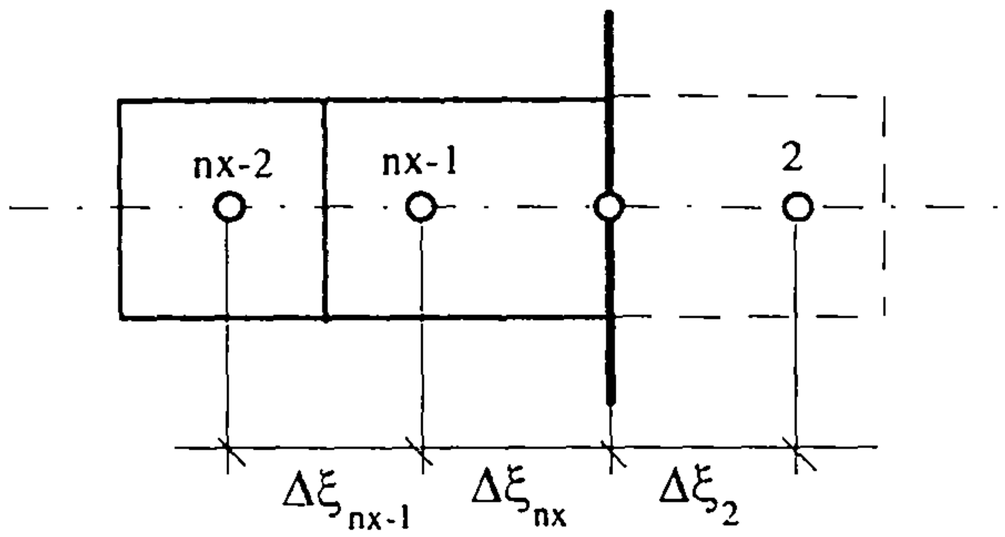

Figure 3.5 - Nodes appearing in the evaluation of the derivatives for i= nx-1.

2) For the conservative property, all the values on the *e* face of the cell *i=nx*-1 should be equal to the corresponding ones on the *w* face of the cell *i*=2 [5]:

$$\phi_e(nx-1,j,m) = \frac{1}{2}\left[\phi(nx-1,j,m) + \phi(2,j,m)\right]$$
$$\phi_w(2,j,m) = \phi_e(nx-1,j,m) \qquad (3.3.5)\ [6]$$

3) the nodes *i*=1 and *i=nx* are not considered during the whole procedure; the values of the variables in these nodes are updated only at the end of the program with an average between the values in the corresponding grid points for *i*=2 and *i=nx*-1.

• Periodic conditions - for the transport equations of the Cartesian velocity components.

The value of the components *u, v, w* on the surfaces with periodic boundary conditions can be obtained from the values of *U, V, W* on the boundaries using the relations (2.2.11). In this case an implicit formulation, like the previous one, cannot be used; instead, the following procedure is used:

1) using the values of *U, V, W* in the nodes *i*=2 and *i=nx*-1, the values on the boundaries with periodic conditions are updated:

---

[5] *As only the e values are stored, the w value for the cell i=2 is memorised as the e value of the cell i=1 (that effectively does not exist).*

[6] *Note that, using a linear interpolation to evaluate the values on the cell faces from the value on the grid nodes, the formula* $\phi_e = 0.5(\phi_P + \phi_E)$ *is accurate, as the cell boundary is exactly in the middle of the distance between the grid points P and E, while the formula (3.3.5) is less accurate as the e face is not necessarily in the middle between the points i=nx-1 and i=2.*

$$U_i(nx,j,m)=\frac{1}{2}\left[U_i(nx-1,j,m)+U_i(2,j,m)\right]$$
$$U_i(1,j,m)=U_i(nx,j,m) \tag{3.3.6}$$

2) the values of u, v, w for i=1 and i=nx are evaluated from the corresponding values (3.3.6) using the relations (2.2.11).

3) these values are used as Dirichlet conditions for the momentum equations.

• Neumann conditions.

The derivative appearing in the condition is discretised with a first order forward or backward difference formula. E.g. referring to figure 3.3:

$$\left(\frac{\partial\phi}{\partial\xi}\right)_{\xi=0}=0 \;\Rightarrow\; \phi(1,j,m)=\phi(2,j,m) \tag{3.3.7}$$

where both $\phi(1,j,m)$ and $\phi(2,j,m)$ are unknown. Notice that the derivative (3.3.7) corresponds to the derivative in the direction normal to the wall in the hypothesis that the local skewness is small, that is if the grid is roughly orthogonal at the wall points. In this case, writing the equation in the node i=2:

$$a_P\phi(2,j,m)=a_E\phi(3,j,m)+a_W\phi(1,j,m)+\ldots \Rightarrow$$
$$\Rightarrow(a_P-a_W)\phi(2,j,m)=a_E\phi(3,j,m)+\ldots \tag{3.3.8}$$

where $a_K=a_K(2,j,m)$. The value $\phi(1,j,m)$ does not appear in the final equation and can be updated with the relation (3.3.7) after the solution of the linear system of equations.

The Neumann conditions, therefore, affect the central coefficient of the grid points near the walls and consequently the diagonal of the matrix of the coefficients of the system of equations.

• Dirichlet conditions.

In this case the value in the node is known and appears in the right hand side of the system of equations, with the source term.

• Blades.

The code assumes that the tip of the blades are positioned exactly in the middle of two grid lines. E.g., indicating with m_i the index in the ζ direction corresponding to the first grid point on the blade, the position of the leading edge in the computational space is supposed to be in the middle of the grid planes $m=m_i$ and $m=m_i-1$ (see figure 3.6). With this approach, the cells on the two sides corresponding to $m=m_i$ cover with one of the faces the leading edge and the beginning of the blade.

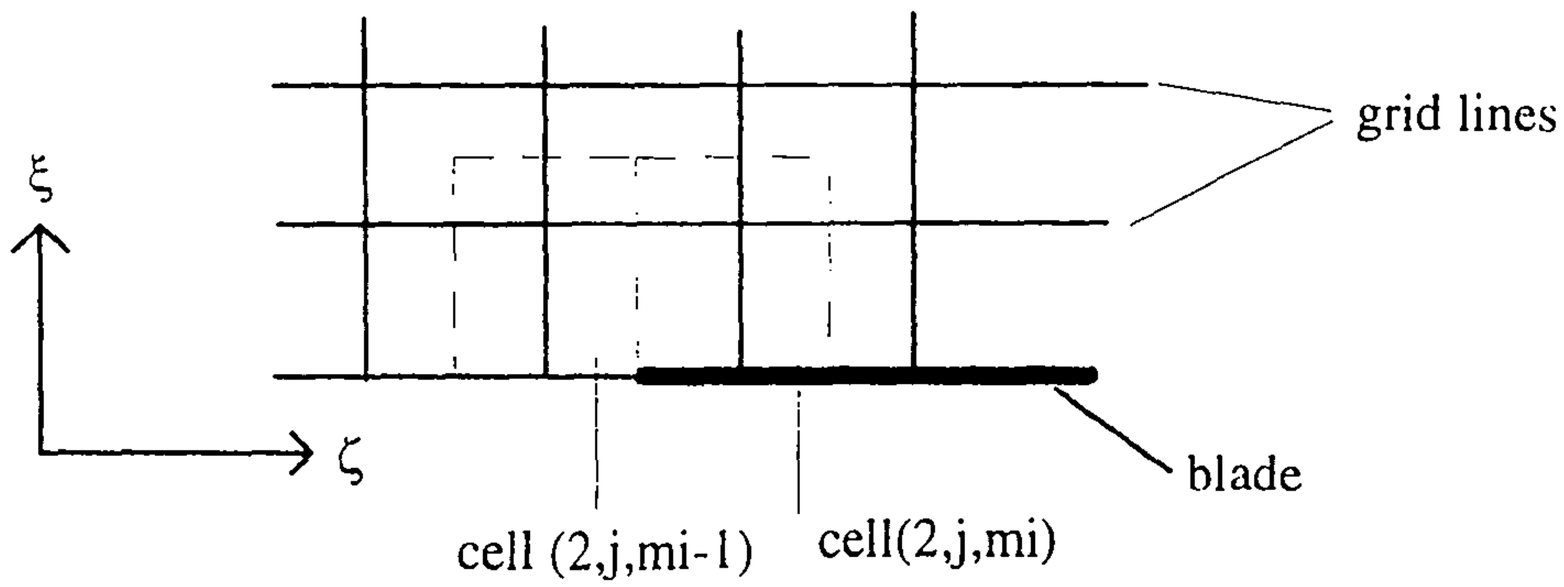

Figure 3.6 - Position of the edge of the blade.

The same approach is used for the position of the tip of the blade, if there is a gap between the tip of the blade and the shroud.

3.4 - The systems of equations.

For each variable ϕ (the Cartesian components of the velocity, the rothalpy, k, ε, the pressure correction) and for each internal cell of the domain an equation linking the value in the node with the values in the surrounding cells can be written, in the form of equations (2.3.12) or (2.4.10). When writing the equations for a variable ϕ the values of the other variables on the previous iterations are used. The systems of equations obtained, therefore, are completely independent one from the other and can be solved separately (segregated approach).

The values at the nodes on the boundaries do not appear in the equations: either the value is known (Dirichlet condition) or is taken into account implicitly (Neumann or periodic conditions). The number of equations is then linked to the number of internal

cells in each direction, e.g. for the ξ direction: i=2,...,nx-1 $\rightarrow$ nx-2 cells; the total number of unknowns, for each variable, is:

$$n = (nx-2)(ny-2)(nz-2) \tag{3.4.1}$$

The shape of the matrix of the coefficients of each system depends on:

1) the ordering of the nodes, from the three indexes i, j and m to a single index s.

2) the number of surrounding nodes involved when writing the equation at each node; this number depends on the convection scheme used. Using a first order Upwind technique the value of the variable at each node P is linked only to the nodes E,W,N,S,F,B.

3) the way the periodic boundary conditions are implemented (cf. equations (3.3.2) and (3.3.3)).

The ordering of the equations in the system that will be used is:

$$s = (m-2)np + (i-2)(nx-2) + (j-1)$$
$$\text{where } \begin{cases} j = 2,...,ny-1 \\ i = 2,...,nx-1 \\ m = 2,...,nz-1 \end{cases} \tag{3.5.1}$$

and np=(nx-2)(ny-2) is the number of cells on a $\xi-\eta$ plane. With this convention the matrix of the coefficients for each system can be written as a block tridiagonal matrix of dimension n in the form:

$$
\begin{Bmatrix}
 & [D] & \begin{bmatrix} a_F & & \\ & \cdots & \\ & & a_F \end{bmatrix} & & & \\
\begin{bmatrix} a_B & & \\ & \cdots & \\ & & a_B \end{bmatrix} & & [D] & \cdots & & \\
 & & \cdots & \cdots & \cdots & \\
 & & & \cdots & [D] & \begin{bmatrix} a_F & & \\ & \cdots & \\ & & a_F \end{bmatrix} \\
 & & & & \begin{bmatrix} a_B & & \\ & \cdots & \\ & & a_B \end{bmatrix} & [D]
\end{Bmatrix}
\tag{3.5.2}
$$

where each block is of dimension np and $a_K = a_K(i,j,m)$ where i, j and m are the indices of the node whose equation is written in the row s following the law (3.5.1). The blocks on the diagonal contain the coefficients involving only variables on the same plane $\xi - \eta$ and depend on the position ζ of the plane: if the plane is before or after the blades, the diagonal block has the form:

$$
\begin{bmatrix}
\begin{pmatrix} d & a_N & & \\ a_S & d & a_N & \\ & \cdots & \cdots & \cdots \\ & & a_S & d \end{pmatrix} & \begin{pmatrix} a_E & & \\ & \cdots & \\ & & a_E \end{pmatrix} & & \begin{pmatrix} a_W & & \\ & \cdots & \\ & & a_W \end{pmatrix} \\
\begin{pmatrix} a_W & & \\ & \cdots & \\ & & a_W \end{pmatrix} & \begin{pmatrix} d & a_N & & \\ a_S & d & a_N & \\ & \cdots & \cdots & \cdots \\ & & a_S & d \end{pmatrix} & \begin{pmatrix} a_E & & \\ & \cdots & \\ & & a_E \end{pmatrix} & \\
(\ldots) & (\ldots) & (\ldots) & \\
(\ldots) & (\ldots) & (\ldots) & \\
\begin{pmatrix} a_E & & \\ & \cdots & \\ & & a_E \end{pmatrix} & \begin{pmatrix} a_W & & \\ & \cdots & \\ & & a_W \end{pmatrix} & \begin{pmatrix} d & a_N & & \\ a_S & d & a_N & \\ & \cdots & \cdots & \cdots \\ & & a_S & d \end{pmatrix} &
\end{bmatrix}
\tag{3.5.3}
$$

where every block has dimension ny-2. The diagonal block (3.5.3) has then the typical form of system with periodic boundary conditions: similar to a tridiagonal form but for

i=2 and i=nx-2 on the corners of the matrix the coefficients corresponding to the periodic conditions do appear. When the plane is between the blades, the periodic conditions do appear only for the cells between the tip of the blade and the shroud (top wall). If no tip leakage exists, the block (3.5.3), for planes between the blades, has a normal tridiagonal form.

The matrix of the coefficients for the system of equations for the transport of the Cartesian velocity components has in any case a tridiagonal form, as the periodic conditions are not implemented implicitly.

The term d in diagonal in the matrix (3.5.3) depends on:

1) the central coefficient a_P;

2) the term $S''_{\phi P}$;

3) for all the variables excluding the pressure correction, d is influenced by the under-relaxation α: rewriting equation (2.3.12) as:

$$\phi_P^{n+1} = \frac{\sum_K a_K \phi_K^{n+1} + S_P}{a_P} = \phi_P^n + \left(\frac{\sum_K a_K \phi_K^{n+1} + S_P}{a_P} - \phi_P^n \right) \tag{3.5.4}$$

where ϕ_p^n is the value of the variable ϕ at the point P obtained at the previous iteration ant the terms in the parentheses represent the change in the magnitude of ϕ_p due to the current iteration. Introducing the relaxation factor $\alpha < 1$:

$$\phi_P^{n+1} = \phi_P^n + \alpha \cdot \left(\frac{\sum_K a_K \phi_K^{n+1} + S_P}{a_P} - \phi_P^n \right) \tag{3.5.5}$$

the equation can be rewritten as:

$$\frac{a_P}{\alpha} \phi_P^{n+1} = \sum_K a_K \phi_K^{n+1} + S_P + \frac{1-\alpha}{\alpha} a_P \phi_P^n \tag{3.5.6}$$

and the last term on the right hand side of equation (3.5.6) is then associated with the source term.

4) Neumann boundary conditions, as in equation (3.3.8). In the same situation, the diagonal term would be:

$$d = \frac{1}{\alpha}\left(a_P - a_W - S''_{\phi P}\right) \tag{3.5.7}$$

Note that the conditioning of the system of equations is strongly influenced by the diagonal dominance of the matrix of the coefficients; the under-relaxation influences positively the system, as increases the diagonal term, while the Neumann boundary conditions affect the matrix in the opposite way, when the diagonal decreases. This means that the system of equations for the pressure correction, without the inclusion of under-relaxation in the matrix and with Neumann conditions on almost all the surfaces, is the worst conditioned.

The matrix (3.5.2) is a banded matrix, with band-width equal to $2np$; only in this region are the coefficients non-zero. The band of the matrix is very narrow, if compared with the dimension of the matrix. For example, for a relatively small case, nx=22, ny=22, nz=52, n is 20×20×50=20,000 while the band is $2np$=800. This situation is graphically represented in figure 3.7.

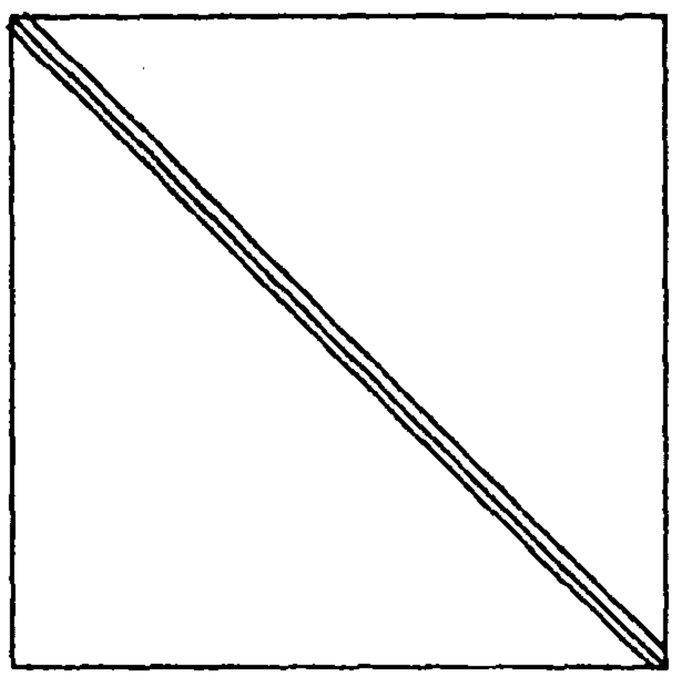

Figure 3.7 - Example of band-width.

However, even in the narrow band region most of the coefficients are zero; in the previous example, for each row of the 800 coefficients in the band only seven are non-zero ($d, a_E, a_W, a_N, a_S, a_F, a_B$).

It is important to note that the dimension of the band depends on the way the nodes are ordered in the system; as the number of the nodes in the ζ direction is generally much higher that in the other two directions, i.e. nz>(nx,ny), the law (3.5.1) insures the minimum width of the band.

The number of non-zero coefficients in the matrix, *nza*, can be easily determined: indicating with m_i and m_f the indices on the ζ direction corresponding, respectively, to the leading edge end the trailing edge of the blades, and with j_{tip} the index in the η direction corresponding to the tip of the blades, there are

- n coefficients d;
- (nz-3) blocks of dimension (nx-2)(ny-2) for a_F and a_B;
- for each of the (nz-2) diagonal blocks: (nx-2)(ny-3) for a_N and a_S, (nx-3)(ny-2) for a_E and a_W, (ny-2) for the periodic a_E and a_W; to this last value the cells on the blades have to be subtracted.

In total:

$$\begin{aligned} nza &= n + 2(nx-3)(ny-2)(nz-2) + 2(nx-2)(ny-3)(nz-2) \\ &+2(nx-2)(ny-2)(nz-3) + 2(nz-2)(ny-2) - 2(m_f - m_i + 1)(j_{tip} - 1) \end{aligned} \tag{3.5.8}$$

For the momentum equations the last two terms on the right-hand side are not to be considered.

The matrix (3.5.2) is not symmetric, also if the disposition of the coefficient is symmetric and is not positive definite. Furthermore the presence of the periodic conditions in the diagonal blocks complicates the use of simple tri- or penta-diagonal linear solvers.

3.5 - The linear solver.

The choice of the linear solver for the solution of the systems of equations is of paramount importance for the efficiency of the whole procedure. As for three-dimensional flow fields the number of grid points is generally of the order of tens or hundreds of thousands, the solution of the systems of equations introduces problems both for the memory required for the storage of the matrix and for the computational time needed to solve each system.

When the number of the unknowns increases, the computational time needed to evaluate the source terms, the coefficients, the transformations between the physical and the computational plane etc., becomes negligible in respect to the time required for the solution of the algebraic system. Therefore the numerical procedure for the solution of the algebraic system has to be optimised in order to have the minimum number of operations performed and to have the best use of the resources of the machine, i.e. the use of vectorisation and/or parallel processing.

Of the two basic problems involved in the choice of the solver, the memory and the computational time required, the first is the most important, as the wrong choice could lead to the completc impossibility of solving the system when the number of unknowns increases. As seen in the previous section, the matrix of the coefficients has a narrow ,band structure; nevertheless, the storing of only the band of the matrix could require more memory than the available one, even for powerful computer mainframes.

Using the same example of the previous chapter, that, as noticed, has a relatively small number of unknowns, the storing of the band of the matrix requires approx. $n \times 2np$=16,000,000 memory locations (for double precision numbers) while the number of non-zero coefficients, using the formula (3.5.8), is only $nza \approx$137,000. The most common way to overcome this problem is to keep track only of the non-zero entries of the matrix and use a linear solver capable to use this form of storage (sparse matrix solvers).

The techniques for the solution of sparse linear systems can be divided into two broad classes: direct and iterative. With a direct solution an explicit factorization of the matrix is computed, and is used for the solution of the linear system given a right hand side. The solution obtained is certain to be as accurate as the problem definition (i.e. the error in the solution is of the order of the machine accuracy); on the other hand direct techniques generate a certain amount of fill-in inside the band, increasing sharply the number of non-zero entries.

With an iterative solver a sequence of approximations is generated iteratively, which (hopefully) converges to the solution of the linear system; iterative solvers require much less memory than direct methods, making iterative methods the only feasiblc approach for very large problems. On the other hand iterative methods are not always robust and are sensitive to the conditioning of the matrix of the coefficients of the system and no general, effective iterative algorithms exist for an arbitrary sparse linear system (Golub and Van Loan, 1989). Hutchinson and Raithby (1986) have shown that in the solution of fluid flow and heat transfer the performance of iterative methods, such as Gauss-Seidel and successive over-relaxation, is very sensitive to the type of boundary conditions, the degree of anisotropy in the coefficients and the number of equations; they have demonstrated that when the magnitude of the coefficients in one direction greatly exceeds those in the other directions, the equation residuals may initially be reduced rapidly with iteration, but later hundreds or thousands of iterations are required to effect a further order of magnitude reduction in the residuals. For ill-conditioned matrices, an iterative solver could converge extremely slowly, or fail to provide a solution of the system (Young, 1971).

The Thomas (1949) algorithm, a technique for rapidly solving tri-diagonal systems, is widely used in CFD programs for the solution of the systems of linear equations. For three-dimensional problems the Thomas algorithm, or three-diagonal matrix algorithm (TDMA), can be applied only in a line-by-line fashion and therefore the spread of boundary information into the calculation domain is slow, and appears to be unsatisfactory for three-dimensional recirculating flows (Versteeg and Malalasekera, 1995). The strongly implicit procedure (SIP) of Stone (1968), that allows an efficient solution of a system of equations with five non-zero diagonals and is closely related to the direct method of triangular decomposition, is also widely used in CFD applications, in particular with the improvements suggested by Schneider and Zedan (1981). Lage (1996) has demonstrated numerically the existence of asymptotic rates of convergence of the residual norm of a system of equations when is solved by the modified strongly implicit procedure (MSIP) of Schneider and Zedan. Based on the prediction of the asymptotic rate of convergence, Lage has developed an algorithm for the adaptive optimisation of the iteration parameter to improve MSIP performance during the solution of heat transfer problems.

Currently the most promising iterative methods for non-symmetric and/or non-positive-definite coefficient matrices are conjugate gradient (CG) type methods, based on matrix factorisation techniques; a complete list and description of the algorithms based on the conjugate gradients, along with related references, can be found in Barrett et al. (1994). Theoretically, the conjugate gradients method is a semidirect method; that is, the exact solution can be reached in a finite number of steps. However, the accumulation of round-off errors will destroy this property. An important property of the CG method is the so-called superlinear convergence behaviour; that is, the convergence rate improves as the iteration proceeds, while in many cases the initial convergence can be very irregular and slow. One of the attractions of methods based upon conjugate gradients is that a large proportion of the computational work will vectorise straight-forwardly and worthwhile gains can therefore be achieved on vector processors (Kightley and Jones, 1985).

Langtangen (1989) compared several conjugate gradients methods with preconditioning for non-symmetric matrix systems with arbitrary sparsity patterns and found that the preconditioned conjugate gradient squared (CGS) turned out to be the best method.

Sheen and Wu (1997) have studied the use of a preconditioned conjugate gradient method for solving the pressure correction equation in the simulation of incompressible flows. They have tested symmetric successive over-relaxation (SSOR), incomplete LU

decomposition (ILU), the modified ILU (MILU) and ADI-type preconditioners in the solution of lid-driven cavity flow and backward-facing step flows. Sheen and Wu argue that a good iterative scheme for the pressure correction must have high and stable convergence rate in the early stage of the iteration, while the asymptotic convergence rate is of relatively less importance. The test results presented in their work show that both ILU- and SSOR-preconditioned conjugate gradient methods have very irregular early-stage convergence, that both MILU- and ADI-preconditioned CG methods can be made very stable by choosing adequate parameters and that good convergence stability comes with lower asymptotic convergence rate.

Kobayashi et al. (1998) have compared the performance of the generalized minimal residual method (GMRES), and the biconjugate gradient stabilized method (BiCGSTAB), both CG type methods, in the numerical solution of several 2D test cases of convection-dominated flows and have found that the BiCGSTAB method requires fewer iterations than GMRES to achieve convergence and that for both methods the use of preconditioning is extremely important.

Sheen and Wu (1998) have investigated the preconditioning techniques for the BiCGSTAB method used in 2-D convection-diffusion problems. The preconditioning matrix was obtained by performing the ILU decomposition of the coefficient matrix produced by the first-order or third-order upwind difference of the convection terms. Because of the one-sided property of the upwind schemes, they were able to reduce the factorisation error of the ILU decomposition by ordering the variable based on the flow direction; this strategy helps reduce the factorisation error and improve the convergence rate. This preconditioning technique is designed for convection-dominant problems. In the test problems Sheen and Wu have found that their ordering technique begins to show its advantage when the convection terms are at least one order of magnitude higher than the diffusion terms in the coefficient matrix.

With conventional solution strategies the rate of convergence of the iterative procedure worsens as the grid is refined, and the computations become very expensive. This is because of the slow rate of convergence of the low-frequency components in the error spectrum. The multigrid technique (Brandtl, 1977) provides an efficient means of smoothing high- and low-frequency errors in the solution that arise during the iterative solution of elliptic equations, by attempting to eliminate uniformly all frequency components of the errors by iterations on a series of grids. A very good description the technique can be found in Briggs (1987).

In recent years, significant progress has been made in the development of multigrid methods for the solution of Navier-Stokes equations; the available results, as

in Vanka (1986a, 1986b) and Sathyamurthy and Patankar (1986), indicate that the multigrid-based solution procedures are significantly faster (factor of 10-20) than the traditional single-grid methods. Karki et al (1989) have shown that, for the same accuracy, improved discretisation schemes require much fewer grid points than the standard Upwind schemes and that the combined use of a multigrid technique and of improved convection schemes is especially attractive for three-dimensional situations, for which the simple upwind schemes require a prohibitively large number of grid points and, in turn, the single-grid methods exhibit poor convergence behaviour. Karki et al (1996) have studied the performance of a multigrid method used in conjunction with a flux-spline scheme for the prediction of the laminar flow in a cubic cavity with a moving wall; the results show that the CPU times for the multigrid method vary almost linearly with the number of grid points and that these CPU times are smaller by factors of 3 to 30 than those for single-grid methods based on the SIMPLE algorithm.

Direct solvers appear to be hardly used in CFD applications of engineering interest.

For this study both an iterative and a direct solver, each one adopting a sparse matrix storage, will be tested. In order to achieve the best use of the available resources, routines developed by Cray Research Inc. to solve a real general sparse system, using a preconditioned conjugate gradient-like method (SITRSOL) or a direct solver (SSTSTRF for the factorization and SSTSTRS for the solution, developed for matrices symmetric in shape), available in the Scientific Library of the Cray mainframes (LIBSCI), have been chosen. These routines are designed to exploit the parallel processing capabilities of Cray systems; matrix-vector operations are designed to achieve significant speed-up on multiple CPUs, especially for large problems. What will be presented in this section will therefore refer to these routines.

• Storage formats.

The data structure used to represent the matrix (3.5.2) is a column-oriented format, which is referred to as the *sparse column format*, in which the entries are grouped by columns. In this format, the row indices of the non-zero elements in the first column are stored contiguously in ascending order in an array called *irowind*; then the row indices are stored for the second column, and so on. The corresponding values are stored in an array named *values*. A pointer array, *icolptr*, points to the first entry in each column of the matrix in *irowind* and *values*; *icolptr*(n+1) is set to nza+1. *irowind* and *values* are

arrays of length *nza* and *icolptr* is of length *n*+1. Hence 2*nza*+*n*+1 words (i.e. memory locations) of storage are required.

E.g., given a matrix *A* with *n*=5 and *nza*=13:

$$A = \begin{bmatrix} 11 & 0 & 0 & 29 & 0 \\ 0 & 22 & 32 & 0 & 52 \\ 0 & 32 & 33 & 43 & 0 \\ 41 & 0 & 23 & 44 & 0 \\ 0 & 52 & 0 & 0 & 55 \end{bmatrix}$$

the sparse column format representation of *A* is:

values=(11, 41, 22, 32, 52, 32, 33, 23, 29, 43, 44, 52, 55)

irowind=(1, 4, 2, 3, 5, 2, 3, 4, 1, 3, 4, 2, 5)

icolptr=(1, 3, 6, 9, 12, 14)

• Because no single robust iterative technique for solving sparse linear systems exists, SITRSOL lets users select from a wide variety of iterative techniques, preconditioning schemes, and a number of tuning parameters. The iterative methods that can be selected are [7] (the words in bold characters are the acronyms for the methods)

- **bcg** - Biconjugate gradient method.
- **cgn** - Conjugate gradient method applied to the equations: $A \cdot A^T \cdot y = b,\ x = A^T \cdot y$ (Craig's method).
- **cgs** - Conjugate gradient squared method.
- **gmr** - Generalized minimum residual (GMRES) method.
- **gmn** - Orthomin or generalised conjugate residual (GCR) method.
- **pcg** - Preconditioned conjugate gradient method.

• The type of preconditioning that can be used are:

- Diagonal (Jacobi) preconditioning.
- Incomplete Cholesky factorization.
- Incomplete LU factorization.
- Truncated Neumann polynomial expansion.
- Truncated least squares polynomial expansion.

---

[7]*Note that not all methods can be used as the matrix is not positive definite. The same can be said for the other features of the routines, such as the preconditioning or the scaling.*

Left, right and two-sided preconditioning of the matrix is available, the last two only for some of the methods.

Each one of these features can be controlled and tuned through several parameters from the user; furthermore the routine returns in output all the information needed to evaluate the efficiency of the procedure, such as the time spent in each one of the phases of the computation. One of the next steps in this study will be, therefore, to find an appropriate combination of these parameters for the present problem and compare with the capabilities of the direct solver; in particular when solving the equations for the pressure correction, where the matrix of coefficients is ill-conditioned, particular care has to be taken.

• When using the direct solver, the structure of the matrix is pre-processed prior to the numerical factorisation, adopting a reordering of the row and columns based on the multiple degree algorithm (Liu, 1985), that reduces the amount of fill-in created during the factorisation. The system is then solved with the multifrontal method (see Liu, 1992), that uses update matrices to carry the intermediate results from the variables being eliminated to the variables that are not yet processed: before the elimination of a variable, update matrices that correspond to previously eliminated variables are assembled to form the current frontal matrix. The partial factorisation of the current frontal matrix is then carried out, and its update matrix is generated.

3.6 - Description of the algorithm.

The computational procedure for the solution of the Reynolds-averaged equations can be described as follows:

begin

Input data and pre-processing:

→ Read physical properties data, inlet conditions and control parameters.

→ Read the grid in the physical space (x,y,z).

→ Generate the grid in the computational space (ξ, η, ζ).

→ Evaluate and store all the geometrical quantities.

→ Obtain an initial guess for all the variables from the values at the inlet.

Start the solution procedure

→ Evaluate and store the transformed velocities on the cell faces.

→ Evaluate and store the components of the pressure gradient.

repeat

→ Evaluate and store density and turbulent viscosity on the cell faces.

→ Evaluate and store the coefficients a_K of the transport equation[8].

→ Evaluate and store the velocities in the middle of the cell edges.

Solve for the Cartesian velocities u^*_i

do i=1,3

→ Add cross derivatives terms of the diffusion to source term.

→ Add pressure term and the component of the centrifugal and Coriolis forces to source term.

→ Add to the source the term:

$\frac{\partial}{\partial \xi_r}\left[J(\mu+\mu_t)\frac{\partial \xi_r}{\partial x_j}\left(\frac{\partial u_j}{\partial \xi_s}\frac{\partial \xi_s}{\partial x_i} - \frac{2}{3}\delta_{ij}\left(\frac{\partial u_m}{\partial \xi_s}\frac{\partial \xi_s}{\partial x_m}\right)\right)\right]$, corresponding to the part of the second term on the right hand side of equation (2.2.2) not included in the diffusion

→ Modify the source term and the coefficients in the cells close to the solid walls to introduce the wall function.

→ Evaluate and store the residual of the transport equation.

Solve the system of equations:

→ Modify the diagonal term and the source to take into account the Neumann boundary conditions and the term $S''_{\phi P}$ and to introduce the relaxation factor.

→ Add in the source term the Dirichlet boundary conditions.

→ Generate the vectors *value*, *irowind* and *icolptr*.

→ Give an initial guess for the solution (only for the iterative solver).

→ Solve the system with SITRSOL or SSTSTRF/SSTSTRS.

→ Evaluate the maximum residual of the system of equations.

→ Update the points with Neumann boundary conditions.

→ Store the diagonal of the system for pressure correction equation.

end do

---

[8]*The coefficients are evaluated using a central difference formula for the normal diffusion terms and a first-order Upwind scheme for the convection. The coefficients do not depend on the variable of the transport equation (i.e. all the systems obtained from the discretisation of a transport equation have the same coefficients).*

→ Update the transformed velocities using formula (2.2.11).

Solve the pressure correction equation:

→ Evaluate and store the coefficients a_K of equation (2.4.10).

→ Modify the diagonal term for the Neumann boundary conditions.

→ Evaluate and store the velocities U^*, V^* and W^* on cell faces.

→ Modify the velocities on the cell faces using the Rhie and Chow scheme.

→ Evaluate and store the mass unbalance (2.4.2) (source term).

→ Generate the vectors *value*, *irowind* and *icolptr*.

→ Give an initial guess for the solution (only for the iterative solver).

→ Solve the system with SITRSOL or SSTSTRF/SSTSTRS.

→ Evaluate the maximum residual of the system of equations.

→ Update the points with Neumann boundary.

→ Obtain the pressure through $p = p^* + \alpha \cdot p'$.

→ Evaluate and store the components of the pressure correction gradient.

→ Update the transformed velocities through formulae (2.4.8).

→ Obtain the Cartesian velocities using relations (2.2.12)

→ Evaluate and store the components of the pressure gradient.

→ Evaluate and store the transformed velocities on the cell faces.

→ Modify the velocities on the cell faces using the Rhie and Chow scheme.

Solve for the scalar quantities: h, k, ε

→ Evaluate and store the generation rate of turbulence G_k.

→ Evaluate the coefficients a_K (as the velocity field has been updated).

Solve the transport equations with the same procedure described for the velocities u^*_i (but with different boundary conditions and different contributions on the source term).

→ Update the turbulent viscosity with formula (2.2.4).

→ Update the density of the fluid, using the perfect gas law.

→ Check the values of k and ε. If an unphysical (negative) value is found, the procedure stops.

→ Check if convergence has been reached comparing the values of the residual of the transport equations and/or of the mass unbalance with a reference value fixed by the user.

until convergence is obtained or the maximum number of iterations fixed by the user has been reached. The pressure field obtained and the velocity fields are used as p^*, u^* etc. for the next iteration.

→ Update the points on the surfaces with periodic boundary conditions.

→ Write in file the values of the variables.

end

3.7 - Implementation on the Cray J916.

As will be shown in the next sections, most of the CPU time required by the code, more then 90% of the total time, is spent for the solution of the systems of equations, and in particular for the solution of the pressure correction equation. This solution, as previously mentioned, is performed using routines available in the scientific library of the Cray, that are designed to give the best performance in terms of vector and parallel processing for the present architecture.

The source code of the solution procedure described in the previous sections is pre-processed by the FORTRAN compiler, that modifies the original code in order to make possible the execution in parallel and/or the use of vectorised computations, mainly for DO loops. To facilitate this process, some principles have been observed in writing the source code, such as:

- One-dimensional vectors have been used to store the variables, instead of three-dimensional variables;
- IF statements are never used inside DO loops, unless no other options are available;
- GOTO instructions are used as least as possible, and never in DO loops;
- Subroutines are never called inside DO loops, that is, every subroutine is brought to the lowest possible level.

Chapter 4
The treatment of the convection

4.1 - Introduction.

The discretisation of the convective term in the transport equations is a fundamental issue both for the convergence of the whole iterative procedure and for the accuracy of the results.

The simple first-order procedures, such as the Upwind scheme or the exponential differencing schemes (Power-Law scheme, Hybrid scheme, etc. see Patankar, 1980) developed several decades ago, are still the most used in the practical application of Computational Fluid Dynamics. Higher-order methods have not been popular because of convergence difficulties and a tendency to generate unphysical overshoots or undershoots during the numerical transition. Recent developments using deferred correction solutions and flux limiters techniques have eliminated all of these difficulties; however these techniques are mostly applied in simple cases, while in complex three-dimensional geometries (such as centrifugal compressors or pumps) first-order methods are still widely used.

In order to test the influence of higher-order methods on the prediction of the flow field in three-dimensional complex geometries, several higher-order approaches have been included in TURBO3D_2 code.

In this chapter the basic Upwind approach and its limitations and some higher-order techniques will be described [9]; the basic reference is the work of B.P.Leonard, who developed the QUICK scheme in 1979.

4.2 - Upwind technique.

As shown in the first chapter, the convective term in the transport equation is integrated over each control volume; with the use of the Gauss's theorem the volume integral is then written as a sum of surface integrals on the cell faces. On each cell face the surface integral is evaluated with the mean value theorem; the contribution to the

---

[9] *Hybrid, Power-Law and other exponential-based schemes will not be considered in this study. In a recent review on convection modelling Leonard and Drummond (1995) demonstrated how these methods, while working well for quasi-one-dimensional flows if the convecting velocity is aligned with one of the grid coordinates, introduce serious cross-wind artificial diffusion in general multidimensional problems. Furthermore, in particular cases the results could become insensitive to the turbulence model used, if the stream direction does not coincide with a grid direction.*

convective term of each face of a generic control volume can therefore be estimated with expressions similar to (2.3.5): the convecting velocities on the cell faces are obtained by linear interpolation between velocity node values evaluated on the previous iteration, while the choice of the interpolation method to obtain the value of the variable on the cell face (i.e. the convected values) is conditioned by stability problems and determines the accuracy of the solution.

In the Upwind approach the convected value is taken as that of the upstream node value, where the upstream direction is based on the convecting velocity on the cell face (see figure 4.1, where $U_w = 0.5(U_P + U_W)$).

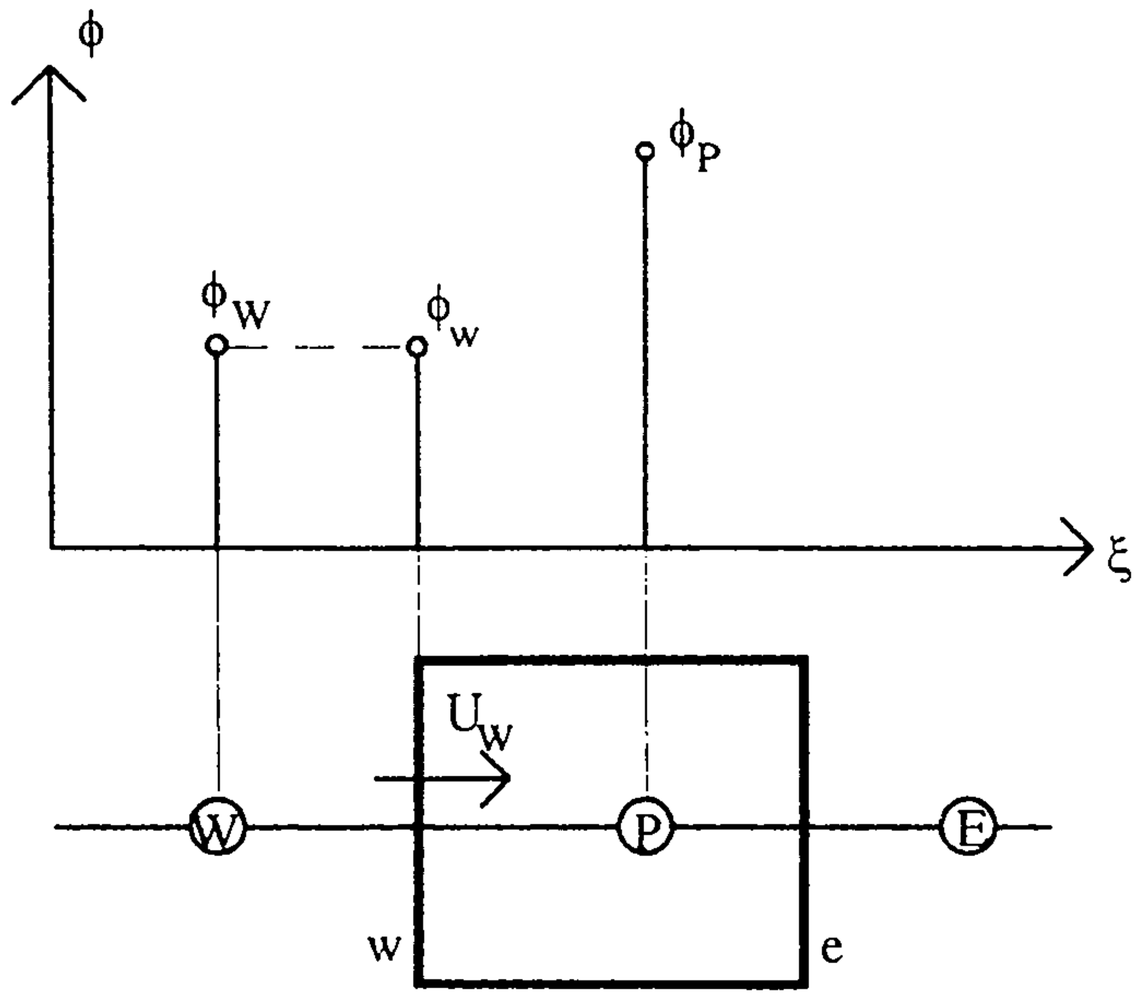

Figure 4.1: Example of use of the Upwind technique for the value of the variable on the west face

The use of an Upwind technique has a very stabilising effect on the convergence of the iterative procedure; this is due to the introduction of artificial damping, or numerical diffusion, that increases the effective diffusion coefficient. The (desired) stabilising effect is therefore obtained at the expense of the accuracy of the calculation. For a one-dimensional problem with constant velocity u_0 and a constant grid spacing Δx_0 the additional numerical diffusion coefficient due to the Upwind technique, in comparision with the use of central differencing (second order accurate), can be easily evaluated and is given by:

$$\nu_{num} = \frac{|u_0| \Delta x_0}{2} \tag{4.2.1}$$

where $\nu = \mu / \rho$.

Thus to obtain physical results an additional condition is required: the additional numerical diffusion coefficient has to be insignificant in comparision with the physical diffusion coefficients; for the previous example, this can be expressed in term of the cell Reynolds number (the Reynolds number based on the dimension of the grid spacing):

$$\mathrm{Re}_{cell} = \frac{|u_0| \Delta x_0}{\nu_0} << 2 \tag{4.2.2}$$

where ν_0 is the physical diffusion coefficient, assumed constant.

The condition (4.2.2) is highly unrealistic in terms of grid requirements to obtain an accurate solution; for problems of engineering interest the refinement of the grid necessary to satisfy the condition (4.2.2) is generally unreachable and the solution obtained is affected by a large error due to the numerical diffusion.

4.3 - Quadratic Upstream Interpolation.

The QUICK (Quadratic Upstream Interpolation for Convective Kinematics) scheme, developed by B.P.Leonard, 1979, is a third-order upwind-weighted method for the convective modelling, that achieves stable convective sensitivity and can be written in a conservative formulation.

The value of the variable on a cell face is obtained using a three point quadratic interpolation; the nodes used for the interpolation are chosen depending on the direction of the convecting velocity on the cell face. Referring to figure 4.2, for a one-dimensional case, the value on the *w* face is obtained from a quadratic interpolation of the values of the three points: Upwind (*U*), Central (*C*) and Downwind (*D*), where the point *C* is the node upstream of the cell face .

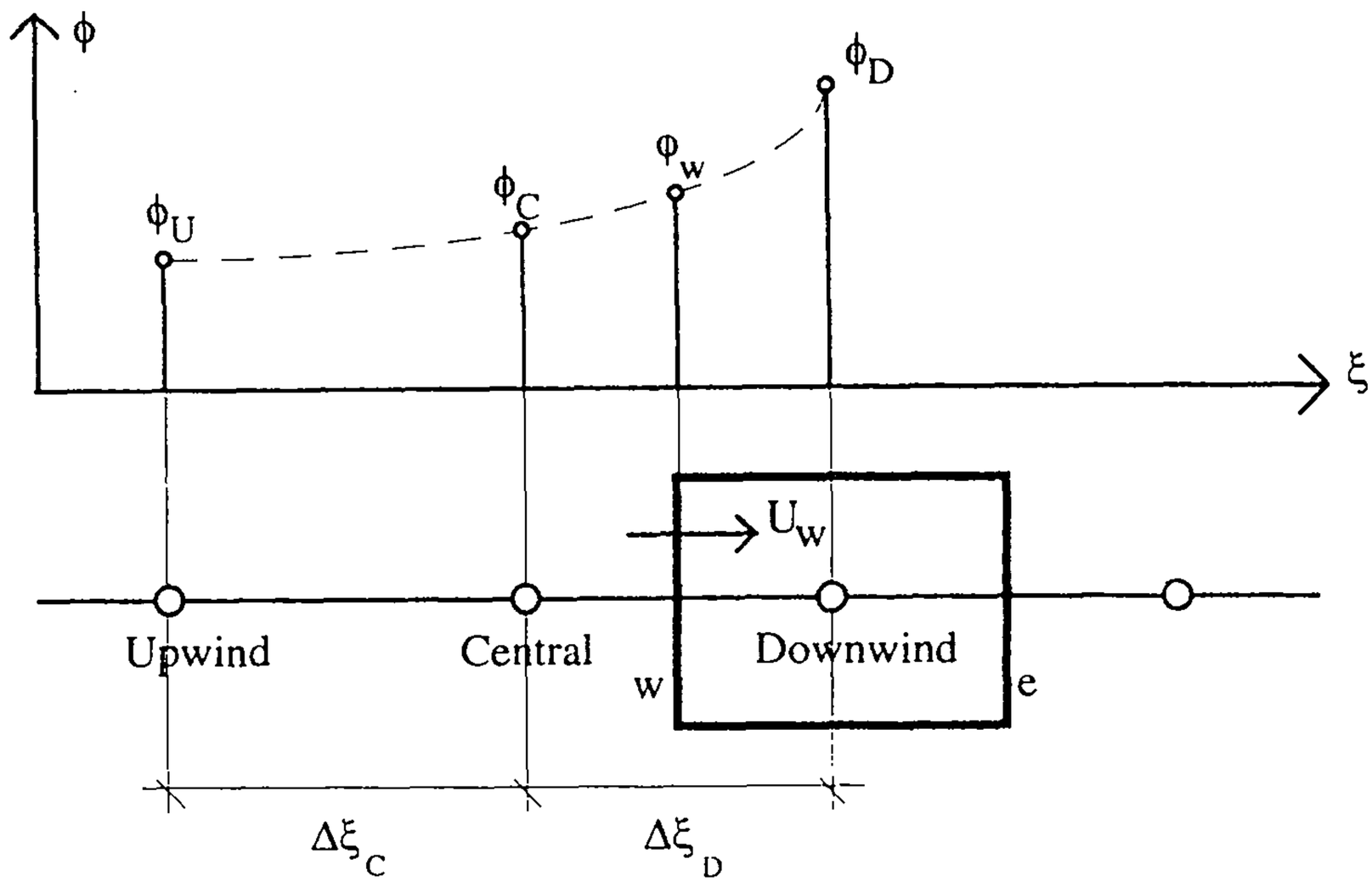

Figure 4.2 - Example of one-dimensional quadratic upstream-weighted interpolation.

Defining with ϕ''_C the value of the second derivative of the variable at the point C (Central point):

$$\phi''_C = \left(\frac{d^2\phi}{d\xi^2}\right)_C = \frac{2}{\Delta\xi_D + \Delta\xi_C}\left(\frac{\phi_D - \phi_C}{\Delta\xi_D} - \frac{\phi_C - \phi_U}{\Delta\xi_C}\right) \tag{4.3.1}$$

the value on the cell face can be written as:

$$\phi_w = \frac{1}{2}(\phi_C + \phi_D) - \frac{\Delta\xi_D^2}{8}\phi''_C \tag{4.3.2}$$

which may be interpreted as a linear interpolation corrected by a term proportional to the upstream-weighted curvature, i.e. the second derivative of the variable at the upstream node C [10].

For a two-dimensional case a simple one-dimensional interpolation could be performed in the direction normal to the cell face; this is, in effect, the most popular way

---

[10] *For a negative velocity on the cell face only the definition of the three nodes is different, while all the formulae are still valid; note that* $\Delta\xi_C = \xi_C - \xi_U$ *and* $\Delta\xi_D = \xi_D - \xi_C$ *are both negative in this case.*

in which the scheme is applied for two or three dimensional flows. However it is important to take into account the transverse curvature of the stream lines, including therefore a correction linked to the second derivative of the variables in the direction non-orthogonal to the cell face.

The effective form of this correction can be found by evaluating the value on the cell face interpolating the values in the surrounding nodes through a quadratic surface. Referring to figure 4.3, depending on the sign of the velocity normal to the cell face, U_w, a local system of coordinates (s,t) is introduced at the upstream node C and the variable is interpolated from the values in the nodes through the quadratic function:

$$\phi(s,t) = C_1 + C_2 \cdot s + C_3 \cdot s^2 + C_4 \cdot t + C_5 \cdot t^2 + C_6 \cdot s \cdot t \tag{4.3.3}$$

the value ϕ_w is then obtained averaging the value of the function (4.3.3) on the cell face with s corresponding to the upstream node C:

$$\phi_w = \frac{2}{\Delta\eta_T + \Delta\eta_C} \int_{-\Delta\eta_C/2}^{\Delta\eta_T/2} \phi\left(\frac{\Delta\xi_D}{2}, t\right) dt \tag{4.3.4}$$

In order to obtain simpler expressions instead of the formula (4.3.4) an approximate average will be used, in which the non-uniformity of the grid in the η direction is neglected only for the integration:

$$\phi_w = \frac{1}{\Delta\eta} \int_{-\Delta\eta/2}^{\Delta\eta/2} \phi\left(\frac{\Delta\xi_D}{2}, t\right) dt \tag{4.3.5}$$

where:

$$\Delta\eta = \frac{2}{\Delta\eta_T + \Delta\eta_C} \tag{4.3.6}$$

is the cell dimension in the η direction. The effect of this approximation is the disappearance from the final expression for ϕ_w of the term in $s \cdot t$ (also called the *twist* term) that is also the only term linked to the cross velocity on the cell face, V_w.

To obtain the value of the six constants in the expression (4.3.3) the quadratic function has to be written in six points where the value of the variable ϕ is known; these points are chosen among the neighbouring nodes depending on the sign of the normal

and of the cross velocities on the cell face, as in the example of figure 4.3. In effect, as the twist term disappears in the integration (4.3.5), the point *BD* is not used and *the choice of the nodes depends only on the sign of the normal velocity* U_w.

Writing the expression (4.3.3) in the nodes:

$$\text{for } s{=}t{=}0 \text{ is } \phi = \phi_C \rightarrow C_1 = \phi_C \tag{4.3.7}$$

$$\text{for } t{=}0,\ s = \Delta\xi_D \text{ is } \phi = \phi_D \rightarrow \phi_D = \phi_C + C_2\Delta\xi_D + C_3\Delta\xi_D^2 \tag{4.3.8}$$

$$\text{for } t{=}0,\ s = -\Delta\xi_C \text{ is } \phi = \phi_U \rightarrow \phi_U = \phi_C - C_2\Delta\xi_C + C_3\Delta\xi_C^2 \tag{4.3.9}$$

Combining equations (4.3.8) and (4.3.9):

$$\begin{aligned} C_2 &= \frac{\phi_D - \phi_C}{\Delta\xi_D} - \frac{\Delta\xi_D}{2}\left(\phi_{\xi\xi}\right)_C \\ C_3 &= \frac{1}{2}\left(\phi_{\xi\xi}\right)_C \end{aligned} \tag{4.3.10}$$

where $\left(\phi_{\xi\xi}\right)_C$ is the value of the second derivative of the variable in the ξ direction in the upstream node *C* evaluated with expression (4.3.1). In the same way:

$$\text{for } s{=}0,\ t = \Delta\eta_T \text{ is } \phi = \phi_{TC} \rightarrow \phi_{TC} = \phi_C + C_4\Delta\eta_T + C_5\Delta\eta_T^2 \tag{4.3.11}$$

$$\text{for } s{=}0,\ t = -\Delta\eta_C \text{ is } \phi = \phi_{BC} \rightarrow \phi_{BC} = \phi_C - C_4\Delta\eta_C + C_5\Delta\eta_C^2 \tag{4.3.12}$$

and combining equations (4.3.11) and (4.3.12):

$$\begin{aligned} C_4 &= \frac{\phi_C - \phi_{BC}}{\Delta\eta_C} - \frac{\Delta\eta_C}{2}\left(\phi_{\eta\eta}\right)_C \\ C_5 &= \frac{1}{2}\left(\phi_{\eta\eta}\right)_C \end{aligned} \tag{4.3.13}$$

where $\left(\phi_{\eta\eta}\right)_C$ is the value of the second derivative of the variable in the η direction in the upstream node *C*. The constant C_6 could be evaluated writing the quadratic function (4.3.3) in the node *BD*.

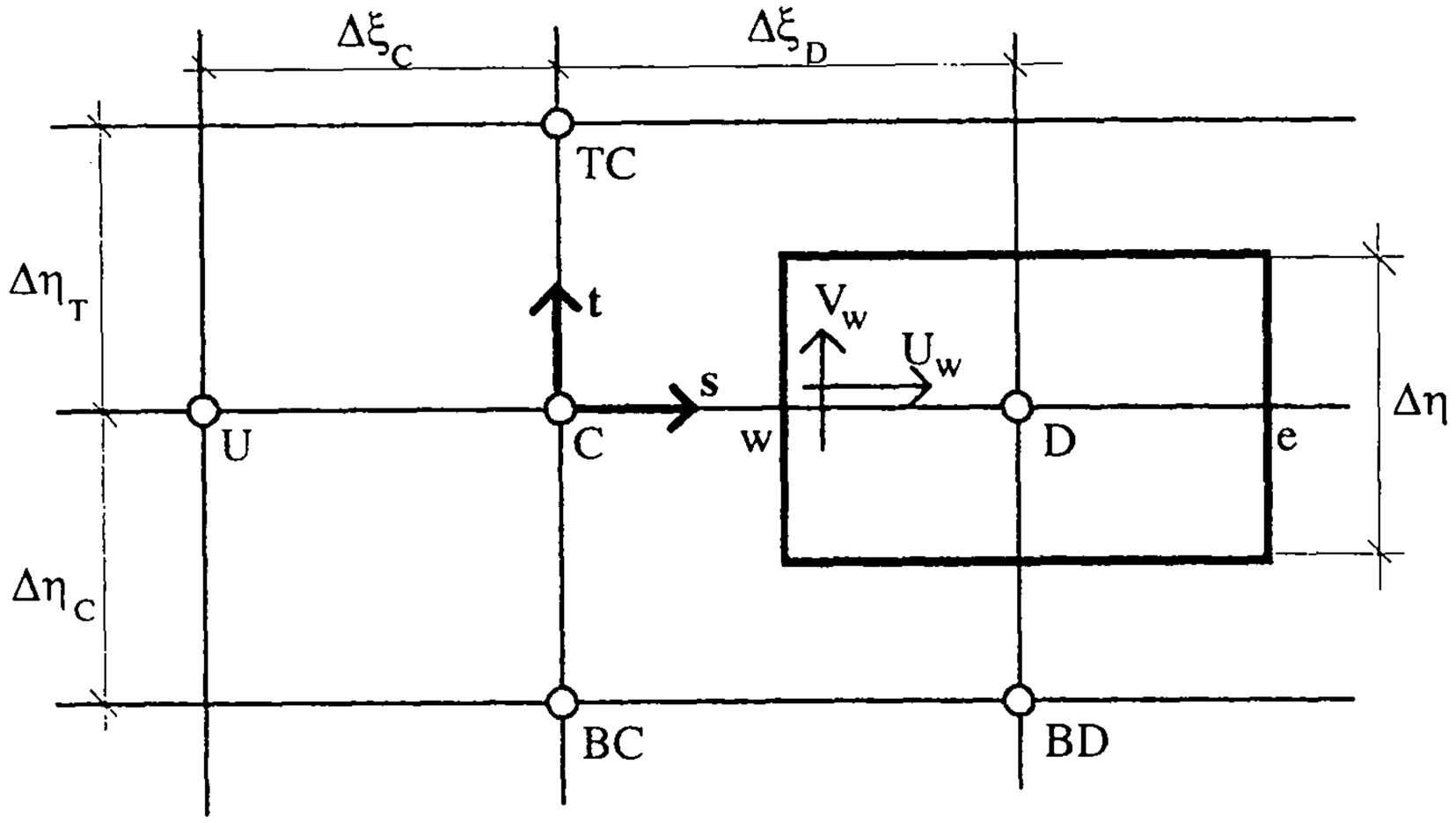

Figure 4.3 - Example of two-dimensional case.

In the integration (4.3.5) the terms in t and $s \cdot t$ disappear; the value on the cell face resulting from this integration is:

$$\phi_w = \frac{1}{2}(\phi_C + \phi_D) - \frac{\Delta\xi_D^2}{8}(\phi_{\xi\xi})_C + \frac{\Delta\eta^2}{24}(\phi_{\eta\eta})_C \qquad (4.3.14)$$

which may be once again interpreted as a linear interpolation corrected by the values of the second derivatives of the variable in the upstream node.

In a three-dimensional case a similar result can be obtained with the same procedure; using the same approximation in the definition of the integration of the cell face, e.g. for the w face:

$$\phi_w = \frac{1}{\Delta\eta \cdot \Delta\zeta} \int_{-\Delta\eta/2}^{\Delta\eta/2} \int_{-\Delta\zeta/2}^{\Delta\zeta/2} \phi\left(\frac{\Delta\xi_C}{2}, t, r\right) dt\, dr \qquad (4.3.15)$$

(where $\Delta\zeta$ is the dimension of the cell in the ζ direction) the scheme used will depend only on the sign of the normal velocity; in figure 4.4 the nodes involved for a positive normal velocity are represented. The value on the face is obtained from equation (4.3.14) simply adding the correction due to the curvature in the third direction:

$$\phi_w = \frac{1}{2}(\phi_C + \phi_D) - \frac{\Delta\xi_D^2}{8}(\phi_{\xi\xi})_C + \frac{\Delta\eta^2}{24}(\phi_{\eta\eta})_C + \frac{\Delta\zeta^2}{24}(\phi_{\zeta\zeta})_C \qquad (4.3.16)$$

The expressions for the other cell faces and for other direction of the normal velocity on the cell faces can be easily obtained following similar procedures.

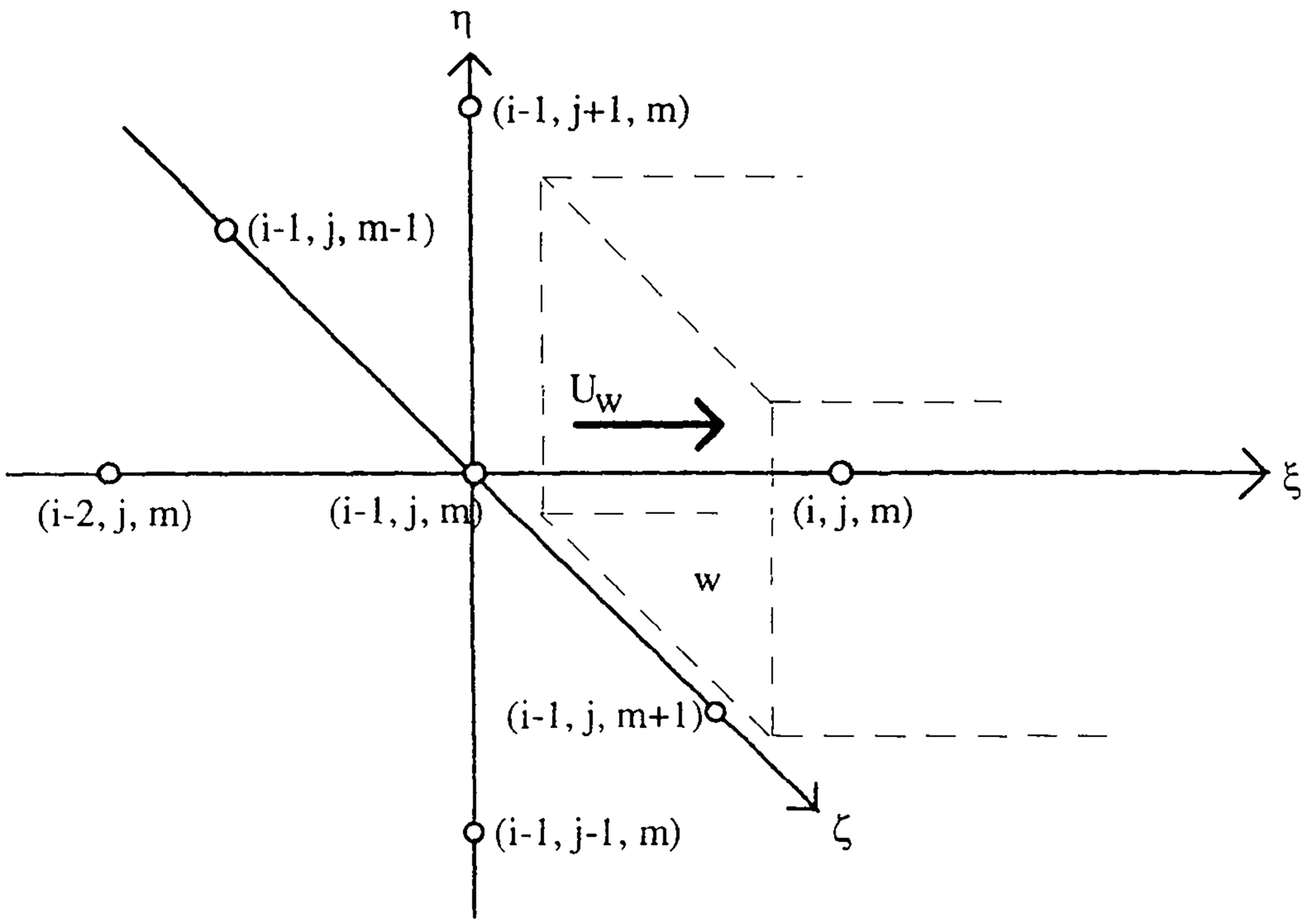

Figure 4.4 - Example of three-dimensional case.

4.4 - Formal accuracy.

From now on the value on the cell face will be indicated with ϕ_f; for a one-dimensional case, making Taylor expansions of the nodes about the control volume face, and referring to figure 4.2, the following expressions are obtained:

$$\phi_D = \phi_f + \phi_f'\left(\frac{\Delta\xi_D}{2}\right) + \frac{1}{2}\phi_f''\left(\frac{\Delta\xi_D}{2}\right)^2 + \frac{1}{6}\phi_f'''\left(\frac{\Delta\xi_D}{2}\right)^3 + \frac{1}{24}\phi_f^{(iv)}\left(\frac{\Delta\xi_D}{2}\right)^4 + \ldots \tag{4.4.1}$$

$$\phi_C = \phi_f - \phi_f'\left(\frac{\Delta\xi_D}{2}\right) + \frac{1}{2}\phi_f''\left(\frac{\Delta\xi_D}{2}\right)^2 - \frac{1}{6}\phi_f'''\left(\frac{\Delta\xi_D}{2}\right)^3 + \frac{1}{24}\phi_f^{(iv)}\left(\frac{\Delta\xi_D}{2}\right)^4 + \ldots \tag{4.4.2}$$

so that linear interpolation across the face would give:

$$\phi_f = \frac{1}{2}(\phi_C + \phi_D) - \frac{\Delta\xi_D^2}{8}\phi_f'' - \frac{\Delta\xi_D^4}{384}\phi_f^{(iv)} + O(\Delta\xi_D^6) \qquad (4.4.3)$$

where the control volume face has been located exactly in the middle of the distance between the two nodes C and D.

The accuracy of a finite difference approximation is conventionally judged in terms of the leading truncation error of the Taylor expansions; the formal accuracy of some of the possible interpolating techniques for ϕ_f will be now evaluated:

• Upwind: the value in upstream node is used: $\phi_f = \phi_C$; from (4.4.2), the leading truncation error term is $\phi_f' \frac{\Delta\xi_D}{2}$;

• Central differencing: the value in the face is written as: $\phi_f = \phi_C + \phi_f' \Delta\xi_D/2$ and the derivative is evaluated with a central formula across the cell face:

$$\phi_f = \phi_C + \frac{\phi_D - \phi_C}{\Delta\xi_D} \cdot \frac{\Delta\xi_D}{2} = \frac{1}{2}(\phi_D + \phi_C) \qquad (4.4.4)$$

from (4.4.3), the leading truncation error is: $-\phi_f'' \frac{\Delta\xi_D^2}{8}$.

• Second-order Upwind: the value in the face is written as: $\phi_f = \phi_C + \phi_C' \Delta\xi_D/2$ and the derivative in the upstream node C is evaluated with a backward formula if the convecting velocity is positive, with a forward formula in the opposite case:

$$\phi_f = \phi_C + \frac{\phi_C - \phi_U}{\Delta\xi_C} \cdot \frac{\Delta\xi_D}{2} = (1 + a)\phi_C - a\phi_U \qquad (4.4.5)$$

where $a = 0.5 * \Delta\xi_D / \Delta\xi_C$, being 0.5 for a uniform grid. A simple expression for the truncation error can be obtained for a uniform grid; in this case, subtracting the Taylor expansion of the U node:

$$\phi_U = \phi_f - \phi_f'\left(\frac{3\Delta\xi}{2}\right) + \frac{1}{2}\phi_f''\left(\frac{3\Delta\xi}{2}\right)^2 + \ldots$$

for the relation (4.4.2) multiplied by 3, the following expression is obtained:

$$\phi_f = \frac{3}{2}\phi_C - \frac{1}{2}\phi_U + \frac{3}{8}\phi''_f \Delta\xi^2 + O\left(\Delta\xi^3\right) \tag{4.4.6}$$

The leading truncation error is therefore proportional to $\Delta\xi^2$.

- QUICK: the value on the control volume face is written as in (4.3.2); expanding the second derivative in the C node:

$$\phi''_C = \phi''_f - \phi'''_f \frac{\Delta\xi_D}{2} + O\left(\Delta\xi_D^2\right)$$

and substituting in the (4.4.3), the following expression is obtained:

$$\phi_f = \frac{1}{2}\left(\phi_C + \phi_D\right) - \frac{\Delta\xi_D^2}{8}\phi''_C + \frac{\Delta\xi_D^3}{16}\phi'''_f + O\left(\Delta\xi_D^4\right) \tag{4.4.7}$$

that shows that the leading truncation error is proportional to $\Delta\xi_D^3$.

4.5 - Convective stability.

Following Leonard (1979), convective stability may be defined as the sensitivity of the convective term, relative to a control volume, to variations of the variable in the corresponding grid point. Considering an unsteady one-dimensional convection-diffusion equation for the scalar ϕ:

$$\frac{\partial\phi}{\partial t} = -\frac{\partial(u\phi)}{\partial x} + \frac{\partial}{\partial x}\left(\Gamma\frac{\partial\phi}{\partial x}\right) \tag{4.5.1}$$

and in the case of constant velocity and uniform grid, the net convective influx per unit volume into the control-volume centered the node C can be written as (referring to figure 4.5):

$$influx = u_0 \frac{\phi_l - \phi_r}{\Delta x} \tag{4.5.2}$$

and the convective stability may be defined as the sensitivity of the convective influx (4.5.2) to the change in ϕ_C:

$$\Sigma_C = \frac{\partial(influx)}{\partial \phi_C} \tag{4.5.3}$$

In order to ensure convective stability, it is important to have a numerical negative feedback mechanism, such that any disturbance to ϕ_C from an outside influence will reduce or enhance *influx* in line with whether ϕ_C increases or decreases, that is:

$\Sigma_C > 0 \Rightarrow$ unstable sensitivity;
$\Sigma_C = 0 \Rightarrow$ neutral sensitivity;
$\Sigma_C < 0 \Rightarrow$ stable sensitivity.

From a purely physical point of view, convection is associated with the transport of fluid properties from upstream to downstream and any numerical approximation to convection should reproduce this transportive feature. This corresponds to having an element of upwind bias, that is giving a greater influence to the values in the upstream direction when evaluating the interpolated value on the cell face. Any numerical approximation to convection which is not upwind biased will lack convective stability.

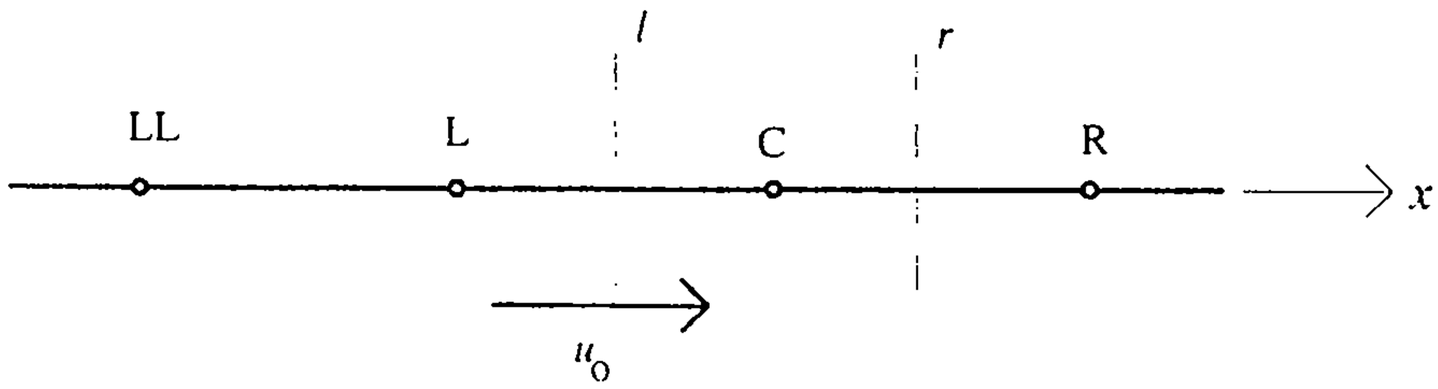

Figure 4.5 - One-dimensional, constant velocity, uniform grid case.

The convective stability of the previous schemes can be easily evaluated in the case of constant velocity and uniform grid:

• Upwind:

$$influx = u_0 \frac{\phi_L - \phi_C}{\Delta x} \Rightarrow \Sigma_C = -\frac{u_0}{\Delta x} \tag{4.5.4}$$

• Central differencing:

$$influx = \frac{u_0}{\Delta x}\left[\frac{1}{2}(\phi_C + \phi_L) - \frac{1}{2}(\phi_C + \phi_R)\right] \Rightarrow \Sigma_C = 0 \tag{4.5.5}$$

• Second-order Upwind:

$$influx = \frac{u_0}{\Delta x}\left[\left(\frac{3}{2}\phi_L - \frac{1}{2}\phi_{LL}\right) - \left(\frac{3}{2}\phi_C - \frac{1}{2}\phi_L\right)\right] \Rightarrow \Sigma_C = -\frac{3}{2}\frac{u_0}{\Delta x} \tag{4.5.6}$$

• QUICK:

$$influx = \frac{u_0}{\Delta x}\left\{\left[\frac{1}{2}(\phi_L + \phi_C) - \frac{1}{8}(\phi_C - 2\phi_L + \phi_{LL})\right] - \left[\frac{1}{2}(\phi_C + \phi_R) - \frac{1}{8}(\phi_R - 2\phi_C + \phi_L)\right]\right\} \Rightarrow \Sigma_C = -\frac{3}{8}\frac{u_0}{\Delta x} \tag{4.5.7}$$

4.6 - The universal limiter constraints.

As is well known, the use of a quadratic interpolation for the value of the variable on the cell face can cause *overshoot* problems; e.g., as schematically represented in figure 4.6 for a one-dimensional case, when $\phi_C \approx \phi_D$ the value obtained from the interpolation can be higher than the values in the surrounding nodes. This phenomenon can lead to non-linear instability; this might happen, for example, when a computed turbulence quantity becomes (unphysically) negative as a result of this oscillation and consequently a negative turbulent viscosity is obtained, causing a computational divergence of the algorithm.

In order to avoid this kind of problem, a convection boundedness criterion is defined, based on simple physical assumptions. The value obtained from the higher-order scheme is therefore limited according to the constraints imposed by the boundedness criterion before being used in the transport equations.

The universal limiter used in TURBO3D_2 is based on the boundedness criterion of Gaskell and Lau (1988), in the formulation with normalised variables of Leonard and Mokhtari (1990).

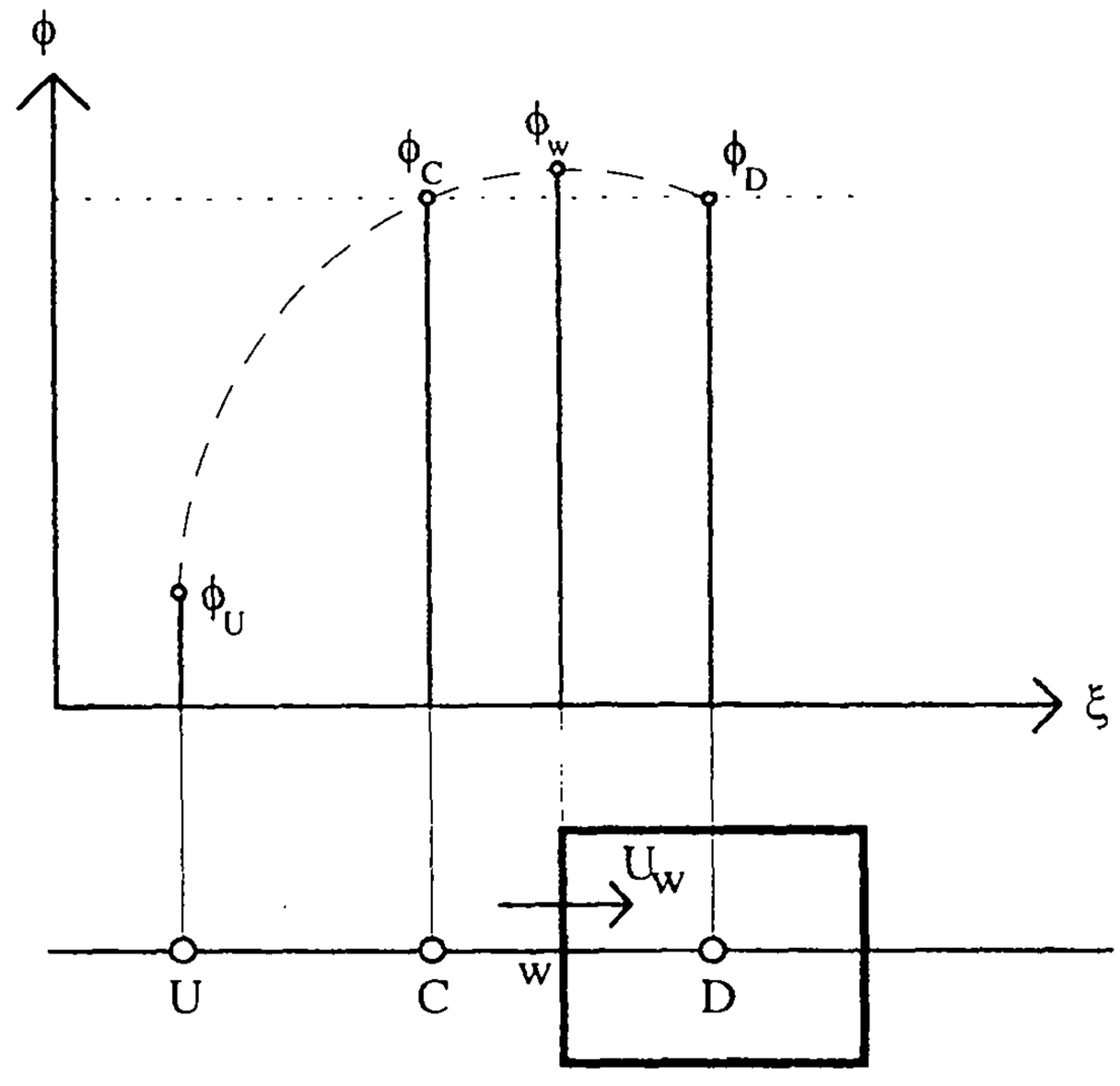

Figure 4.6 - Example of overshoot in the evaluation of the variable on the cell face with a quadratic interpolation.

Depending on the direction of the convecting velocity the three nodes *D* (downwind), *U* (Upwind) and *C* (upstream respect to the cell face, centrally located between the other two) are chosen, as in the previous figures for a positive velocity.

The logic of the constraint is the following:

• in locally monotonic regions, that is if the upstream value (*C*) is bounded by the values in the upwind and downwind nodes (*D* and *U*), i.e. $\phi_C \in [\phi_U, \phi_D]$, the interpolated value on the cell face should lie between adjacent node values, i.e. $\phi_f \in [\phi_C, \phi_D]$.

• if $\phi_C \notin [\phi_U, \phi_D]$ no information is available to limit the interpolated value; in this case a lower-order scheme is used, for example the first order Upwind (that is always bounded).

In the formulation of Leonard second-order schemes are used in the last case.

A normalised variable $\tilde{\phi}$ is defined as:

$$\tilde{\phi}(\xi,\eta,\zeta) = \frac{\phi(\xi,\eta,\zeta) - \phi_U}{\phi_D - \phi_U} \tag{4.6.1}$$

leading therefore to $\tilde{\phi}_U = 0$ and $\tilde{\phi}_D = 1$.

The universal limiter constraints can now be written using the following assumptions, referring to figure 4.7 for the representation of the constraints in the Normalised Variable Diagram (NVD):

1) If the value of ϕ_C is between ϕ_U and ϕ_D then the value on the cell face must be between ϕ_C and ϕ_D. In normalised variables:

$$\tilde{\phi}_C \le \tilde{\phi}_f \le 1 \quad \text{for} \quad 0 < \tilde{\phi}_C \le 1 \tag{4.6.2}$$

This relation is satisfied in the interior of the triangle in figure 4.7, which is referred to as the *monotonic region* of the criterion.

2) If $\phi_C = \phi_D$ then it follows that $\phi_f = \phi_D$. In normalised variables:

$$\tilde{\phi}_f = 0 \quad \text{at} \quad \tilde{\phi}_C = 0 \tag{4.6.3}$$

corresponding to the point *O* in figure 4.7.

3) To avoid the non-uniqueness near $\tilde{\phi}_C \to 0_+$ the boundary *OB* in figure 4.7 has a steep but finite positive slope. This introduces an additional constraint:

$$\tilde{\phi}_f \le const \times \tilde{\phi}_C \quad \text{near} \quad \tilde{\phi}_C \to 0_+ \tag{4.6.4}$$

4) The extension beyond $\tilde{\phi}_C = 1$ (point *A* in figure 4.7) is given with the central differencing scheme (4.4.4):

$$\tilde{\phi}_f = 1 + \frac{1}{2}\left(\tilde{\phi}_C - 1\right) \quad \text{for} \quad \tilde{\phi}_C > 1 \tag{4.6.5}$$

5)The extension to values of $\tilde{\phi}_C$ less then zero (point *O* in figure 4.7) is given with the second-order Upwind scheme (4.4.5):

$$\tilde{\phi}_f = (1+a)\tilde{\phi}_C \quad \text{for} \quad \tilde{\phi}_C < 0 \tag{4.6.6}$$

Note that both lines pass through the *second-order* point *C*, located at $(1/(1+2a),(1+a)/(1+2a))$, corresponding to the point (0.5, 0.75) for a uniform grid.

Alternatively, the two extension formulae (4.6.5) and (4.6.6) could be given with a first order Upwind (corresponding to the diagonal of the first and the third quadrants):

$$\tilde{\phi}_f = \tilde{\phi}_C \quad \text{for} \quad \tilde{\phi}_C \notin [0,1] \tag{4.6.7}$$

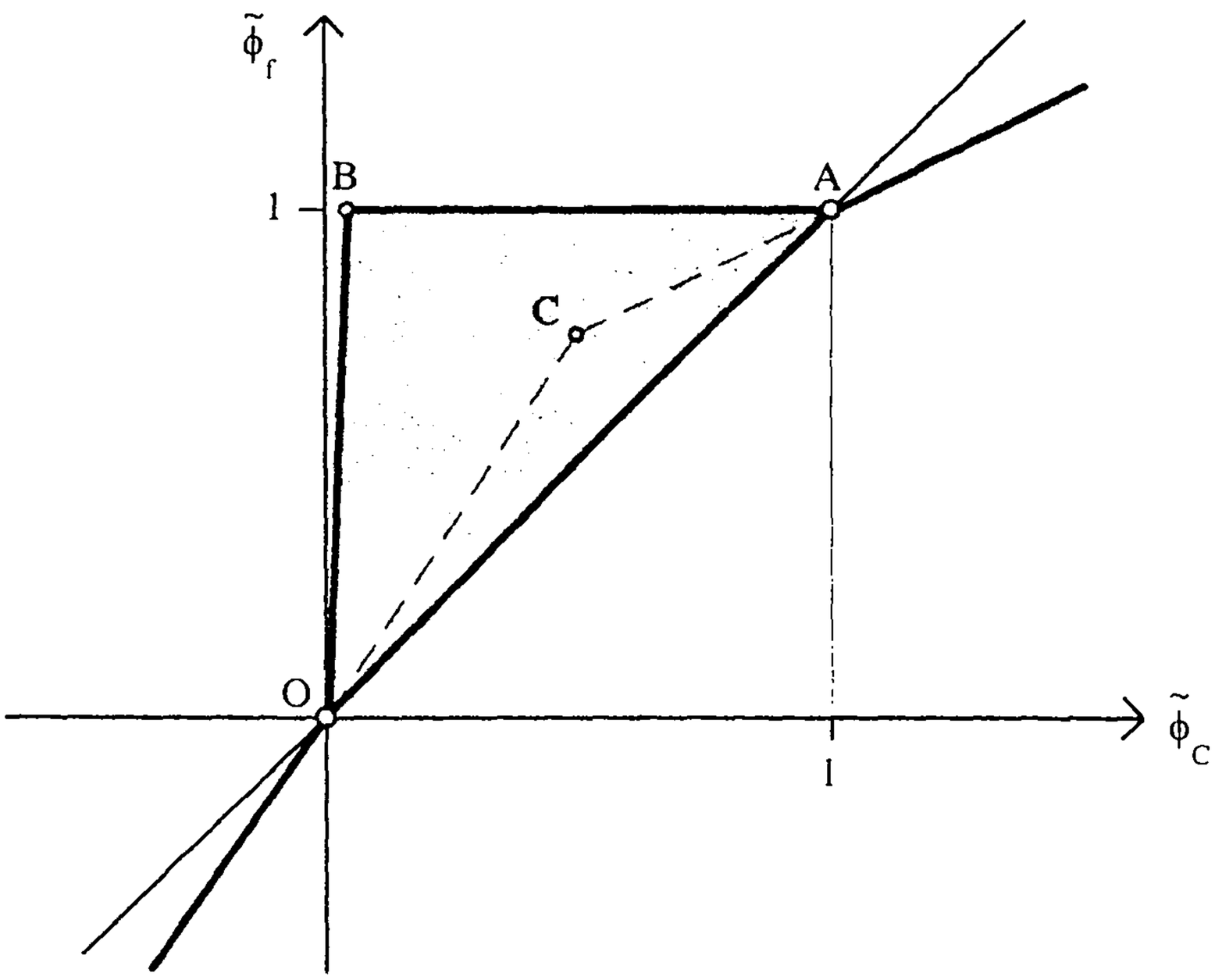

Figure 4.7 - Universal limiter constraints in the Normalised Variable Diagram.

It is important to note that the previous constraints are implemented in a one-dimensional way, which means that only the values in the Central, Upwind and Downwind nodes in the direction normal to the cell face are considered when limiting ϕ_f and not the surrounding nodes in the other two directions, also if the value on the cell face has been evaluated with a three-dimensional stencil, such as the one in figure 4.4. This kind of procedure, obviously needed for simplicity reasons, is partially

justified from the consideration that the main contribution to the convected value is given from the interpolation of the values in the nodes in the normal direction (e.g. the first two terms in equation (4.3.16)) and that this interpolation is most likely the cause of an overshoot.

The universal limiter constraint is therefore applied, for each face of each control volume (in effects using the conservative property only half of the cell faces has to be considered), as follows:

1) note the direction of the normal velocity component, the nodes U, C and D are identified.

2) the value of ϕ_f is obtained with a high-order upwind-weighted method, as the one presented in the previous section, taking also into account the three-dimensional effects.

3) the normalised values $\tilde{\phi}_f$ and $\tilde{\phi}_C$ are computed.

4) if the point $(\tilde{\phi}_C, \tilde{\phi}_f)$ does not fall within the triangular region of figure 4.7, $\tilde{\phi}_f$ is limited to the nearest appropriate constraint boundary at the given $\tilde{\phi}_C$ value.

5) the non-normalised face value is then reconstructed by:

$$\phi_f = \tilde{\phi}_f(\phi_D - \phi_U) + \phi_U \tag{4.6.8}$$

4.7 - The Deferred Correction.

As reported previously, the use of the first-order Upwind technique, introducing a considerable amount of numerical viscosity, has a strong stabilising effect on the procedure and the corresponding matrix of the coefficients becomes more diagonally dominant. In order to maintain these positive effects, while at the same time using a more accurate higher-order scheme, the value on the cell face (to be computed) can be written in terms of the first-order Upwind face value plus a correction term:

$$\phi_f^{n+1} = \left(\phi_f^{n+1}\right)_{upwind} + \left[\left(\phi_f^{n}\right)_{higher-order} - \left(\phi_f^{n}\right)_{upwind}\right] \tag{4.7.1}$$

The contribution of the correction term, evaluated with the values of the variables at the previous iteration, is incorporated in the source term; therefore the system will have the same matrix of coefficients to the Upwind approach. As the converged solution is reached, the first order contributions cancel, and the solution is consistent with using the higher-order face values everywhere.

4.8 - The Downwind Weighting Factor.

Another possible way of using higher-order schemes is through the introduction of an auxiliary variable, called the Downwind Weighting Factor (*DWF*), that is function of the cell face, as originally proposed by Leonard (1990).

For every cell face (with the usual adoption of a conservative calculation) a value of ϕ_f is computed with a high-order multidimensional upwind-weighted method using the values of the variable at the previous iteration. The *DWF* then is defined as:

$$DWF = \frac{\phi_f - \phi_C}{\phi_D - \phi_C} \tag{4.8.1}$$

or, in normalised variables:

$$DWF = \frac{\tilde{\phi}_f - \tilde{\phi}_C}{1 - \tilde{\phi}_C} \tag{4.8.2}$$

where the points C and D are defined as shown in previous sections. All the values of variable ϕ appearing in these formulae and in the following ones are the known values evaluated at the previous iteration.

The constraints for ϕ_f are now rewritten as limits for the *DWF* :

$$1)\ 0 \le DWF \le 1 \text{ for } 0 < \tilde{\phi}_C \le 1 \tag{4.8.3}$$

$$2)\ DWF = 0 \text{ at } \tilde{\phi}_C = 0 \tag{4.8.4}$$

$$3)\ DWF \le \frac{(const\ 1)\tilde{\phi}_C}{1 - \tilde{\phi}_C} \quad \text{near} \quad \tilde{\phi}_C \to 0_+ \tag{4.8.5}$$

$$4)\ DWF = 0.5 \text{ for } \tilde{\phi}_C > 1 \tag{4.8.6}$$

$$5)\ DWF = \frac{a\phi_C}{\left(1 - \tilde{\phi}_C\right)} \text{ for } \tilde{\phi}_C \le 0 \tag{4.8.7}$$

The universal limiter constraints for the *DWF* are represented in figure 4.8, where the same letters of figure 4.7 have been used. Note that the point A in figure 4.7 has been stretched out into a vertical line in figure 4.8. The point C is now at $(1/(2a+1), 1/2)$.

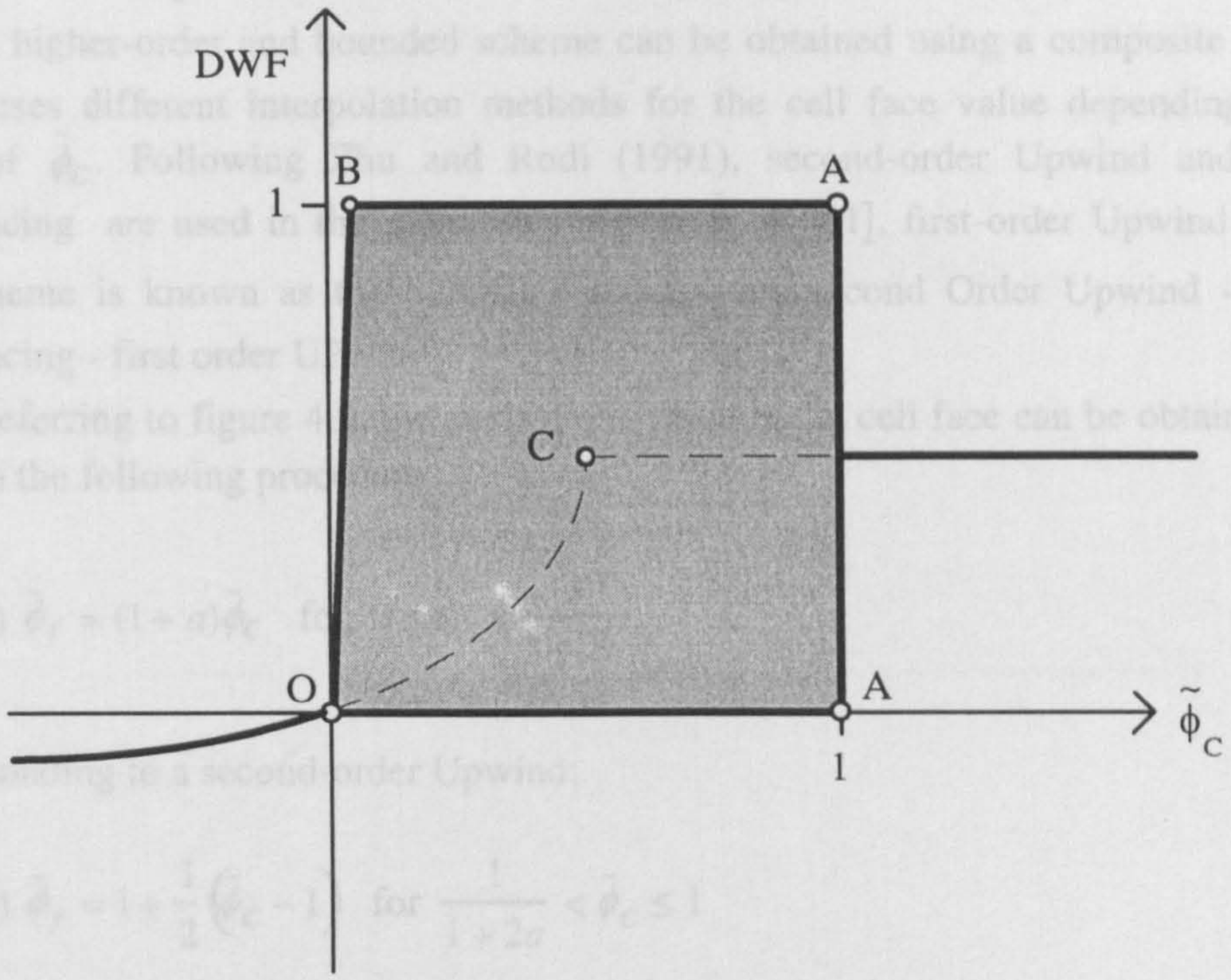

Figure 4.8 - Universal limiter constraints in terms of the DWF.

Once the *DWF* has been evaluated and limited, the face value is rewritten in term of the known *DWF* as:

$$\phi_f = DWF \cdot \phi_D^{n+1} + (1 - DWF) \cdot \phi_C^{n+1} \tag{4.8.8}$$

where the values of the variable appearing in the right-hand side have to be evaluated solving the system of equations; the *DWF* will therefore appear in the coefficients of these variables in the matrix of the system. For example when evaluating the variable on the w face for a positive value of U_w the term in *DWF* appears in the coefficient a_P (being P the downwind node) while the term in (1-*DWF*) appears in the coefficient a_W.

When evaluating the convective flux on a control volume face, therefore, only the adjacent nodes are involved, exactly as in the Upwind procedure, but the *DWF* contains a higher-order wide stencil information and the universal limiter constraints.

With the *DWF* technique the matrix of the system of linear equations keeps the same form as the Upwind technique, but the positive effects of the Upwind in the conditioning of the matrix are no longer present.

4.9 - A composite second order scheme (SOUCUP).

A higher-order and bounded scheme can be obtained using a composite scheme, which uses different interpolation methods for the cell face value depending on the value of $\tilde{\phi}_C$. Following Zhu and Rodi (1991), second-order Upwind and central differencing are used in the monotonic region $\tilde{\phi}_C \in [0,1]$, first-order Upwind outside; this scheme is known as the SOUCUP (composite Second Order Upwind - Central differencing - first order UPwind).

Referring to figure 4.9, the normalised value at the cell face can be obtained from $\tilde{\phi}_C$ with the following procedure:

$$1)\ \tilde{\phi}_f = (1+a)\tilde{\phi}_C \quad \text{for } 0 \le \tilde{\phi}_C \le \frac{1}{1+2a} \tag{4.9.1}$$

corresponding to a second-order Upwind;

$$2)\ \tilde{\phi}_f = 1 + \frac{1}{2}\left(\tilde{\phi}_C - 1\right) \quad \text{for } \frac{1}{1+2a} < \tilde{\phi}_C \le 1 \tag{4.9.2}$$

corresponding to central differencing;

$$3)\ \phi_f = \phi_C \quad \text{for } \phi_C \notin [0,1] \tag{4.9.3}$$

corresponding to a first-order Upwind.

The non-normalised value on the cell face is then evaluated with formula (4.6.8).

This choice of the scheme used in the monotonic region is in agreement with the physical consideration that if $\tilde{\phi}_C \approx 0$ the face value must be dominated by the upstream conditions (therefore a second-order Upwind is used), while, if $\tilde{\phi}_C \approx 1$ the downstream conditions prevail (central differencing).

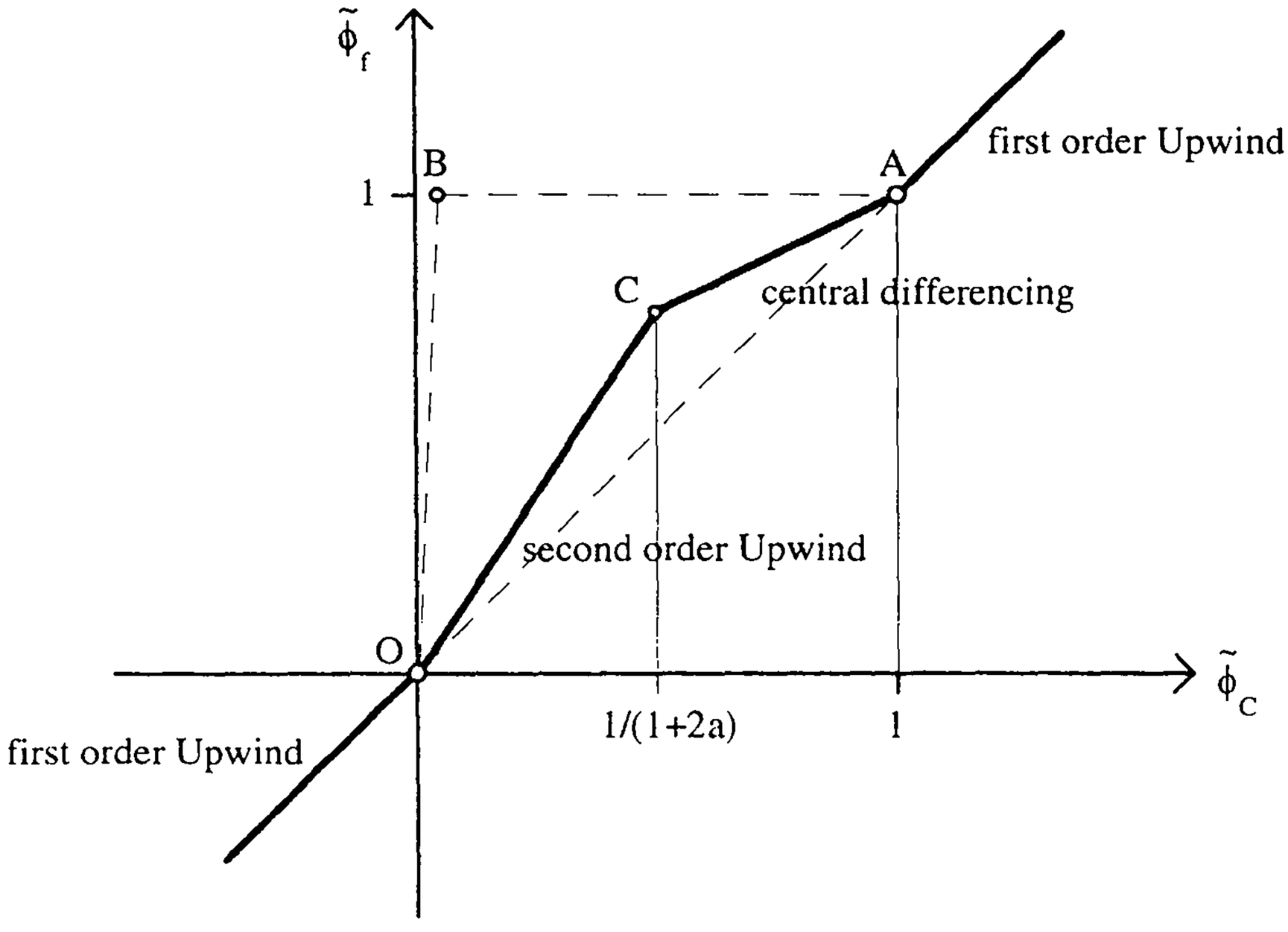

Figure 4.9 - The SOUCUP scheme in the Normalised Variable Diagram.

4.10 - A composite third order scheme (SMART).

To obtain an expression for $\tilde{\phi}_f$ as a function of $\tilde{\phi}_C$ the transverse terms have to be neglected; rewriting expressions (4.3.1) and (4.3.2) in normalised variables:

$$\tilde{\phi}_f = \left(\frac{1}{2} + \frac{\Delta\xi_D}{4\Delta\xi_C}\right)\tilde{\phi}_C + \left[\frac{1}{2} - \frac{\Delta\xi_D}{4(\Delta\xi_C + \Delta\xi_D)}\right] \tag{4.10.1}$$

In the Normalised Variable Diagram this is represented by the line intersecting the boundary $\tilde{\phi}_f = 1$ for

$$\tilde{\phi}_C = \left[\frac{\Delta\xi_D}{4(\Delta\xi_D + \Delta\xi_C)} + \frac{1}{2}\right] \Big/ \left(\frac{\Delta\xi_D}{4\Delta\xi_C} + \frac{1}{2}\right) \tag{4.10.2}$$

(being 5/6 for an uniform grid), corresponding to point D of figure 4.10, and the boundary $\tilde{\phi}_C = 0$ for

$$\tilde{\phi}_f = \frac{1}{2} - \frac{\Delta\xi_D}{4(\Delta\xi_D + \Delta\xi_C)} \qquad (4.10.3)$$

(being 3/8 for a uniform grid), corresponding to the point E of figure 4.10.

In order to avoid the non-uniqueness near $\tilde{\phi}_C \to 0_+$ and to have at any point a monotonic behaviour, the scheme is modified as in figure 4.10, introducing the points D' and E' (with a certain degree of arbitrariety in the choice of the slope of the lines).

The scheme in figure 4.10 is similar to the SMART (Sharp and Monotonic Algorithm for Realistic Transport) of Gaskell and Lau, although the original scheme had been developed for a uniform grid and used a different approach near $\tilde{\phi}_C \to 0_+$ where the point O was connected to point (1/6, 1/2) (thin line in figure 4.10) on the basis of considerations about the property of the quadratic profile for a uniform grid.

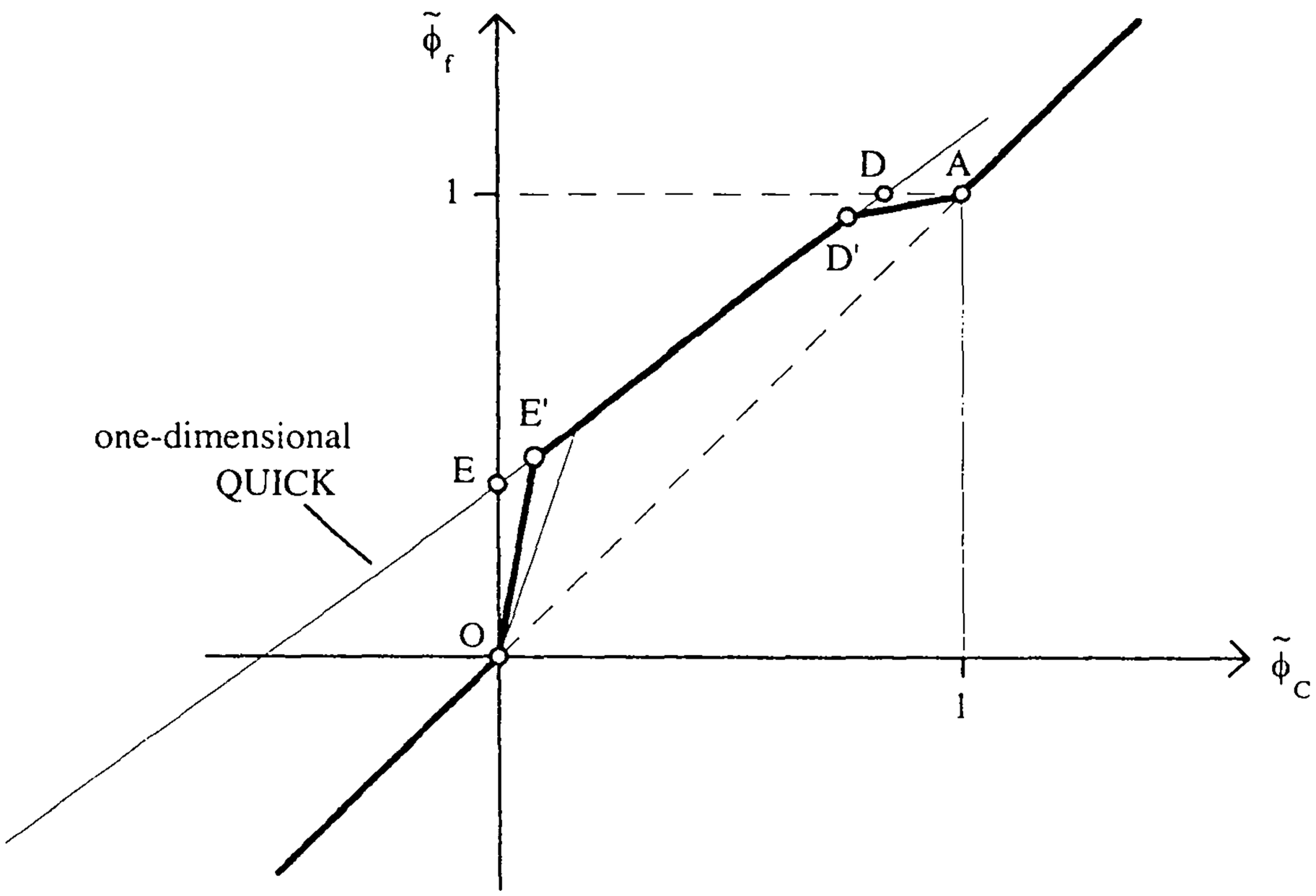

Figure 4.10 - The SMART scheme in the Normalised Variable Diagram.

4.11 - Fifth-order Upwind.

Expanding in Taylor series across the cell face the second derivatives at the nodes C and D, an expression for the second derivative on the cell face, similar to (4.4.3), can be obtained:

$$\phi''_f = \frac{1}{2}\left(\phi''_C + \phi''_D\right) - \frac{\Delta\xi_D^2}{8}\phi_f^{(\mathrm{iv})} + O\left(\Delta\xi_D^4\right) \tag{4.11.1}$$

and substituting in (4.4.3):

$$\phi_f = \frac{1}{2}\left(\phi_C + \phi_D\right) - \frac{1}{8}\Delta\xi_D^2\left(\phi''_C + \phi''_D\right) + \frac{5}{384}\Delta\xi_D^4\phi_f^{(\mathrm{iv})} + O\left(\Delta\xi_D^6\right) \tag{4.11.2}$$

Following a procedure similar to the one used to obtain expression (4.4.7) for the QUICK, the fourth derivative can be written as:

$$\phi_f^{(\mathrm{iv})} = \phi_C^{(\mathrm{iv})} + \frac{\Delta\xi_D}{2}\phi_f^{(\mathrm{v})} + O\left(\Delta\xi_D^2\right)$$

and therefore:

$$\phi_f = \frac{1}{2}\left(\phi_C + \phi_D\right) - \frac{1}{8}\Delta\xi_D^2\left(\phi''_C + \phi''_D\right) + \frac{5}{384}\Delta\xi_D^4\phi_C^{(\mathrm{iv})} + \frac{5}{768}\Delta\xi_D^5\phi_f^{(\mathrm{v})} + O\left(\Delta\xi_D^6\right) \tag{4.11.3}$$

Considering only the first three terms on the right-hand side of expression (4.10.3), a fifth-order method (upwind-biased, as more points in the upstream direction are involved) for the evaluation of ϕ_f could be obtained. This formula in any case is one-dimensional.

The convective stability, for a uniform grid with uniform velocity, is:

$$\Sigma_C = -10\cdot\frac{5}{384}\frac{u_0}{\Delta x} \tag{4.11.4}$$

where only the upwind-biased term contributes to the convective stability.

The fourth derivative in the (4.11.3) can be easily obtained from the second derivatives, with the same procedure used to evaluate the second derivatives:

$$\left(\frac{\partial^4\phi}{\partial\xi^4}\right)_C = \frac{2}{\Delta\xi_D + \Delta\xi_C}\left[\frac{(\phi_{\xi\xi})_D - (\phi_{\xi\xi})_C}{\Delta\xi_D} - \frac{(\phi_{\xi\xi})_C - (\phi_{\xi\xi})_U}{\Delta\xi_C}\right] \qquad (4.11.5)$$

The use of the interpolation formula (4.11.4) requires three upstream nodes to the cell face; for this reason, in all the near boundary control volumes a third order formula (QUICK) is used. The value obtained from the interpolation is then eventually limited according to the universal limiter constraints of figure 4.7.

Finally, a three-dimensional formula can be obtained adopting the third-order curvature correction of expression (4.3.16):

$$\phi_f = \frac{1}{2}(\phi_C + \phi_D) - \frac{1}{8}\Delta\xi_D^2(\phi_C'' + \phi_D'') + \frac{5}{384}\Delta\xi_D^4\phi_C^{(iv)} + \\ + \frac{\Delta\eta^2}{24}(\phi_{\eta\eta})_C + \frac{\Delta\zeta^2}{24}(\phi_{\zeta\zeta})_C \qquad (4.11.6)$$

4.12- Near boundary control volumes.

All the higher-order schemes presented in this chapter involve two upstream nodes for each cell face; it may seem necessary to follow special practices for the near boundary control volumes, in order to avoid the use of values outside the flow domain.

In effect, due to the chosen definition of the cells near to the boundaries, this is not necessary in TURBO3D_2. Referring to figure 2.3, when evaluating the contribution of the convection in the cell i=2, the value of the variable on the w face is assigned, corresponding to the value in the node i=1, therefore only the value on the e face has to be evaluated with a higher-order scheme. For the e face two upstream nodes are always available (e.g., for a positive U_e, the nodes i=1 and i=2). In the same way, the value on the b face of the cell m=2 is assigned (inlet values), while the value on the f face of the cell m=nx-1 can be obtained from the upstream value, with the hypothesis of the convection dominating the flow at the outlet.

Chapter 5
Initial validation of the code

5.1 - Introduction.

An initial testing of the solution procedure presented in the previous sections has to be carried out before the modified formulation for the turbulence modelling is introduced, in order to validate the convection schemes presented in the previous section and to select the appropriate linear solver among the ones that are available in the chosen libraries.

The flow in a 90° bend of square cross section is the first test case chosen for the validation of the code, as a large amount of experimental measurements are available for comparison (Taylor, Whitelaw and Yianneskis (1981)) both for laminar and turbulent flow. The duct used in the flow measurements has a 90° bend of mean radius 92*mm* and of radius ratio 2.3, with a square section of 40×40*mm* in a water tunnel; the bulk velocity for the laminar case is 0.0198 *m/sec*, corresponding to a Reynolds number of 790; for the turbulent case the bulk velocity is 1.0 *m/sec*, corresponding to a Reynolds number of 40,000. In figure 5.1 the coordinate system used in the flow measurements is illustrated.

In figures 5.2 and 5.3 the grid used for the discretisation of the duct is presented; in each cross-section plane 20×20 grid points have been used, with a clustering of the nodes near to the walls, and 100 planes in the main flow direction, with a clustering of the nodes near to the bend entry and exit planes, giving a total of 40,000 nodes. The relaxation factor used is 0.2 for all variables.

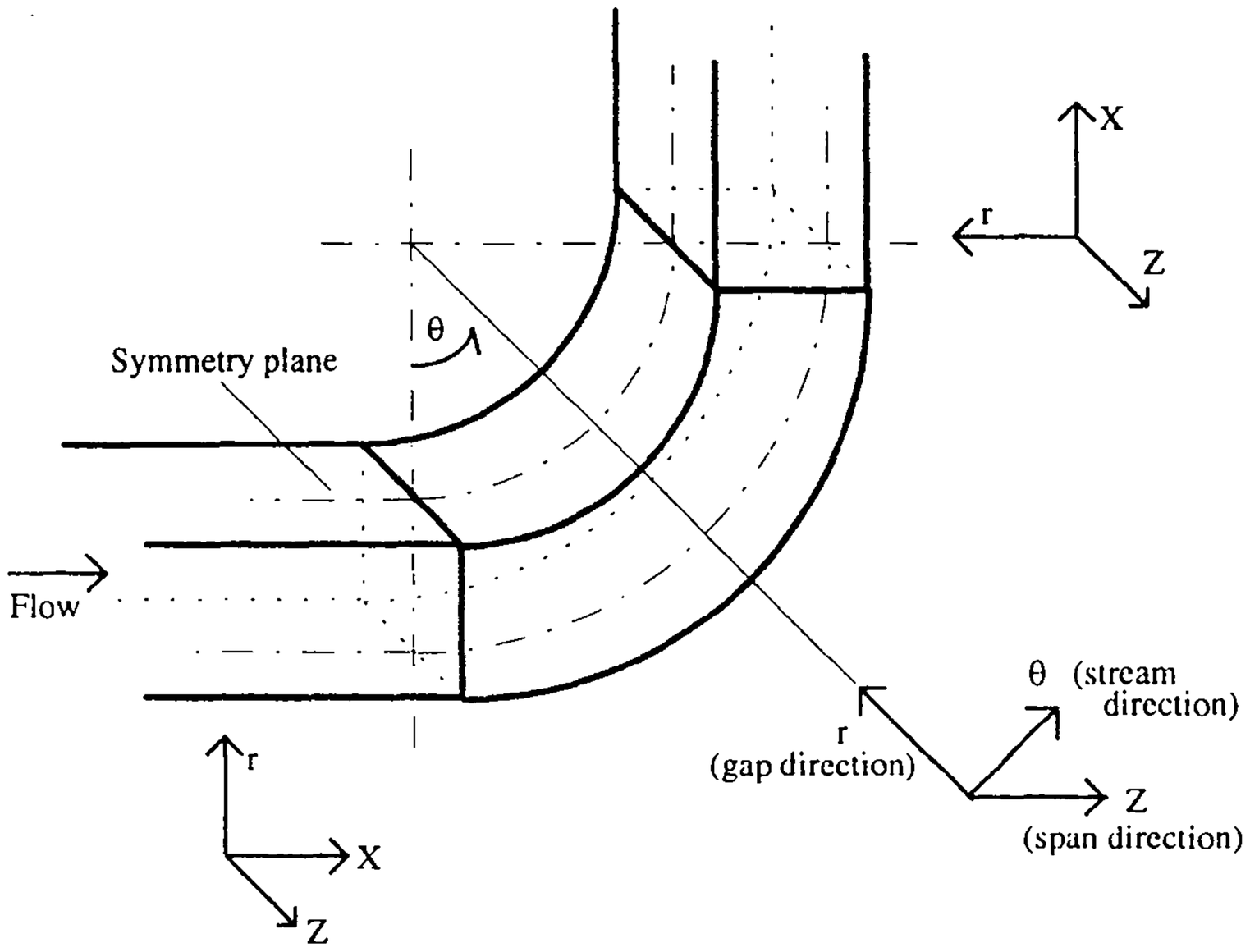

Figure 5.1 - Coordinate definition used in the flow measurements.

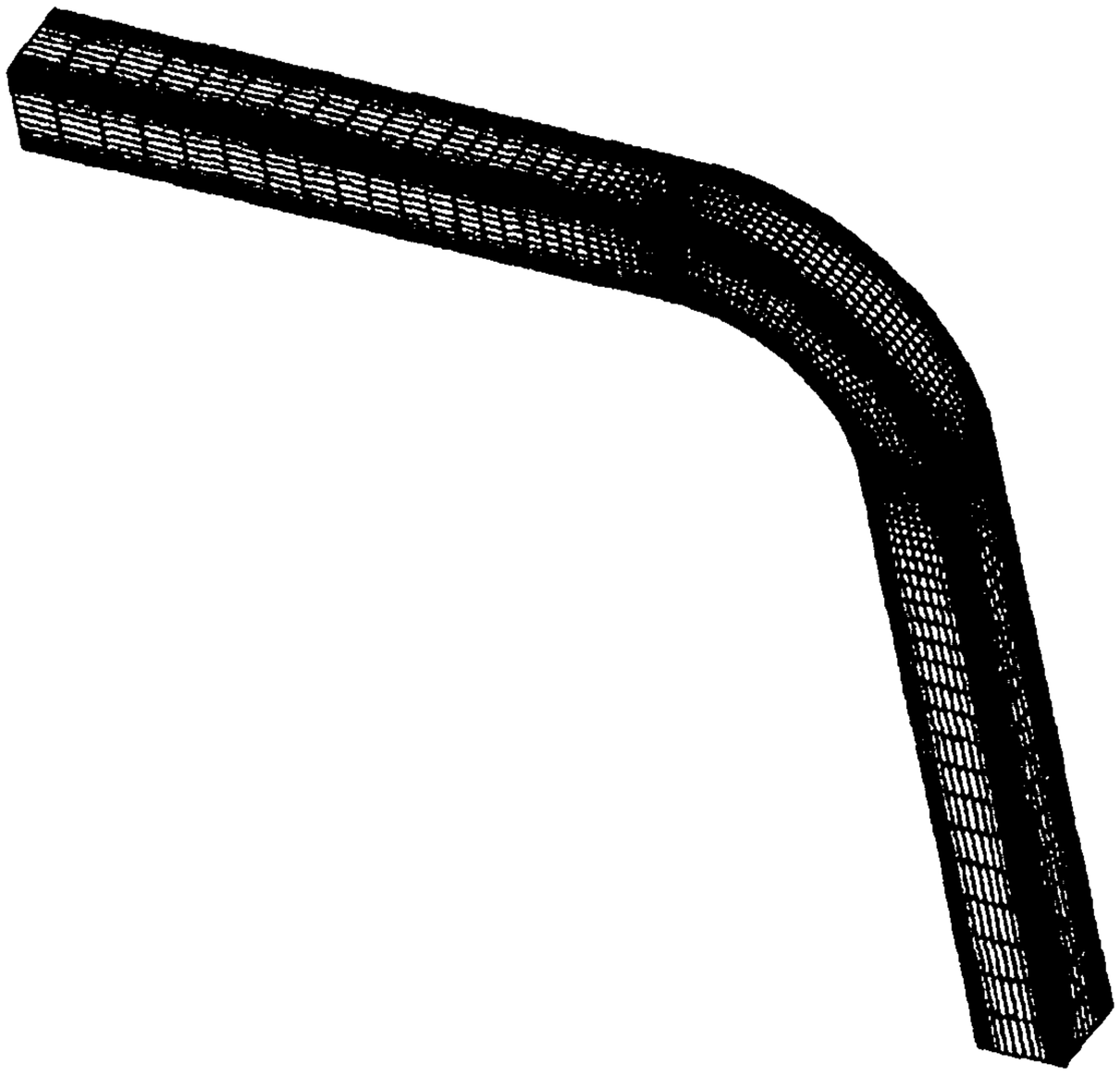

Figure 5.2 - View of the grid.

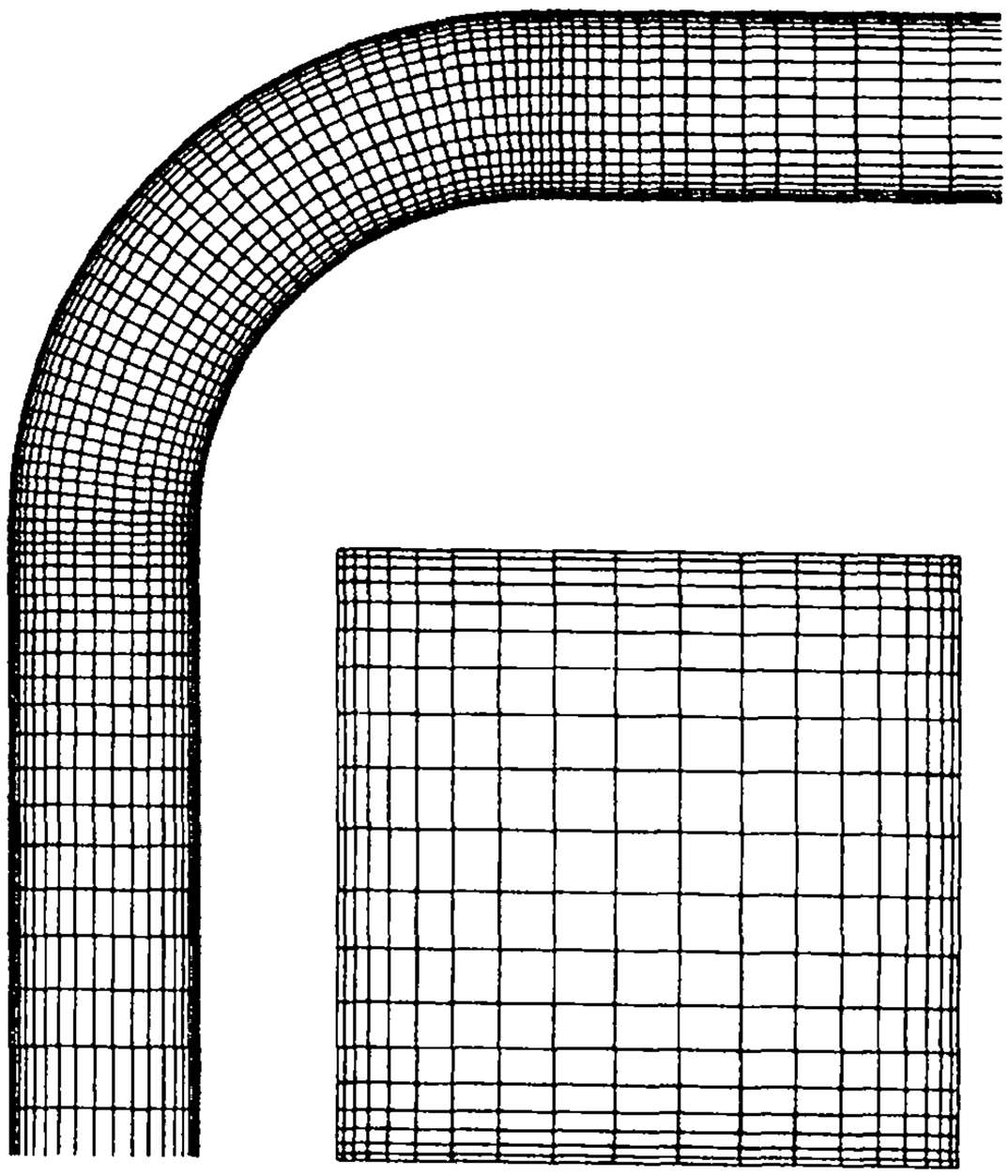

Figure 5.3 - Details of the mesh in the symmetry plane and in the cross section.

5.2 - Boundary condition for the pressure at the inlet.

At the inlet of the duct, where the value of the velocity is prescribed, the value of the pressure cannot be assigned, as it is linked to the given velocity field through the momentum equations. The boundary condition for the pressure used at the inlet is the Neumann condition (2.6.3).

In figure 5.17 the distribution of the pressure at the inlet obtained for the laminar flow is represented; although this distribution corresponds to the physical distribution *p=const*, the presence of a numerical error in the solution of the momentum equations generates the distribution of the figure, having the typical behaviour of the numerical error in the solution of an elliptic equation.

If the value *p=const* had been prescribed at the inlet, a strong oscillation in the values of the pressure and the velocity would have appeared in the neighbouring planes. This behaviour is typical of the previous version of the code (TURBO3D), where the pressure at the inlet was assigned; in the plane-by-plane approach, in any case, it would be very difficult to impose correctly the Neumann condition at the inlet.

At the outlet, where the velocity distribution is not explicitly assigned, the distribution of the pressure can be assigned in TURBO3D_2 without any limitations. In

the case that a Neumann condition is used also at the outlet, the matrix of the coefficients of the system of equation for the pressure correction is singular (Neumann conditions on all the boundaries) and the pressure field is determined with an arbitrary additive constant. The effective pressure field can then be obtained imposing a reference value in at a specific point: e.g., if the pressure field is required to have the value $p = p_{ref}$ in the grid node $(i_{ref}, j_{ref}, m_{ref})$, this can be obtained as follows:

$$\begin{aligned} &\Delta p = p(i_{ref}, j_{ref}, m_{ref}) - p_{ref} \\ &p_{eff}(i,j,m) = p(i,j,m) - \Delta p \quad \text{for} \quad i = 1,nx;\ j = 1,ny;\ m = 1,nz \end{aligned} \tag{5.2.1}$$

In the results presented in this chapter, where the flow is incompressible and only the gradients of pressure influence the behaviour of the flow, the value p=1 has been imposed at the node (i=2, j=2, m=1) of the inlet plane.

5.3 - The choice of the linear solver.

The choice of the iterative technique to adopt among the ones available in the SITRSOL routine, described in the second chapter, is conditioned by the following considerations:

1) As all the systems are not symmetric or positive definite, only GMRES (generalised minimum residual), BiCG (biconjugate gradient) and CGS (conjugate gradient squared) methods can be used.

2) Both CGS and BiCG can break down in particular situations; this has occurred with both methods in the first tests of the code.

3) The system of equations for the pressure correction can be singular and in any case is ill-conditioned; both CGS and BiCG seem to be very sensitive to the ill-conditioning of the matrix (CGS seems to diverge completely for the p' system).

Only GMRES, therefore, could be used; also this method, in any case, seems to be extremely sensitive to the conditioning of the system, being able to solve the systems for the momentum equations in no more than 10 iterations, while showing a very slow convergence for the pressure correction equation.

In particular, the following behaviour has been observed in the use of GMRES for the solution of the pressure correction equation for the laminar case:

1) Using a first-order Upwind, in the first steps of the solution procedure there is a crisis of the linear solver, that is incapable of reducing the error beyond a certain limit (figure 5.4). In order to allow the computation to proceed, a maximum number of

iterations has been fixed (5000) and the solution obtained has been used in the procedure, even if the convergence criterion had not been reached. This approach has been proven to be successful: after a certain number of steps of the procedure in which the maximum number of iterations in GMRES had been reached, a converged solution was obtained for the pressure correction equation for every step (figure 5.6).

As well known from the theory, GMRES computes a sequence of orthogonal vectors and combines these through a least-squares solve and update, but it requires storing the whole sequence, so that the amount of storage needed grows rapidly with the iterations. For this reason, a restarted version of GMRES is used: after a chosen number *rs* of iterations, the accumulated data are cleared and the intermediate results are used as the initial data for the next *rs* iterations. The value of *rs* has been set to a relatively small number (*rs*=10); extensive tests have shown that this choice of *rs* is not the cause of the slow convergence in the solution of the pressure correction equation, as using higher values has not produced any improvements. Furthermore, all the preconditioning procedures present in SITRSOL have failed to produce any improvements for this problem.

As reported in the previous chapter, the higher-order schemes can be applied both with the deferred correction, adding the corresponding contribution in the source and keeping the same matrix of the coefficients as in the case of Upwind for the momentum equations, or with a procedure like the *DWF*, in which the coefficients of the matrix are affected. The numerical tests have proven that with the use of the *DWF* the system for the momentum equations becomes ill-conditioned as well and a quite small value of the relaxation factor is required to re-establish the diagonal dominance of the matrix of the coefficients, that is necessary to achieve a fast solution in GMRES, as shown in figure 5.5. For this reason, as the convergent solution is equivalent for the two methods, only the deferred correction has been used in the other tests.

2) Using higher-order convection schemes there are larger areas in which there is a crisis of the linear solver in the solution of the pressure correction equation, and can be noted that this effect increases with the order of the scheme (figures 5.7, 5.8 and 5.9).

3) Using *a* flux limite*r* a converged solution for the pressure correction equation is obtained only in few points (figure 5.10).

4) If a constant pressure is imposed at the outlet, instead of the Neumann condition, the solver is incapable of obtaining an accurate solution and divergence occurs, unless the under-relaxation coefficients are lowered (figure 5.11).

If the matrix of the coefficients is not singular, a direct solver can be used. In this case a very accurate solution of the system can be achieved (of the order of machine accuracy, e.g.: 10^{-15} for the residual, while with GMRES the minimum value of the residual achieved was of the order of 10^{-8}); however much more memory is required; the amount of computational time necessary for the solution of the system depends only on the number of unknowns and is generally much larger than the one required by an iterative solver. In this particular case this is not necessarily true, as the crisis of the iterative solver experienced in the solution of the pressure correction equation, especially using higher-order convection schemes, causes a sharp increase in the time required by the solution with GMRES.

In figure 5.13 the results of the tests performed on this particular case are presented, showing how the use of the direct solver actually reduces the time required for the solution if higher-order schemes are used, especially in conjunction with a flux limiter. The results with the GMRES solver have been obtained imposing a Neumann condition at the outlet for the pressure, while the direct solver has been used in conjunction with a constant pressure at the outlet; the difference between the flow fields obtained is completely negligible. Furthermore, using a direct solver a much better performance is achieved, both in vectorisation and parallelisation of the code.

It is important to point out that this is true only if an accurate solution of the pressure correction is required; if extremely low-values of the under-relaxation have to be used a stable convergence could be achieved using much fewer iterations of GMRES for the pressure correction equation.

The amount of memory required by the direct solver grows rapidly when increasing the number of unknowns, so that a very strict limit on the number of unknowns that can be used could be imposed by this procedure.

Finally, figures 5.14 and 5.15 show how in both cases the solution of the pressure correction equation is responsible for most of the computational time required by the code.

5.4 - Analysis of the numerical tests.

In figures 5.6 to 5.12 the convergence history of the whole procedure for the laminar case is illustrated, where the maximum values of the absolute residual of the

momentum equation and the maximum value of the mass inbalance (*mp*) are reported; only the residual of one of the three components of the velocity is given, as the other two follow an identical behaviour. It is interesting to note that, using GMRES, the mass inbalance tends towards a minimum value and becomes constant, this minimum value being reached only when an accurate solution for the pressure correction is obtained. At the same time, when using a direct solver, the mass unbalance tends towards a much lower value (figure 5.12). Furthermore, it is important to point out that when using the flux limiter the residual of the equations cannot be reduced beyond a certain point (figure 5.10), although it can be shown that this affects only marginally the accuracy of the solution.

In figures 5.16 to 5.18 the results of the numerical tests for the laminar case are represented. The effect of higher-order schemes can be clearly seen in the prediction of the secondary flows at the exit of the bend: while the first-order Upwind predicts a single pair of counter-rotating vortices, higher-order schemes predict two pairs of counter-rotating vortices, in agreement with the measurements.

In figures 5.19 to 5.24 the comparison with the measured data is reported. The results are given as a function of the distance from the plane of symmetry normalised by the duct half-span, z^*, and of the distance from the outer wall normalised by the duct gap, r^*. The increase in accuracy obtained with higher-oreder schemes, especially in the regions of high curvature, is evident.

In figures 5.25 to 5.33 the corresponding results for the turbulent flow analysis are represented. Note that the residual values are higher than in the laminar case as non-normalised values have been plotted and the momentum at the inlet is much higher for the turbulent case. The considerations on the behaviour of GMRES, presented for the laminar case, appear to be valid also for the turbulent case.

From the analysis of the secondary flows at the exit of the bend (figure 5.32) and the comparison with the experimental data in the region of strong curvature (figure 5.33) it is evident that the use of higher-order methods, while produces a sharp increase in the accuracy of the solution for the laminar case, seems to affect the turbulent solution in a much minor way. The links between turbulence modelling and the increase in accuracy expected with higher-order schemes will be examined in detail in the next chapters, where a complete study of the turbulent flow in the bend will be presented.

The computer power available does not allow a considerable increase of the size of the grid, as necessary to study the grid independence of the solution with the presented algorithm, but the use of higher-order schemes, such as the third and fifth

order schemes used in this work, should reduce drastically such a dependence. Tamamidis and Assanis (1993), who have studied the effects of higher-order schemes on the prediction of the laminar and turbulent flow in the same 90° bend, using a standard k-ε model, have shown that grid independence is actually obtained in this case using either a third-order or a fifth-order one-dimensional convection scheme with a similar number of points in the cross sections (22×22). The results of Tamamidis and Assanis are represented in figures 5.34 to 5.36; the predicted secondary flow patterns at the exit of the bend appear to be identical to the ones presented in this thesis. In figures 5.37 and 5.38 the predicted distributions of streamwise velocities obtained with the method used in this thesis are presented in the same form adopted by Tamamidis and Assanis, so that a comparison can be made with the results displayed in figure 5.36. Further comparisons with the results of Tamamidis and Assanis can be made with the results presented at the end of the seventh chapter, where an improved turbulence model will be used for the prediction of the turbulent flow in the bend.

In section 2.5 of this thesis it has been shown how the use of the Rhie and Chow scheme to eliminate pressure oscillations can produce a solution that is dependent on the value of under-relaxation α adopted for the velocity solution. In the following table the turbulent flow streamwise and gapwise velocity profiles at 0.25 hydraulic diameters downstream of the bend exit plane for r^*=0.3, predicted using three different values of α, have been presented; the QUICK scheme and the direct solver have been used in all the cases. The solution dependence on under-relaxation appears to be minimal. All the other velocity profiles show a similar behaviour

Z^*	*Streamwise velocity*			*Gapwise velocity*		
	α = 0.2	**α = 0.15**	**α = 0.1**	**α = 0.2**	**α = 0.15**	**α = 0.1**
0.1	1.11892	1.11860	1.11882	-0.12041	-0.12044	-0.12034
0.2	1.11897	1.11885	1.11924	-0.11818	-0.11820	-0.11810
0.3	1.11972	1.11992	1.12063	-0.11389	-0.11391	-0.11380
0.4	1.12008	1.12014	1.12055	-0.10559	-0.10562	-0.10557
0.5	1.11879	1.11882	1.11877	-0.09589	-0.09590	-0.09590
0.6	1.11698	1.11705	1.11707	-0.07057	-0.07056	-0.07055
0.7	1.10773	1.10766	1.10776	-0.02538	-0.02537	-0.02539
0.8	1.08557	1.08577	1.08585	0.03715	0.03715	0.03718
0.9	1.03308	1.03307	1.03342	0.11981	0.11982	0.11978

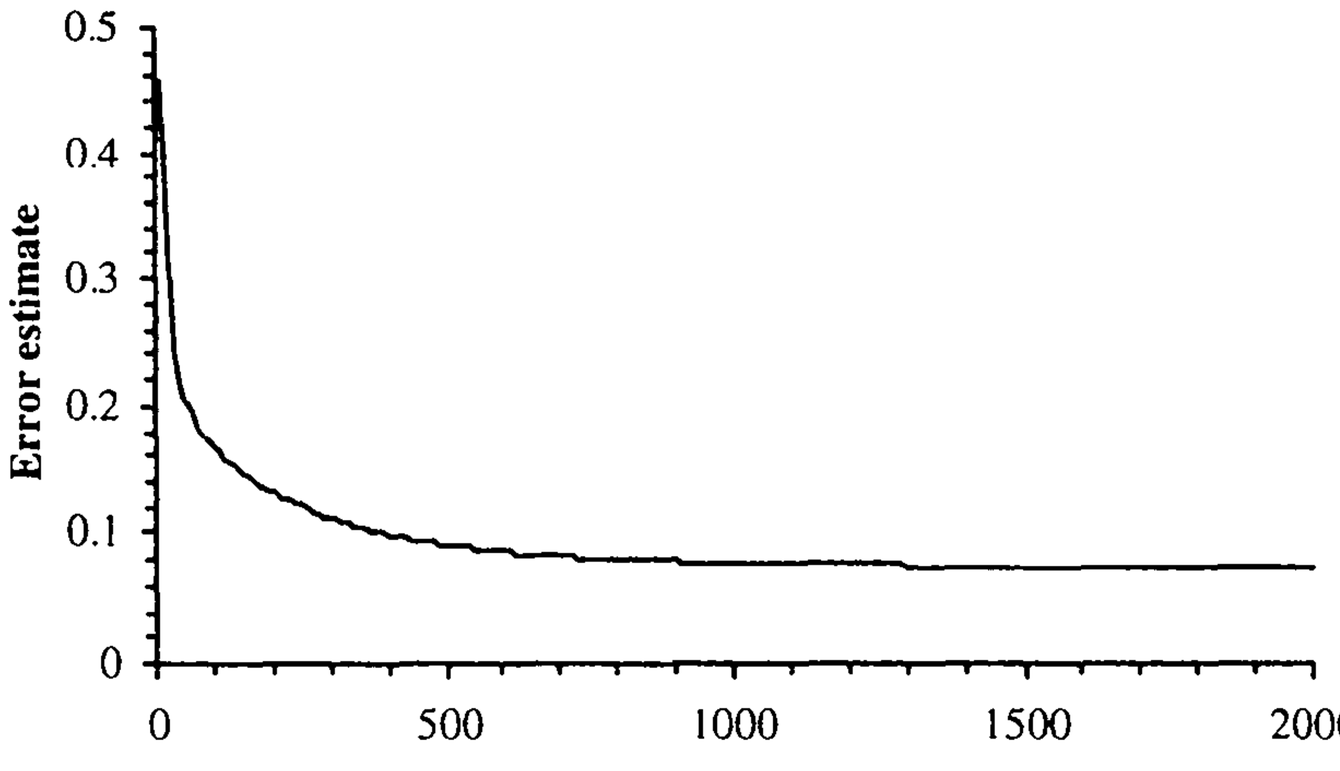

Figure 5.4 - GMRES: convergence history for the pressure correction equation in the first step of the procedure (using first-order Upwind).

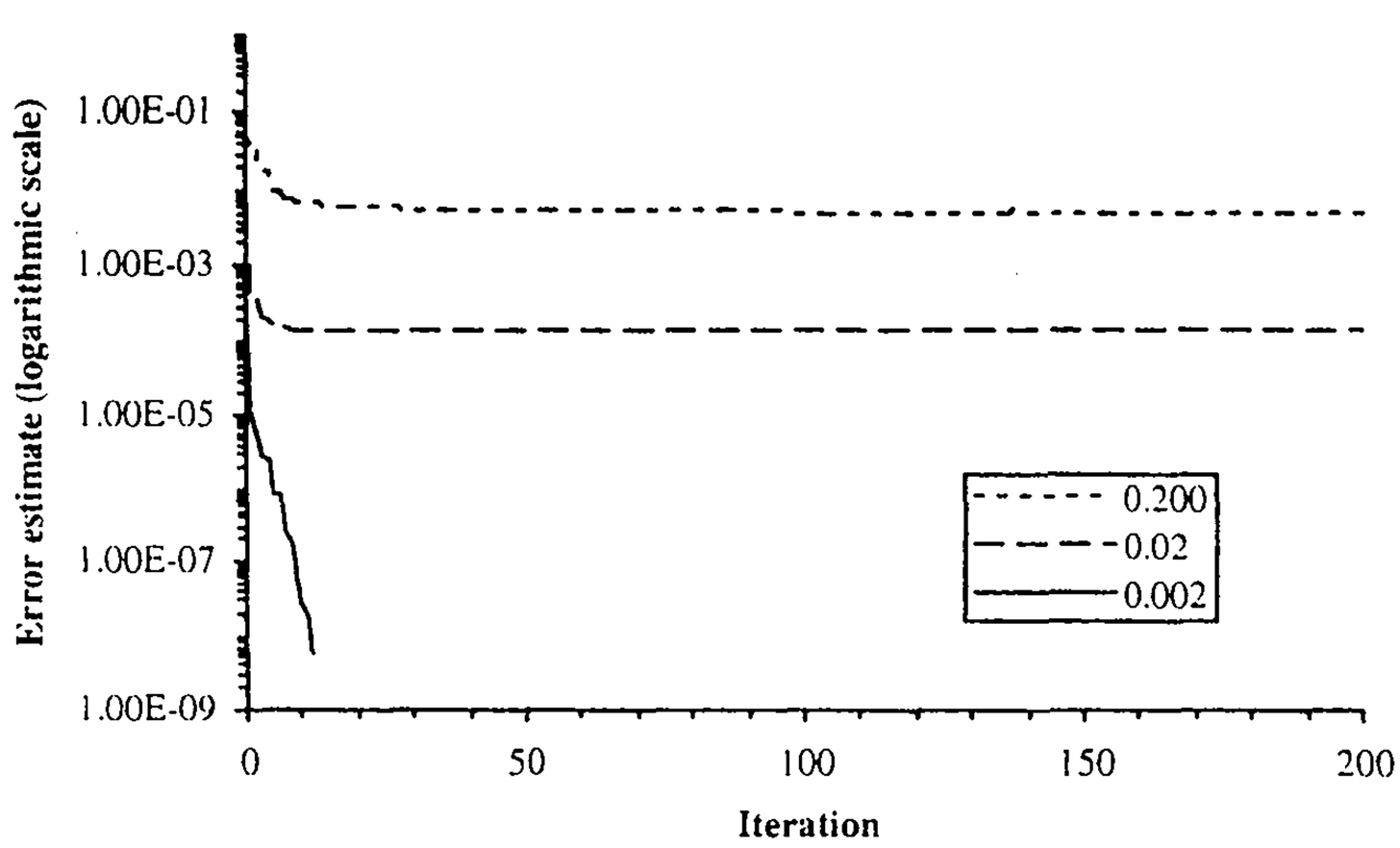

Figure 5.5 - GMRES: convergence history in the solution of the v- velocity equation using the limited DWF (using first-order Upwind) for several values of the underrelaxation factor.

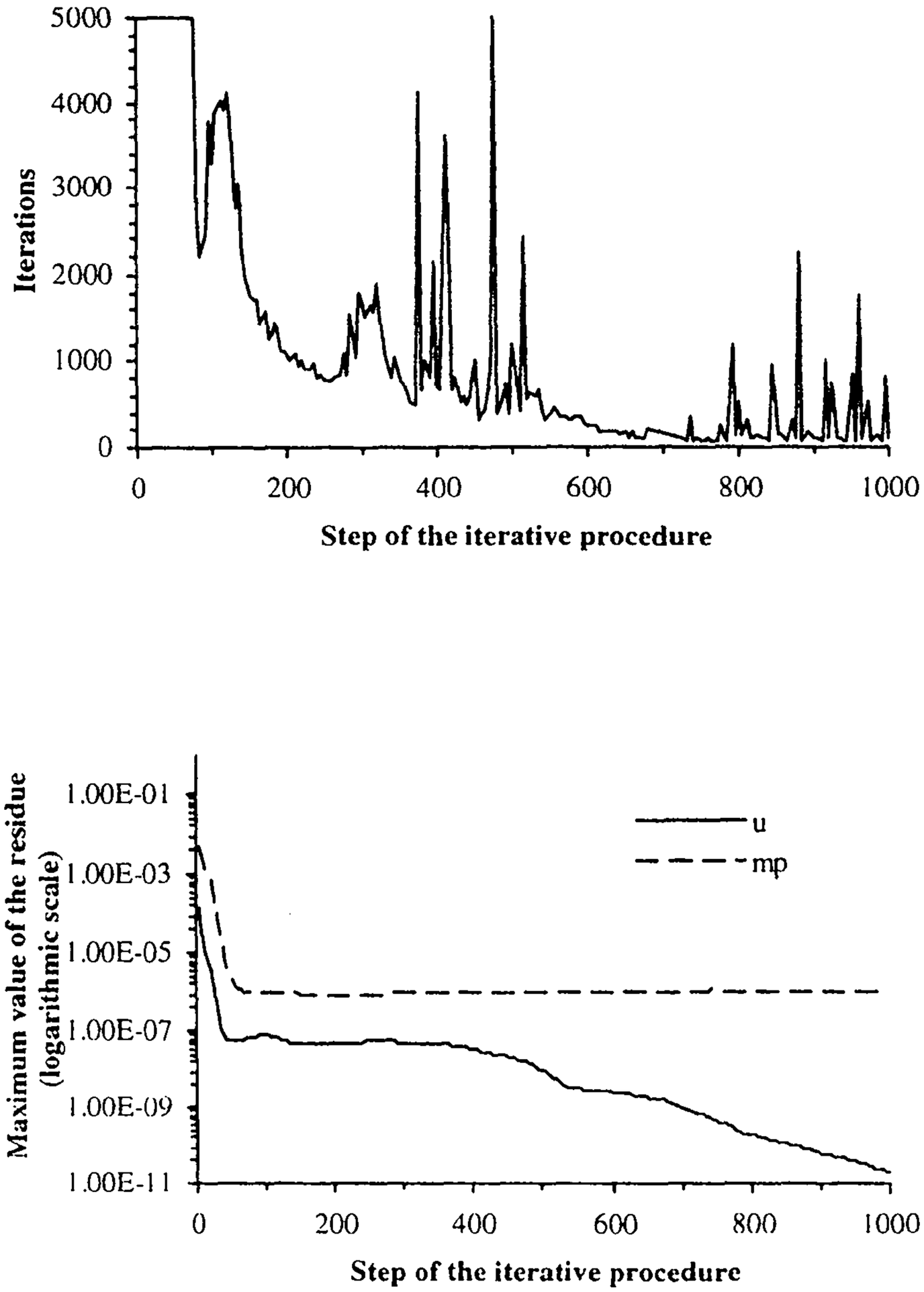

Figure 5.6 - Number of iterations of GMRES to solve the pressure correction equation (top) and convergence history of the procedure (bottom) using the ***first-order Upwind*** *scheme.*

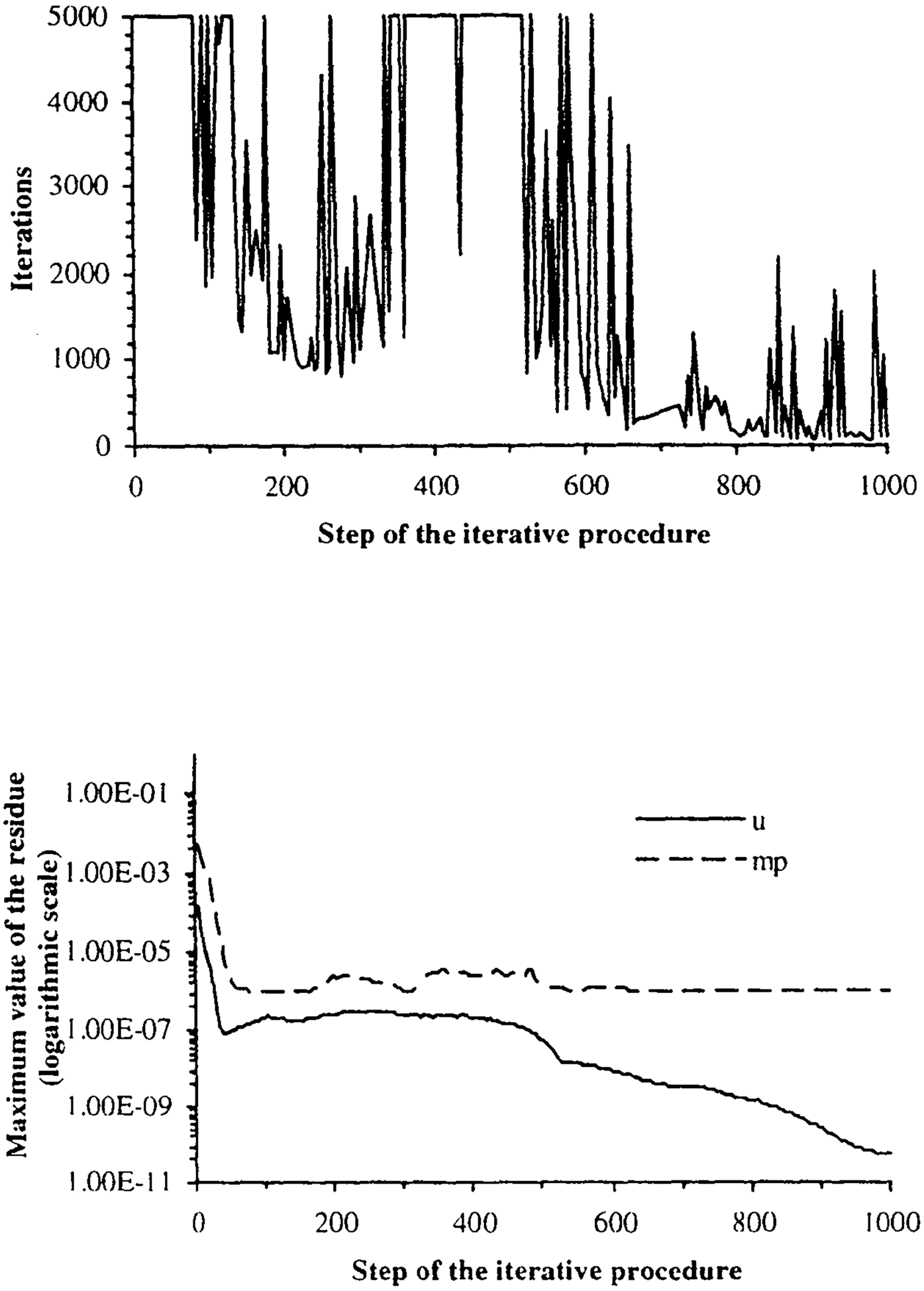

Figure 5.7 - Number of iterations of GMRES to solve the pressure correction equation (top) and convergence history of the procedure (bottom) using the ***SOUCUP*** *scheme.*

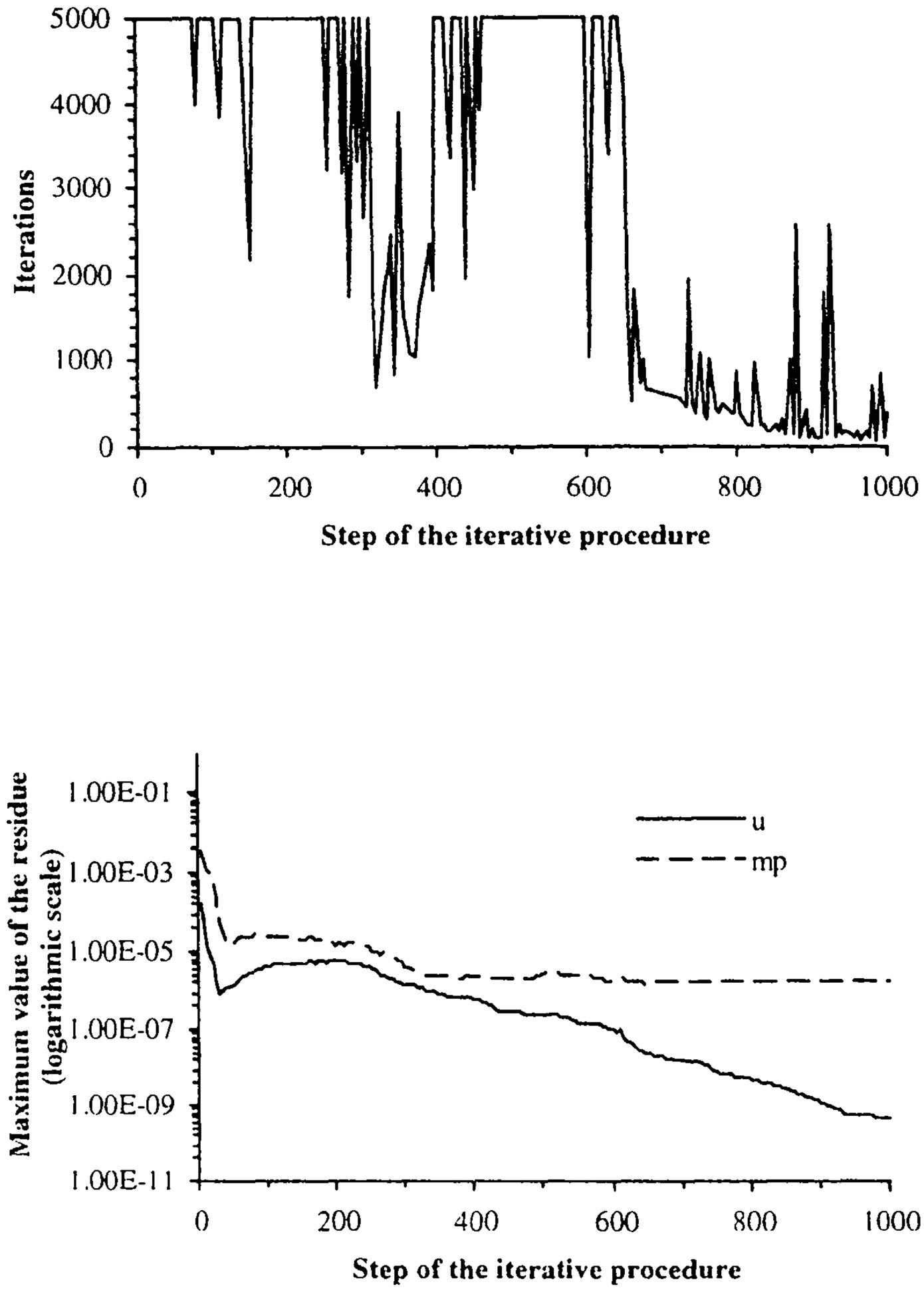

Figure 5.8 - Number of iterations of GMRES to solve the pressure correction equation (top) and convergence history of the procedure (bottom) using the three-dimensional ***QUICK*** *scheme.*

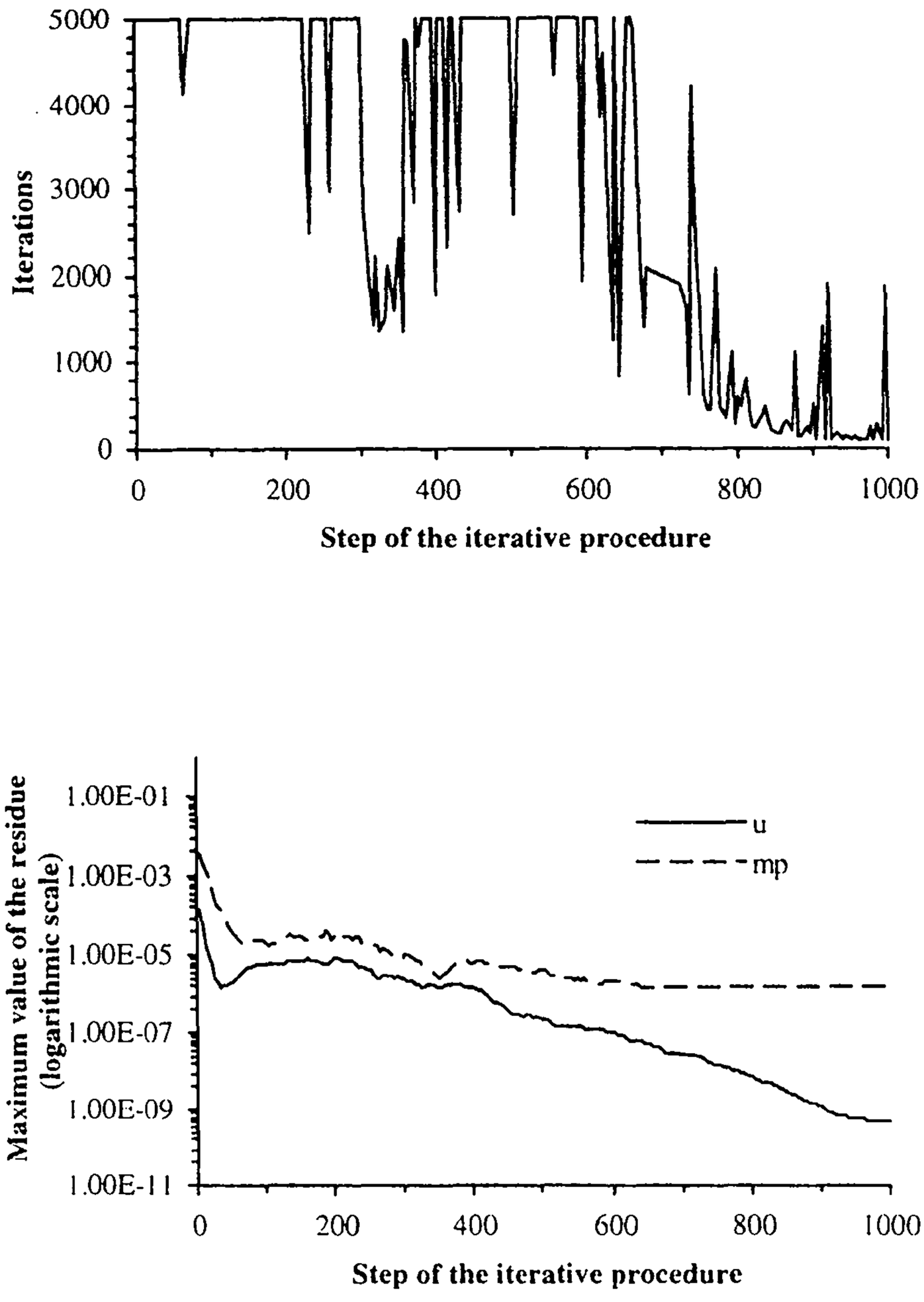

Figure 5.9 - Number of iterations of GMRES to solve the pressure correction equation (top) and convergence history of the procedure (bottom) using the one-dimensional ***fifth-order*** *scheme.*

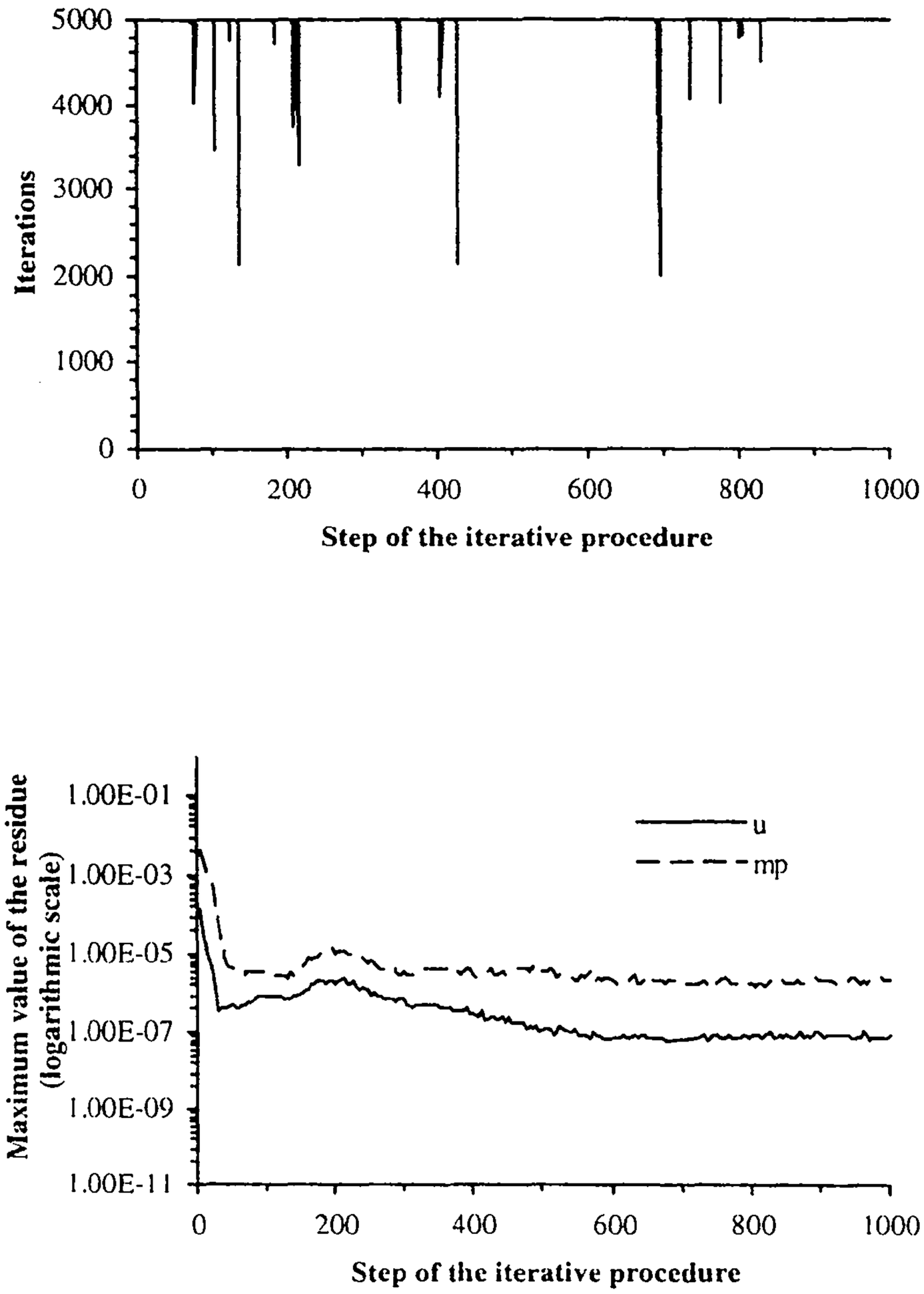

Figure 5.10 - Number of iterations of GMRES to solve the pressure correction equation (top) and convergence history of the procedure (bottom) using the three-dimensional ***QUICK*** *scheme and the* ***flux-limiter****.*

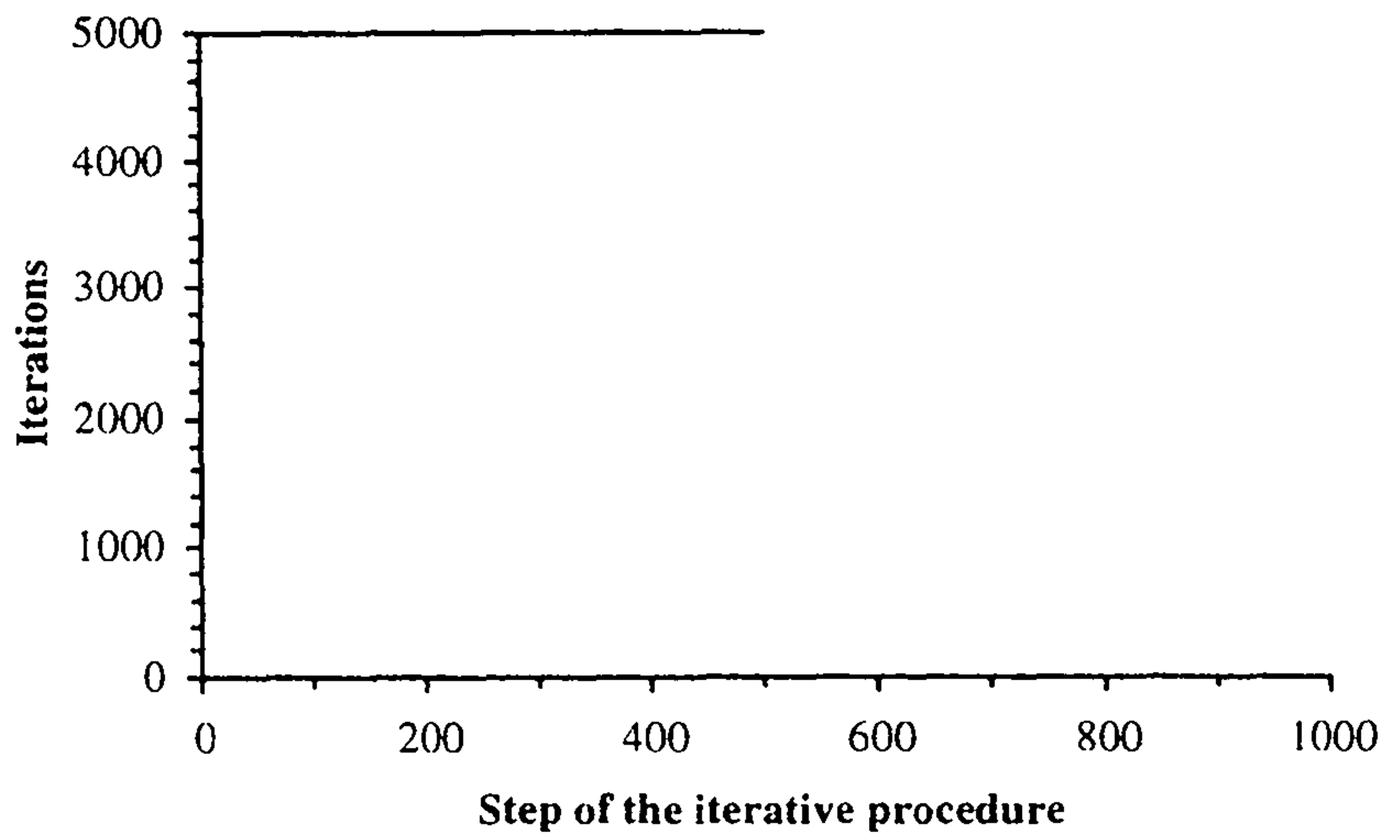

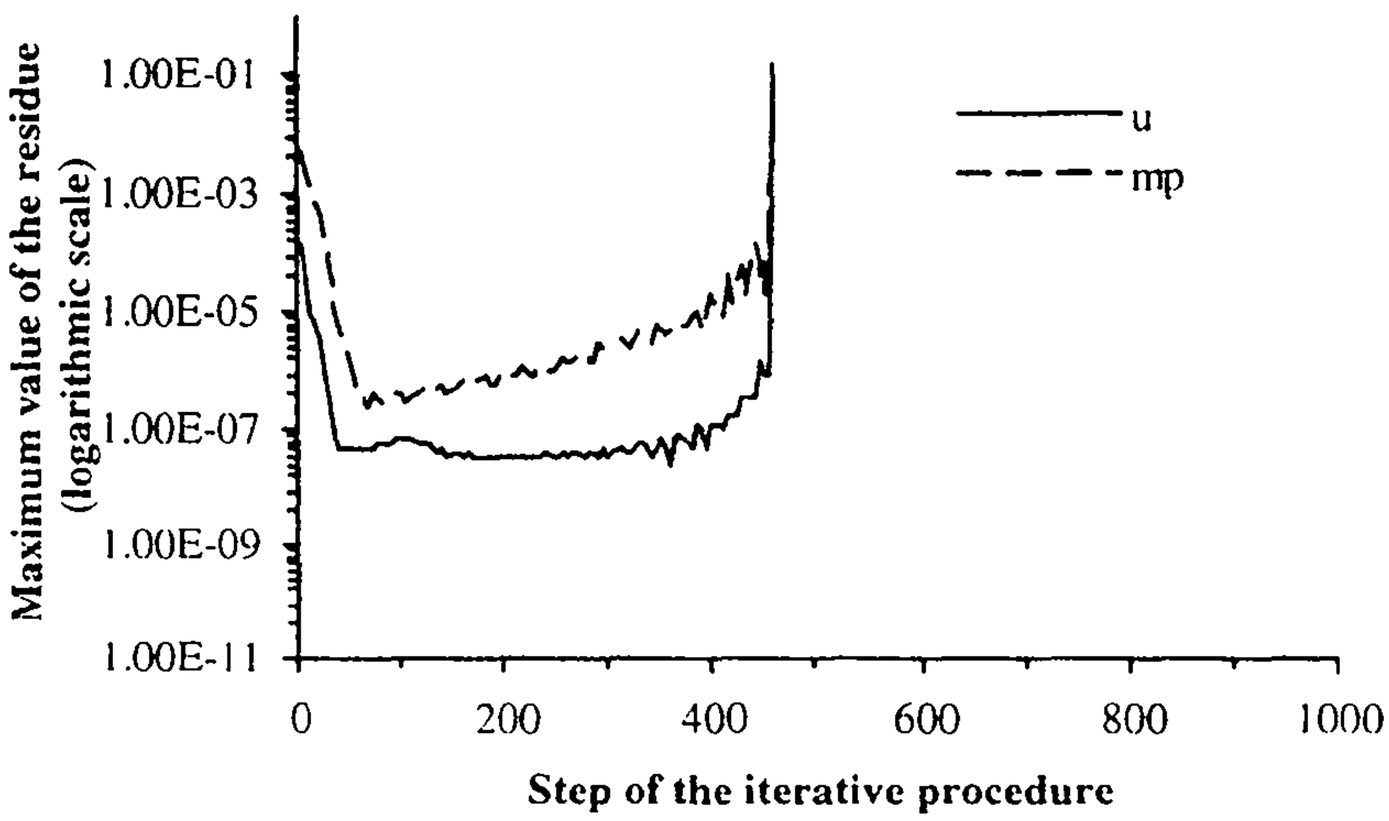

Figure 5.11 - Number of iterations of GMRES to solve the pressure correction equation (top) and convergence history of the procedure (bottom) using the ***first-order Upwind*** *and* ***a constant pressure for the boundary condition at the outlet.***

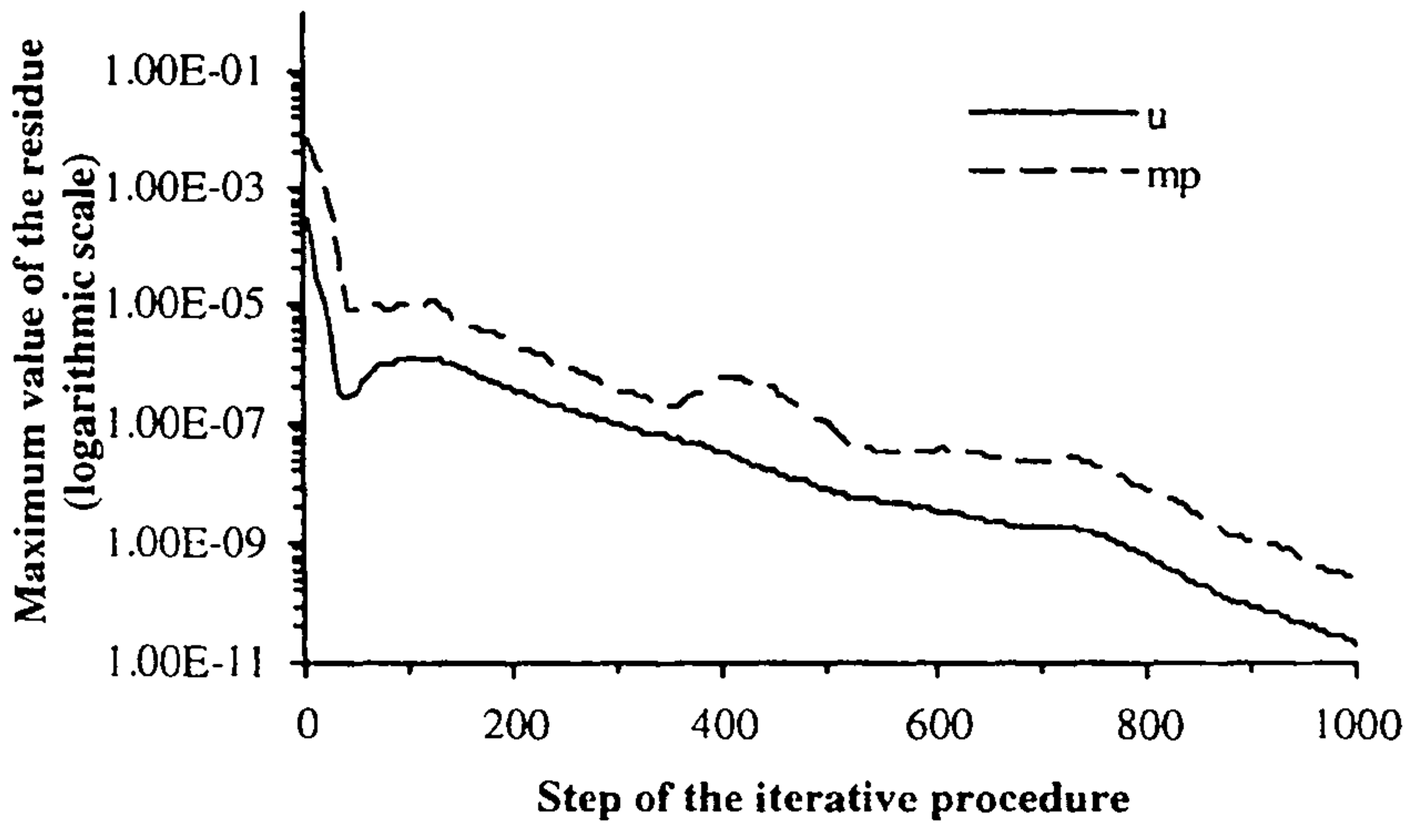

*Figure 5.12 - Convergence history of the procedure using a **direct solver** for the solution of the pressure correction equation, and a first-order Upwind.*

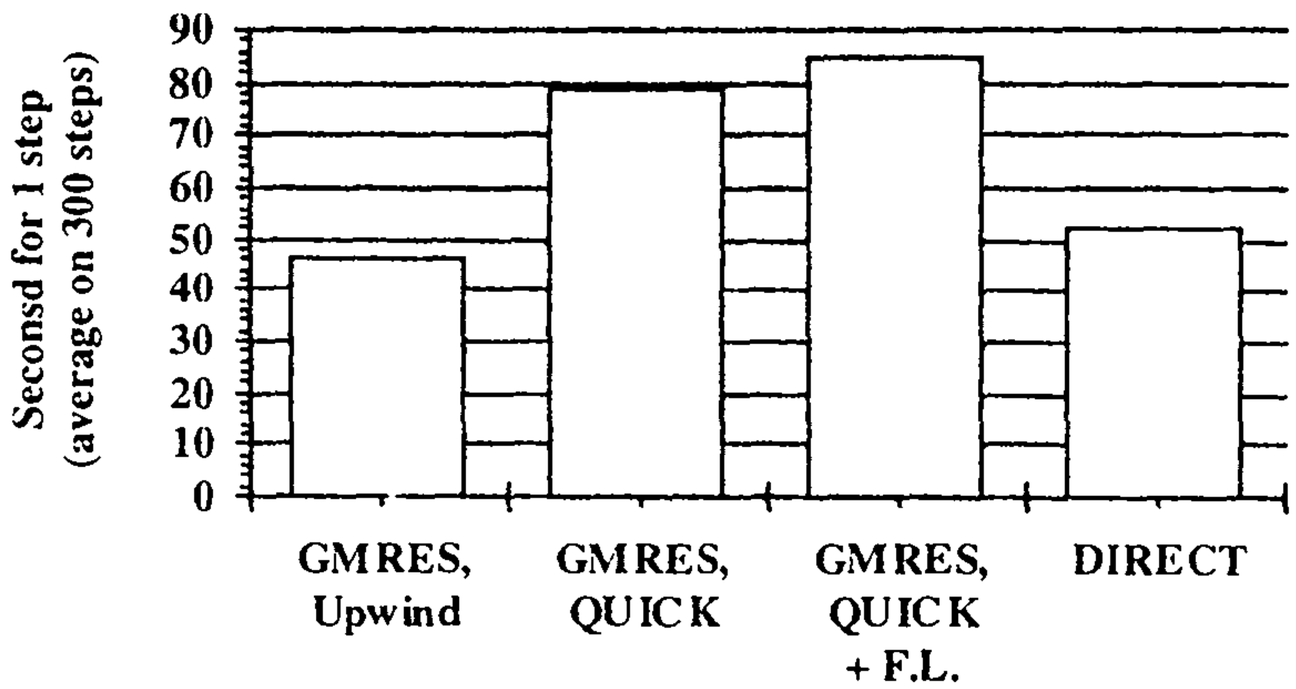

Figure 5.13 - Number of seconds for a single step of the solution procedure (averaged on 300 steps) on a Cray J90.

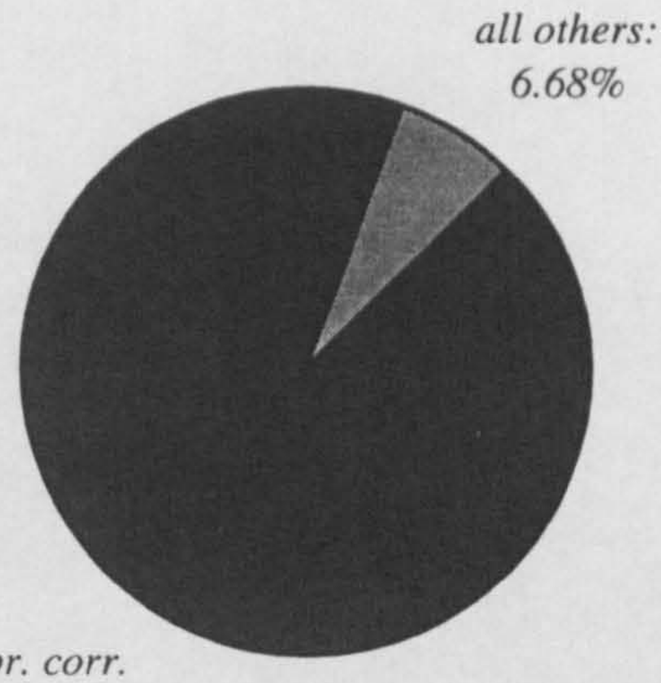

Figure 5.14 - Percentage of CPU time used by the routine for the solution of the pressure correction equation and all the others routines, using ***GMRES*** *and the first-order Upwind scheme (for 300 steps).*

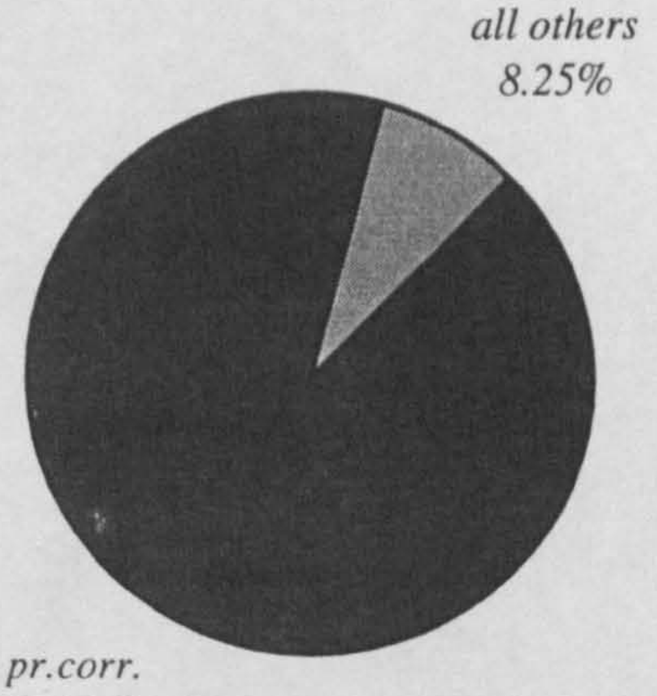

Figure 5.15 - Percentage of CPU time used by the routine for the solution of the pressure correction equation and all the others routines, using the ***direct*** *solver and the first-order Upwind scheme (for 300 steps).*

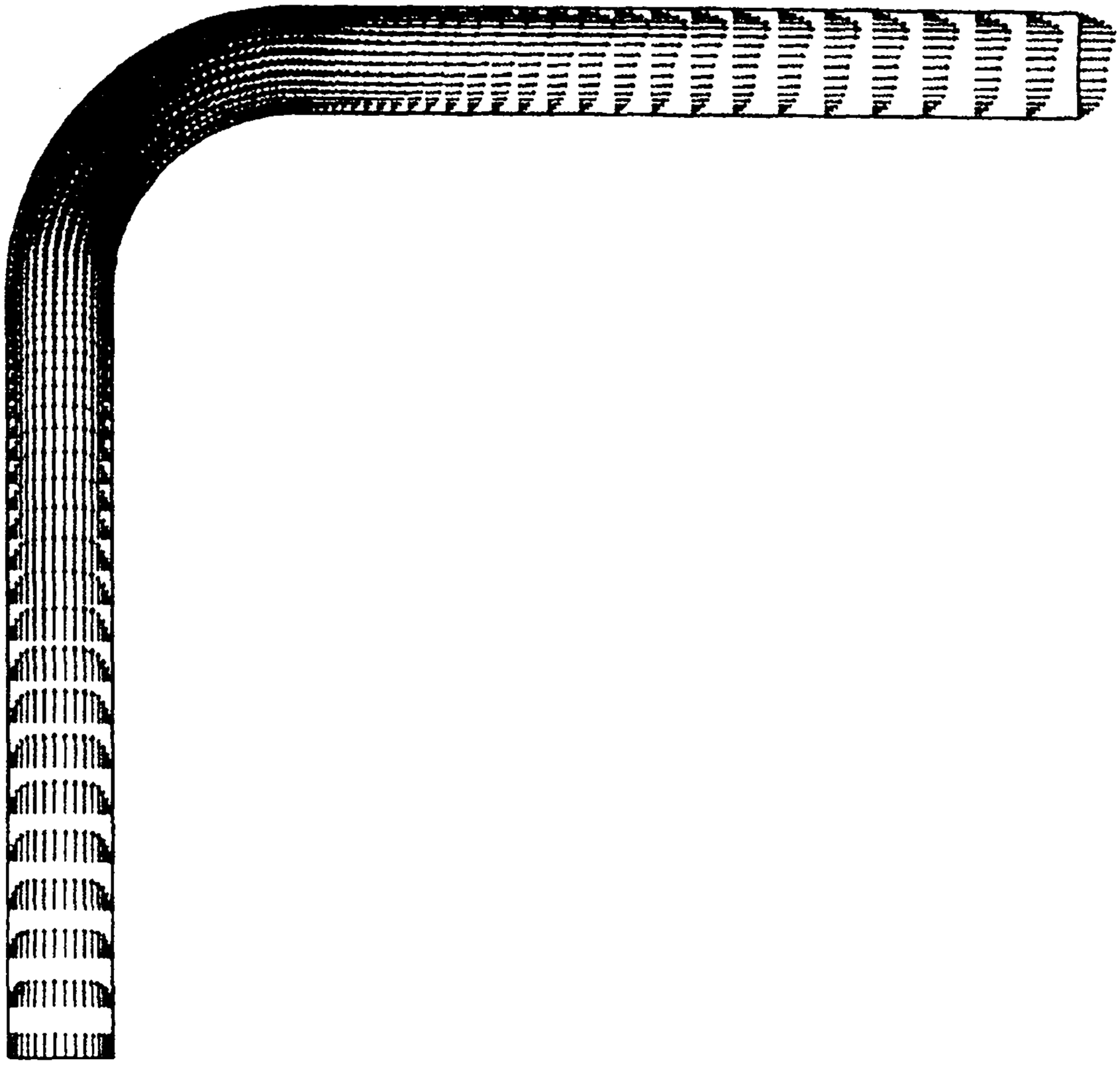

Figure 5.16 - First-order Upwind, laminar case: velocity in the symmetry plane.

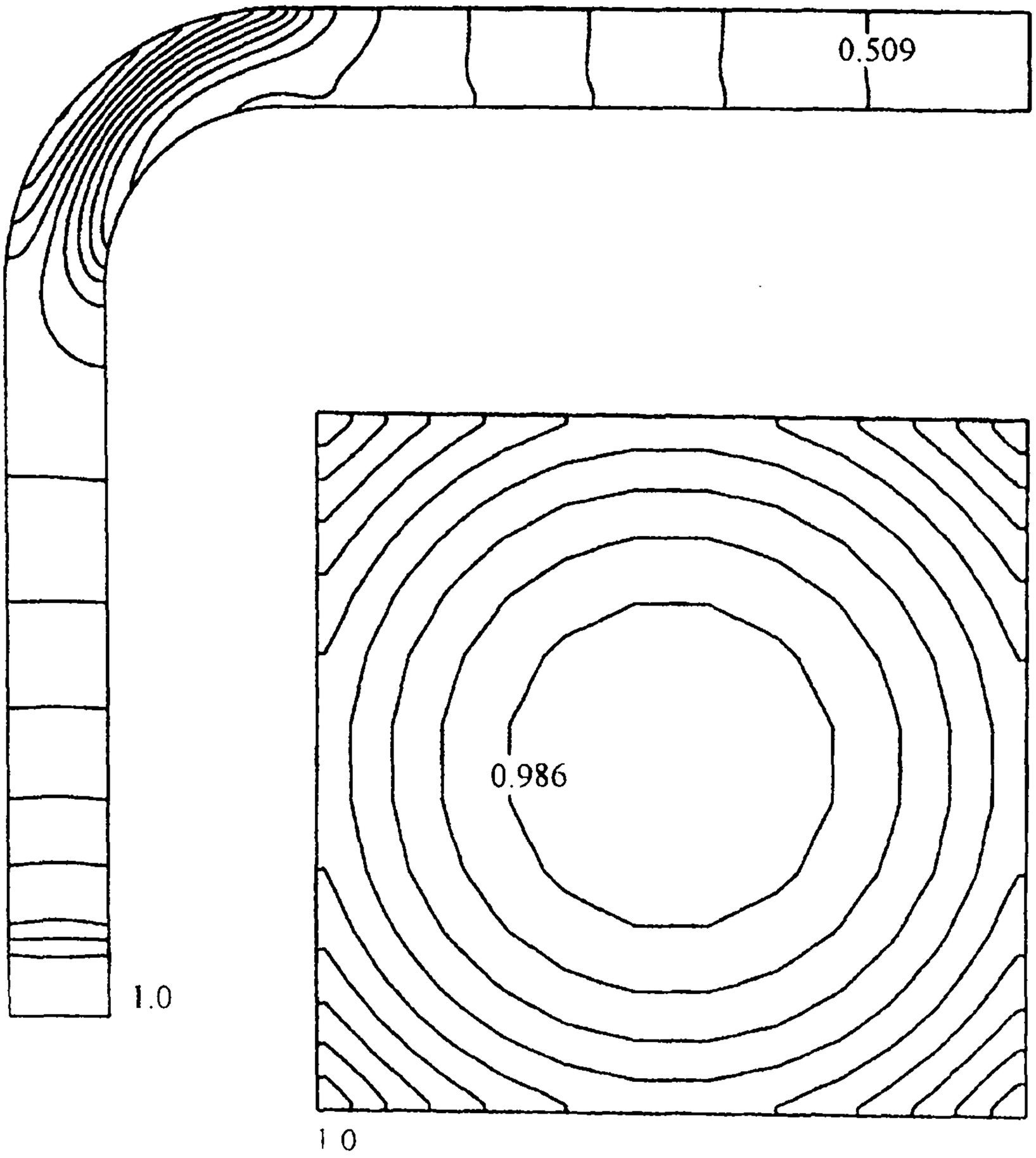

Figure 5.17 - First-order Upwind, laminar case: pressure in the symmetry plane and pressure at the inlet plane.

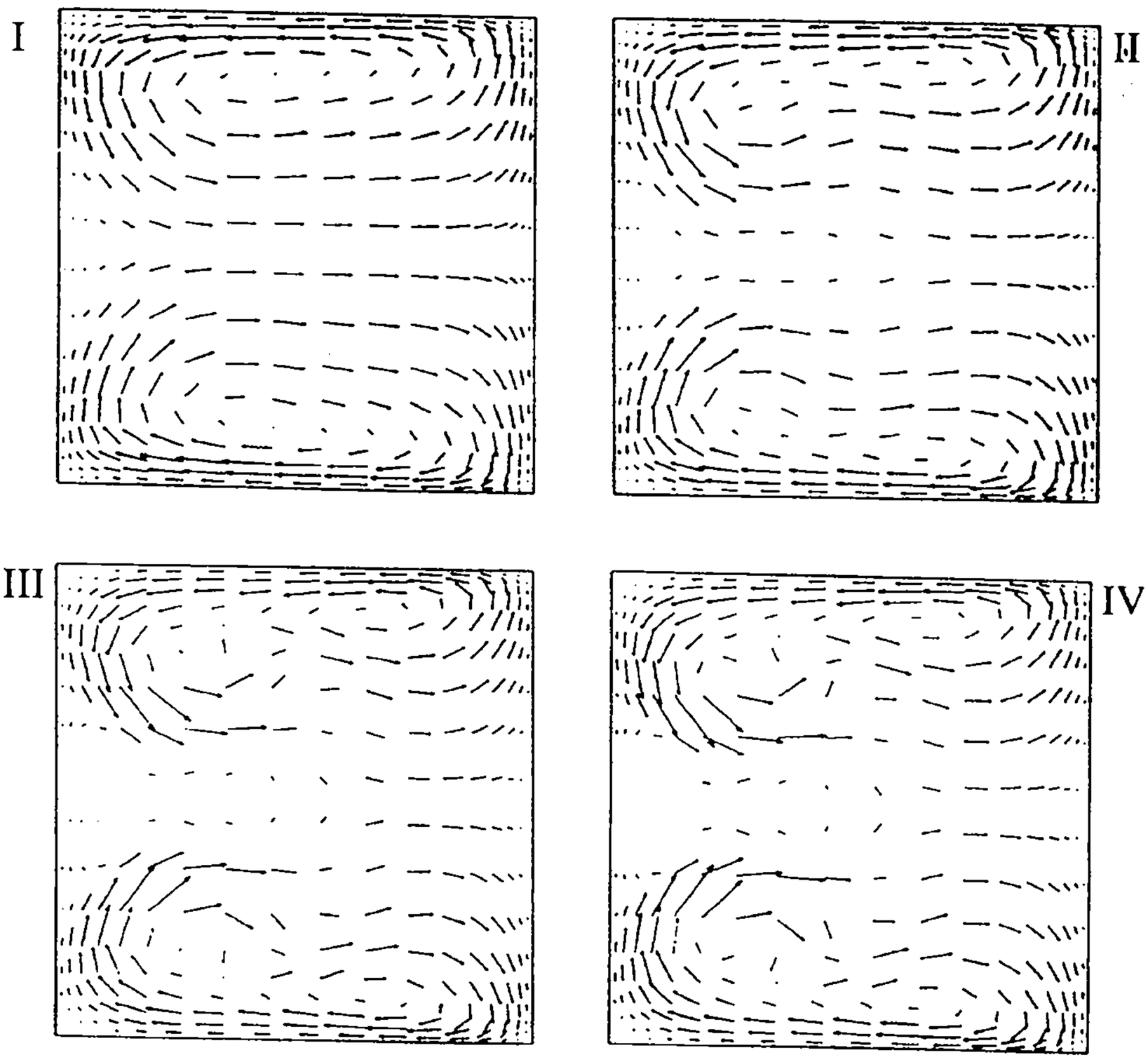

Figure 5.18 -Laminar flow: secondary velocity at the exit of the bend using (I) first-order Upwind,(II) SOUCUP, (III) QUICK and (IV) the one-dimensional fifth-order Upwind.

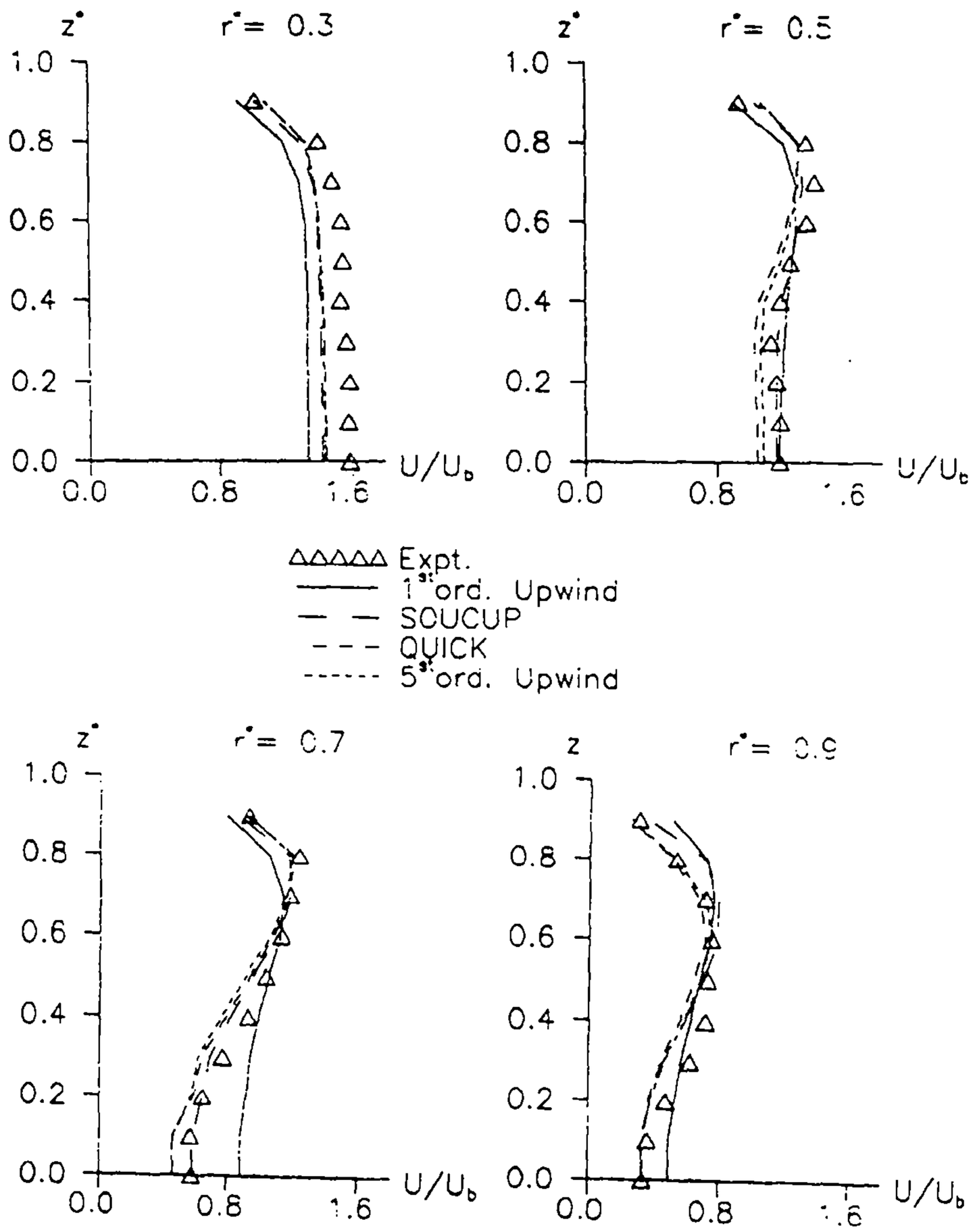

Figure 5.19 - Laminar case: streamwise velocity at 60° from the bend entry plane, comparison with experimental measurements.

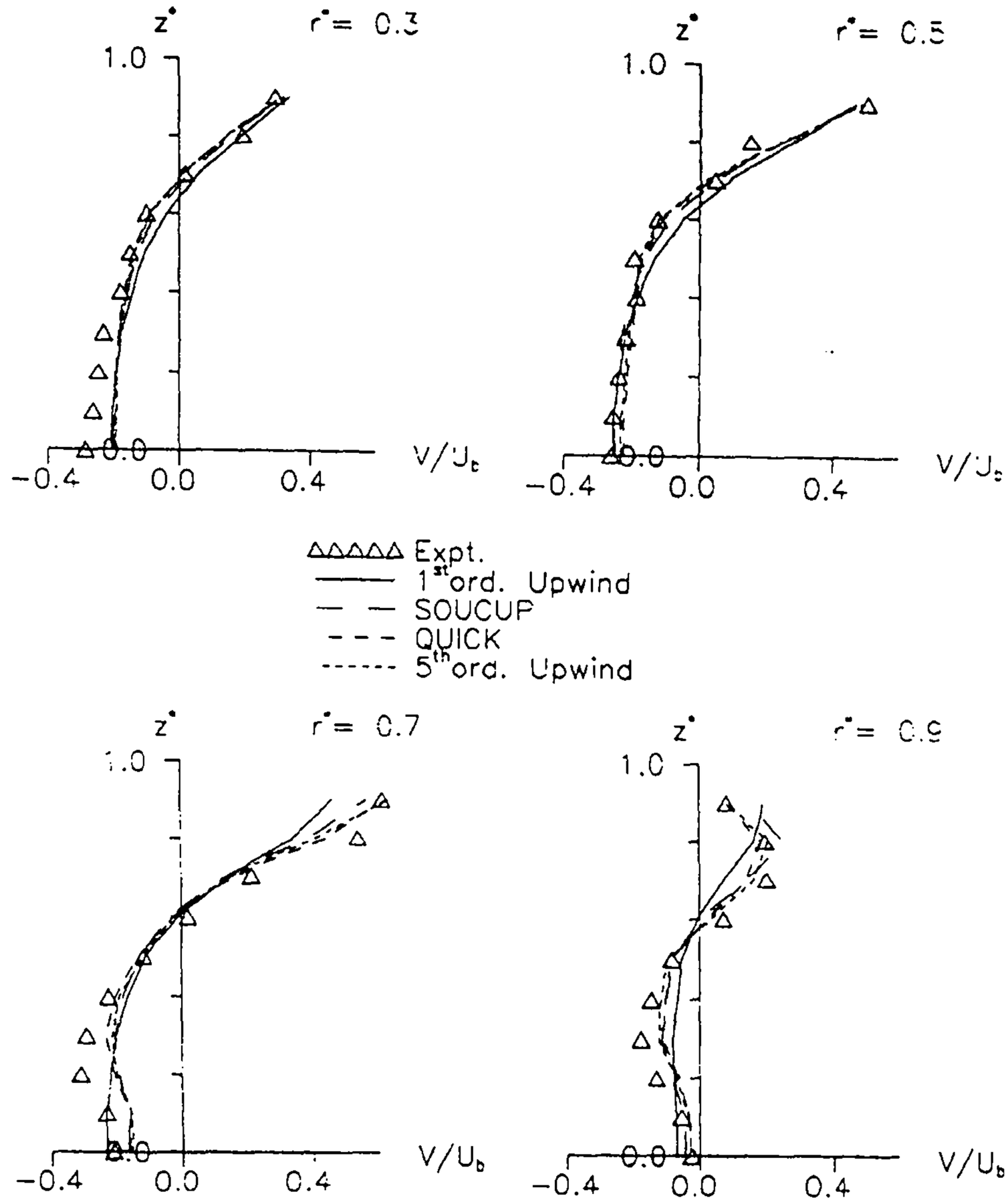

Figure 5.20 - Laminar case: gapwise velocity at 60° from the bend entry plane, comparison with experimental measurements.

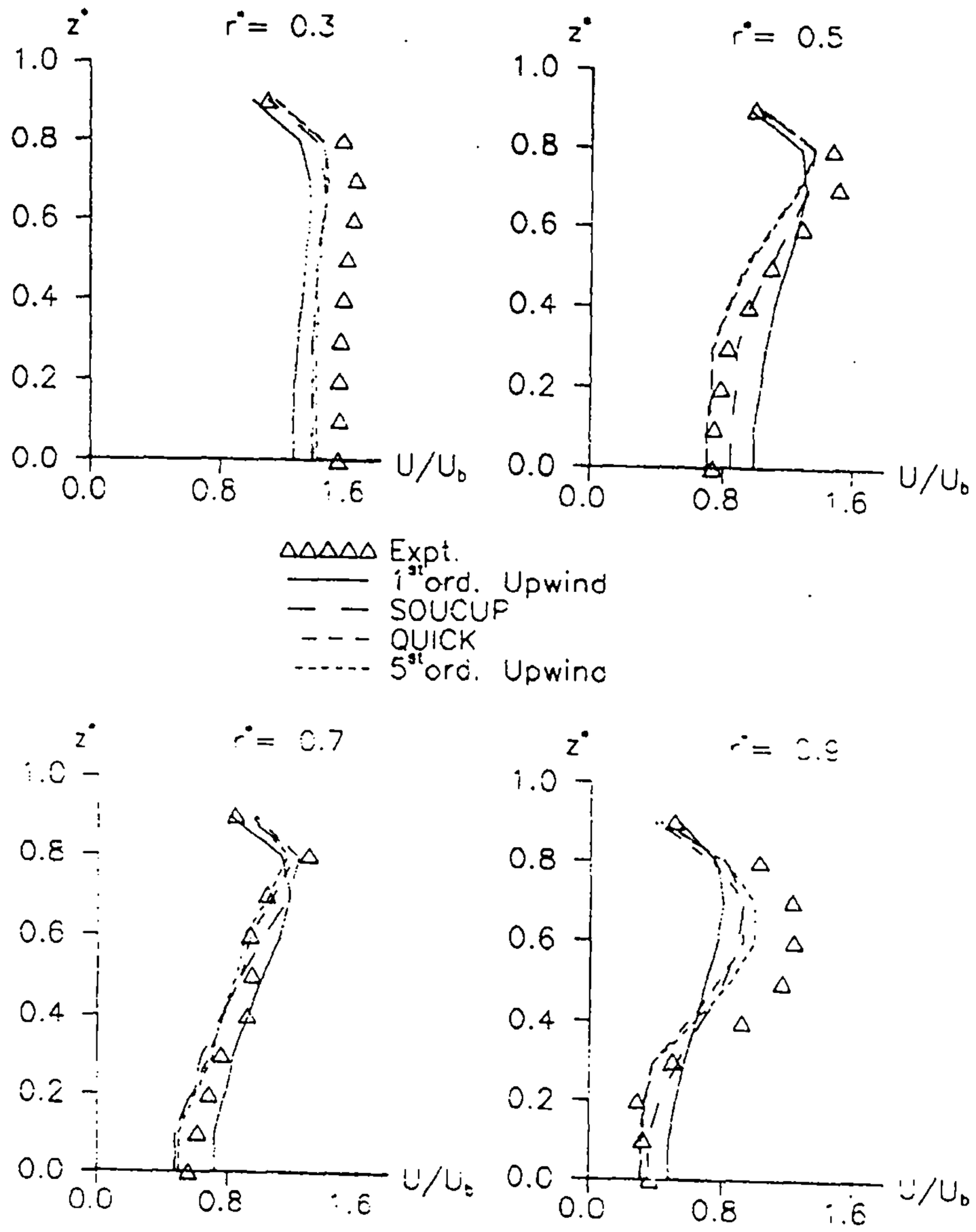

Figure 5.21 - Laminar case: streamwise velocity at 77.5° from the bend entry plane, comparison with experimental measurements.

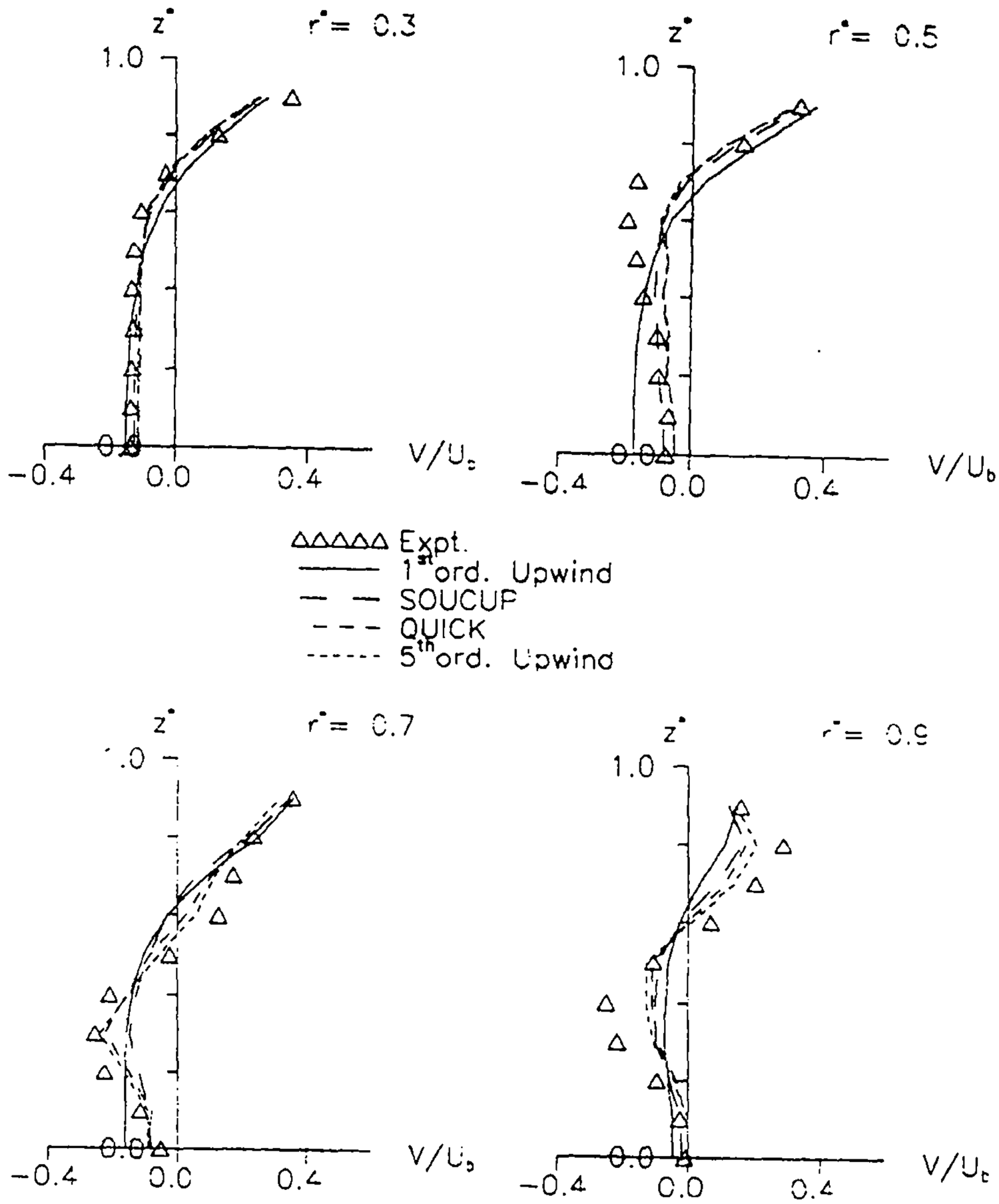

Figure 5.22 - Laminar case: gapwise velocity at 77.5° from the bend entry plane, comparison with experimental measurements.

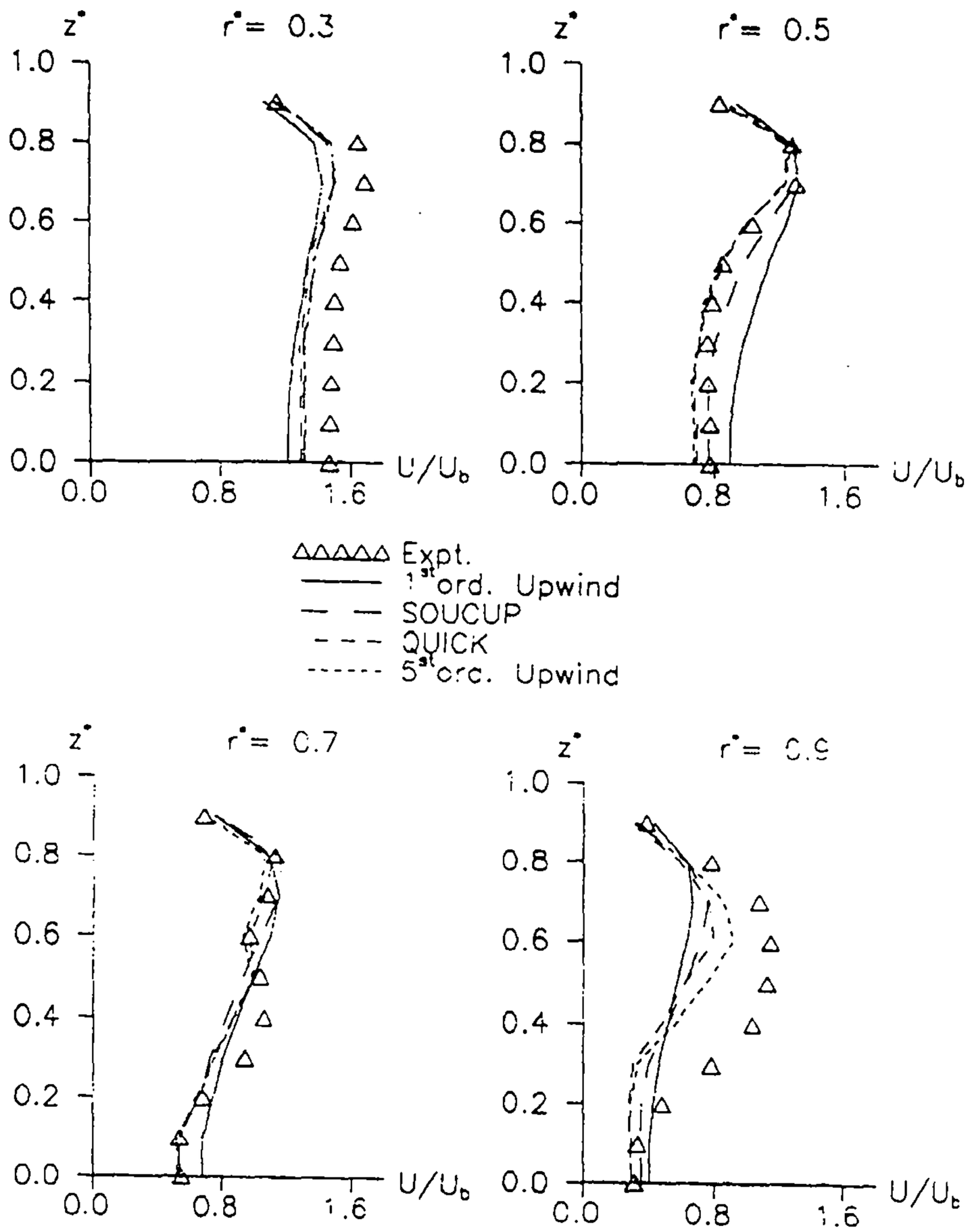

Figure 5.23 - Laminar case: streamwise velocity at 0.25 hydraulic diameters downstream of the bend exit plane, comparison with experimental measurements.

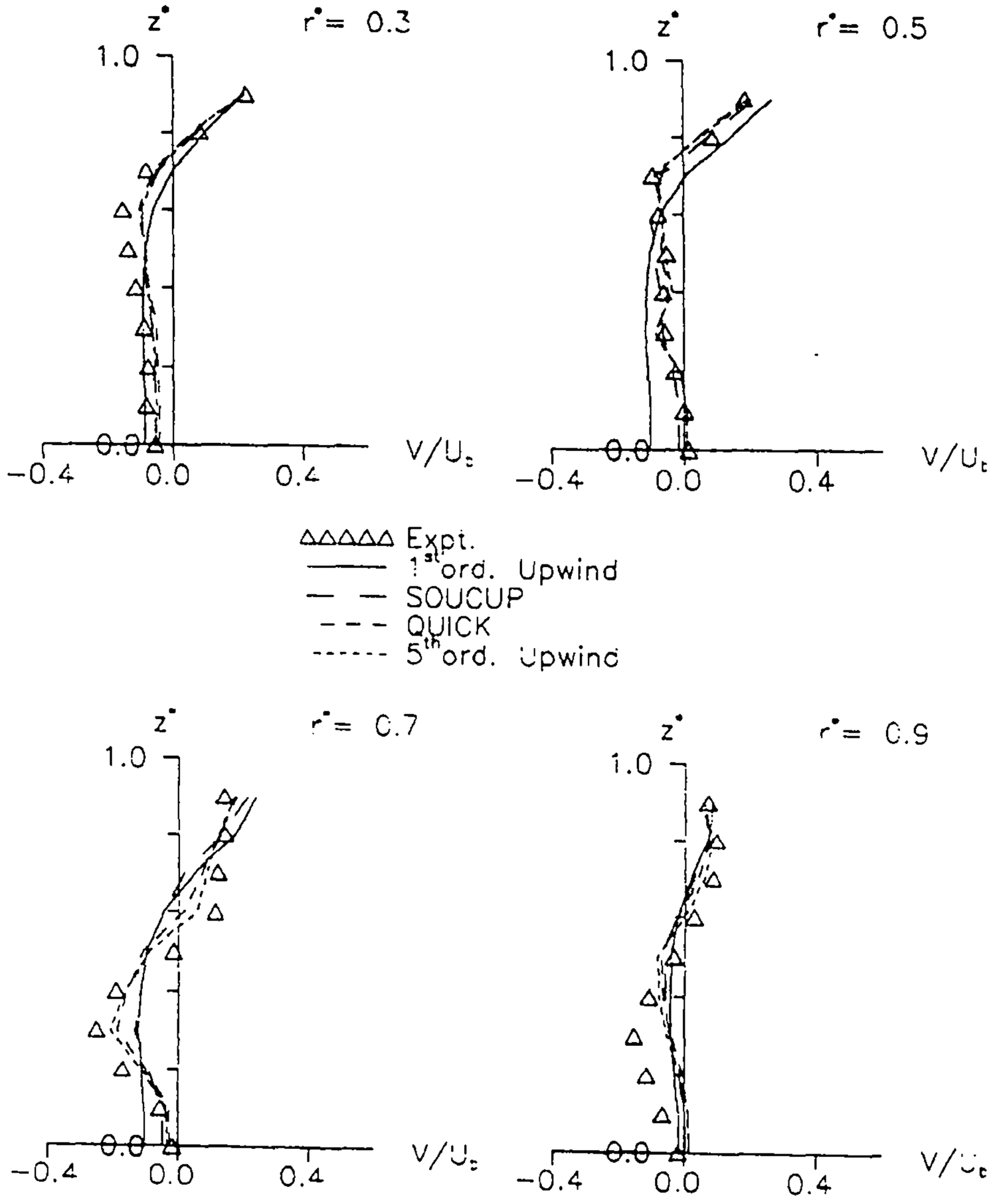

Figure 5.24 - Laminar case: gapwise velocity at 0.25 hydraulic diameters downstream of the bend exit plane, comparison with experimental measurements.

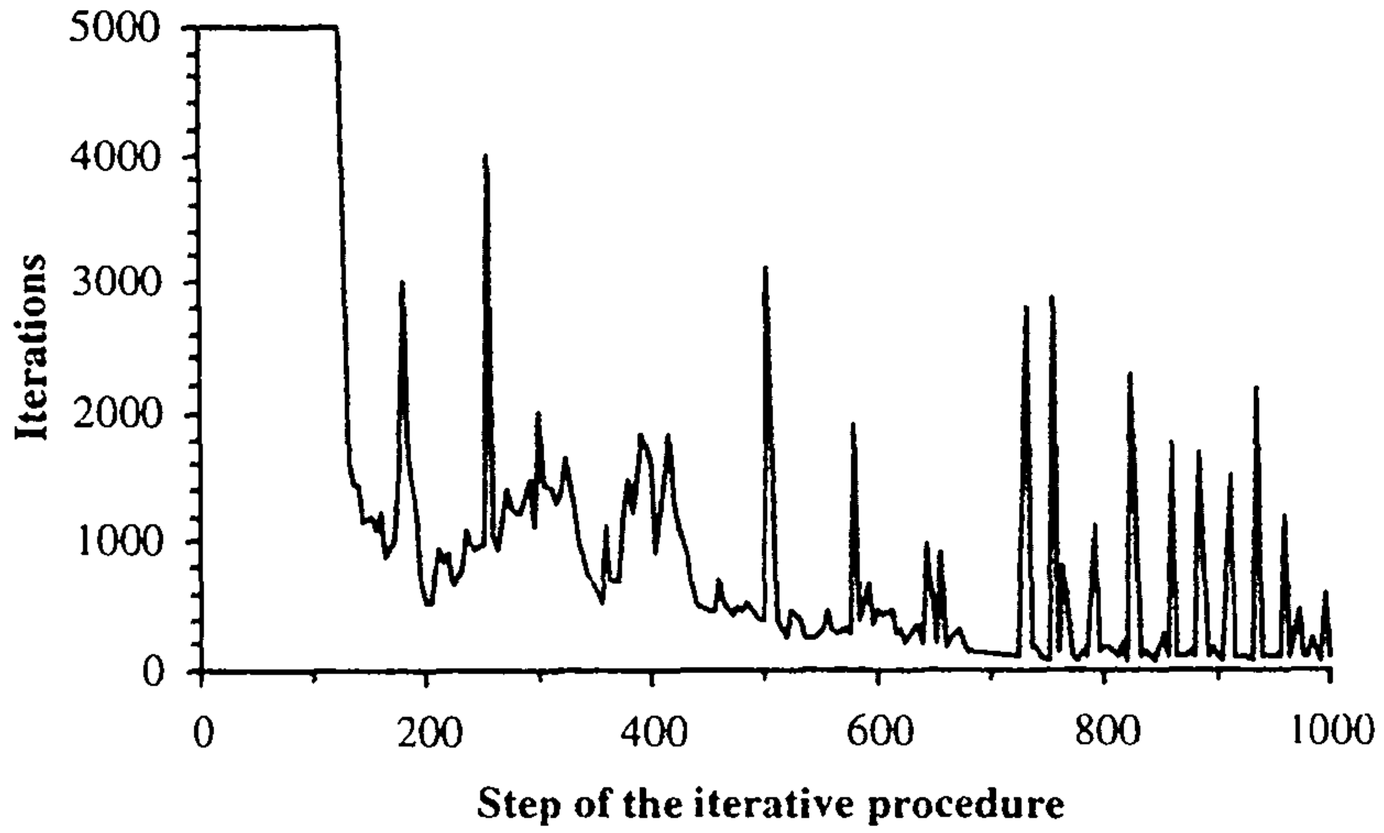

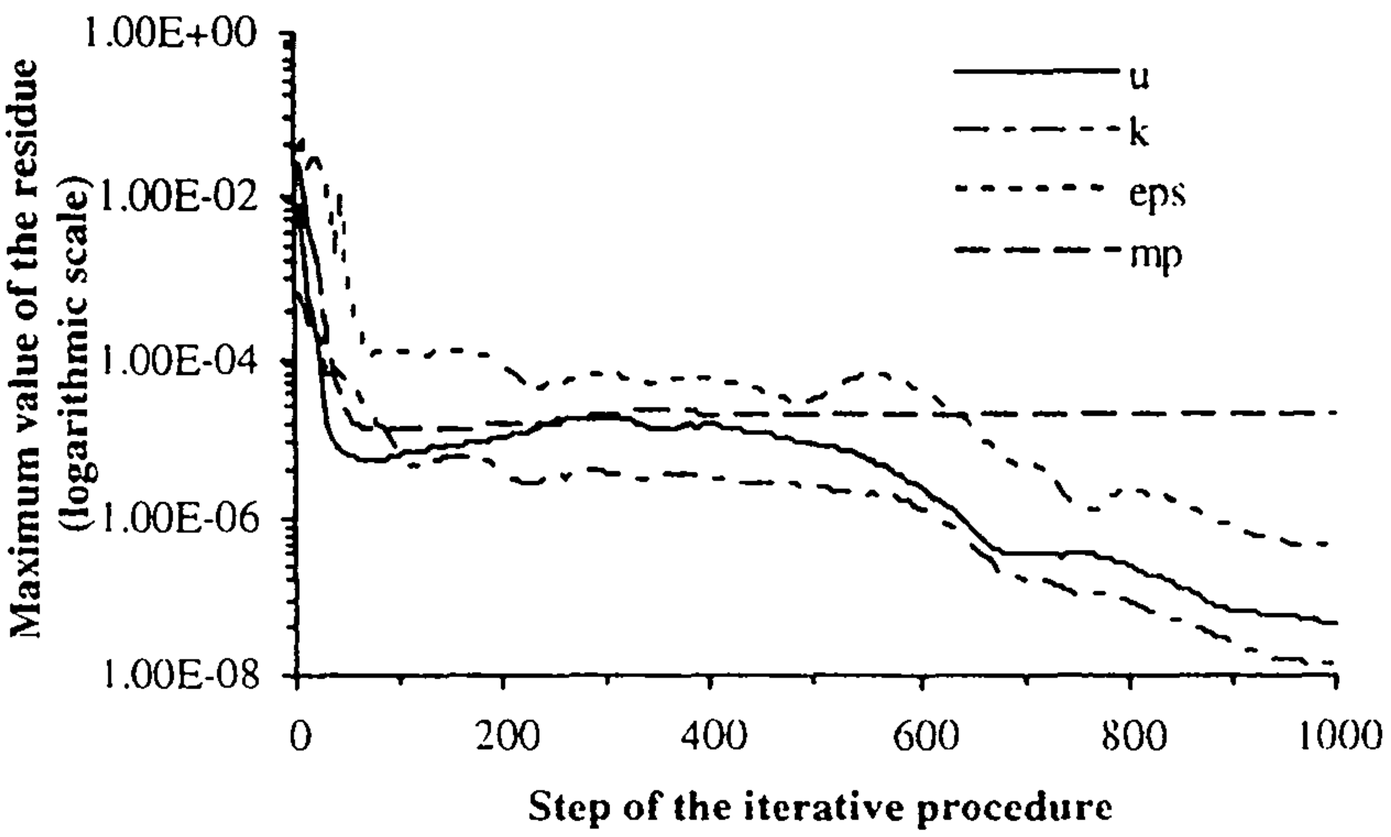

Figure 5.25 - Turbulent flow: number of iterations of GMRES to solve the pressure correction equation (top) and convergence history of the procedure (bottom) using the ***first-order Upwind*** *scheme.*

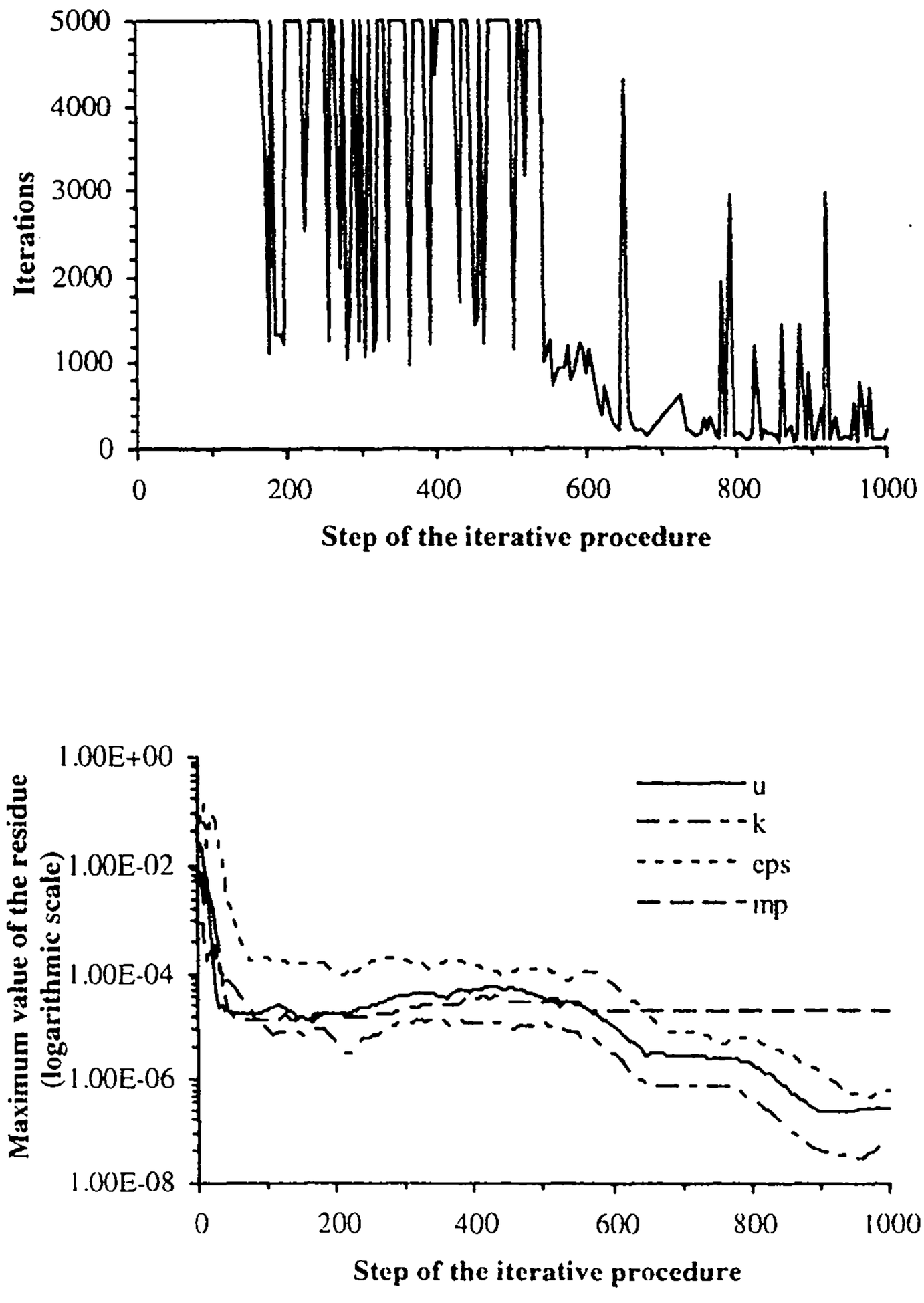

Figure 5.26 - Turbulent flow: number of iterations of GMRES to solve the pressure correction equation (top) and convergence history of the procedure (bottom) using the ***SOUCUP*** *scheme.*

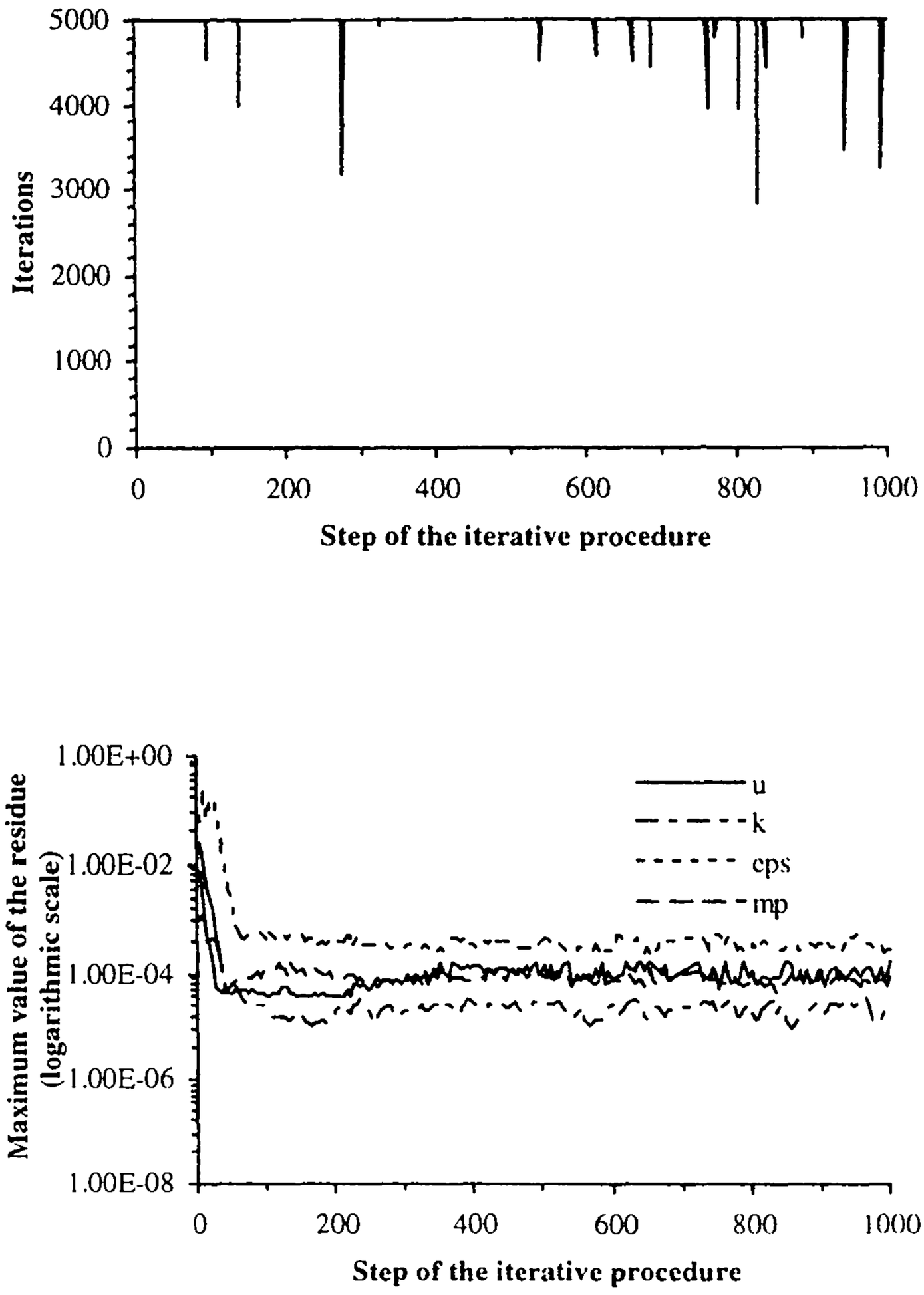

*Figure 5.27 - Turbulent flow: number of iterations of GMRES to solve the pressure correction equation (top) and convergence history of the procedure (bottom) using the three-dimensional **QUICK** scheme and the **flux-limiter**.*

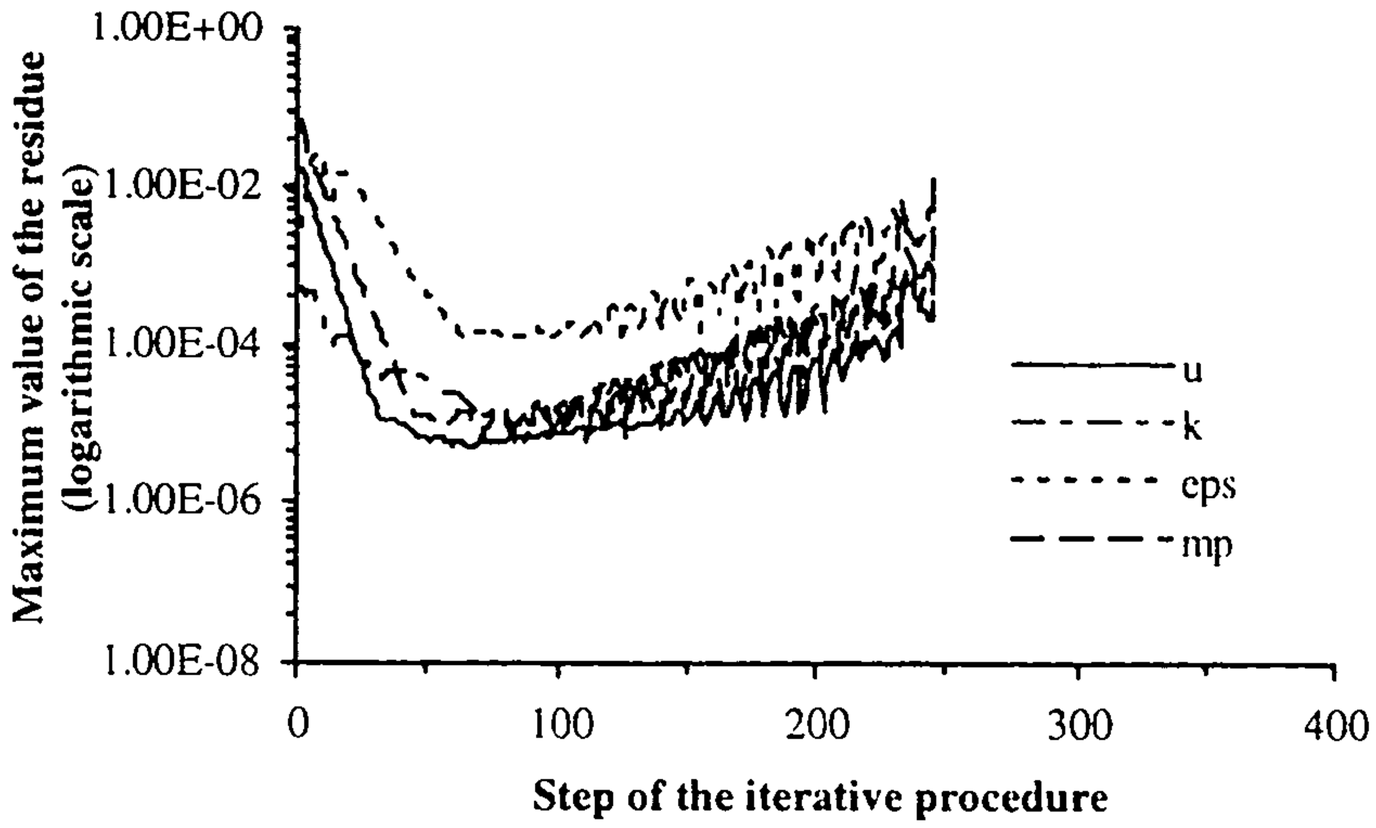

Figure 5.28 - Turbulent flow: convergence history of the procedure using ***GMRES****, the* ***first-order Upwind*** *and* ***a constant pressure for the boundary condition at the outlet****.*

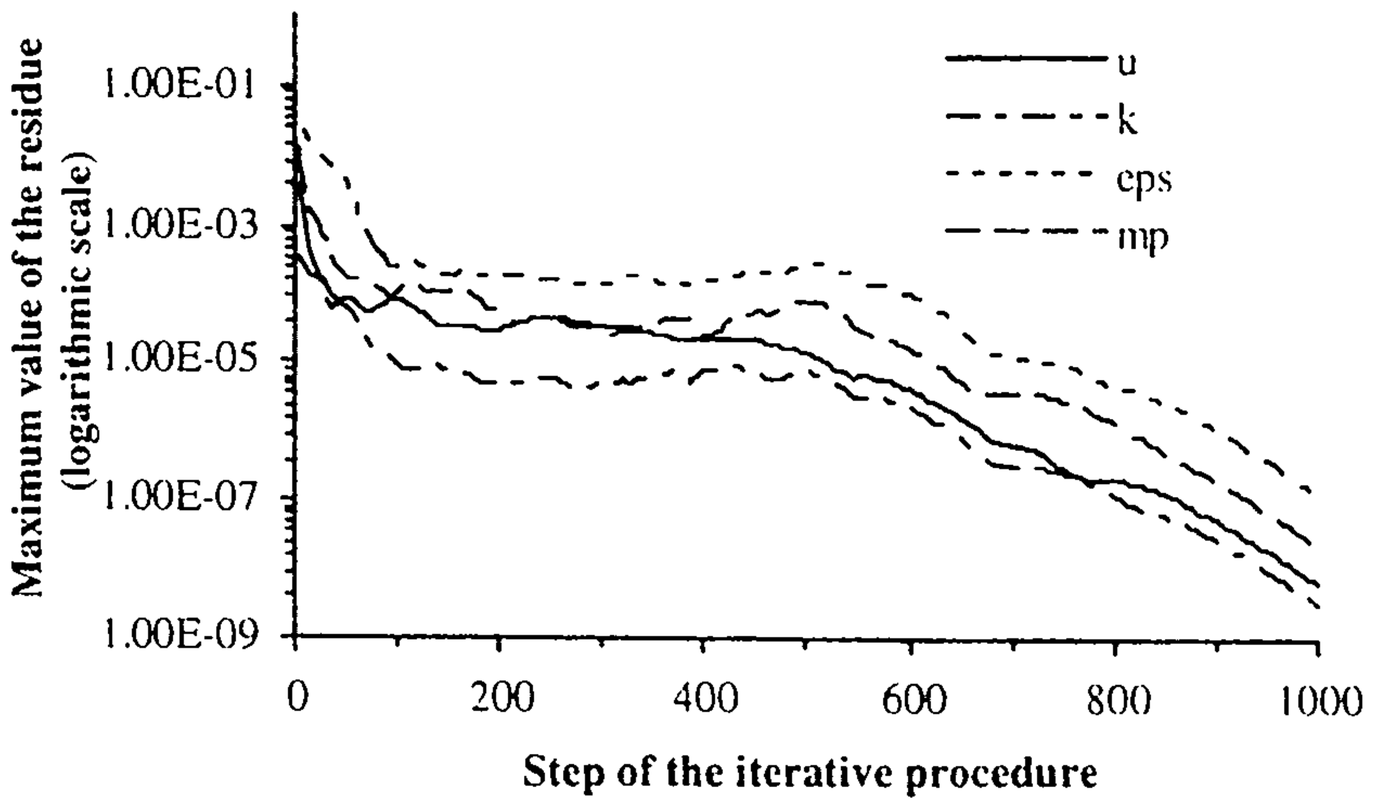

Figure 5.29 - Turbulent flow: convergence history of the procedure using a ***direct solver*** *for the solution of the pressure correction equation, and a first-order Upwind.*

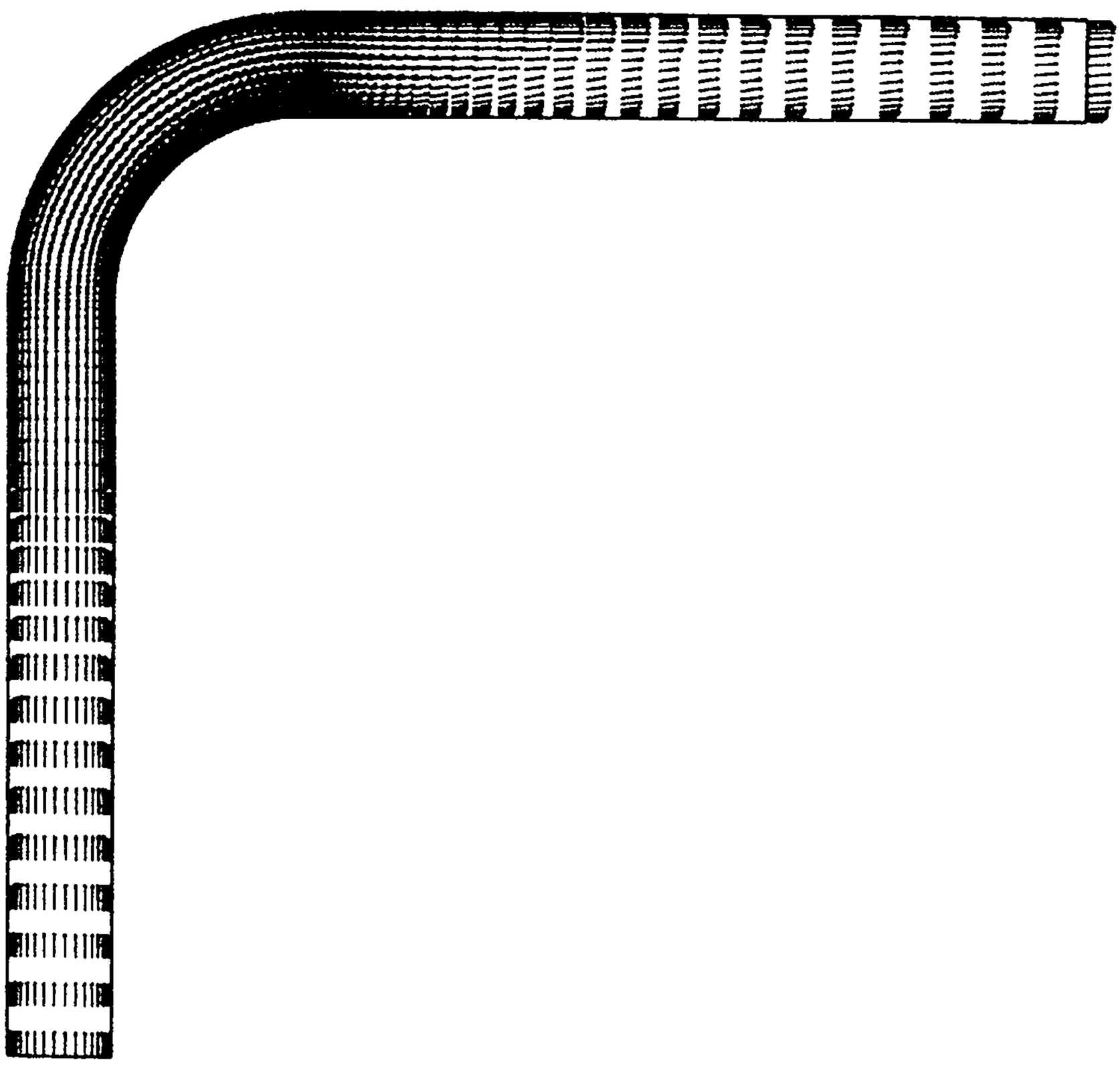

Figure 5.30 - First-order Upwind, turbulent case: velocity in the symmetry plane.

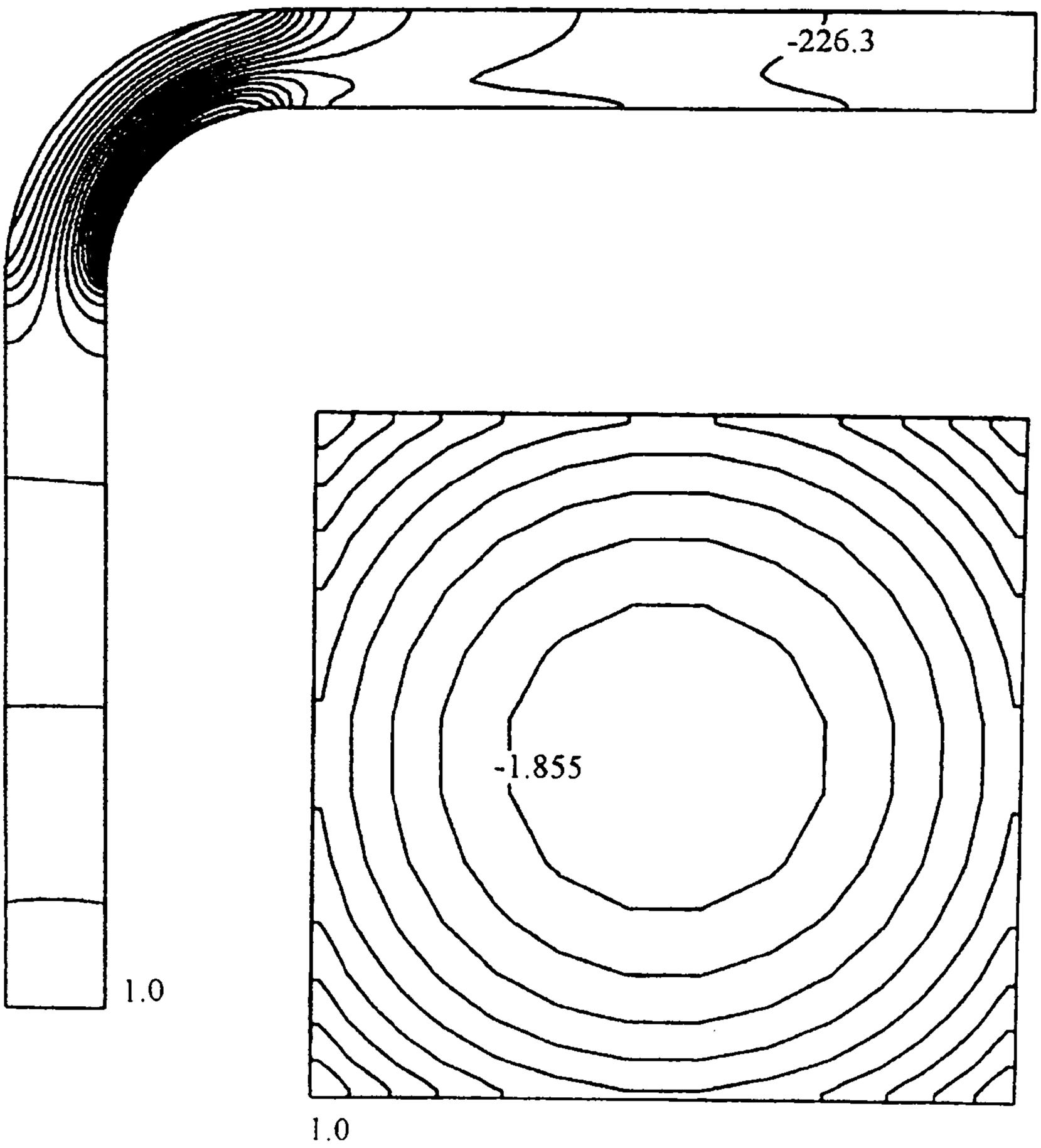

Figure 5.31 - First-order Upwind, turbulent case: pressure in the symmetry plane and pressure at the inlet plane

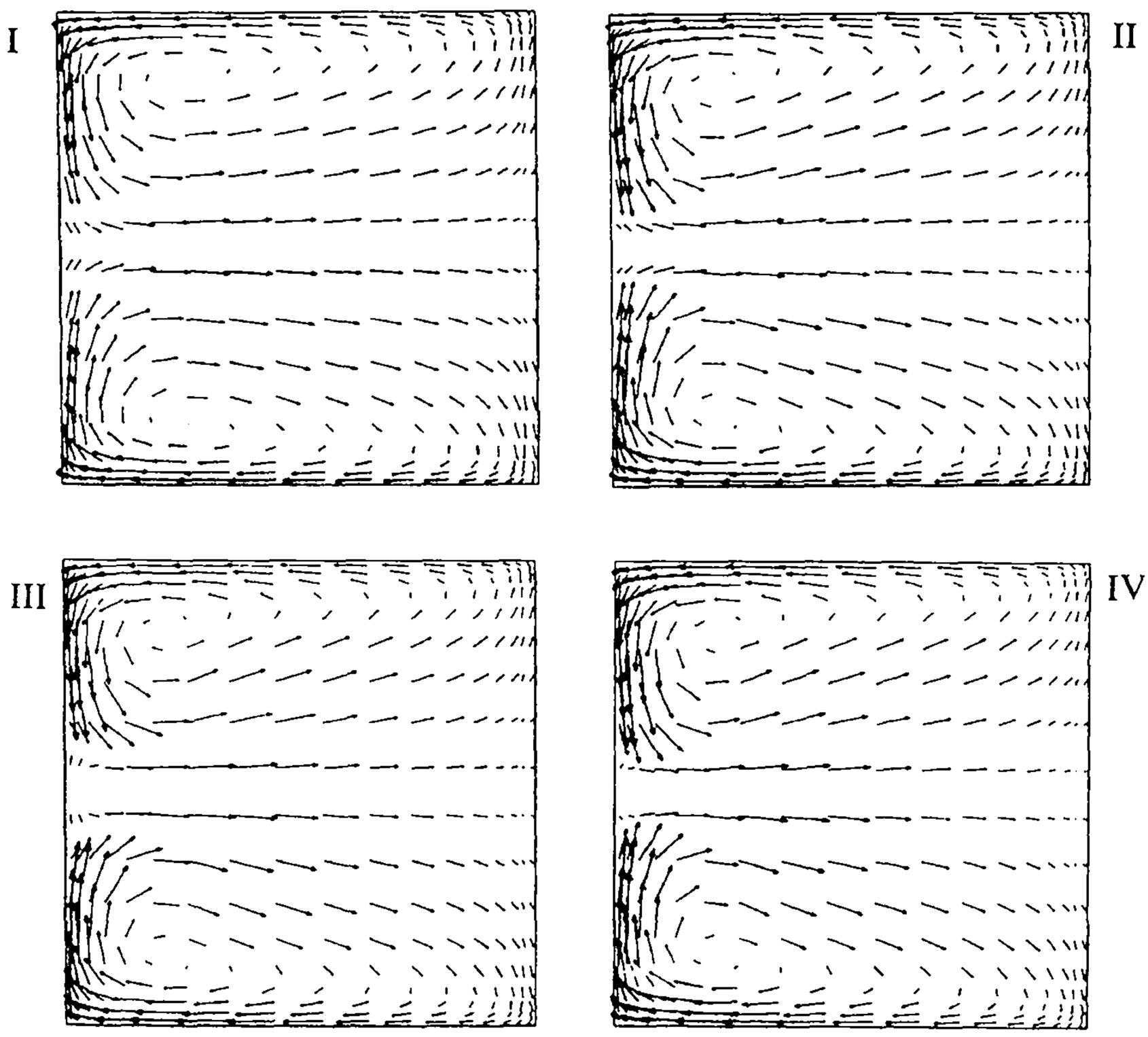

Figure 5.32 - Turbulent flow: secondary velocity at the exit of the bend using (I) first-order Upwind, (II) SOUCUP, (III) QUICK with flux limiter and (IV) fifth-order Upwind with flux limiter.

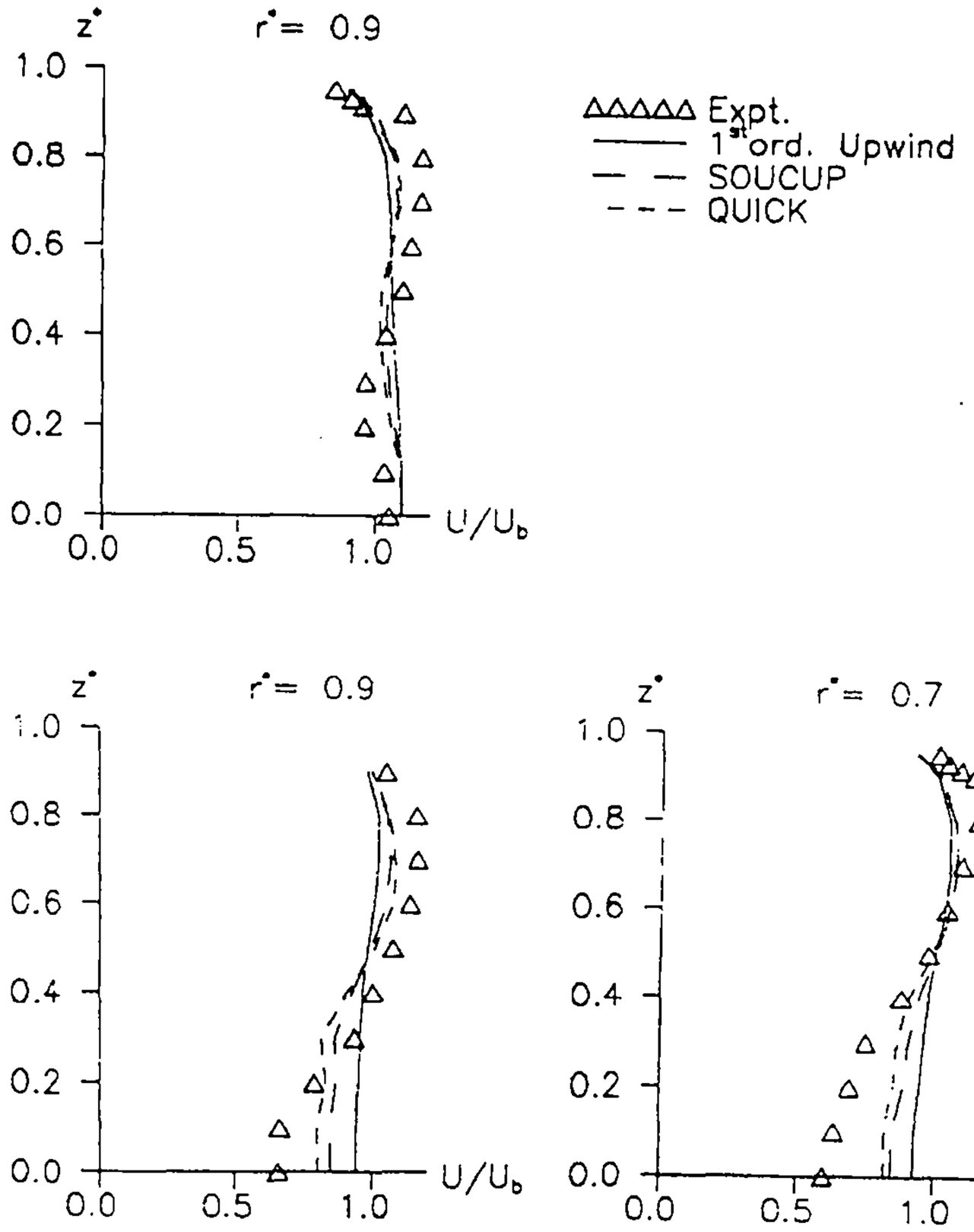

Figure 5.33 - Turbulent flow: streamwise velocity at ϑ=60° (top), ϑ=77.5° (bottom left) and X=0.25h (bottom right), comparison with experimental measurements.

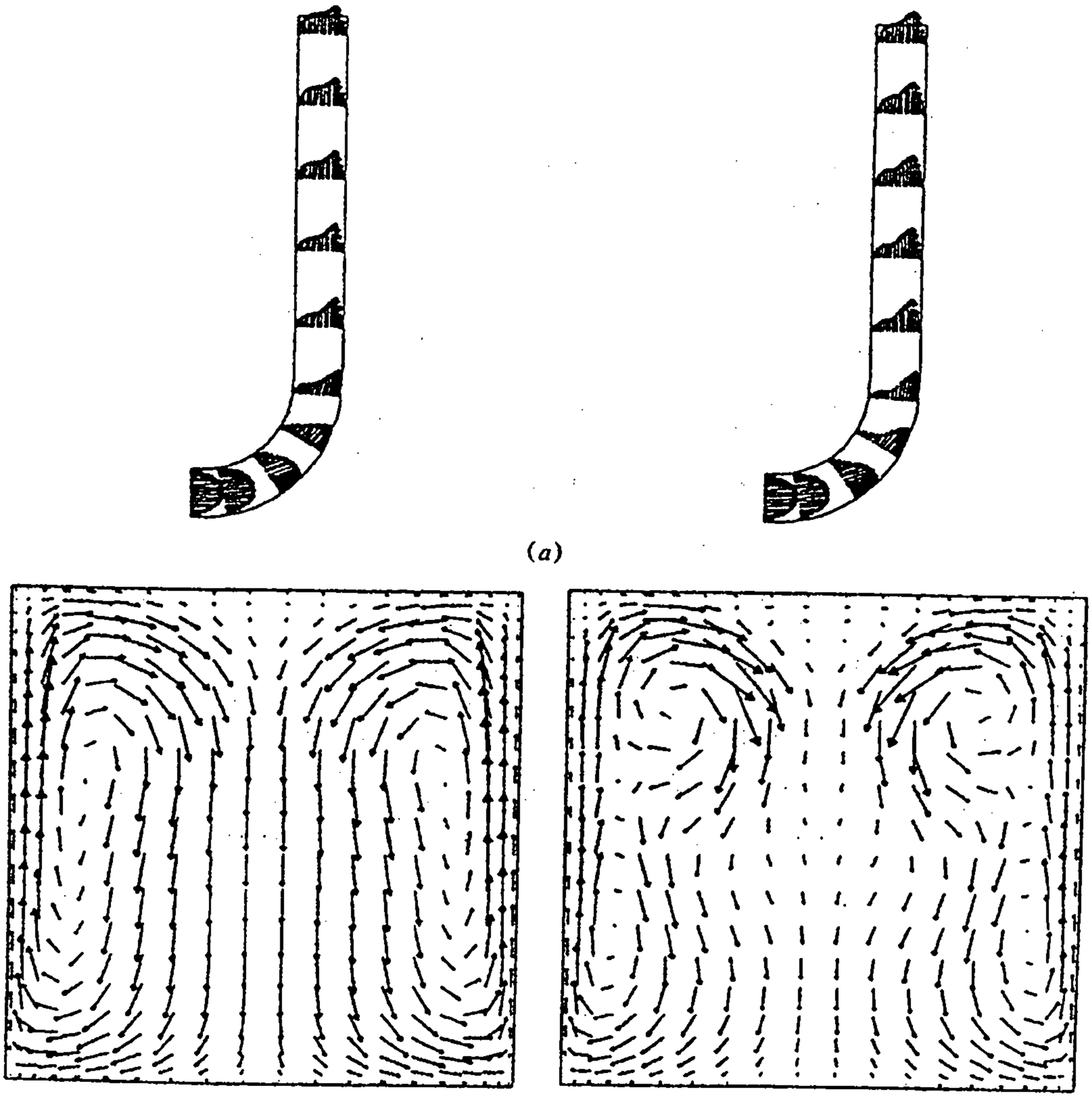

(a)

(b)

Figure 5.34 – Laminar flow field in the 90° bend predicted by Tamamidis and Assanis(1993) with a 22×22×71 grid and using the hybrid scheme (left hand side) and the QUICK scheme (right hand side): (a) flow in the symmetry plane and (b) secondary flow at the exit of the bend.

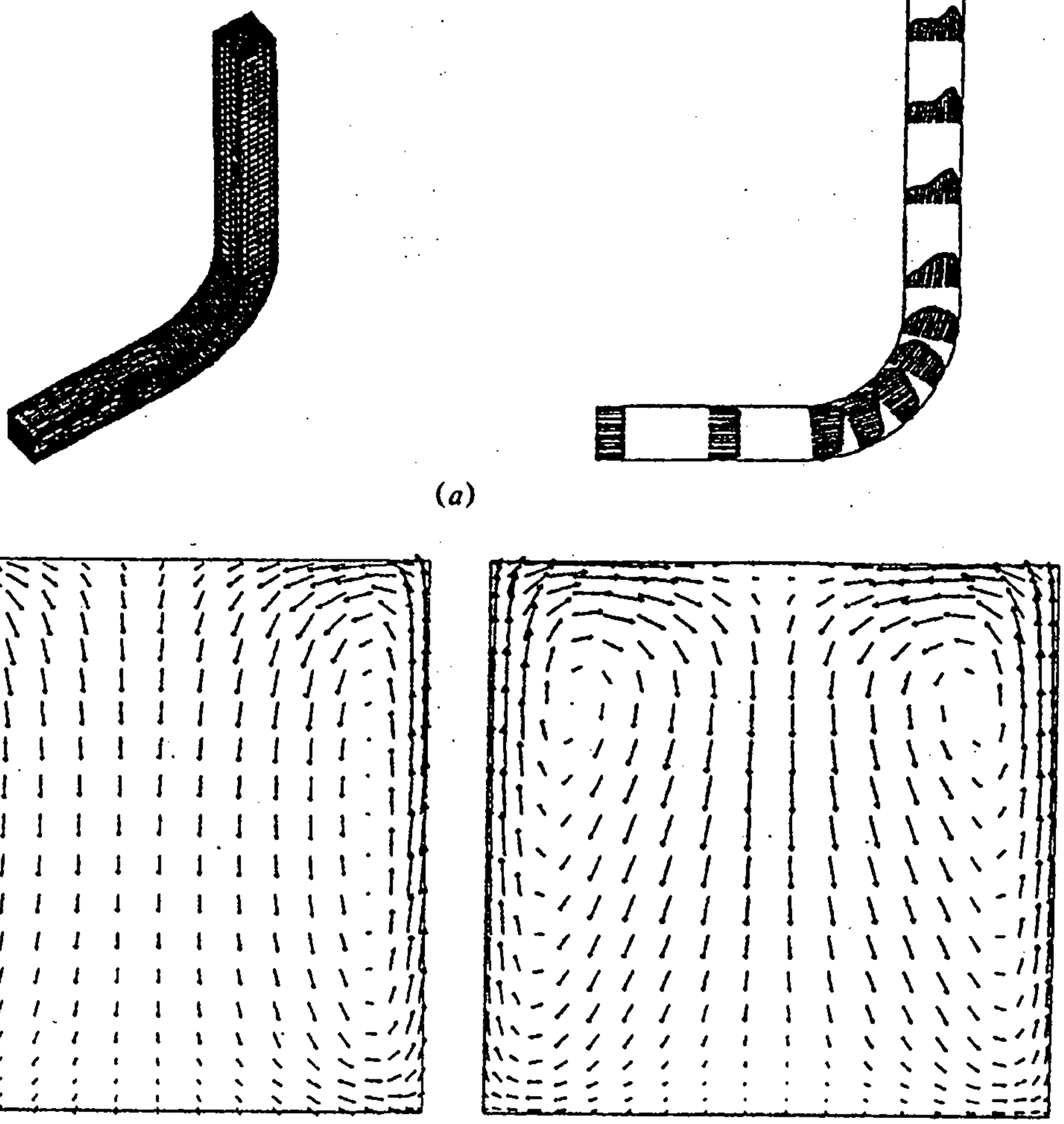

(a)

(b)

Figure 5.35 – Turbulent flow field in the 90° bend predicted by Tamamidis and Assanis(1993) using a standard k-ε model and the QUICK scheme: (a) grid used (22×22×71 nodes) and flow in the symmetry plane, (b) secondary flow at $\theta = 30^0$ and at the exit of the bend. Tamamidis and Assanis have shown that grid-independent solutions have been produced by the QUICK scheme with this grid size.

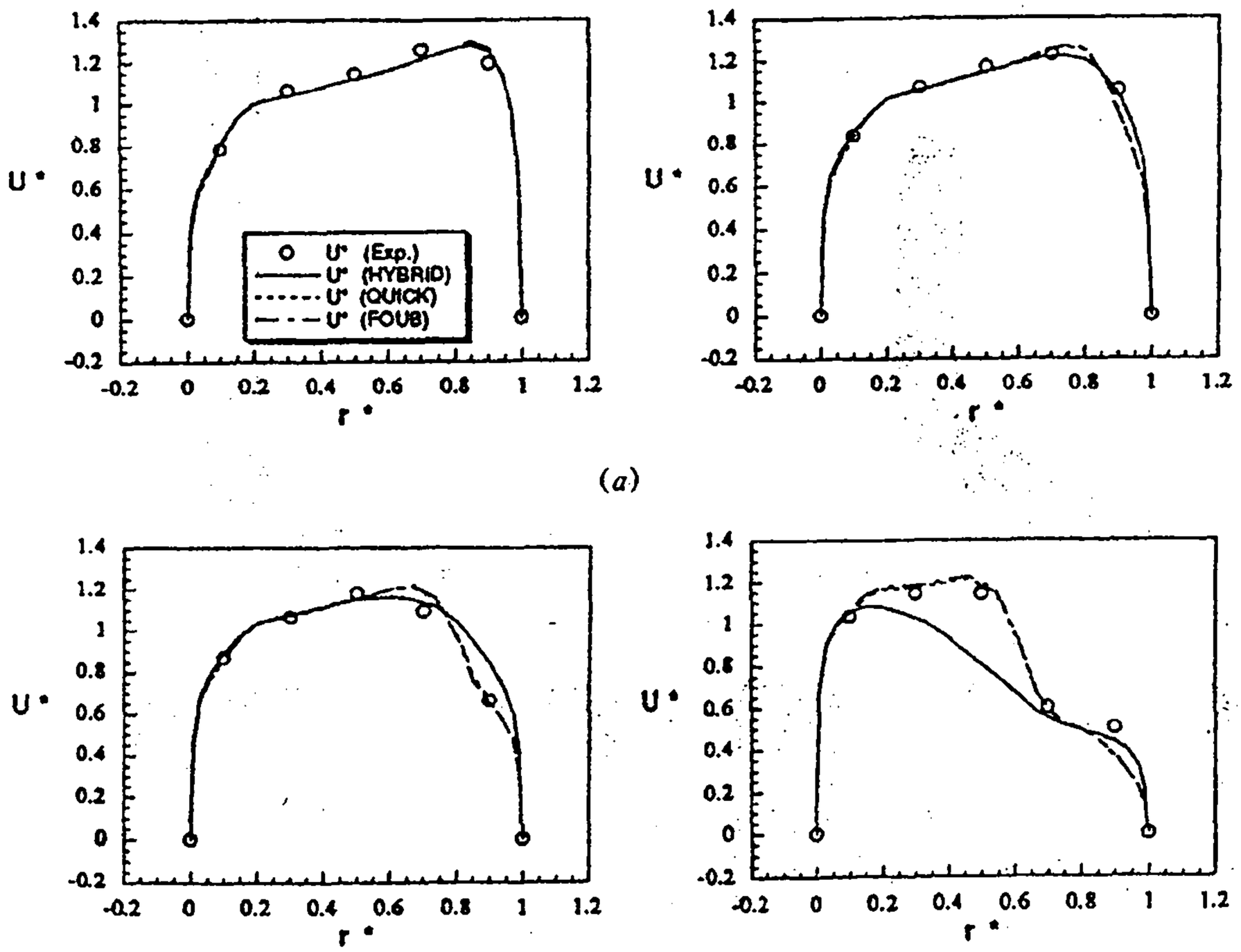

Figure 5.36 - Turbulent flow field in the 90° bend predicted by Tamamidis and Assanis(1993), using an hybrid scheme, a QUICK scheme, and a fifth-order Upwind scheme (FOUB): comparison between calculated and measured distributions of streamwise velocities at various midspan locations: (a) 30° station (left) and 60° station; (b) 77.5° station (left) and 0.25 hydraulic diameters from the bend exit plane.

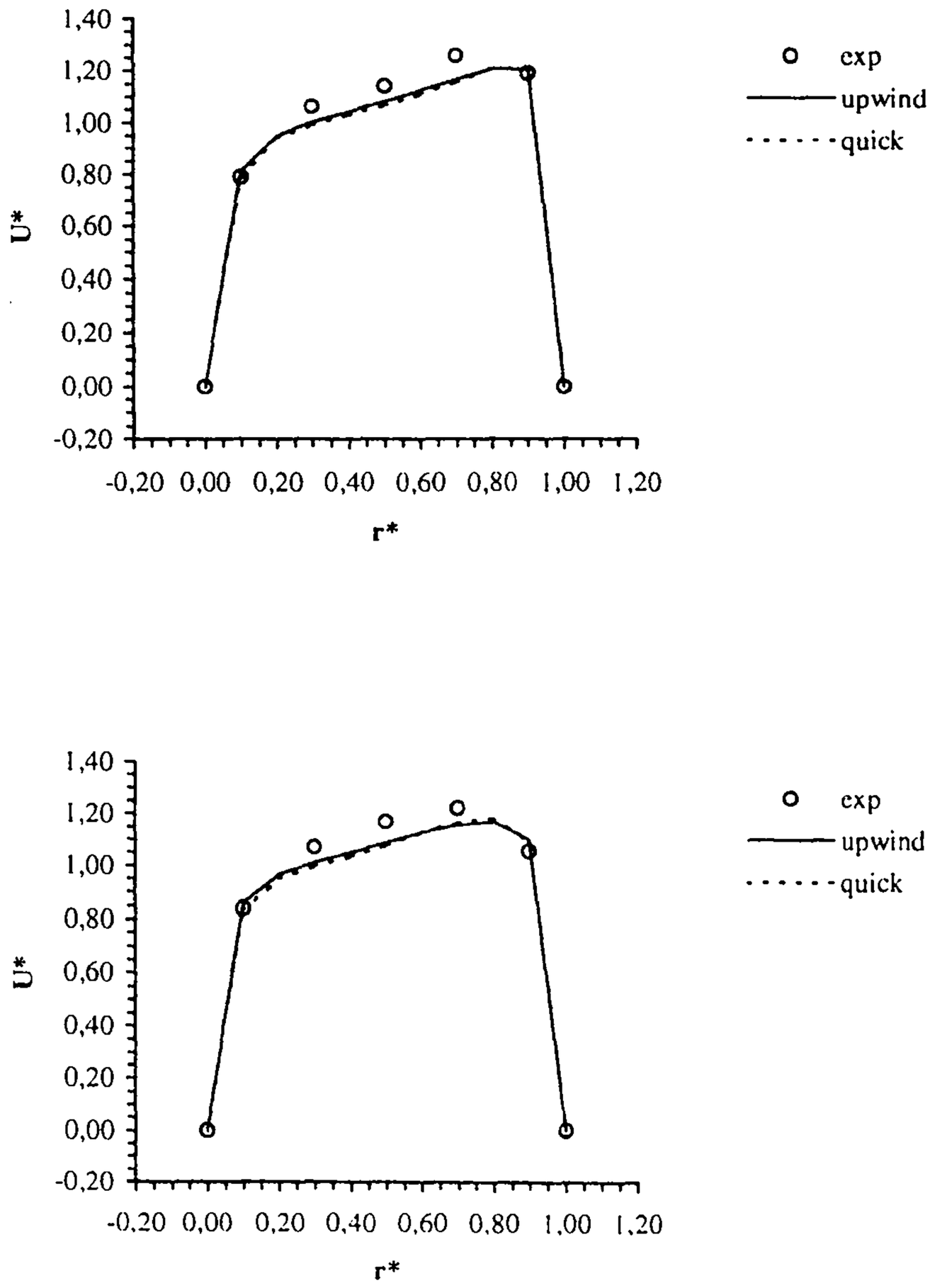

Figure 5.37 – Turbulent flow: comparison between calculated and measured distributions of streamwise velocities at the 30° (top) and 60° (bottom) stations.

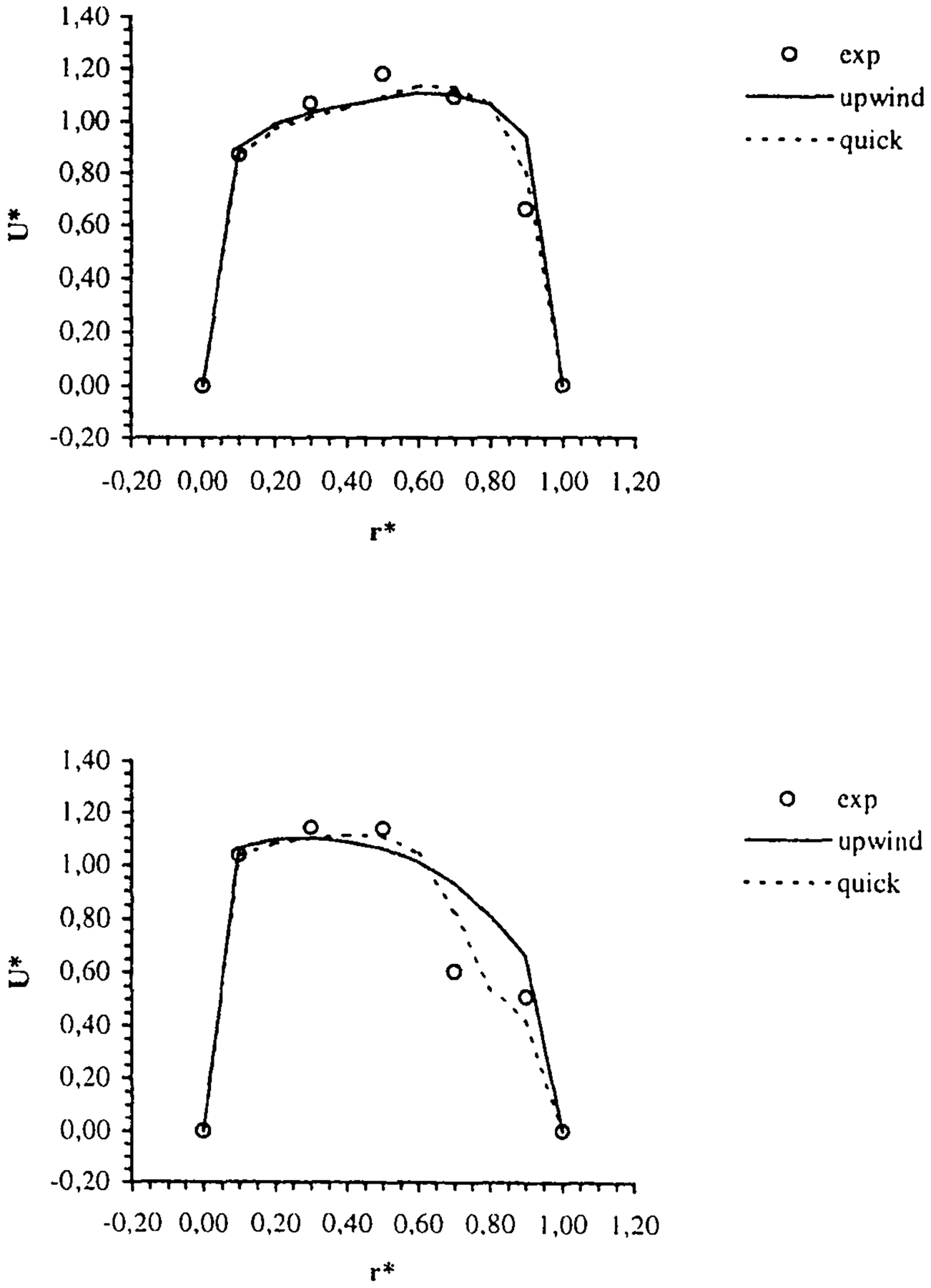

Figure 5.38 – Turbulent flow: comparison between calculated and measured distributions of streamwise velocities at the 77.7° station (top) and at 0.25 hydraulic diameters from the bend exit plane (bottom).

Chapter 6
Turbulence modelling

6.1 - Introduction.

In this section the proposed modification to the standard $k-\varepsilon$ method, that is introduced to avoid the use of the eddy viscosity and to adopt arbitrary modelling of the Reynolds stresses, will be presented.

In order to clarify the nature and the purpose of the modification introduced, the derivation of the Reynolds-averaged Navier-Stokes equation and of the standard $k-\varepsilon$ method will be also presented.

At the end of this section a simple quadratic formulation of the Reynolds stresses, that will be used to test the capability of the new code to adopt arbitrary modelling of the Reynolds stresses, is introduced.

6.2 - Derivation of the Reynolds-averaged Navier-Stokes equations.

The Navier-Stokes equations for a viscous fluid will be first determined.

Assuming that the fluid is Newtonian, the total internal stresses can be written as:

$$\underline{\underline{\sigma}} = -p\underline{\underline{I}} + \underline{\underline{\tau}} \tag{6.2.1}$$

where $\underline{\underline{I}}$ is the unit tensor, p is the isotropic pressure and $\underline{\underline{\tau}}$ is the viscous shear stress tensor, equal to:

$$\tau_{ij} = \mu D_{ij} + \lambda(\underline{\nabla} \cdot \underline{V})\delta_{ij} \tag{6.2.2}$$

where D_{ij} is twice the mean strain rate tensor defined by:

$$D_{ij} = \frac{\partial u_j}{\partial x_i} + \frac{\partial u_i}{\partial x_j} \tag{6.2.3}$$

and μ and λ are the first and second viscosity coefficient. With the exception of very high temperature and pressure range, the second viscosity coefficient can be considered as dependent on μ, following the Stokes relation:

$$2\mu + 3\lambda = 0 \tag{6.2.4}$$

Therefore the viscous shear stress tensor (6.2.2) can be written as:

$$\tau_{ij} = \mu\left[\left(\frac{\partial u_j}{\partial x_i} + \frac{\partial u_i}{\partial x_j}\right) - \frac{2}{3}(\underline{\nabla}\cdot\underline{V})\delta_{ij}\right] \tag{6.2.5}$$

The term multiplying the viscosity in the right hand side of equation (6.2.5) is in effect twice the traceless, symmetric part of the gradient of the velocity (second order tensor):

$$\left[\frac{1}{2}\left(\frac{\partial u_j}{\partial x_i} + \frac{\partial u_i}{\partial x_j}\right) - \frac{1}{3}(\underline{\nabla}\cdot\underline{V})\delta_{ij}\right] = (\underline{\nabla}\otimes\underline{V})_0^s \tag{6.2.6}$$

As can be easily seen, the antisymmetric part of the gradient of the velocity corresponds to a rigid rotation, while its trace (the divergence) corresponds to a volume variation; the component (6.2.6) of the gradient of velocity, therefore, gives a pure shear stress.

A differential form for the equation of motion can be easily obtained from the momentum conservation equation:

$$\frac{\partial}{\partial t}(\rho\underline{V}) + \underline{\nabla}\cdot\left(\rho\underline{V}\otimes\underline{V} + p\underline{\underline{I}} - \underline{\underline{\tau}}\right) = \underline{F} \tag{6.2.7}$$

where $\underline{F}$ are the external volume forces.

Introducing the form (6.2.5) into equation (6.2.7), the conservative form of the Navier-Stokes equations is obtained, which for a steady flow reduces to:

$$\frac{\partial}{\partial x_j}(\rho u_j u_i) = -\frac{\partial p}{\partial x_i} + \frac{\partial}{\partial x_j}\left[\mu\left(\frac{\partial u_i}{\partial x_j} + \frac{\partial u_j}{\partial x_i} - \frac{2}{3}\delta_{ij}\frac{\partial u_m}{\partial x_m}\right)\right] + F_i \qquad i = 1,2,3 \tag{6.2.8}$$

In order to obtain the laws of motion for the mean turbulent quantities, a time averaging process is introduced: for any scalar quantity ϕ the following separation is adopted:

$$\phi = \overline{\phi} + \phi' \tag{6.2.9}$$

where $\overline{\phi}$ is the mean value in the time Δt, large enough compared with the same time scale of the turbulence (Reynolds mean):

$$\overline{\phi}(x,t) = \frac{1}{\Delta t}\int_{-\Delta t/2}^{\Delta t/2} \phi(x, t+\vartheta)\, d\vartheta \tag{6.2.10}$$

and

$$\overline{\phi'} = 0 \tag{6.2.11}$$

For compressible flows the averaging process leads to products of fluctuations between density and other variables. In order to avoid their explicit occurrence a density-weighted average can be introduced:

$$\tilde{\phi} = \frac{\overline{\rho\phi}}{\overline{\rho}} \tag{6.2.12}$$

$$\phi = \tilde{\phi} + \phi'' \tag{6.2.13}$$

$$\overline{\rho\phi''} = 0 \tag{6.2.14}$$

Applying the averaging process to the momentum equation (6.2.7) the averaged Navier-Stokes, respectively for incompressible and compressible flows, are obtained:

$$\rho\frac{\partial}{\partial t}\left(\overline{\underline{V}}\right) + \underline{\nabla}\cdot\left(\rho\overline{\underline{V}}\otimes\overline{\underline{V}} - \overline{p}\underline{\underline{I}} - \underline{\underline{\tau}}^{V} - \underline{\underline{\tau}}^{R}\right) = \overline{E} \tag{6.2.15a}$$

$$\frac{\partial}{\partial t}\left(\overline{\rho}\tilde{\underline{V}}\right) + \underline{\nabla}\cdot\left(\overline{\rho}\tilde{\underline{V}}\otimes\tilde{\underline{V}} - \overline{p}\underline{\underline{I}} - \underline{\underline{\tau}}^{V} - \underline{\underline{\tau}}^{R}\right) = \overline{E} \tag{6.2.15b}$$

where $\underline{\underline{\tau}}^{V}$ is the averaged viscous shear stress tensor (6.2.4) and $\underline{\underline{\tau}}^{R}$ is the Reynolds stresses tensor, defined by:

$$\underline{\underline{\tau}}^R = -\rho\overline{\underline{V'} \otimes \underline{V'}} \tag{6.2.16a}$$

$$\tau_{ij}^R = -\rho\overline{u_i' u_j'} \tag{6.2.17a}$$

for incompressible flows, and:

$$\underline{\underline{\tau}}^R = -\overline{\rho\underline{V''} \otimes \underline{V''}} \tag{6.2.16b}$$

$$\tau_{ij}^R = -\overline{\rho u_i'' u_j''} \tag{6.2.17b}$$

for compressible flows, that can be interpreted as an additional shear stress due to the fluctuating part of the turbulent velocity.

From now all the variables will be intended as time-averaged and the corresponding symbols will be omitted. Equation (6.2.8) can now be written as:

$$\frac{\partial}{\partial x_j}\left(\rho u_j u_i\right) = -\frac{\partial p}{\partial x_i} + \frac{\partial}{\partial x_j}\left[\mu\left(\frac{\partial u_i}{\partial x_j} + \frac{\partial u_j}{\partial x_i} - \frac{2}{3}\delta_{ij}\frac{\partial u_m}{\partial x_m}\right) + \tau_{ji}^R\right] + F_i \qquad i = 1,2,3 \tag{6.2.18}$$

The relations between the Reynolds stresses (6.2.17) and the mean flow quantities are unknown. Being the Reynolds stresses tensor symmetric, $\tau_{ij}^R = \tau_{ji}^R$, there are 6 new scalar quantities to be evaluated. Therefore the application of the Reynolds-averaged equations to the computation of turbulent flows requires the introduction of some modelling of these unknown relations, based on theoretical considerations coupled to inevitable empirical information.

According to Markovin (1961), the effects of density fluctuations on the turbulence structure will remain small for Mach numbers below 5 for boundary layers and wakes. This implies that the turbulence models, based on density-averaged quantities will remain valid with the empirical data taken from incompressible flow experiments, within these limits on Mach number.

6.3 - The eddy viscosity.

Boussinesq (1877) suggested that the Reynolds stresses tensor could be expressed in a similar way than the viscous shear stress tensor (6.2.5) introducing an eddy viscosity μ_t, based on the assumption of an analogy between turbulent and molecular mixing:

$$\tau_{ij}^{R} = \mu_t \left[\left(\frac{\partial u_j}{\partial x_i} + \frac{\partial u_i}{\partial x_j} \right) - \frac{2}{3} (\underline{\nabla} \cdot \underline{V}) \delta_{ij} \right] - \frac{2}{3} \rho k \delta_{ij} \tag{6.3.1}$$

where k is the kinetic energy (per unit mass) of the turbulent fluctuations, or turbulence energy:

$$k = \frac{1}{2} \overline{u_i' u_i'} = \frac{1}{2} \left(\overline{u'^2} + \overline{v'^2} + \overline{w'^2} \right) \tag{6.3.2}$$

and the last term in the (6.2.1) has to be introduced to ensure consistency for $i=j$, since:

$$\tau_{11}^{R} + \tau_{22}^{R} + \tau_{33}^{R} = -\rho \left(\overline{u'^2} + \overline{v'^2} + \overline{w'^2} \right) = -2\rho k \tag{6.3.3}$$

Notice that for compressible flows, the turbulence energy should be defined as:

$$k = \frac{1}{2\bar{\rho}} \overline{\rho u_i'' u_i''} \tag{6.3.4}$$

for consistency with the definition (6.2.17b) of the Reynolds stresses; for the reported hypothesis on the influence of the compressibility on the turbulence structure, only the definition (6.3.2) will be used.

For the analogy with the molecular viscosity, which dimension is:

$$\mu \propto [\text{density}] \times \begin{bmatrix} \text{mean free path} \\ \text{(length)} \end{bmatrix} \times \begin{bmatrix} \text{average molecular} \\ \text{velocity} \end{bmatrix} \tag{6.3.5}$$

the eddy viscosity is taken as (Prandtl, 1925):

$$\mu_t \propto [\text{density}] \times \begin{bmatrix} \text{length scale of} \\ \text{turbulence, } l \end{bmatrix} \times \begin{bmatrix} \text{average velocity of} \\ \text{the turbulent flow} \end{bmatrix} \tag{6.3.6}$$

It is important to notice that while the molecular viscosity μ is a physical property of the fluid, the eddy viscosity μ_t depends on the particular flow.

Choosing the turbulence energy (6.3.2) as the basis for the velocity scale of the turbulent flow (Prandtl, 1945), the eddy viscosity is given by:

$$\mu_t = \text{constant} \times \rho l \sqrt{k} \tag{6.3.7}$$

Introducing the expression (6.3.1) of the Reynolds stresses into the turbulent-averaged Navier-Stokes leads to a system that has the same form of the laminar one with the molecular viscosity μ replaced by an effective viscosity $(\mu + \mu_t)$, equation (6.2.18) can now be written as:

$$\frac{\partial}{\partial x_j}(\rho u_j u_i) = -\frac{\partial p}{\partial x_i} + \frac{\partial}{\partial x_j}\left[(\mu + \mu_t)\left(\frac{\partial u_i}{\partial x_j} + \frac{\partial u_j}{\partial x_i} - \frac{2}{3}\delta_{ij}\frac{\partial u_m}{\partial x_m}\right)\right] + \\ -\frac{2}{3}\frac{\partial}{\partial x_i}(\rho k) + F_i \qquad i = 1,2,3 \tag{6.3.8}$$

Note that the term in ρk, coming from the last term of equation (6.3.1), is usually included in the pressure term (as an extra pressure due to turbulence).

Using the analogy between turbulent and molecular mixing, the flux of the generic scalar quantity ϕ, in the turbulent transport of the specie ϕ, can be written for similarity with Fick's law:

$$\underline{J}_\phi = -\Gamma_\phi \underline{\nabla}\phi \tag{6.3.9}$$

where Γ_ϕ is a turbulent exchange coefficient for the specie ϕ. The effective turbulent Prandtl number for the transport of ϕ can be introduced as:

$$\sigma_\phi = \frac{\mu_t}{\Gamma_\phi} \tag{6.3.10}$$

6.4 - The turbulence energy equation.

An exact equation for the turbulence energy can be derived from the Navier-Stokes equations, multiplying by a fluctuating property and time averaging the product. Using this procedure, and assuming incompressible flow (as the structure of turbulence

is not influenced by compressibility effects), the following transport equation is obtained:

$$\rho\frac{\partial k}{\partial t}+\rho u_j\frac{\partial k}{\partial x_j}=\frac{\partial}{\partial x_j}\left(\mu\frac{\partial k}{\partial x_j}-\frac{1}{2}\rho\overline{u_i'u_i'u_j'}-\overline{p'u_j'}\right)+\tau_{ij}^R\frac{\partial u_i}{\partial x_j}-\rho\varepsilon \qquad (6.4.1)$$

The terms on the left-hand side of equation (6.4.1) are, respectively, the unsteady term and the convection. The term $\mu\,\partial k/\partial x_j$ represents the diffusion of turbulence energy caused by the fluid's natural molecular transport processes (molecular diffusion).

The term $\rho\overline{u_i'u_i'u_j'}$ can be considered as turbulent transport, that is the rate at which turbulence energy is transported through the fluid by turbulent fluctuations; the term $\overline{p'u_j'}$ is another form of turbulent transport resulting from correlations of pressure and velocity fluctuations (pressure diffusion). The turbulent transport term is represented with the law (6.3.9), introducing the effective turbulent Prandtl number σ_k as in (6.3.10); the pressure diffusion term is generally grouped with the turbulent transport:

$$\frac{1}{2}\rho\overline{u_i'u_i'u_j'}+\overline{p'u_j'}=-\frac{\mu_t}{\sigma_k}\frac{\partial k}{\partial x_j} \qquad (6.4.2)$$

The term: $\tau_{ij}^R\,\partial u_i/\partial x_j$ is the production term, representing the rate at which kinetic energy is transferred from the mean flow to the turbulence.

The last term is the dissipation term, that is the rate at which turbulence kinetic energy is converted into thermal internal energy, where ε is the dissipation of turbulence energy per unit mass defined by:

$$\varepsilon=\frac{\mu}{\rho}\overline{\frac{\partial u_i'}{\partial x_m}\frac{\partial u_i'}{\partial x_m}} \qquad (6.4.3)$$

for purely dimensional arguments it is:

$$\varepsilon=\text{constant}\times\frac{k^{3/2}}{l} \qquad (6.4.4)$$

For a steady flow, the turbulence energy equation obtains, therefore, the following form:

$$\rho u_j \frac{\partial k}{\partial x_j} = \frac{\partial}{\partial x_j}\left[\left(\mu + \frac{\mu_t}{\sigma_k}\right)\frac{\partial k}{\partial x_j}\right] + \tau_{ij}^R \frac{\partial u_i}{\partial x_j} - \rho\varepsilon \qquad (6.4.5)$$

$$[\text{convection}] = [\text{diffusion}] + [\text{production}] - [\text{dissipation}]$$

At high Reynolds numbers it is common practice to neglect the molecular diffusion with respect to the turbulent one; at the same time the term ρk in the definition (6.4.1) of the Reynolds stresses is neglected in the production term; the most common way of writing equation (6.4.5) is therefore:

$$\rho u_j \frac{\partial k}{\partial x_j} = \frac{\partial}{\partial x_j}\left[\frac{\mu_t}{\sigma_k}\frac{\partial k}{\partial x_j}\right] + \mu_t\left(\frac{\partial u_j}{\partial x_i} + \frac{\partial u_i}{\partial x_j}\right)\frac{\partial u_i}{\partial x_j} - \rho\varepsilon \qquad (6.4.6)$$

6.5 - The $k - \varepsilon$ method.

An exact transport equation for ε could be derived from the Navier-Stokes equations, following the same procedure adopted for the derivation of equation (6.4.1). The equation obtained is far more complicated than the turbulence energy equation and involves several new unknown double and triple correlations of fluctuating velocity, pressure and velocity gradients.

A simplified procedure is therefore used: the transport equation for ε is written in the same form of the (6.4.5), with:

$$[\text{production of } \varepsilon] = C_1 \frac{\varepsilon}{k}[\text{production of } k]$$

$$[\text{dissipation of } \varepsilon] = C_2 \frac{\varepsilon}{k}[\text{dissipation of } k]$$

where the term ε/k is introduced to obtain the correct dimensions and the two constants C_1 and C_2 have to be evaluated from the comparison with the experimental data available.

For a stationary flow, the equation assumes, therefore, the following form:

$$\rho u_j \frac{\partial \varepsilon}{\partial x_j} = \frac{\partial}{\partial x_j}\left[\left(\mu + \frac{\mu_t}{\sigma_\varepsilon}\right)\frac{\partial \varepsilon}{\partial x_j}\right] + C_1 \frac{\varepsilon}{k}\left(\tau_{ij}^R \frac{\partial u_i}{\partial x_j}\right) - C_2 \frac{\varepsilon}{k}(\rho\varepsilon) \qquad (6.5.1)$$

$$[\text{convection}] = [\text{diffusion}] + [\text{production}] - [\text{dissipation}]$$

This equation is generally used in the simplified form:

$$\rho u_j \frac{\partial \varepsilon}{\partial x_j} = \frac{\partial}{\partial x_j}\left[\frac{\mu_t}{\sigma_\varepsilon}\frac{\partial \varepsilon}{\partial x_j}\right] + C_1 \frac{\varepsilon}{k}\mu_t\left(\frac{\partial u_j}{\partial x_i} + \frac{\partial u_i}{\partial x_j}\right)\frac{\partial u_i}{\partial x_j} - C_2\rho\frac{\varepsilon^2}{k} \qquad (6.5.2)$$

From equations (6.3.7) and (6.4.4) an expression for the eddy viscosity in terms of k and ε can be obtained:

$$\mu_t = C_\mu \rho \frac{k^2}{\varepsilon} \qquad (6.5.3)$$

The $k-\varepsilon$ method (Jones and Launder, 1972; Launder and Spalding, 1972) is therefore based on:

- the definition (6.3.1) for the Reynolds stresses τ_{ij}^R;
- the definition (6.5.3) for the eddy viscosity μ_t;
- the momentum equations in the form (6.3.8);
- the transport equation (6.4.5) or (6.4.6) for k;
- the transport equation (6.5.1) or (6.5.2) for ε.

The values of the constants recommended are:

C_μ	C_1	C_2	σ_k	σ_ε
0.09	1.44	1.92	1.0	1.3

The two transport equations (6.4.5) and (6.5.1) have to be associated with appropriate boundary conditions. For the turbulence energy equation the non-slip condition has to be prescribed:

$$k = 0 \text{ on solid walls.} \qquad (6.5.3)$$

It can easily proven that expanding ε using Taylor series in terms of the distance from the wall and considering only the first term of such series, the following boundary condition for ε could be adopted:

$$\frac{\partial \varepsilon}{\partial n} = 0 \text{ on solid walls.} \qquad (6.5.4)$$

The validity of this assumption is supported from experimental measurements indicating that the level of the turbulence energy dissipation rate is constant in the immediate neighbourhood of a wall (Patel et al., 1985).

However, the form of the $k-\varepsilon$ method that has been presented is valid only for fully turbulent flows. Close to solid walls there are inevitably regions where the local Reynolds number of turbulence is so small that viscous cffects predominate over turbulent ones. The basic model has to be modified to take into account these effects (low-Reynolds number methods) and a considerable number of points in the vicinity of the walls is needed to describe the laminar regions and the transition. An easier (and very popular) alternative, although much more approximate, is to impose the boundary conditions using of a wall function, as described in Appendix B.

6.6 - Equations in generalised coordinates.

Implementing the coordinate transformation (2.2.8), the turbulent-averaged Navier-Stokes equations (6.2.18) are transformed in:

$$\frac{1}{J}\frac{\partial}{\partial\xi_r}(\rho U_r u_i)=\frac{\partial p}{\partial\xi_r}\frac{\partial\xi_r}{\partial x_i}+\frac{1}{J}\frac{\partial}{\partial\xi_r}\Bigg[J\mu g^{rs}\frac{\partial u_i}{\partial\xi_s}+$$
$$+J\mu\frac{\partial\xi_r}{\partial x_j}\left(\frac{\partial u_i}{\partial\xi_s}\frac{\partial\xi_s}{\partial x_i}-\frac{2}{3}\delta_{ij}\frac{\partial u_m}{\partial\xi_s}\frac{\partial\xi_s}{\partial x_m}\right)+J\frac{\partial\xi_r}{\partial x_j}\tau_{ji}^{R}\Bigg]+F_i \qquad i=1,2,3 \tag{6.6.1}$$

where

$$g^{rs}=\frac{\partial\xi_r}{\partial x_j}\frac{\partial\xi_s}{\partial x_j} \tag{6.6.2}$$

Boussinesq's relation for the Reynolds stresses tensor (6.6.1) becomes:

$$\tau_{ij}^{R}=\mu_t\left[\left(\frac{\partial u_j}{\partial\xi_r}\frac{\partial\xi_r}{\partial x_i}+\frac{\partial u_i}{\partial\xi_r}\frac{\partial\xi_r}{\partial x_j}\right)-\frac{2}{3}\left(\frac{\partial u_m}{\partial\xi_r}\frac{\partial\xi_r}{\partial x_m}\right)\delta_{ij}\right]-\frac{2}{3}\rho k\delta_{ij} \tag{6.6.3}$$

and the corresponding form of the Navier-Stokes (6.3.8) is:

$$\frac{1}{J}\frac{\partial}{\partial\xi_r}(\rho U_r u_i)=\frac{\partial p}{\partial\xi_r}\frac{\partial\xi_r}{\partial x_i}+\frac{1}{J}\frac{\partial}{\partial\xi_r}\Bigg[J(\mu+\mu_t)g^{rs}\frac{\partial u_i}{\partial\xi_s}+$$

$$+J(\mu+\mu_t)\frac{\partial\xi_r}{\partial x_j}\left(\frac{\partial u_i}{\partial\xi_s}\frac{\partial\xi_s}{\partial x_i}-\frac{2}{3}\delta_{ij}\frac{\partial u_m}{\partial\xi_s}\frac{\partial\xi_s}{\partial x_m}\right)\Bigg]-\frac{2}{3}\frac{\partial(\rho k)}{\partial\xi_r}\frac{\partial\xi_r}{\partial x_i}+F_i \qquad i=1,2,3 \tag{6.6.4}$$

The k and ε equation are respectively rewritten as:

$$\frac{1}{J}\frac{\partial}{\partial\xi_r}(\rho U_r k)=\frac{1}{J}\frac{\partial}{\partial\xi_r}\left[J\left(\mu+\frac{\mu_t}{\sigma_k}\right)g^{rs}\frac{\partial k}{\partial\xi_s}\right]+G-\rho\varepsilon \tag{6.6.5}$$

$$\frac{1}{J}\frac{\partial}{\partial\xi_r}(\rho U_r \varepsilon)=\frac{1}{J}\frac{\partial}{\partial\xi_r}\left[J\left(\mu+\frac{\mu_t}{\sigma_\varepsilon}\right)g^{rs}\frac{\partial\varepsilon}{\partial\xi_s}\right]+C_1\frac{\varepsilon}{k}G-C_2\frac{\varepsilon}{k}(\rho\varepsilon) \tag{6.6.6}$$

where G is the production of turbulence energy:

$$G=\tau_{ij}^R\frac{\partial u_i}{\partial\xi_r}\frac{\partial\xi_r}{\partial x_j} \tag{6.6.7}$$

6.7 - A more general form of the k and ε equations.

A form of the k and ε equations not depending on the Boussinesq approximation and on the eddy viscosity can be obtained writing the turbulent diffusive transport term as function of the components of the Reynolds stresses tensor. Following Hanjalic and Launder (1972), and the hypothesis presented in their work, the turbulent diffusive transport of Reynolds stresses can be written as:

$$\overline{u_i'u_j'u_m'}=-C_s\frac{k}{\varepsilon}\left(\overline{u_i'u_l'}\frac{\partial\overline{u_j'u_m'}}{\partial x_l}+\overline{u_j'u_l'}\frac{\partial\overline{u_m'u_i'}}{\partial x_l}+\overline{u_m'u_l'}\frac{\partial\overline{u_i'u_j'}}{\partial x_l}\right) \tag{6.7.1}$$

where C_s is a constant, that gives for the turbulent transport term in the turbulence energy equation:

$$\overline{u_i'u_i'u_j'}=-C_s\frac{k}{\varepsilon}\left(2\overline{u_i'u_l'}\frac{\partial\overline{u_i'u_j'}}{\partial x_l}+\overline{u_j'u_l'}\frac{\partial\overline{u_i'u_i'}}{\partial x_l}\right)=-C_s\frac{k}{\varepsilon}\left(2\frac{\tau_{jl}^R}{\rho^2}\frac{\partial\tau_{ij}^R}{\partial x_l}-2\frac{\tau_{jl}^R}{\rho}\frac{\partial k}{\partial x_l}\right) \tag{6.7.2}$$

$$-\frac{1}{2}\rho\overline{u_i'u_i'u_j'} = C_s\frac{k}{\rho\varepsilon}\left(\tau_{il}^R\frac{\partial\tau_{ij}^R}{\partial x_l} - \rho\tau_{jl}^R\frac{\partial k}{\partial x_l}\right) \tag{6.7.3}$$

where C_s is a constant to be determined, and neglecting once again the pressure diffusion term $\overline{p'u_j'}$, the resulting equation for the turbulent energy is:

$$\rho u_j\frac{\partial k}{\partial x_j} = \frac{\partial}{\partial x_j}\left[\mu\frac{\partial k}{\partial x_j} + C_s\frac{k}{\rho\varepsilon}\left(\tau_{il}^R\frac{\partial\tau_{ij}^R}{\partial x_l} - \rho\tau_{jl}^R\frac{\partial k}{\partial x_l}\right)\right] + \tau_{ij}^R\frac{\partial u_i}{\partial x_j} - \rho\varepsilon \tag{6.7.4}$$

and in generalised coordinates:

$$\begin{aligned}\frac{1}{J}\frac{\partial}{\partial\xi_r}(\rho U_r k) = \frac{1}{J}\frac{\partial}{\partial\xi_r}\Bigg[J\mu g^{rs}\frac{\partial k}{\partial\xi_s} + \\ + JC_s\frac{k}{\rho\varepsilon}\frac{\partial\xi_r}{\partial x_j}\left(\tau_{il}^R\frac{\partial\xi_s}{\partial x_l}\frac{\partial\tau_{ij}^R}{\partial\xi_s} - \rho\tau_{jl}^R\frac{\partial\xi_s}{\partial x_l}\frac{\partial k}{\partial\xi_s}\right)\Bigg] + G - \rho\varepsilon\end{aligned} \tag{6.7.5}$$

Hanjalic and Launder suggest for m-th component of the turbulent diffusive transport term in the ε equation the following form:

$$-\rho\overline{u_m'\varepsilon'} = C_\varepsilon\rho\frac{k}{\varepsilon}\overline{u_m'u_l'}\frac{\partial\varepsilon}{\partial x_l} = -C_\varepsilon\frac{k}{\varepsilon}\tau_{ml}^R\frac{\partial\varepsilon}{\partial x_l} \tag{6.7.6}$$

where C_ε is a constant; therefore the resulting equation is:

$$\rho u_j\frac{\partial\varepsilon}{\partial x_j} = \frac{\partial}{\partial x_j}\left[\mu\frac{\partial\varepsilon}{\partial x_j} - C_\varepsilon\frac{k}{\varepsilon}\tau_{jl}^R\frac{\partial\varepsilon}{\partial x_l}\right] + C_{\varepsilon1}\frac{\varepsilon}{k}\left(\tau_{ij}^R\frac{\partial u_i}{\partial x_j}\right) - C_{\varepsilon2}\frac{\varepsilon}{k}(\rho\varepsilon) \tag{6.7.7}$$

and, in generalised coordinates:

$$\begin{aligned}\frac{1}{J}\frac{\partial}{\partial\xi_r}(\rho U_r\varepsilon) = \frac{1}{J}\frac{\partial}{\partial\xi_r}\left[J\mu g^{rs}\frac{\partial\varepsilon}{\partial\xi_s} - JC_\varepsilon\frac{k}{\varepsilon}\frac{\partial\xi_r}{\partial x_j}\tau_{jl}^R\frac{\partial\xi_s}{\partial x_l}\frac{\partial\varepsilon}{\partial\xi_s}\right] + \\ + C_{\varepsilon1}\frac{\varepsilon}{k}G - C_{\varepsilon2}\frac{\varepsilon}{k}(\rho\varepsilon)\end{aligned} \tag{6.7.8}$$

The values recommended for the constants are:

C_s	C_ε	$C_{\varepsilon 1}$	$C_{\varepsilon 2}$
0.08	0.13	1.45	2.0

The $k-\varepsilon$ method presented is therefore based on:

- the momentum equations in the original form (6.2.18) or (6.6.1);
- the transport equation (6.7.4) or (6.7.5) for k;
- the transport equation (6.7.7) or (6.7.8) for ε.
- an algebraic modelling for the Reynolds stresses τ_{ij}^R (e.g. with the Boussinesq assumption (6.3.1) or (6.6.3), but any modelling can be used).

The use of a turbulence model not based on the eddy viscosity for the modelling of the turbulent diffusive transport causes a deterioration in the stability of the numerical procedure.

In the standard procedure, the value of the variable appearing in the convection and in the normal diffusion terms, both laminar and turbulent, is evaluated implicitly, e.g. for the k equation:

$$\frac{1}{J}\frac{\partial}{\partial \xi_r}\left(\rho U_r k^{n+1}\right)=\frac{1}{J}\frac{\partial}{\partial \xi_r}\left[J\left(\mu+\frac{\mu_t}{\sigma_k}\right)g^{rr}\frac{\partial k^{n+1}}{\partial \xi_r}+J\left(\mu+\frac{\mu_t}{\sigma_k}\right)\sum_{s\neq r}g^{rs}\frac{\partial k^{n}}{\partial \xi_s}\right]+\ldots \tag{6.7.9}$$

where the superscript n indicates that the values of the variable at the previous step of the procedure are used, while $n+1$ indicates that the value of the variable is obtained from the solution of the corresponding system of linear equations.

In the modified formulation, instead, only the laminar part of the normal diffusion term contributes to the implicit evaluation, while the turbulent diffusive transport term is associated to the source:

$$\begin{aligned}\frac{1}{J}\frac{\partial}{\partial \xi_r}\left(\rho U_r k^{n+1}\right)&=\frac{1}{J}\frac{\partial}{\partial \xi_r}\left\{J\mu g^{rr}\frac{\partial k^{n+1}}{\partial \xi_r}+J\mu\sum_{s\neq r}g^{rs}\frac{\partial k^{n}}{\partial \xi_s}+\right.\\&\left.+\left[JC_s\frac{k}{\rho\varepsilon}\frac{\partial \xi_r}{\partial x_j}\left(\tau_{il}^R\frac{\partial \xi_s}{\partial x_l}\frac{\partial \tau_{ij}^R}{\partial \xi_s}-\rho\tau_{jl}^R\frac{\partial \xi_s}{\partial x_l}\frac{\partial k}{\partial \xi_s}\right)\right]^n\right\}+\ldots\end{aligned} \tag{6.7.10}$$

With the laminar diffusion being practically negligible with respect to the turbulent one ($\mu_t >> \mu$), this procedure modifies drastically the balance between the implicit and the explicit part in the transport equation. A deterioration of the stability of the procedure is therefore expected, bringing the necessity of lowering the under-relaxation parameters in respect to the original procedure.

The turbulent diffusive transport term is evaluated with the Gauss's theorem and added in the source term; e.g., referring once again to the k equation, defining:

$$T_j = \tau_{il}^R \frac{\partial \xi_s}{\partial x_l} \frac{\partial \tau_{ij}^R}{\partial \xi_s} - \rho \tau_{jl}^R \frac{\partial \xi_s}{\partial x_l} \frac{\partial k}{\partial \xi_s}, \qquad j = 1,2,3 \tag{6.7.11}$$

the integration to the control volume is given by:

$$\begin{aligned}
&\int_{\Theta_P} \frac{1}{J} \frac{\partial}{\partial \xi_r} \left[JC_S \frac{k}{\rho \varepsilon} \frac{\partial \xi_r}{\partial x_j} T_j \right] J d\Theta = \\
&= \int_{A_e} JC_S \frac{k}{\rho \varepsilon} \frac{\partial \xi}{\partial x_j} T_j dA - \int_{A_w} JC_S \frac{k}{\rho \varepsilon} \frac{\partial \xi}{\partial x_j} T_j dA + \\
&+ \int_{A_n} JC_S \frac{k}{\rho \varepsilon} \frac{\partial \eta}{\partial x_j} T_j dA - \int_{A_s} JC_S \frac{k}{\rho \varepsilon} \frac{\partial \eta}{\partial x_j} T_j dA + \\
&+ \int_{A_t} JC_S \frac{k}{\rho \varepsilon} \frac{\partial \zeta}{\partial x_j} T_j dA - \int_{A_b} JC_S \frac{k}{\rho \varepsilon} \frac{\partial \zeta}{\partial x_j} T_j dA
\end{aligned} \tag{6.7.12}$$

where Θ_P is the volume of the cell centred in P, A_e is the surface of the *east* face of the cell, etc.

The surface integrals on the solid walls are not evaluated, as the diffusion due to the walls is taken into account separately, with the wall function method, as reported in Appendix B.

6.8 - Modelling of the Reynolds stresses.

The $k-\varepsilon$ method presented in the previous section allows the use of an arbitrary modelling of the Reynolds stresses.

The linear relationship between stresses and strain in the Boussinesq's modelling (6.3.1), with the assumption of isotropic turbulence (i.e. C_μ is assumed to be a scalar), produces acceptable results for thin shear flows, but fails to determine any form of turbulence anisotropy. In reality, anisotropy is significant for three-dimensional flows even in plane thin shear layers, while streamline curvature introduces additional complication, due to the remarkably strong interaction between curvature strain and the normal stresses (Bradshaw, 1973).

Methods based on the linear modelling (6.3.1) generally produce inaccurate prediction for the normal Reynolds stresses, and are incapable to predict properly flows where the normal Reynolds stresses play an important role, such as in recirculation and secondary flows. For example, adopting the modelling (6.3.1) is impossible to predict the presence of secondary flows in fully developed turbulent flow in a rectangular duct, a physical effect that has been observed experimentally (Melling and Whitelaw, 1976). Speziale (1982) has proven that in order for secondary flows to occur in a rectangular duct, the axial mean velocity must give rise to a difference in the transverse normal stresses: $\tau^R_{xx} \neq \tau^R_{yy}$ (z being the axial direction), while in this case the modelling (6.3.1) produces $\tau^R_{xx} = \tau^R_{yy}$.

A simple way to overcome the limitations of the Boussinesq assumption, both in the prediction of anisotropy and in the sensitivity of the stress components to secondary strains associated with curvature, is to maintain the basic assumption of the dependence of the Reynolds stresses on the strain rate tensor, but adopting a non-linear, e.g. quadratic or cubic, relationship. Several quadratic stress-strain relationships have been proposed in recent years, by Baker and Orzechowski (1983), Speziale (1987), Nosizima & Yoshizawa (1987), Rubinstein & Barton (1990), Myong & Kasagi (1990), Shih *et al.* (1993). Craft *et al.* (1996) have presented a cubic stress-strain relationship, claiming that no quadratic form is capable to correctly account for the effects of streamline curvature on the turbulent stresses. It is interesting to notice that most of these formulations are extremely similar, while presenting very different values for the modelling coefficients (as shown by Craft *et al.*), depending on the flows that have been chosen to evaluate the recommended constants. In effects, all the models appear to be calibrated by reference to a certain number of simple flows, mostly two-dimensional, so that none of the models can guarantee an accurate resolution of anisotropy for arbitrary, complex three-dimensional flows, as has been shown in several assessment of turbulence models (for

example, Lien & Leschziner, 1994). This apparent lack of universality, together with the complexity of the formulations proposed so far, especially if written in generalised coordinates, complicate the choice of a modelling of the Reynolds stresses for practical three-dimensional computations.

In this work, in order to test the capability of a non-linear stress-strain relationship to predict accurately three-dimensional flows with streamline curvature, a correction, quadratic in the strain rate, will be added to the linear relation (6.3.1). The formulation adopted for the Reynolds stresses has to satisfy the consistency condition (6.3.3) that can be satisfied by taking:

$$\tau_{ij}^{R} = -\frac{2}{3}\rho k \delta_{ij} + \tau_{ij}^{0} \tag{6.8.1}$$

where τ_{ij}^{0} is a traceless tensor. In addition, the model has to be frame-indifferent, that is having the same form whether or not the frame of reference is inertial; this can be achieved allowing τ_{ij}^{R} to depend only on the frame-indifferent parts of the tensor $\underline{\nabla} \otimes \underline{V}$ and its derivatives (Speziale, 1983).

Defining D_{ij} as twice the main strain rate tensor (frame indifferent part of $\underline{\nabla} \otimes \underline{V}$):

$$D_{ij} = \frac{\partial u_j}{\partial x_i} + \frac{\partial u_i}{\partial x_j} = \frac{\partial u_j}{\partial \xi_s}\frac{\partial \xi_s}{\partial x_i} + \frac{\partial u_i}{\partial \xi_s}\frac{\partial \xi_s}{\partial x_j} \tag{6.8.2}$$

the simplest quadratic formulation, that satisfies both conditions and the symmetry requisites, can be written as follows:

$$\tau_{ij}^{R} = -\frac{2}{3}\rho k \delta_{ij} + C_{\mu}\rho\frac{k^2}{\varepsilon}D_{ij} + C\rho\frac{k^3}{\varepsilon^2}\left(D_{im}D_{mj} - \frac{1}{3}D_{mn}D_{mn}\delta_{ij}\right) \tag{6.8.3}$$

which, as can be easily seen, corresponds to Speziale's model without the additional term containing the frame-indifferent part of the convective derivative of $\underline{\nabla} \otimes \underline{V}$ (term containing the Oldroyd derivative).

It can be easily seen that for the turbulent flow in rectangular duct the simplified formulation (6.8.3) still introduces the anisotropy between the normal stresses that is necessary to produce secondary flows: substituting $\underline{V} = w\underline{k}$ into (6.8.3), $\underline{k}$ being the

direction of the z axis and w the corresponding velocity, the following difference between the transverse normal stresses is obtained:

$$\tau_{yy}^{R} - \tau_{xx}^{R} = C\rho\frac{k^3}{\varepsilon^2}\left[\left(\frac{\partial w}{\partial y}\right)^2 - \left(\frac{\partial w}{\partial x}\right)^2\right] \tag{6.8.4}$$

this is equivalent to the result obtained by the complete Speziale's formulation. At the same time, the proposed modelling fails to predict correctly the normal stresses in a fully developed two-dimensional channel flow; in this case, supposing that the flow direction coincides with the x axis, the modelling (6.8.3) predicts $\tau_{xx}^{R} = \tau_{yy}^{R}$, which is in contradiction with the experimental observations (Laufer,1952).

The proposed simplified modelling (6.8.3), although obviously lacking in universality, provides a very simple way to test the effects of the introduction of terms quadratic in the strain rate in the formulation of the Reynolds stresses for the prediction of three-dimensional complex flows. The constant C, on which the contribution of the non-linear part depends, will be obtained through comparison with the experimental data available for a three-dimensional geometry with strong streamline curvature.

The algorithm of the proposed formulation can be schematically written as follows, where the additional computations introduced are underlined:

repeat

Solve for the Cartesian velocities:

- evaluate the coefficients of the transport eq. using 1st ord. Upwind.
- evaluate the Reynolds stresses.

for *u, v, w*

- add to the source the pressure gradient term.
- add to the source the turbulent diffusion term.
- add to the source the deferred correction for the high-order scheme.
- solve the three-dimensional system with GMRES.

next

- update the contravariant velocities *U, V, W.*

Solve for the pressure correction:

- correct the contravariant velocities using the Rhie and Chow scheme.
- evaluate the coefficients and the source (mass unbalance).

- solve the three-dimensional system using the direct solver.
- update the pressure and correct *U, V, W*. Update *u, v, w*.

Solve for the turbulence quantities:
- evaluate the coefficients of the transport eq. using 1st ord. Upwind.
- evaluate the Reynolds stresses.
- evaluate the production of turbulence energy.

for *k, ε*
- add to the source the generation and dissipation terms.
- add to the source the turbulent diffusion term.
- add to the source the deferred correction for the high-order scheme.
- solve the three-dimensional system with GMRES.

next

until convergence.

Chapter 7
Validation of the turbulence modelling: turbulent flow in the 90° bend

7.1 - Introduction.

The different formulations for the turbulence modelling described in the previous chapter have been tested for the turbulent water flow analysis inside the 90° bend described in the fourth chapter. This test case appears to be particularly appropriate to study the capability of the proposed formulation in the prediction of anisotropic turbulent flow fields: the experimental data for the turbulent fields show higher shear stress towards the outer radius and large anisotropy at the exit of the bend, with high gapwise normal Reynolds stresses near the pressure surface (outer wall) and high streamwise normal Reynolds stresses near the suction surface (inner wall, or wall towards the centre of curvature).

For simplicity, in the rest of this study the standard k-ε formulation will be referred to as the **eddy viscosity** formulation, while the model based on the Hajanlic and Launder formulation for the turbulence diffusion will be referred to as the **modified** formulation.

The value of the under-relaxation coefficients used is 0.2 for the eddy viscosity formulation and 0.1 for the modified formulation; in both cases the same value of under-relaxation has been used for all the transport equations and for the pressure correction.

For the modified formulation the underrelaxation coefficients for k and ε have been lowered to 0.08 when using the QUICK and the fifth-order Upwind. The third and fifth order schemes have been used in conjunction with the flux limiter.

The modified formulation shows convergence properties similar to those of the eddy viscosity formulation, as can be seen comparing figures 7.1 and 7.2 with the corresponding figures for the eddy viscosity formulation (figures 5.25 and 5.26).

In all the other figures the streamwise velocity is indicated with U and gapwise velocity is indicated with V; both velocities have been normalised by the bulk velocity $U_b = 1.002\ m/s$ (corresponding to Re=40,000), and the gapwise velocity has been multiplied by a factor of 100. The results are given as function of the distance from the plane of symmetry normalised by the duct half-span, z^*, and of the distance from the outer wall normalised by the duct gap, r^*.

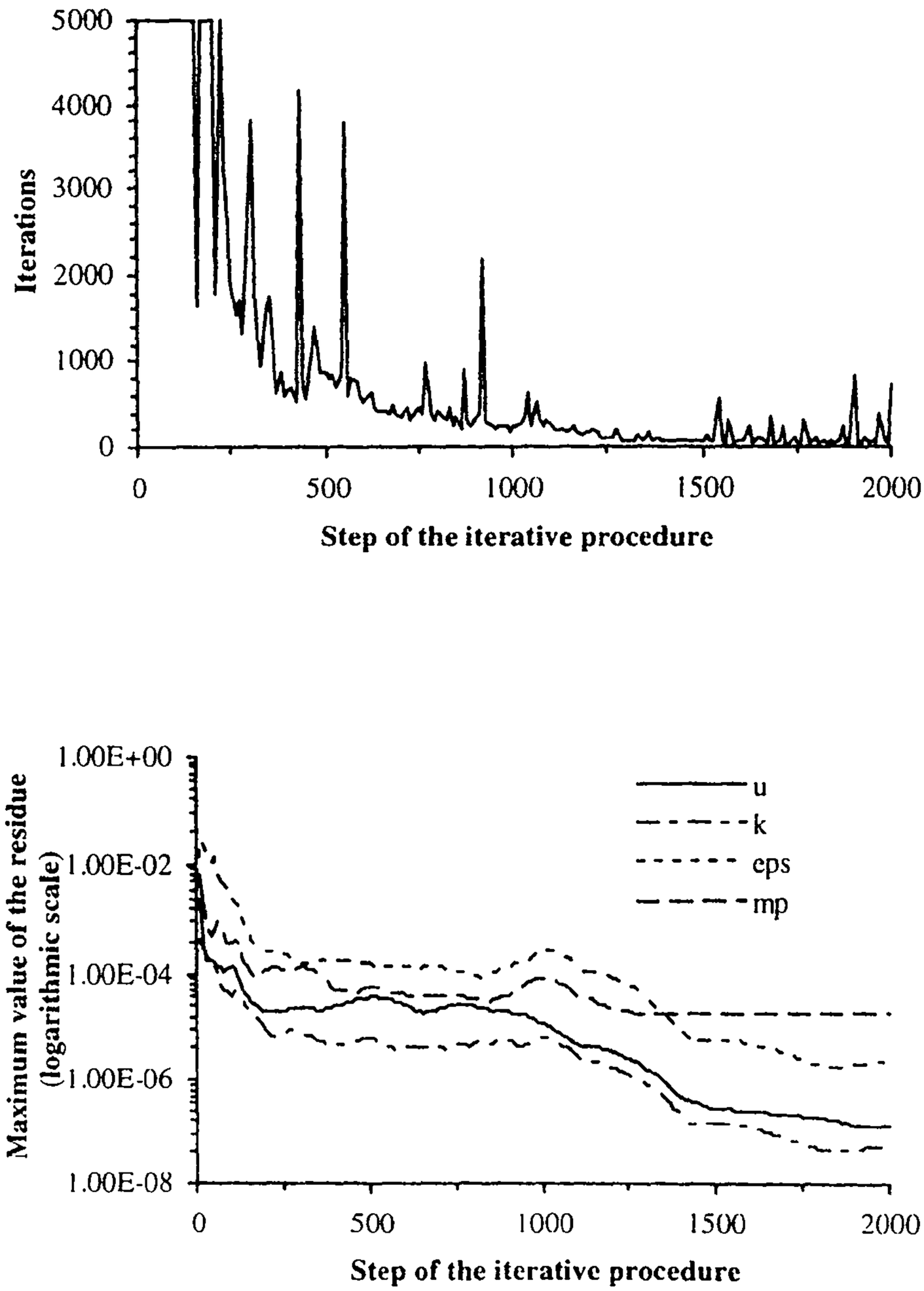

Figure 7.1 - Modified formulation: number of iterations of GMRES to solve the pressure correction equation (top) and convergence history of the procedure (bottom) using the ***first-order Upwind*** *scheme.*

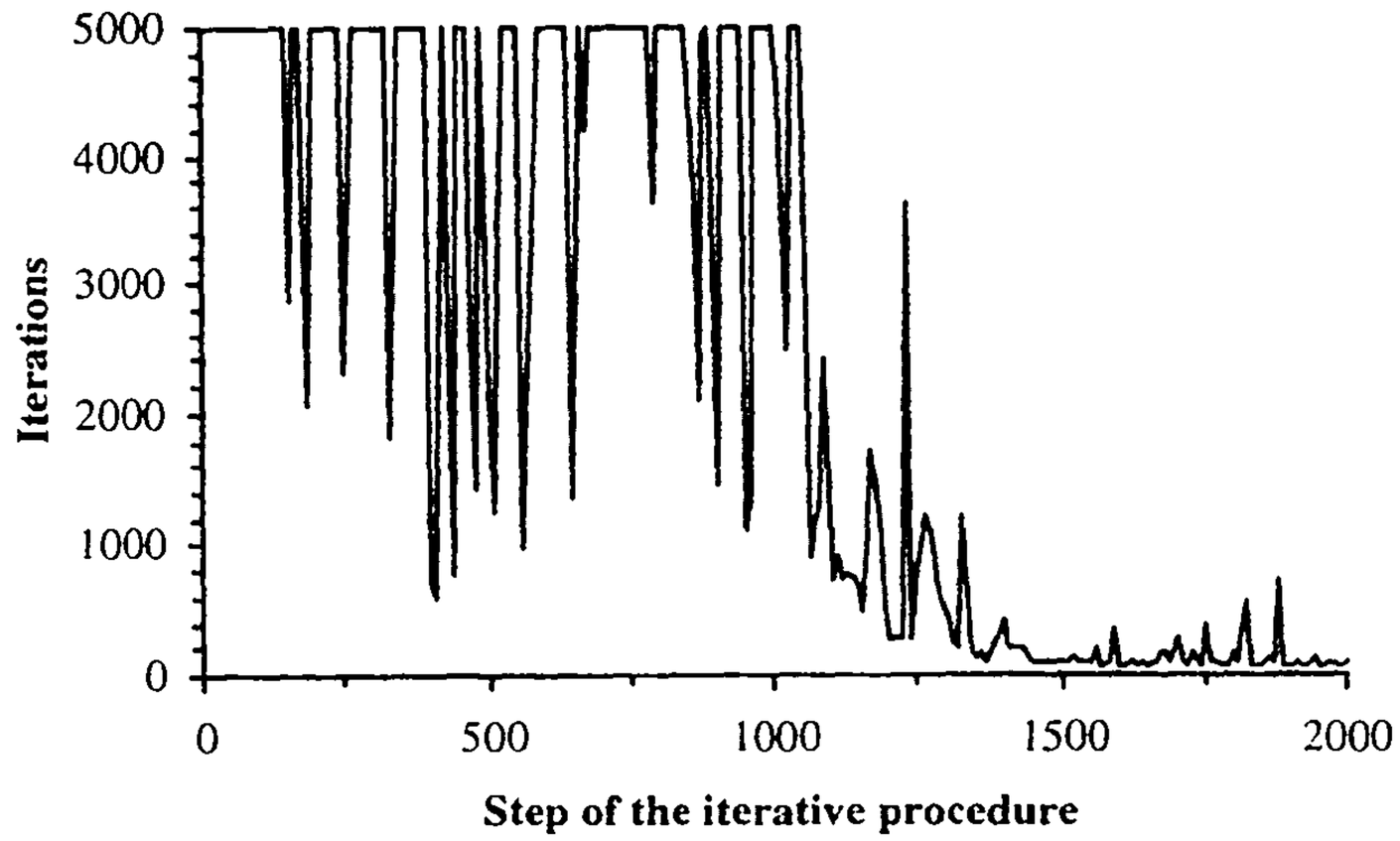

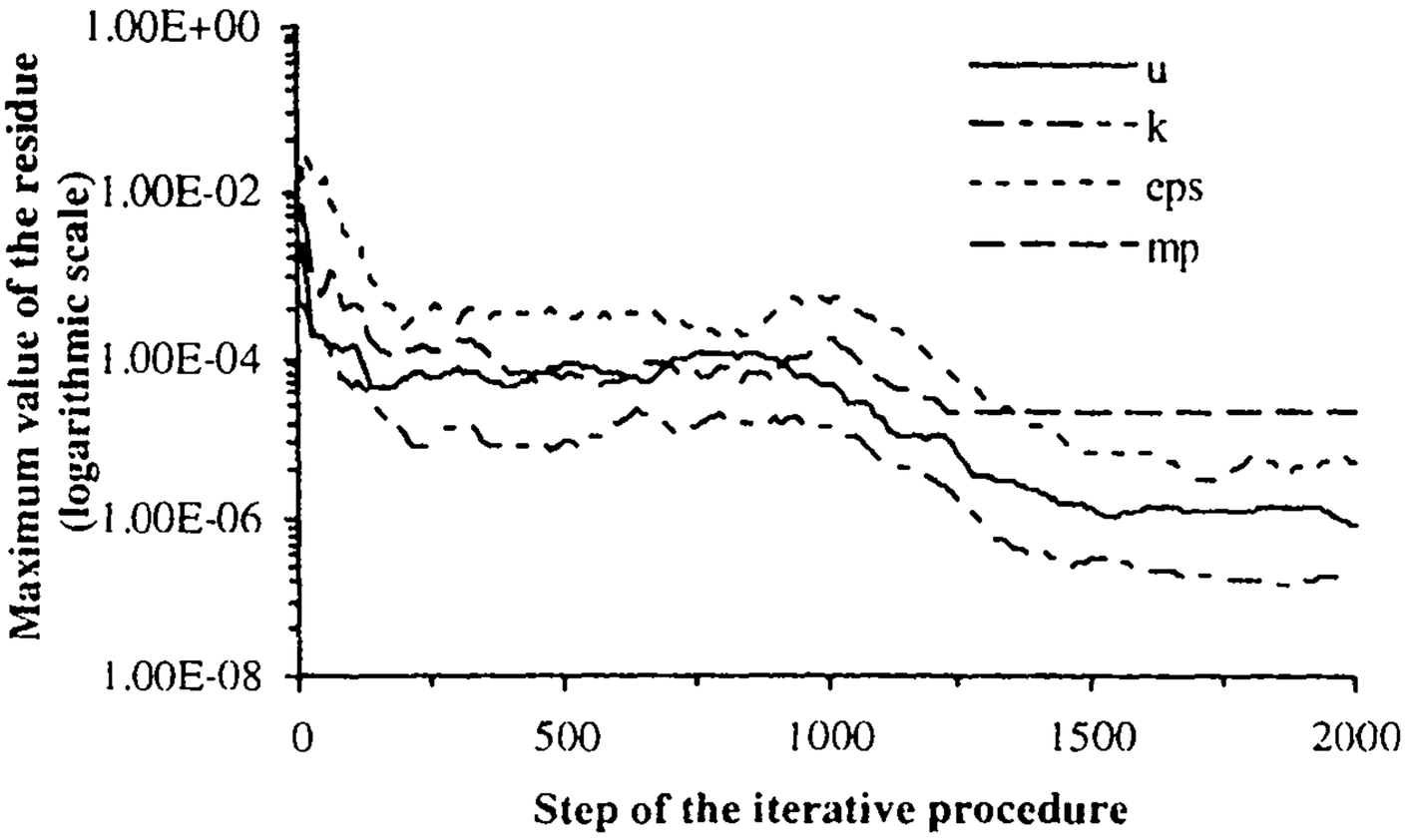

Figure 7.2 - Modified formulation: number of iterations of GMRES to solve the pressure correction equation (top) and convergence history of the procedure (bottom) using the ***SOUCUP*** *scheme.*

7.2 - Comparison between the eddy viscosity formulation and the modified formulation: effect of the modelling of the turbulent transport term.

A modelling of the Reynolds stresses has to be associated with the modified formulation; in order to have a meaningful comparison of the results with the eddy viscosity formulation, the Boussinesq assumption for the Reynolds stresses, on which the eddy viscosity formulation is based, has been adopted.

In the figures 7.3 and 7.4 a comparison of the turbulence energy profiles obtained with the two formulations is represented; as can be easily seen, the modified formulation produces a more accurate prediction of the measurements. In particular, the main difference between the two formulation seems to be the impact of the higher-order convection schemes on the accuracy of the solution. This is probably due to the fact that the eddy viscosity formulation tends to over-predict the physical diffusion in the k and ε equations, and therefore the reduction in numerical viscosity due to the use of higher-order schemes appears to be less effective, producing a smaller increase in accuracy in respect to the increase observed when using the modified formulation.

An increase in the efficacy of the higher-order schemes is then observed in the prediction of the streamwise velocity in regions of strong curvature of the velocity profiles, as can be seen in the figures 7.5, 7.6 and 7.7. Also in this case, the explanation can be that the values of k and ε, that in the momentum equations determine the additional diffusion due to the turbulence, tend to generate an over-prediction of the physical diffusion when evaluated with the eddy viscosity formulation.

A very effective way to show the global increase in efficacy of higher-order schemes in the prediction of the streamwise and gapwise velocity, when using the modified formulation, is through isovalue lines. All the isovalue lines presented refer to the cross section at 0.25 hydraulic diameters downstream the bend exit plane of which only half is represented, due to the spanwise symmetry of the problem.

In figure 7.8 the isovalue lines of the measured streamwise and gapwise velocities at 0.25 hydraulic diameters downstream the bend exit plane, as reported in Taylor et al. (1981), are presented.

In figure 7.9 the isovalue lines of the calculated streamwise velocity using the eddy viscosity formulation and the several convection schemes are reported. The increase in accuracy due to the use of higher-order schemes can be observed in the position of the line U/U_b=0.6, that progressively moves from the walls towards the inside of the domain, and in the increase in the inclination of the lines U/U_b=0.7 to U/U_b=1.0 towards the pattern present in the experimental data. Noticeably, the use of

the fifth-order scheme does not seem to increase the accuracy of the solution when compared with the third-order scheme.

In figure 7.10 the corresponding isovalue lines calculated with the modified formulation are reported. As can be observed, while the Upwind calculation produces very similar results to the one obtained with the standard formulation, the effect of the increase in accuracy due to the use of higher-order schemes is much more noticeable, especially with the third and fifth-order schemes.

In figure 7.11 the isovalue lines of the calculated gapwise velocity using the eddy viscosity formulation are reported. In this case an even smaller difference between the results obtained with the several convection schemes can be observed; the line V/U_b=0 appears to be well predicted, while there is a certain tendency of the lines V/U_b=-15 and V/U_b=-10 towards the pattern observed in the measured data. This tendency appears in any case to be quite small.

In figure 7.12 the corresponding isovalue lines calculated with the modified formulation are illustrated. In this case the effect of the use of higher-order convection schemes is even more marked than the one observed with the streamwise velocity: the line V/U_b=0 appears, once again, to be well predicted while the lines V/U_b=-15 and V/U_b=-10, starting from a pattern similar to the one obtained with the standard formulation, are strongly modified by the higher-order schemes, tending rapidly towards the shape present in the measured data.

From these results it can be deduced that the modified k-ε formulation is more sensitive to the increase in accuracy due to the use of higher-order convection schemes, thus showing that the modelling of the turbulent diffusive transport term in the standard k-ε equations could be the cause of the excessive diffusivity of the method.

In any case a closer agreement between the prediction and the measured results has been obtained.

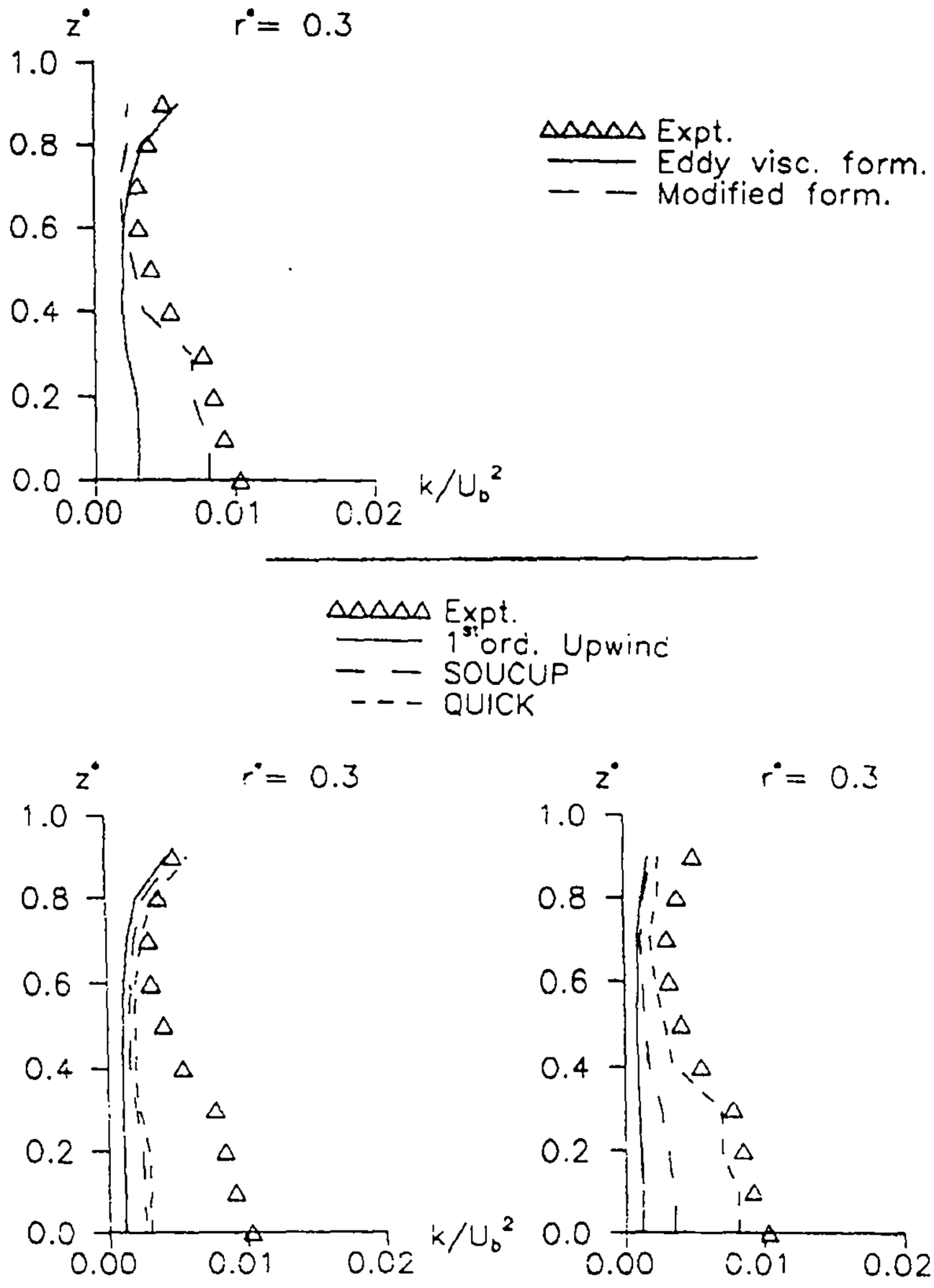

Figure 7.3 - Turbulence energy profiles at 2.5 hydraulic diameters downstream of the bend exit plane, comparison with experimental measurements; ***top****:comparison between the two formulations, using the QUICK scheme;* ***bottom****: comparison of the several convection schemes using the eddy visc. fom. (****left****) or the modified (****right****).*

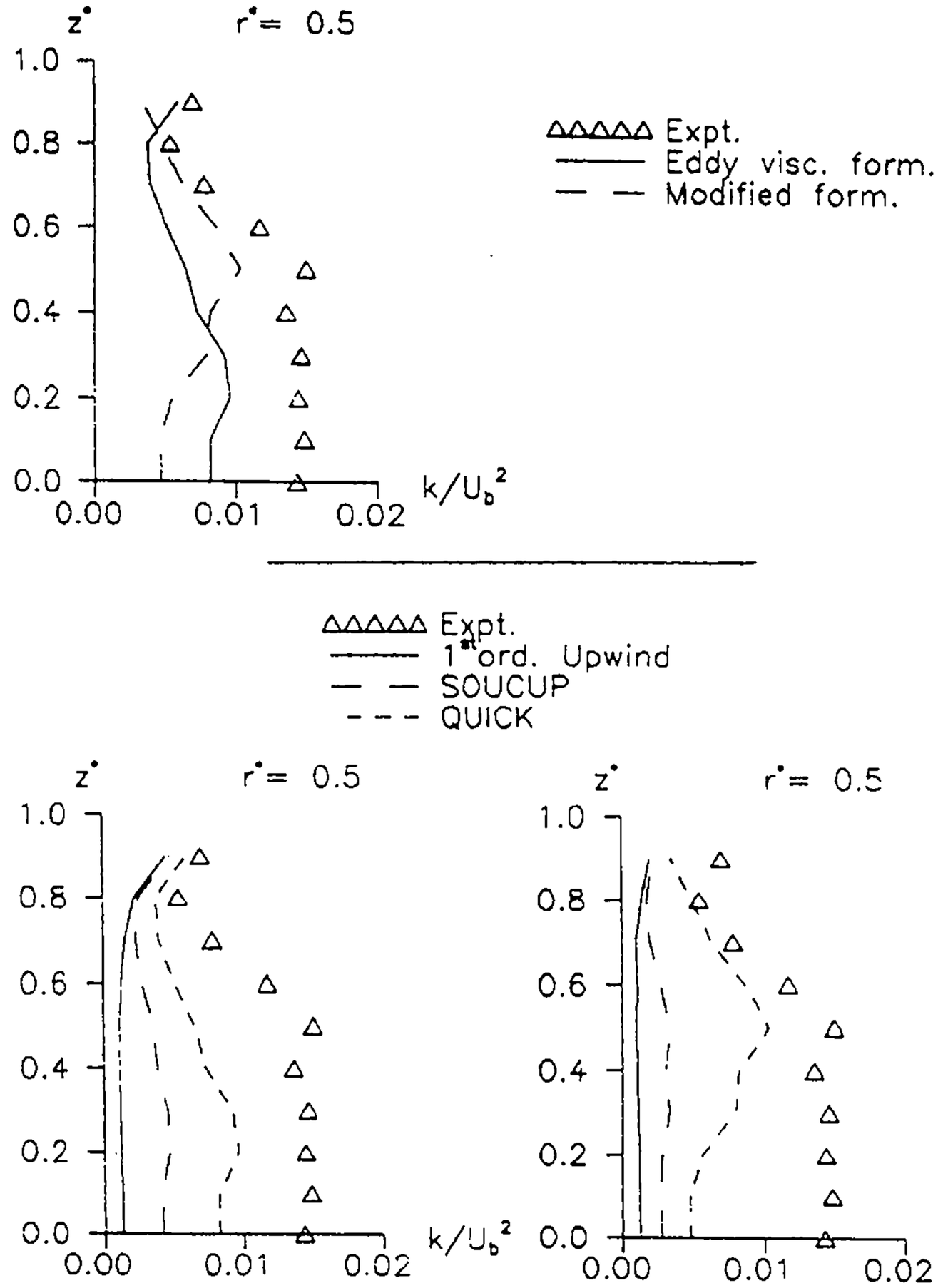

Figure 7.4 - Turbulence energy profiles at 2.5 hydraulic diameters downstream of the bend exit plane, comparison with experimental measurements; ***top****:comparison between the two formulations, using the QUICK scheme;* ***bottom****: comparison of the several convection schemes using the eddy visc. fom. (****left****) or the modified (****right****).*

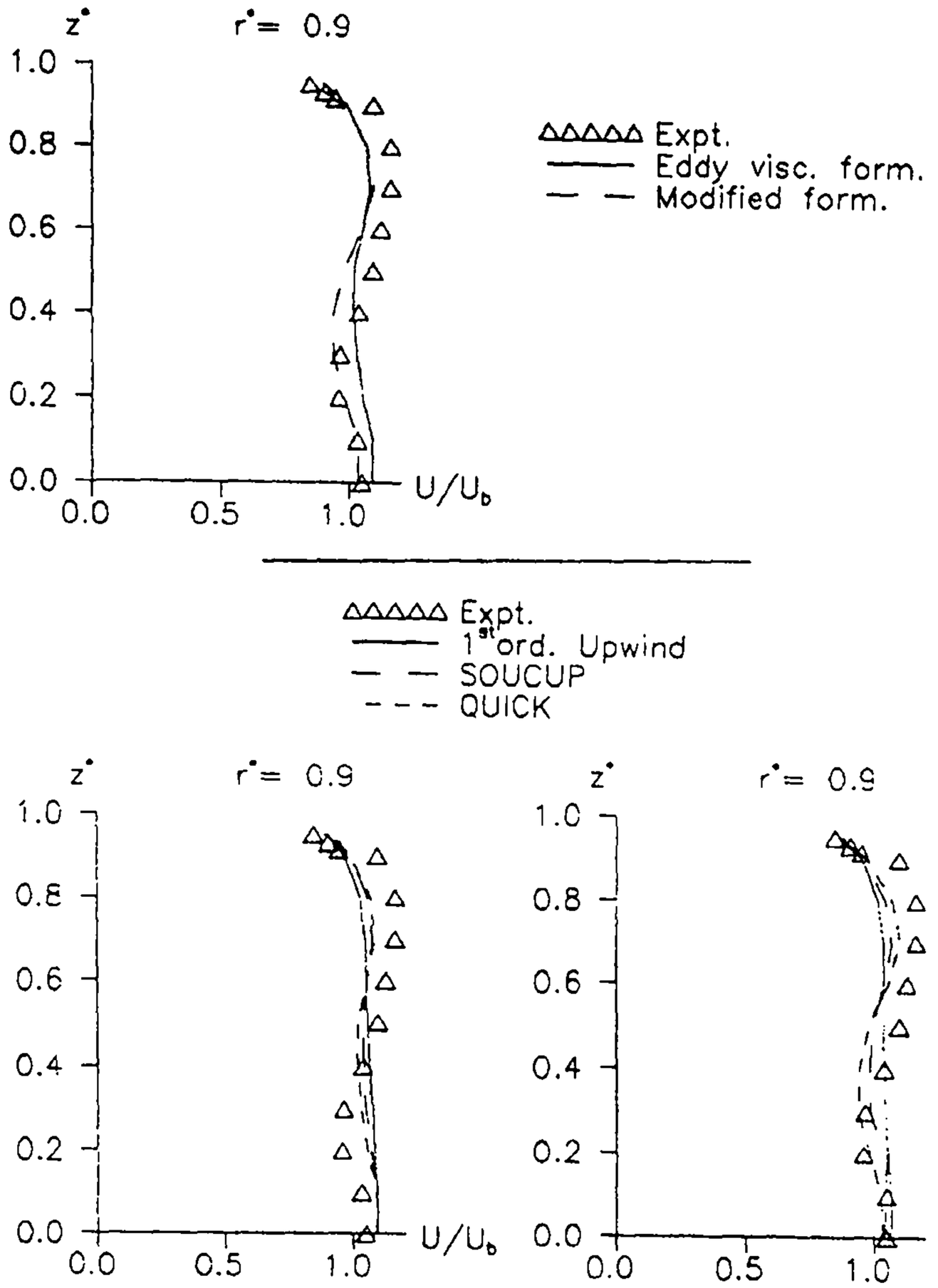

Figure 7.5 - Streamwise velocity profiles at 60° from the bend entry plane, comparison with experimental measurements; ***top****:comparison of the two formulations, using the QUICK scheme;* ***bottom****: comparison between the several convection schemes using the eddy visc. fom. (****left****) or the modified (****right****).*

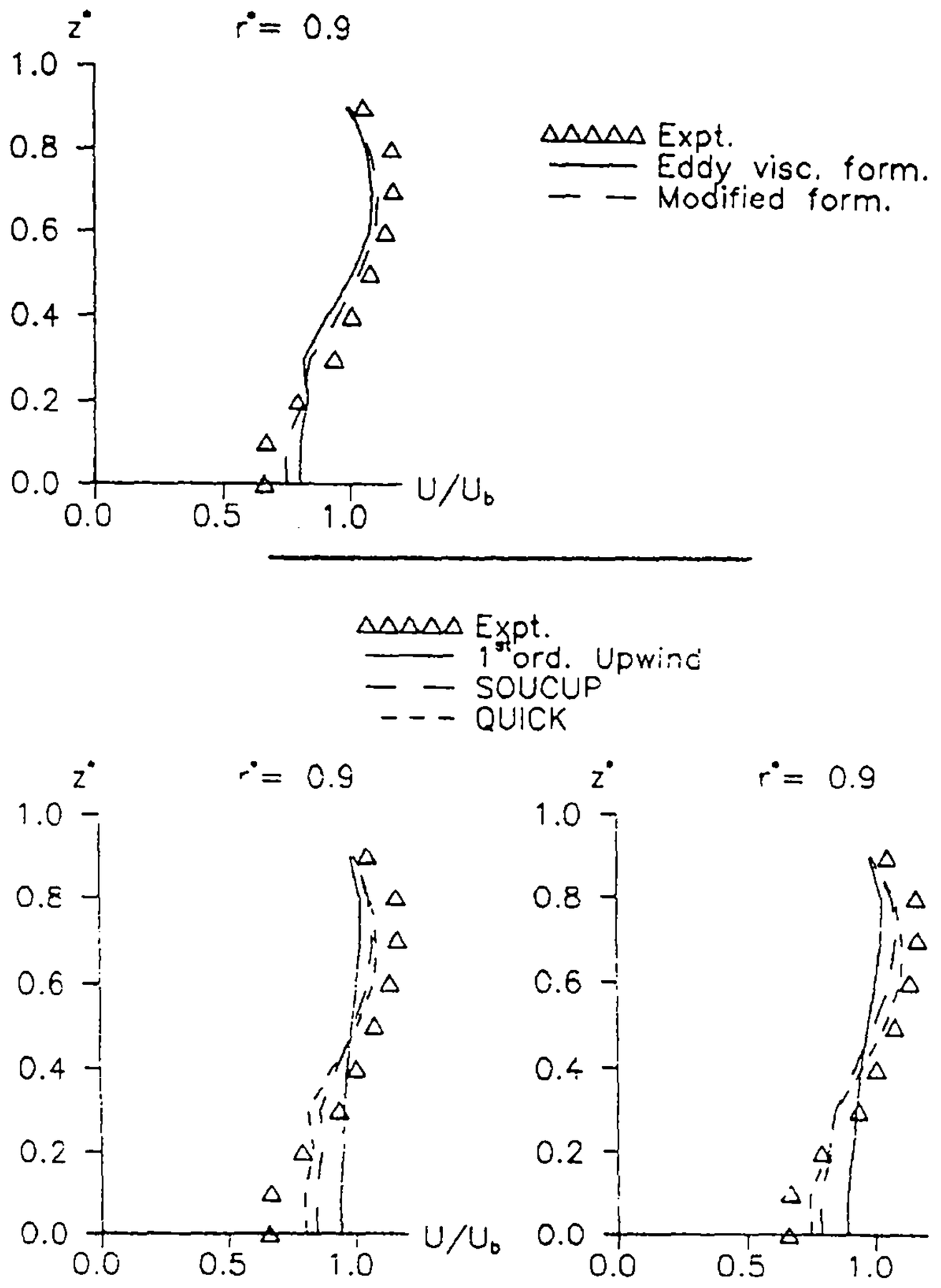

Figure 7.6 - Streamwise velocity profiles at 77.5° from the bend entry plane, comparison with experimental measurements; ***top****:comparison between the two formulations, using the QUICK scheme;* ***bottom****: comparison of the several convection schemes using the eddy visc. fom. (****left****) or the modified (****right****).*

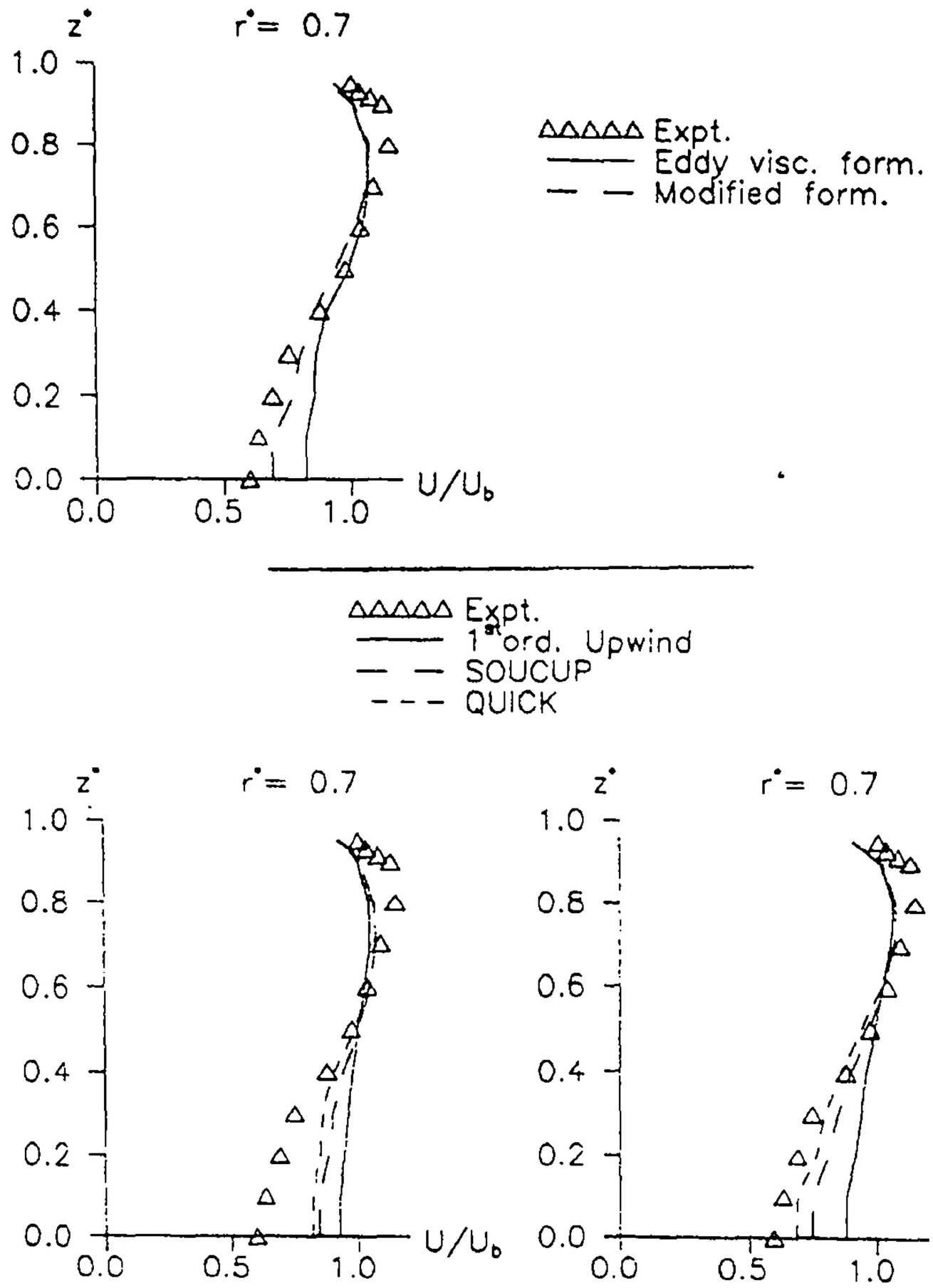

Figure 7.7 - Streamwise velocity profiles at 0.25 hydraulic diameters downstream of the bend exit plane, comparison with experimental measurements; ***top****:comparison between the two formulations, using the QUICK scheme;* ***bottom****: comparison of the several convection schemes using the eddy visc. fom. (****left****) or the modified (****right****).*

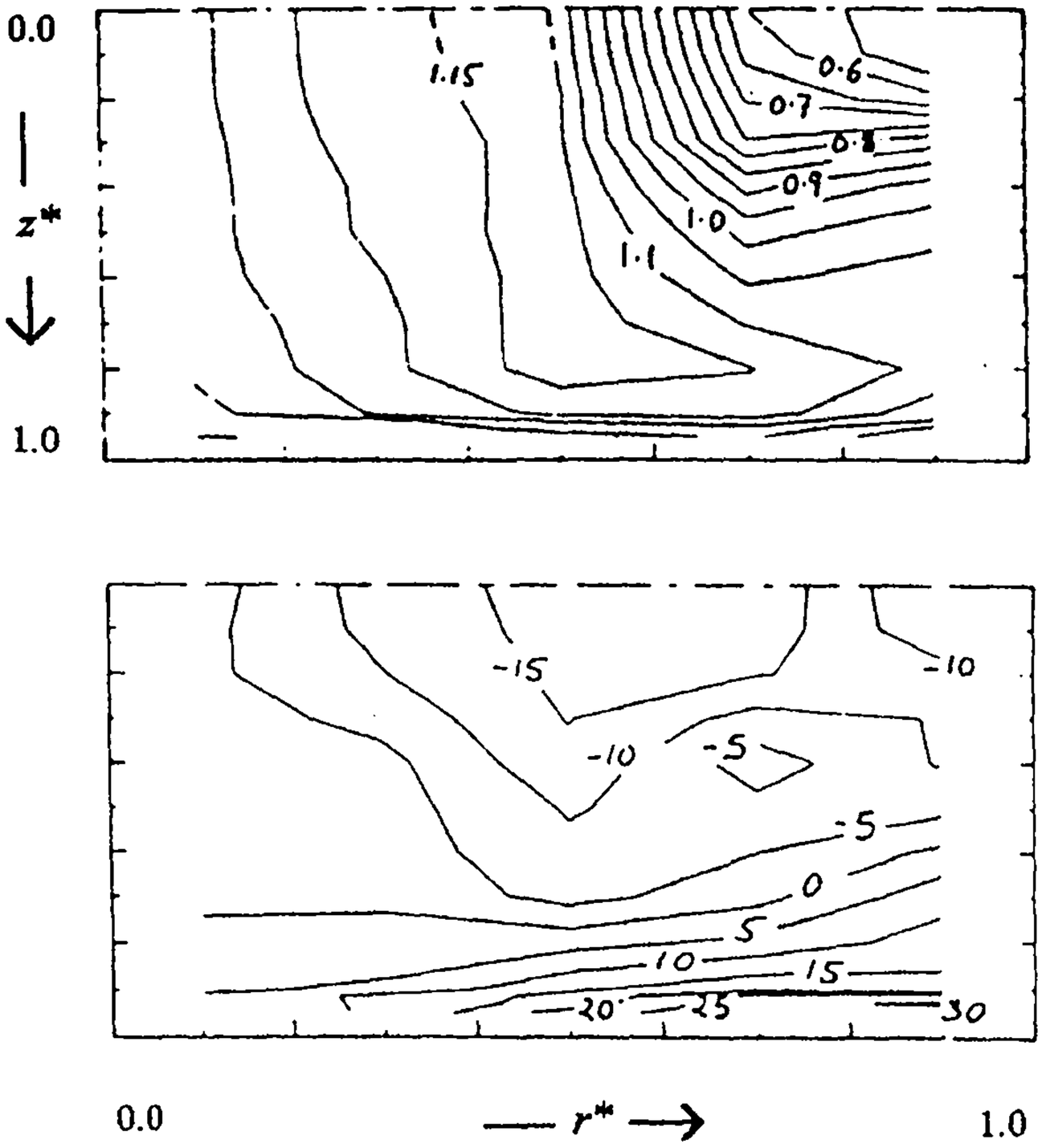

Figure 7.8 - Isovalue lines of the measured values of U/U_b (top) and V/U_b (bottom) at 0.25 hydraulic diameters downstream of the bend exit plane, taken from Taylor et al. (1981).

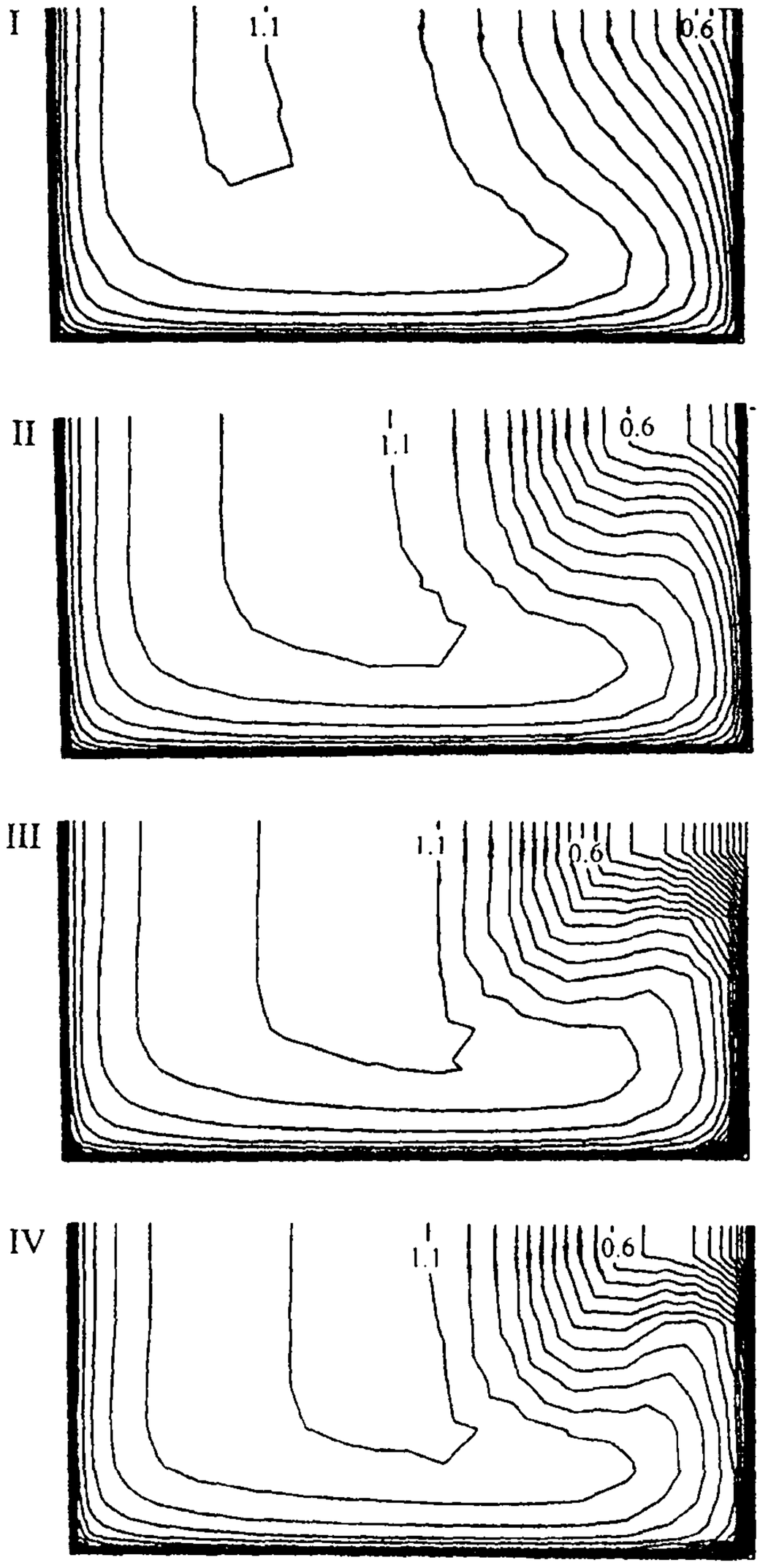

Figure 7.9 - Isovalue lines of U/U_b calculated with the ***eddy viscosity formulation****, using:(I) first-order Upwind, (II) the SOUCUP scheme, (III) the QUICK scheme and (IV) the fifth-order Upwind.*

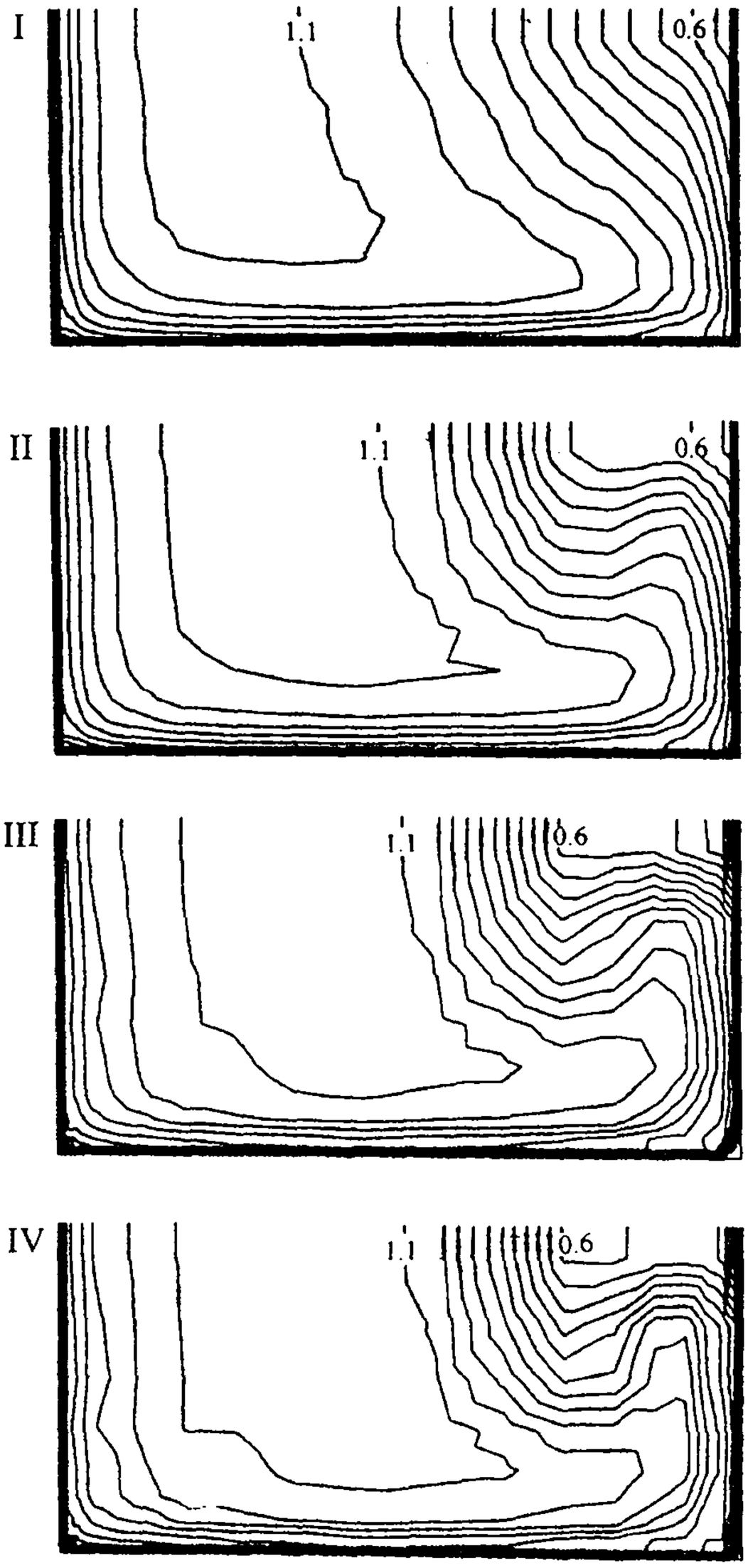

Figure 7.10 - Isovalue lines of the values of U/U_b, calculated with the ***modified formulation*** *using: (I) first-order Upwind, (II) the SOUCUP scheme, (III) the QUICK scheme and (IV) the fifth-order Upwind.*

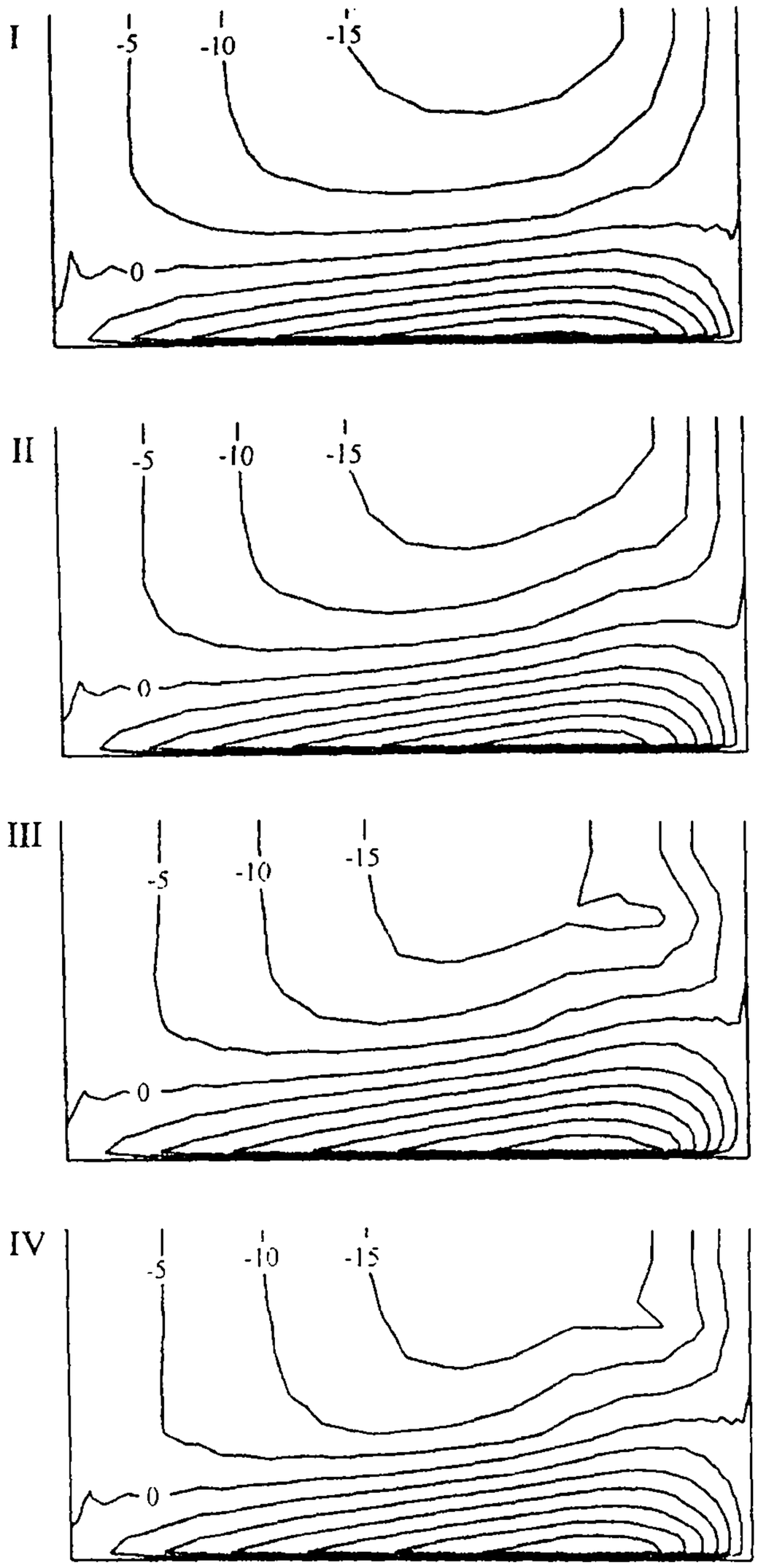

Figure 7.11 - Isovalue lines of V/U_b calculated with the ***eddy viscosity formulation*** *using: (I) first-order Upwind, (II) the SOUCUP scheme, (III) the QUICK scheme and (IV) the fifth-order Upwind.*

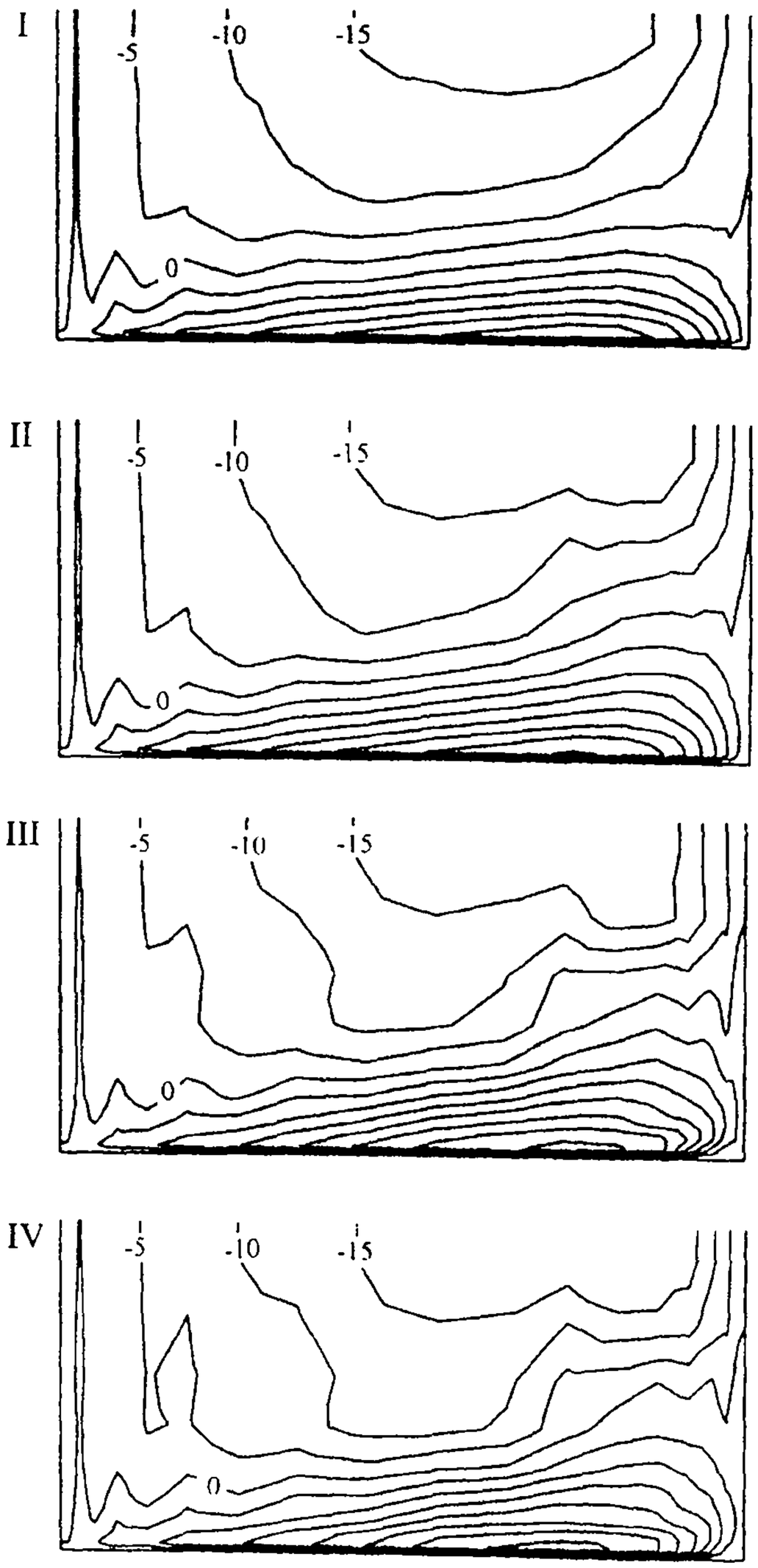

*Figure 7.12 - Isovalue lines of V/U_b calculated with the **modified formulation** using: (I) first-order Upwind,(II) the SOUCUP scheme, (III) the QUICK scheme and (IV) the fifth-order Upwind.*

7.3 - Results with the non-linear modelling of the Reynolds stresses.

Before attempting to determine the value of the constant C that multiplies the non-linear term in the expression (6.8.3) of the Reynolds stresses, it is important to notice that the different modelling of the Reynolds stresses will affect principally the diffusion term in the governing equations. The effect on the diffusion of the non-linear term, that has been introduced as a correction to the linear formulation of the Reynolds stresses and presumably contributing in a lesser part to the turbulent diffusion term, could be hidden by the additional numerical diffusion introduced by a low-order convection scheme as the first-order Upwind. For this reason the non-linear modelling of the Reynolds stresses will be initially tested in conjunction with the three-dimensional QUICK (third-order) scheme.

In figure 7.13 the isovalue lines of U/U_b in the reference section (cross section at 0.25 hydraulic diameters downstream the bend exit plane) calculated with the non-linear modelling of the Reynolds stresses, for several values of the constant C, are presented. For C=0.002 an increase of the velocity towards the pattern present in the measured data is observed (line U/U_b=1.15); increasing the constant to C=0.004 both the lines U/U_b=1.15 and U/U_b=1.1 reach a position very close to the corresponding lines in the measured data (figure 7.8). A further increase of the constant to C=0.006 does not produce additional effects. The value C=0.004 is therefore adopted; notice that this value is very close to the one proposed by Baker and Orzechowki for their model (although in their work it is not clear which convection model has been used, that, as has been pointed out and will be shown later, affects the contribution of the non-linear part).

In figure 7.14 the isotachs of the values of V/U_b in the reference section calculated with the non-linear modelling of the Reynolds stresses, for several values of the constant C, are presented. In this case the effects of the non-linear term can be clearly observed in the shape of the line V/U_b=-10 that, for C=0.004, reaches a position very similar to the corresponding line in the measured data. Also in this case, an increase in the value of the constant does not produce additional effects.

If a first-order Upwind is used for the treatment of the convection, a small increase in the value of the streamwise velocity is observed for the much higher value C=0.01 while no effect can be observed on the gapwise velocity (figure 7.15).

The non-linear model causes the movement of the position of the minimum value of the pressure towards the plane of symmetry, while the value itself increases in absolute value. This effect corresponds to the movement of the centre of each of the secondary vortices towards the symmetry plane and an increase in the intensity of the secondary flows (figure 7.16).

The comparison with the measured data available shows an improvement in the prediction of the pressure field, as can be seen in figures 7.17 and 7.18, where both the streamwise and gapwise distributions of the non-dimensional pressure coefficient *Cp* defined as:

$$Cp = \frac{p - p_{ref}}{\frac{1}{2}\rho V_C^2}$$

where p_{ref} is the pressure at the bend entry on the wall on the suction side of the bend (wall towards the centre of curvature) in the plane of symmetry, are represented for the pressure side of the bend.

Finally, in figures 7.19 and 7.20 the comparison with the experimental measurements of the predicted streamwise velocity profiles obtained with the eddy viscosity formulation and the modified formulation with both the linear and non-linear modelling, is presented, while in figures 7.21 and 7.22 the predicted distributions of streamwise velocities are presented in the form adopted by Tamamidis and Assanis (as in figure 5.36 in the fifth chapter).

Although the results presented for the 90° bend show that the simple quadratic correction introduced in the modelling of the Reynolds stresses allows a very close prediction of the streamwise velocity profiles, therefore contributing positively to the resolution of both the anisotropy in the turbulence introduced by the bend and the effects of streamline curvature on the stresses, the proposed modelling (6.8.3) is certainly not an universal formulation for the Reynolds stresses, while the modelling constant *C* cannot be defined by this single test alone.

It is interesting to notice that increasing the value of the constant *C*, even doubling it, no difference can be observed in the results, while much higher values of *C* cause the complete divergence of the procedure. At the same time, a comparison with some of the other non-linear models proposed in the literature seems to suggest a much higher value of the modelling constant than the one used in the previous section.

As the introduction of additional terms in the modelling of the Reynolds stresses appears to cause a further deterioration in the stability of the procedure, it could be argued that, for three-dimensional applications, the choice of the formulation for the Reynolds stresses should be made also on the basis of considerations of stability and 'practicality'. Convergence with Reynolds stresses formulations designed to represent a large number of more or less complex flows could prove to be impossible, while the

introduction of simple *ad hoc* corrections, as in this study, could lead to a sharp improvement in the prediction without an excessive computational cost.

Furthermore, as has been partially seen in this study, numerical diffusion plays an important role in the choice of the modelling constant; some of the values obtained in the previous works through computer optimisation could therefore depend on the convection scheme adopted, while the values proposed for stress-strain relationships calibrated through eddy viscosity formulations could be severely affected by an over-prediction of the physical diffusion caused by the simplified modelling of the turbulent diffusion term, as in (6.4.2). It is clear that much more work has yet to be done in this field.

In the form presented for the modified $k-\varepsilon$ method any modelling of the Reynolds stresses can be directly adopted, in a completely general formulation, while keeping the simple formulation of the standard $k-\varepsilon$ method.

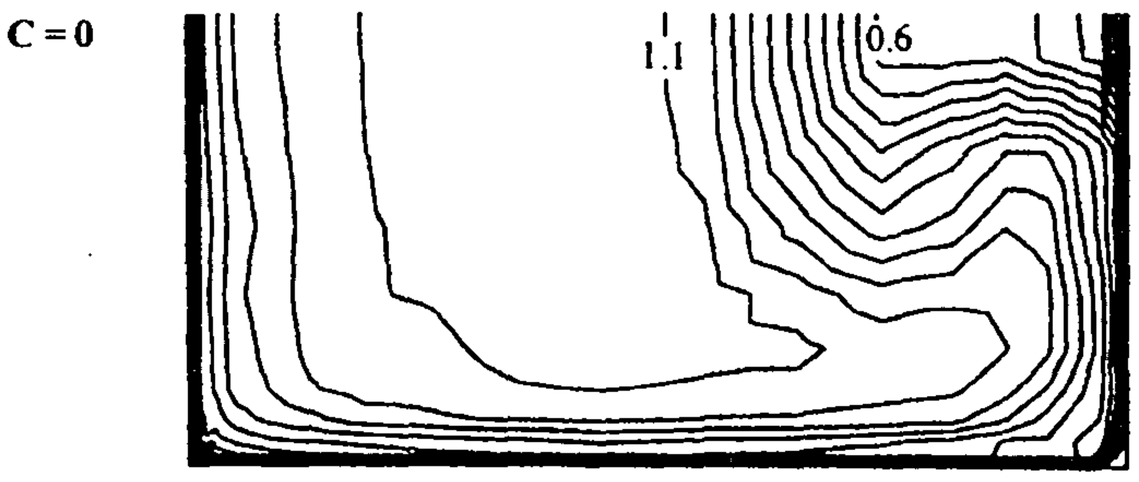

*Figure 7.13 - Isovalue lines of U/U_b calculated with the non-linear modelling of the Reynolds stresses for several values of the constant C, using the **QUICK** scheme.*

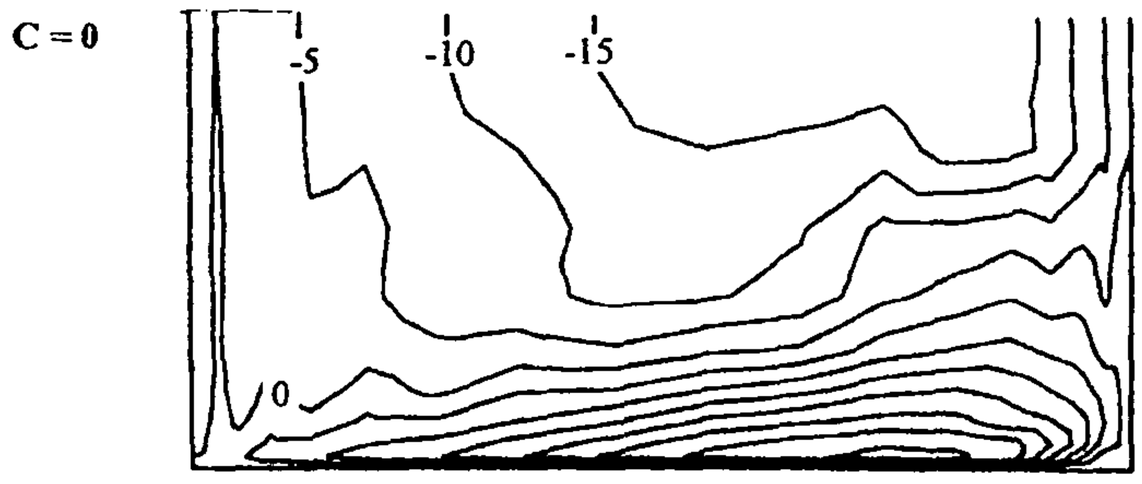

*Figure 7.14 - Isovalue lines of V/U_b calculated with the non-linear modelling of the Reynolds stresses for several values of the constant C, using the **QUICK** scheme.*

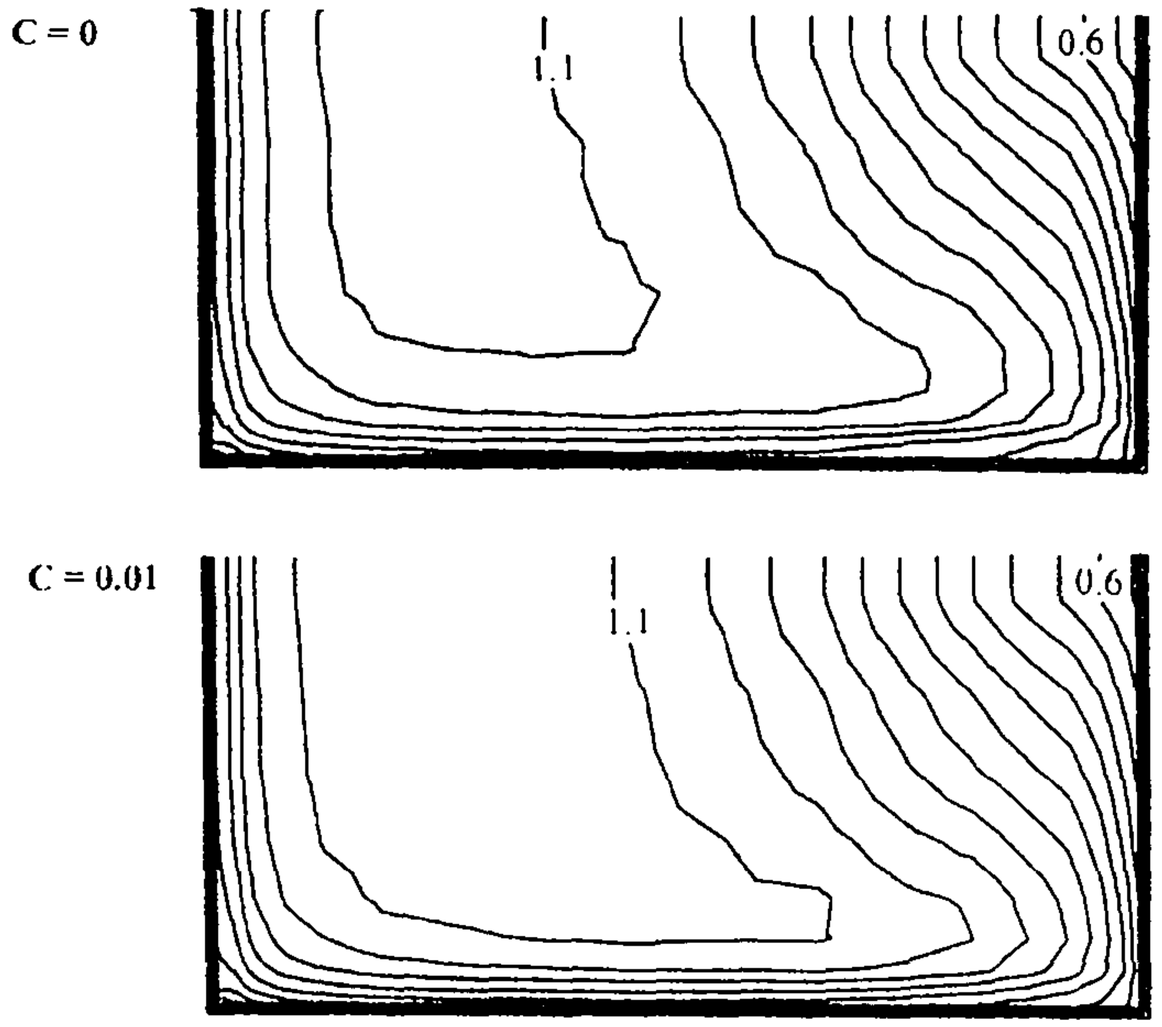

Figure 7.15 - Isovalue lines of U/U_b (top two) and V/U_b (bottom two) calculated with the non-linear modelling of the Reynolds stresses for several values of the constant C, using the first-order ***Upwind*** *scheme.*

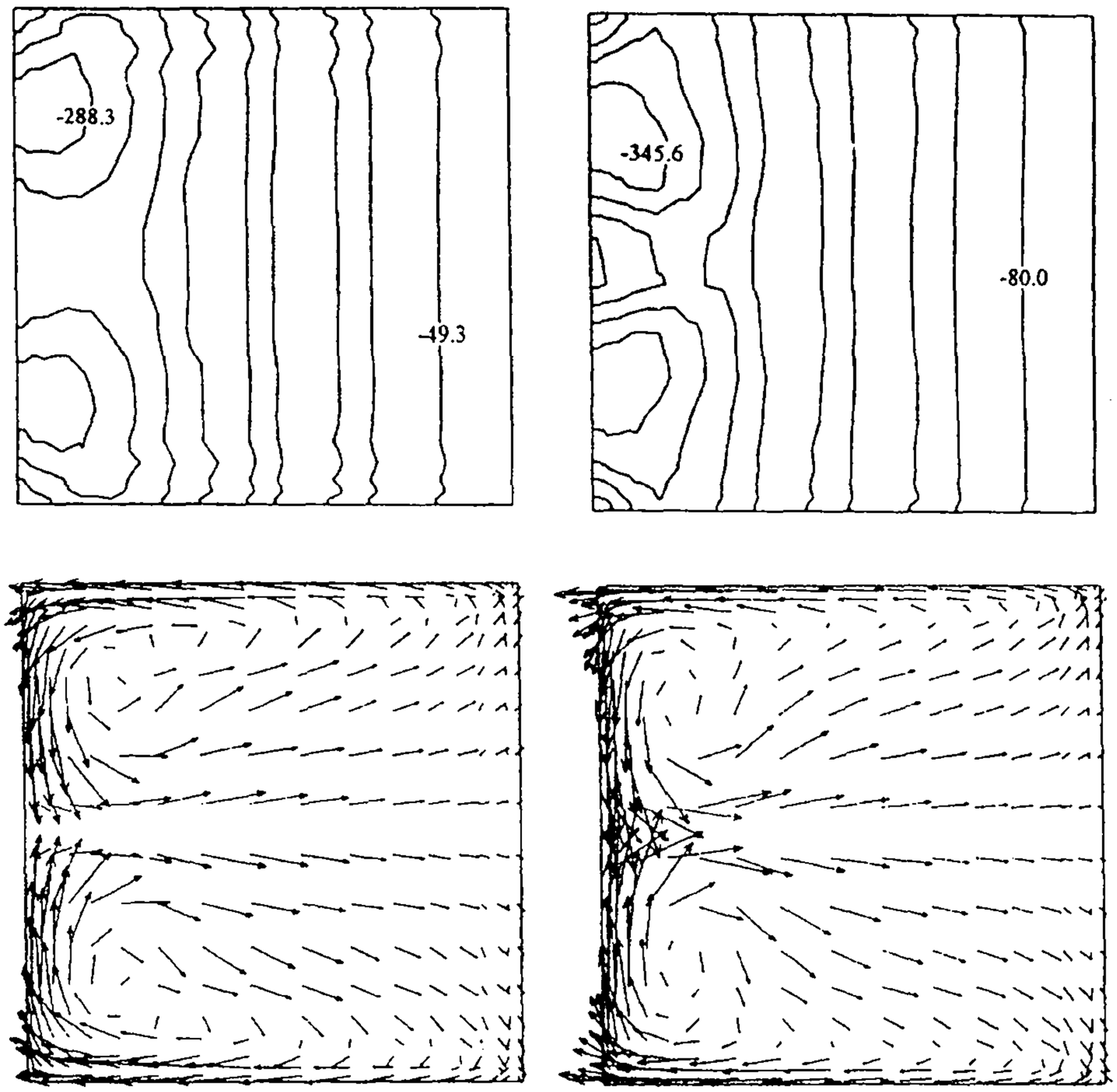

*Figure 7.16 - **Top:** Isobars of p-p(inlet) in N / m^2 calculated using the linear modelling of the Reynolds stresses (left) and the non-linear modelling (right). **Bottom:** secondary flow (at 0.25 hydraulic diameters downstream the bend exit plane) calculated using the linear modelling of the Reynolds stresses (left) and the non-linear modelling (right).*

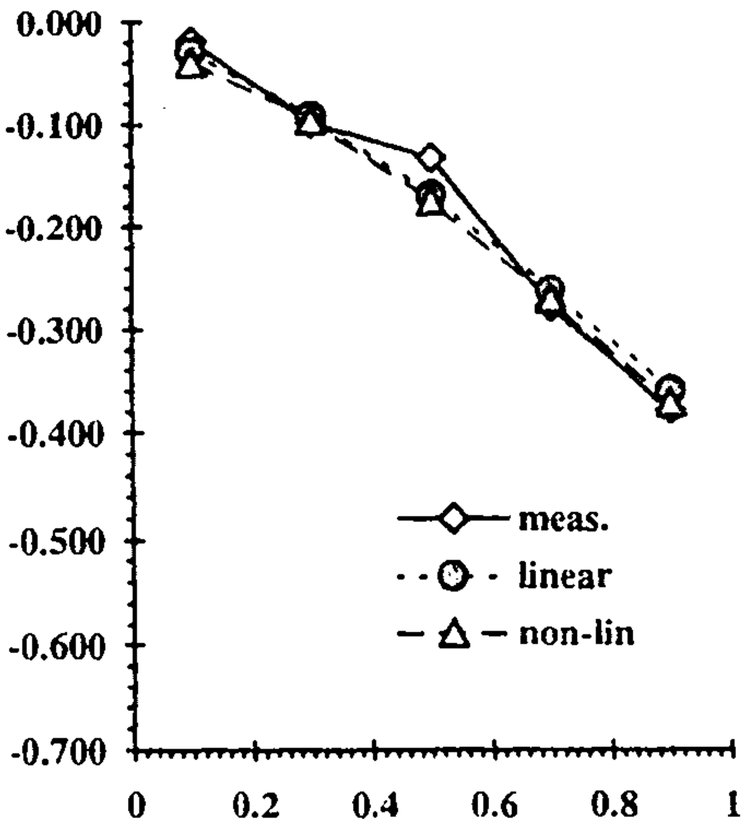

Streamwise location $\vartheta = 0°$

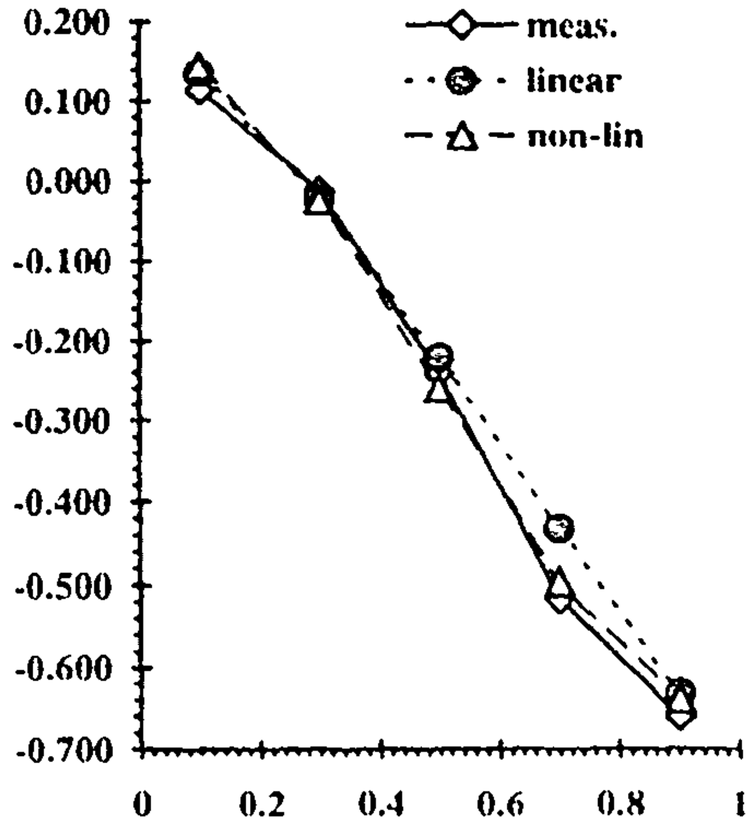

Streamwise location $\vartheta = 45°$

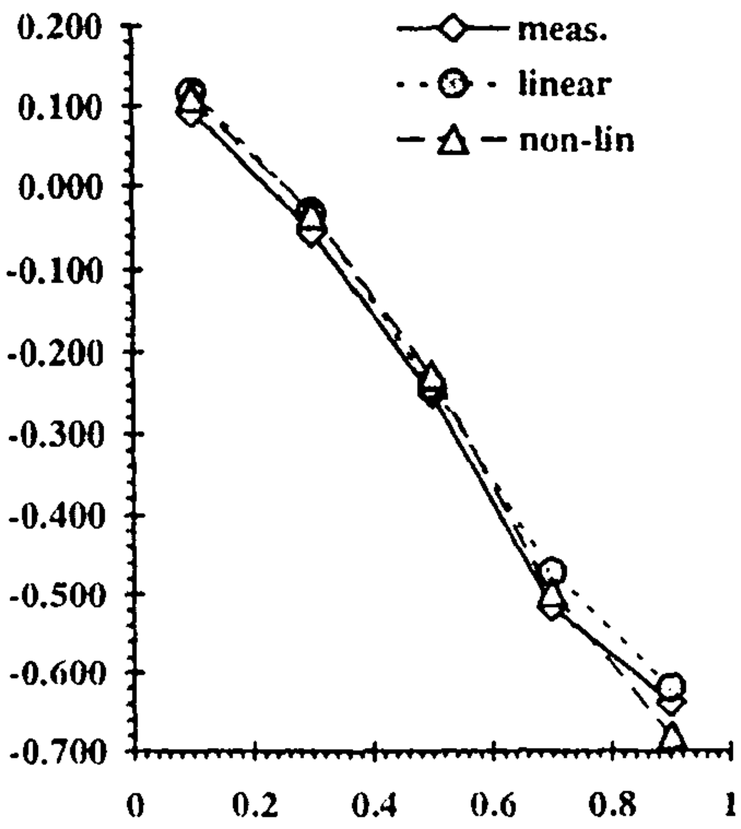

Streamwise location $\vartheta = 71°$

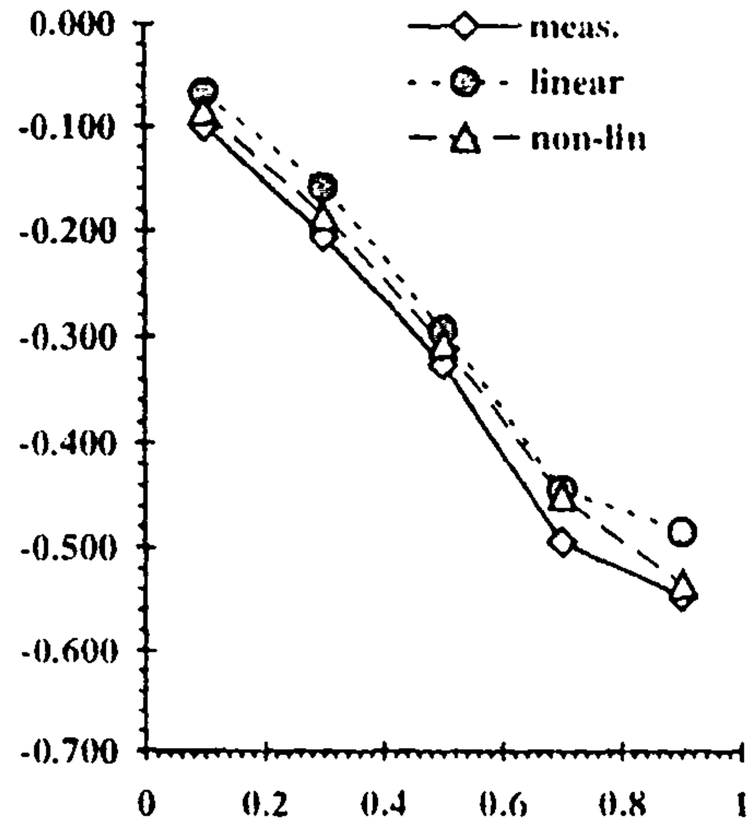

Streamwise location $\vartheta = 90°$

Figure 7.17 - Gapwise distribution of the pressure coefficient Cp on the wall on the pressure side of the bend, in function of the distance from the symmetry plane normalised by the duct half-span, at different streamwise planes (given by the angle formed with the bend entry plane).

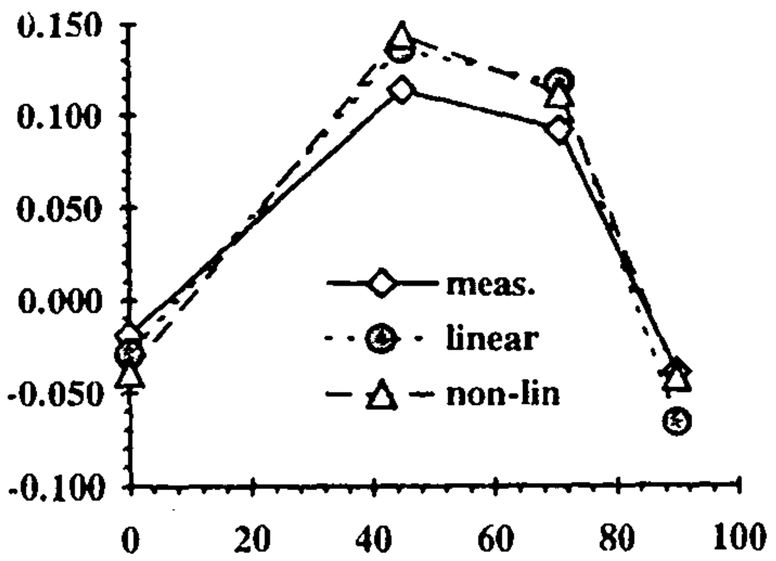

Gapwise position = 0.1

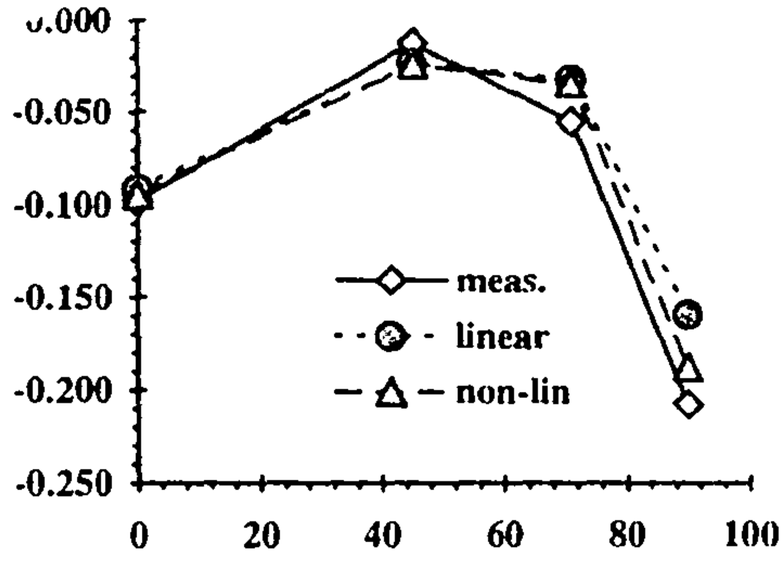

Gapwise position = 0.3

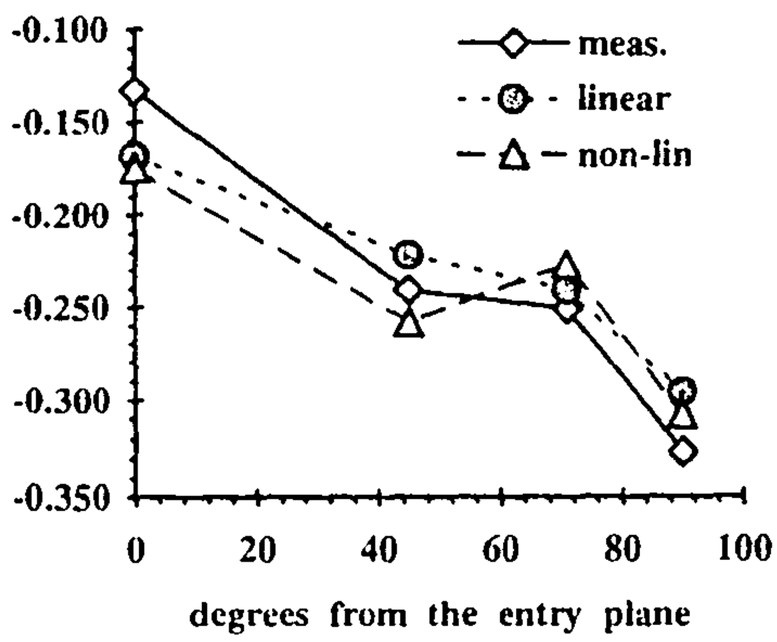

Gapwise position = 0.5

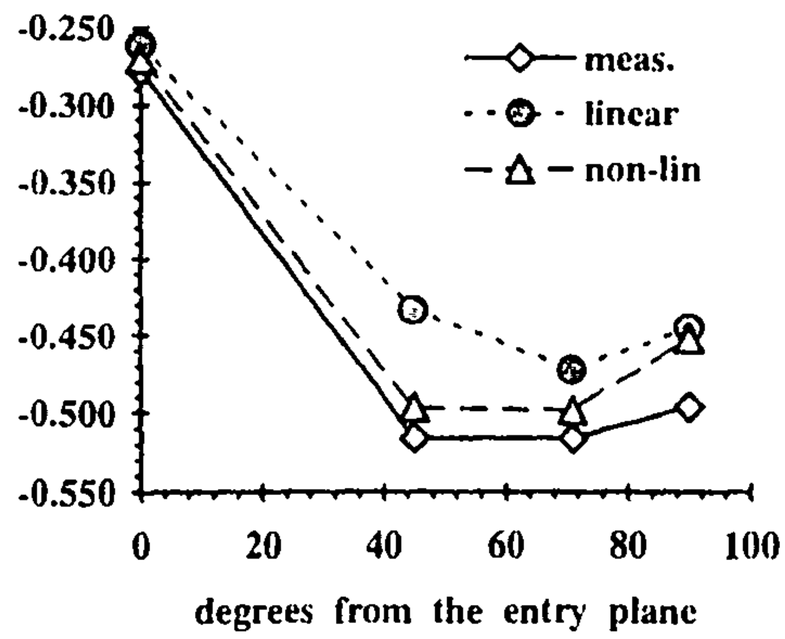

Gapwise position = 0.7

Figure 7.18 - Streamwise distribution of the pressure coefficient Cp on the wall on the pressure side of the bend, at different gapwise positions.

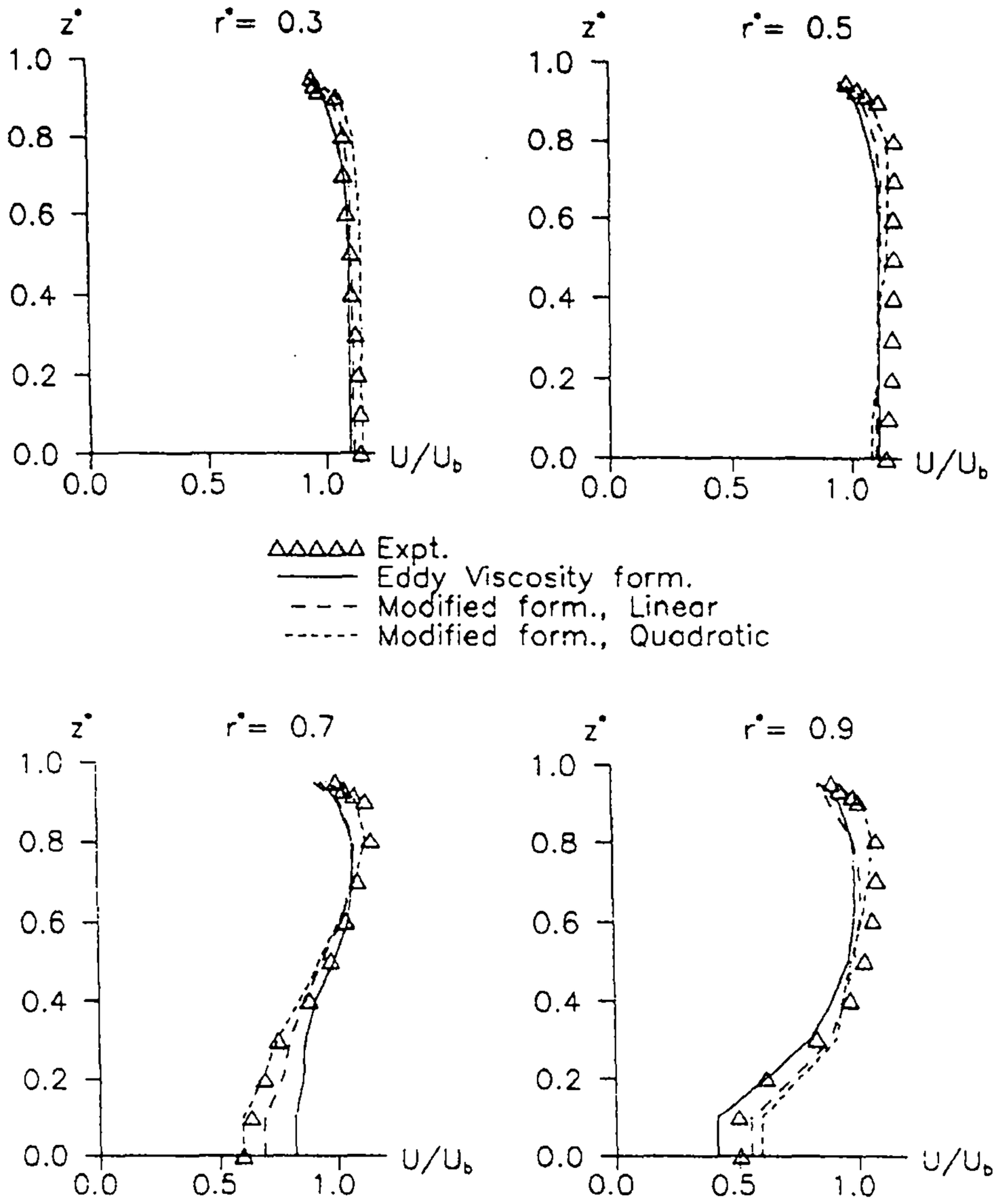

Figure 7.19 -Streamwise velocity at 77.5° from the bend entry plane, comparison with experimental measurements.

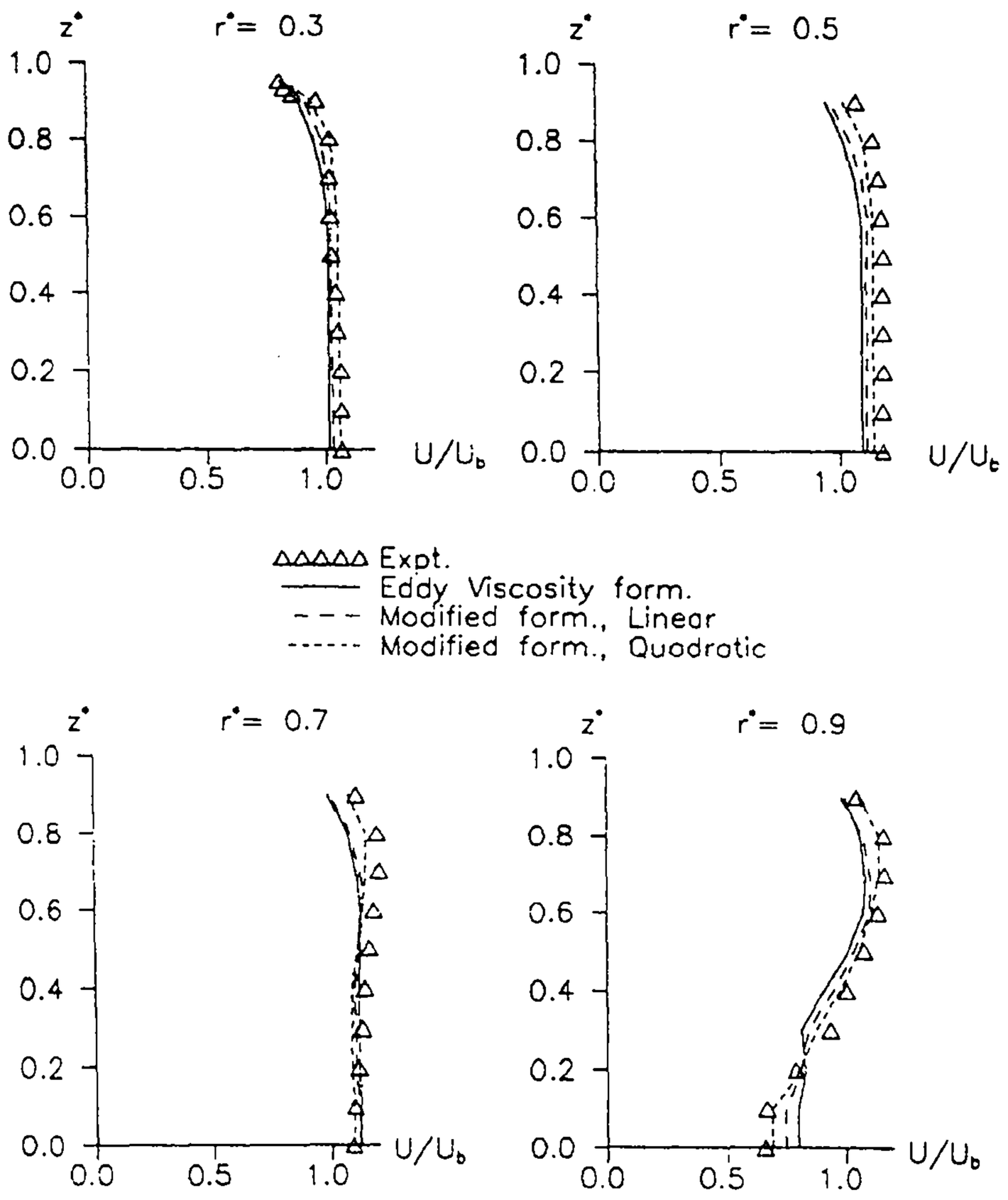

Figure 7.20 - Streamwise velocity at 0.25 hydraulic diameters downstream of the bend exit plane, comparison with experimental measurements.

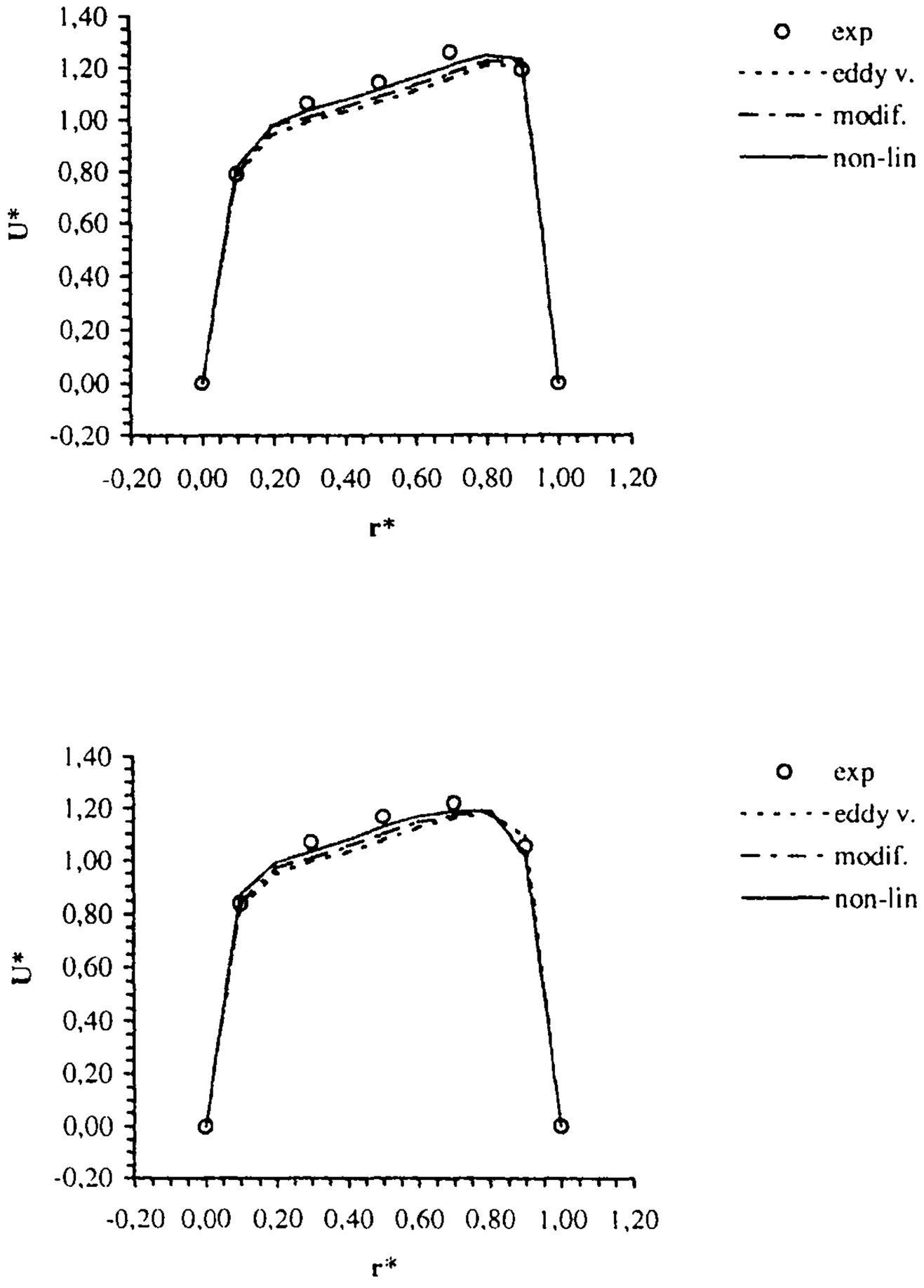

Figure 7.21 – Turbulent flow: comparison between calculated and measured distributions of streamwise velocities at the 30° (top) and 60° (bottom) stations.

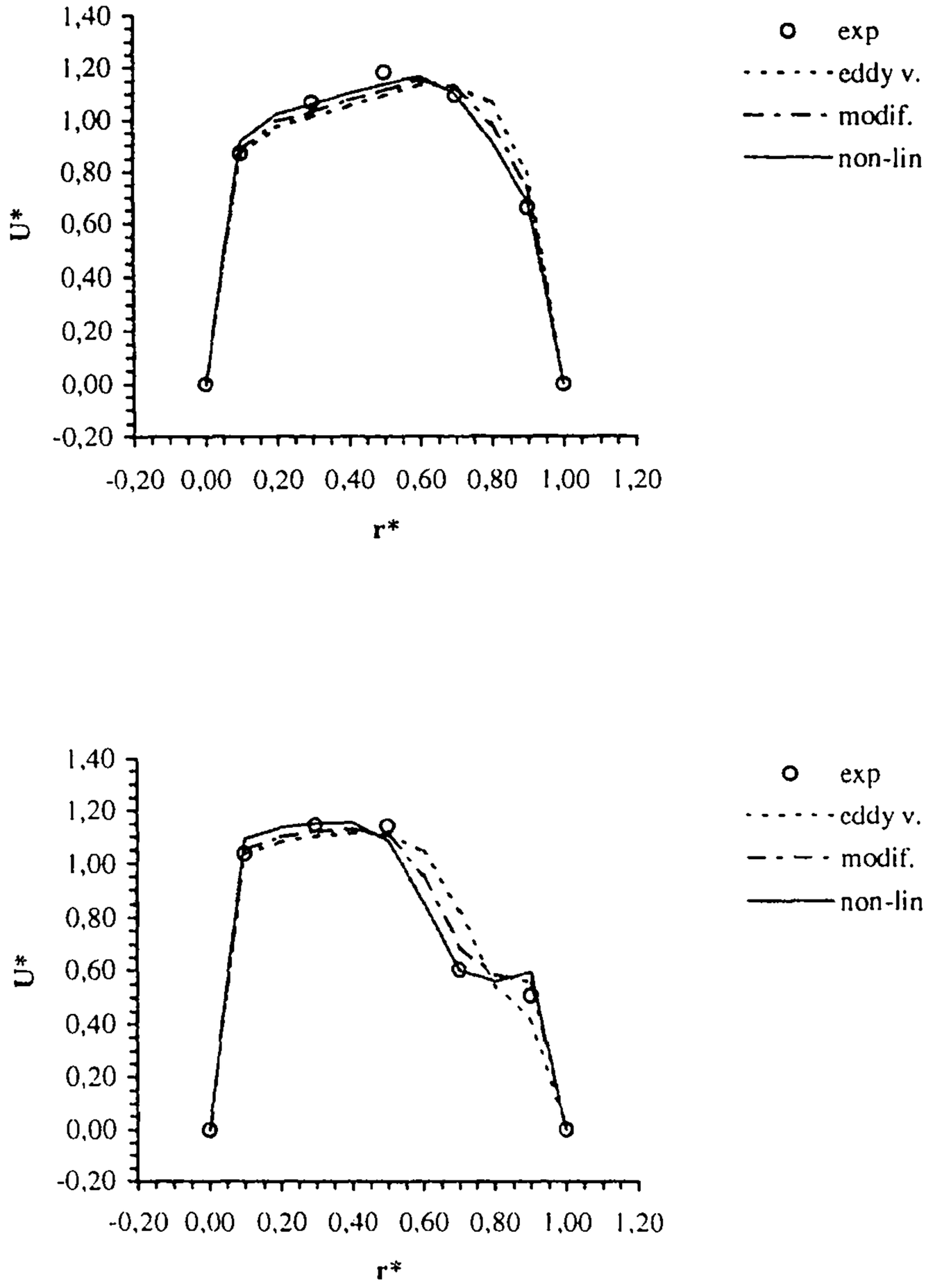

Figure 7.22 – Turbulent flow: comparison between calculated and measured distributions of streamwise velocities at the 77.7° station (top) and at 0.25 hydraulic diameters from the bend exit plane (bottom).

Chapter 8
The rotating diffuser

8.1 - Geometry and boundary conditions.

A single, rotating radial-outflow channel of simple geometry, as the one used by Moore (1973) for his experimental measurements, can be extremely useful in describing the effects of rotation and secondary flows in rotating flow passages. In particular, at high flow rates the measurements indicate the formation of a large wake region on the suction (trailing) side of the passage.

A qualitative description of the wake formation can be given as follows (Dean, 1968): it appears that in the diffusing flow the boundary layer thickens and the flow separates on the trailing side of the rotating passage (suction side); the flow separation is followed by the formation of a wake which appears to be fed by secondary flows.

The test section used by Moore, shown in figure 8.1, had a constant height of $0.0762m$ (3") and the side walls were radii with an included angle of 15°. The length of the test section was $0.6096m$ with a square inlet at a radius of $0.3048m$. The test section was located at the end of an inlet 90° bend, which turned the flow from an axial to a radial direction; the inlet bend was designed to deliver a potential flow, with thin boundary layer, at the inlet of the test section:

$$U = \overline{U} + 2\Omega y \tag{8.1.1}$$

where the coordinate system is defined in figure 8.1, Ω is the rotational speed ($206rpm$ in the tests) and $\overline{U}$ is the mean velocity on the section. In figure 8.1 a comparison at channel mid-height of the measured velocity profiles and equation (8.1.1), is also represented for several flow rates.

The flow used was air, with $\rho = 1.2013875 Kg/m^3$ and $\mu = 0.00001853 Ns/m^3$. Only the 'large' flow rate will be considered in this study, corresponding to an inlet mean velocity of $\overline{U} = 34.56m/s$. The flow is incompressible.

As only a schematic view of the bend is given, only the test section (diffuser) can be adequately modelled; 32×28×60 grid points, respectively in the width, height and length directions, have been used (figure 8.2). No information is given in Moore's work on the velocity distribution at the inlet at large flow rate, other than the comparison with equation (8.1.1) in the mid-height plane. As was shown in the previous chapters, a 90° bend induces both a deformation in the streamwise velocity profiles and extensive

secondary flows, but, as no data is available on these effects, only equation (8.1.1) can be used: at the inlet the potential flow is assigned to the streamwise velocity, while the other two components of the velocity are assumed to be zero. Although introducing a large discrepancy with the test case, no other choice of boundary conditions at the inlet, due to the lack of data, is possible.

Furthermore, a pressure distribution has to be assigned at the outlet of the diffuser: if a Neumann condition is assumed for the pressure at the outlet, so that the pressure equation is closed by all Neumann conditions, an unphysical pressure distribution is obtained, with a decrease of the pressure from inlet to outlet, as can be seen in figure 8.3. As no value of pressure can be imposed at the inlet, where the velocity field had already been assigned, it is necessary to assign the pressure distribution at the outlet.

The only information available for the pressure are the measurements of a 'static pressure recovery coefficient' on the side walls of the channel at mid-height, in which the static pressure, the centrifugal pressure and the pressure of the potential flow appear. Using this data, supposing that the total pressure is constant across the section of the diffuser and using the additional arbitrary constant for the pressure (being the flow incompressible), an approximate relation for the pressure difference between the pressure side and the suction side of the walls at the outlet at mid-height can be obtained:

$$p_{ps} - p_{ss} \cong 45 N / m^2 \tag{8.1.2}$$

where the subscripts *ps* and *ss* refer, respectively, to the pressure and suction sides of the diffuser.

The most obvious way of imposing the pressure difference (8.1.2) at the outlet is through a linear variation:

$$p(y) = p_{ps} - \frac{y - y_{ps}}{y_{ss} - y_{ps}} \left(p_{ps} - p_{ss} \right) \tag{8.1.3}$$

(with the y axis directed from pressure side to suction side). The effective pressure distribution at the outlet of the diffuser is obviously very different from the linear variation (8.1.3); in particular, in the area where the wake is present, a region of approximately constant pressure is expected. In the absence of additional information, the relation (8.1.3) has been adopted to assign the boundary conditions for the pressure at the outlet.

Due to the approximations adopted both for the inlet and outlet boundary conditions, the results presented in this chapter have to be considered not as an attempt to predict the experimental data obtained by Moore but as a study on the effects of the different convection schemes and turbulence formulation on the prediction of the flow in a rotating passage, having Moore's measurements as a reference in analysing the results.

8.2 - On the stability of the k and ε equations.

One of the major problems in predicting turbulent flows in rotating passages is that the transport equations for k and ε can be affected by problems of stability, with the appearance of (unphysical) negative values, that cause the divergence of the whole procedure. The regions of the domain most likely to be affected by the appearance of negative values of the turbulence parameters are the one close to the solid walls, where a wall function is used to assign the boundary conditions. Generally, while a converged solution can easily be obtained for the k and ε equations when using a first-order Upwind as convection scheme, when higher-order convection schemes are used for these equations negative values of k or ε often appear near the walls.

In order to avoid this problem, while using at the same time higher-order schemes for the k and ε equations, a 'buffer' region is defined in the close vicinity of the walls; in this region first-order Upwind is always used, while in the rest of the domain higher-order schemes are adopted. This approach has proven to be very successful and can be easily implemented simply not adding the deferred correction, that contains the variation due to higher-order schemes, in the buffer region. In this study the buffer region near each wall is composed by just two cells.

A similar problem of stability for the k and ε equations is obtained when using the modified turbulence formulation, not based on the eddy viscosity. Also in this case, the appearance of negative values of the turbulence parameters is mostly concentrated in the cells close to the solid walls, even when using a first-order Upwind for the convection. In order to adopt a strategy similar to the previous one, the modified formulation is written as a correction to the eddy viscosity formulation; in the case of constant density, the modified formulation is written, in transformed coordinates:

$$\frac{1}{J}\frac{\partial}{\partial \xi_r}\left(\rho U_r u_i\right) = \frac{\partial p}{\partial \xi_r}\frac{\partial \xi_r}{\partial x_i} + \frac{1}{J}\frac{\partial}{\partial \xi_r}\left[J(\mu+\mu_t)g^{rs}\frac{\partial u_i}{\partial \xi_s}\right] + F_i + \\ + \frac{1}{J}\frac{\partial}{\partial \xi_r}\left[J\frac{\partial \xi_r}{\partial x_j}\left(\tau_{ji}^{R} - \tau_{ji}^{R,B}\right)\right] \quad i = 1,2,3 \tag{8.2.1}$$

$$\frac{1}{J}\frac{\partial}{\partial\xi_r}(\rho U_r k)=\frac{1}{J}\frac{\partial}{\partial\xi_r}\left[J\left(\mu+\frac{\mu_t}{\sigma_k}\right)g^{rs}\frac{\partial k}{\partial\xi_s}\right]+G-\rho\varepsilon+$$

$$+T_b\frac{1}{J}\frac{\partial}{\partial\xi_r}\left[JC_s\frac{k}{\rho\varepsilon}\frac{\partial\xi_r}{\partial x_j}\left(\tau_{il}^R\frac{\partial\xi_s}{\partial x_l}\frac{\partial\tau_{ij}^R}{\partial\xi_s}-\rho\tau_{jl}^R\frac{\partial\xi_s}{\partial x_l}\frac{\partial k}{\partial\xi_s}\right)-J\frac{\mu_t}{\sigma_k}g^{rs}\frac{\partial k}{\partial\xi_s}\right] \tag{8.2.2}$$

$$\frac{1}{J}\frac{\partial}{\partial\xi_r}(\rho U_r\varepsilon)=\frac{1}{J}\frac{\partial}{\partial\xi_r}\left[J\left(\mu+\frac{\mu_t}{\sigma_\varepsilon}\right)g^{rs}\frac{\partial\varepsilon}{\partial\xi_s}\right]+C_1\frac{\varepsilon}{k}G-C_2\frac{\varepsilon}{k}(\rho\varepsilon)+$$

$$+T_b\frac{1}{J}\frac{\partial}{\partial\xi_r}\left[-JC_\varepsilon\frac{k}{\varepsilon}\frac{\partial\xi_r}{\partial x_j}\tau_{jl}^R\frac{\partial\xi_s}{\partial x_l}\frac{\partial\varepsilon}{\partial\xi_s}-J\frac{\mu_t}{\sigma_\varepsilon}g^{rs}\frac{\partial\varepsilon}{\partial\xi_s}\right] \tag{8.2.3}$$

where the last term in all the equations is the correction to the eddy viscosity formulation, $\tau_{ij}^{R,B}$ are the Reynolds stresses calculated with the Boussinesq's modelling (6.5.3), and a blend parameter T_b has been introduced, to eventually reduce the effect of the correction in the k and ε equations, obtaining the original modified formulation for T_b=1.0 and the eddy viscosity formulation for T_b=0.0. For this test case T_b has been left to 1.0.

The correction to the eddy formulation is not added in the buffer regions; this procedure actually eliminates the appearance of negative values for the turbulence parameters in the cells close to the walls when using the modified formulation, although the relaxation parameters have to be lowered from the value adopted for the eddy viscosity formulation, to avoid a global divergence of the procedure.

Numerical tests have also shown that a small increase in the value of the modelling constant C_2 in equation (8.2.3) can provide an improvement in the stability of the procedure. For this test case, it has been found that an increase of 5% in respect to the value used in the previous chapter; that is adopting C_2=2.1, has sharply improved the stability of the procedure, while it was not possible to achieve convergence when the original value C_2=2.0 was used. In order to test the effect of this alteration of one of the modelling constants of the modified turbulence formulation on the accuracy of the solution, the predicted flow fields obtained for the turbulent flow in the 90° bend using the two different values of the constant C_2, that is 2.0 and 2.1, have been compared, where the QUICK scheme and the direct solver have been used. The differences between the two predicted flow fields have been found to be quite small, as can be seen

in the following table, where the predicted streamwise velocity at 0.25 hydraulic diameters downstream of the bend exit plane for r^*=0.3 has been presented:

Z^*	C_2=2.0	C_2=2.1
0.1	1.12736	1.12648
0.2	1.12404	1.12450
0.3	1.12721	1.12802
0.4	1.11636	1.11637
0.5	1.11413	1.11411
0.6	1.11643	1.11754
0.7	1.09929	1.09843
0.8	1.08646	1.08557
0.9	1.05350	1.05425

All the other velocity profiles show a similar behaviour; the adoption of the value C_2=2.1 appears, therefore, not to affect significantly the accuracy of the solution for this particular case. At the same time it is important to notice that this arbitrary change of one of the modelling constant is not defensible on physical modelling grounds and should not be used in general. The value of C_2 determines the decay of turbulence in shear free conditions (grid turbulence), and the experimental evidence indicated that a value between 1.8 and 2.0 is possible. The value adopted here, C_2=2.1, goes outside this range but, as said previously, convergence has not been achieved with lower values.

8.3 - Analysis of the numerical results.

All the results presented have been obtained using a direct solver for the pressure correction equation; the under-relaxation parameters used are 0.2 for all the variables when using the eddy viscosity formulation and 0.1 for u,v,w,p' and 0.05 for k and ε when using the modified formulation. Only the linear (Boussinesq) modelling of the Reynolds stresses has been adopted for the results presented in this chapter.

In the figures 8.4 to 8.14 the results obtained with the eddy viscosity formulation and the modified formulation, using both a first-order Upwind and the QUICK scheme, are presented. Three transversal reference planes have been chosen, at $0.8m$, $0.85m$ and $0.9m$ from the axis of rotation, the latter (plane III) being close to the exit of the diffuser; the position of the planes is illustrated in figure 8.1. In the figures the isovalue lines of pressure and u velocity in the mid-height plane, the isovalue lines of the u velocity and the secondary velocity in reference plane III, and the comparison of the u

velocity profiles in the three reference planes at channel mid-height, are presented. These velocity profiles, in particular, provide an interesting comparison with the measured velocity profile showing the appearance of the wake, taking into account the large approximations introduced with the choice of the boundary conditions.

As can be easily seen in the figures, a region of backflow is obtained on the suction side of the diffuser, towards the end of the duct; the comparison of the predicted velocity profiles and secondary flows in this region can provide useful information on the effects of the different convection schemes and turbulence formulation.

In particular, the following conclusions can be drawn:

1) The QUICK scheme appears to have a limited effect when used in conjunction with the eddy viscosity formulation: there appears to be a small difference between the results obtained with the two convection schemes, particularly in the region of backflow. The u velocity in the reference plane III shows a tendency towards a more steep profile towards the pressure side, as shown in the measured profiles, when using a QUICK scheme, although the variation due to the higher-order scheme remains quite small.

2) A drastic change in the solution is instead obtained when using the QUICK scheme with the modified formulation. The region of backflow appears to be the most affected by the use of the scheme, as can be easily seen comparing the results with the one obtained using the first-order Upwind. In particular, there is a sharp variation of the slope of the velocity profile in reference plane III, towards an extremely steep variation towards the suction side. These results are in agreement with the general tendency observed in the previous chapter, that show how the higher-order schemes appear to be more effective when used with the modified formulation of the k and ε equations.

3) The secondary flows in reference plane III predicted with the modified formulations appear to be quite different from the ones evaluated with the eddy viscosity formulation, even when using a first-order Upwind. In particular, the modified formulation predicts, with a first-order Upwind, a couple of well-defined counter-rotating vortices in the area of backflow that do not appear, or are not so well defined, in the solution obtained with the eddy viscosity formulation, both with first-order Upwind and QUICK. It is very interesting to notice that, when using a QUICK scheme, the modified formulation predicts that some of the flows close to top and bottom walls

'turns' towards the suction side and the two vortices, in a sense 'feeding' this area with additional flow.

Finally, it has to be pointed out that precise conclusions on the performance of the modified turbulence model cannot really be made on the sole basis of the results presented here, since it would be unsafe to draw conclusions from predictions obtained using a single mesh and just switching the order of accuracy of the convection scheme

Until grid refinement calculations are done, it cannot be absolutely clear that the differences that have been observed are really related to the turbulence model. Such calculations were not achievable with the computational power available for this study.

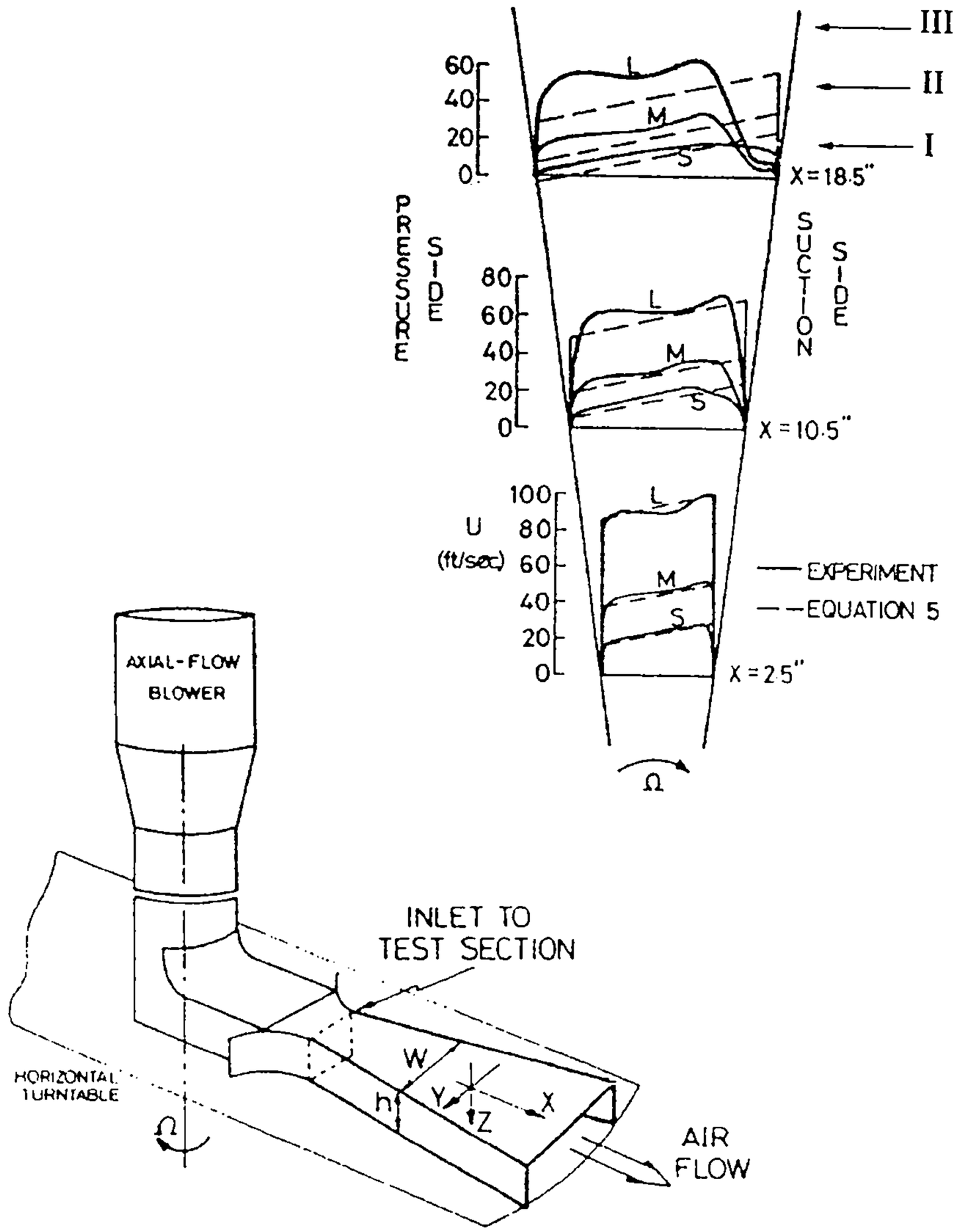

Figure 8.1 - Schematic view of the test section and comparison of measured velocity profiles and the potential velocity distribution for L-large, M-medium, S-small flow rates, at channel mid-height (taken from Moore,1973). The position of the planes chosen for reference in this study is also represented.

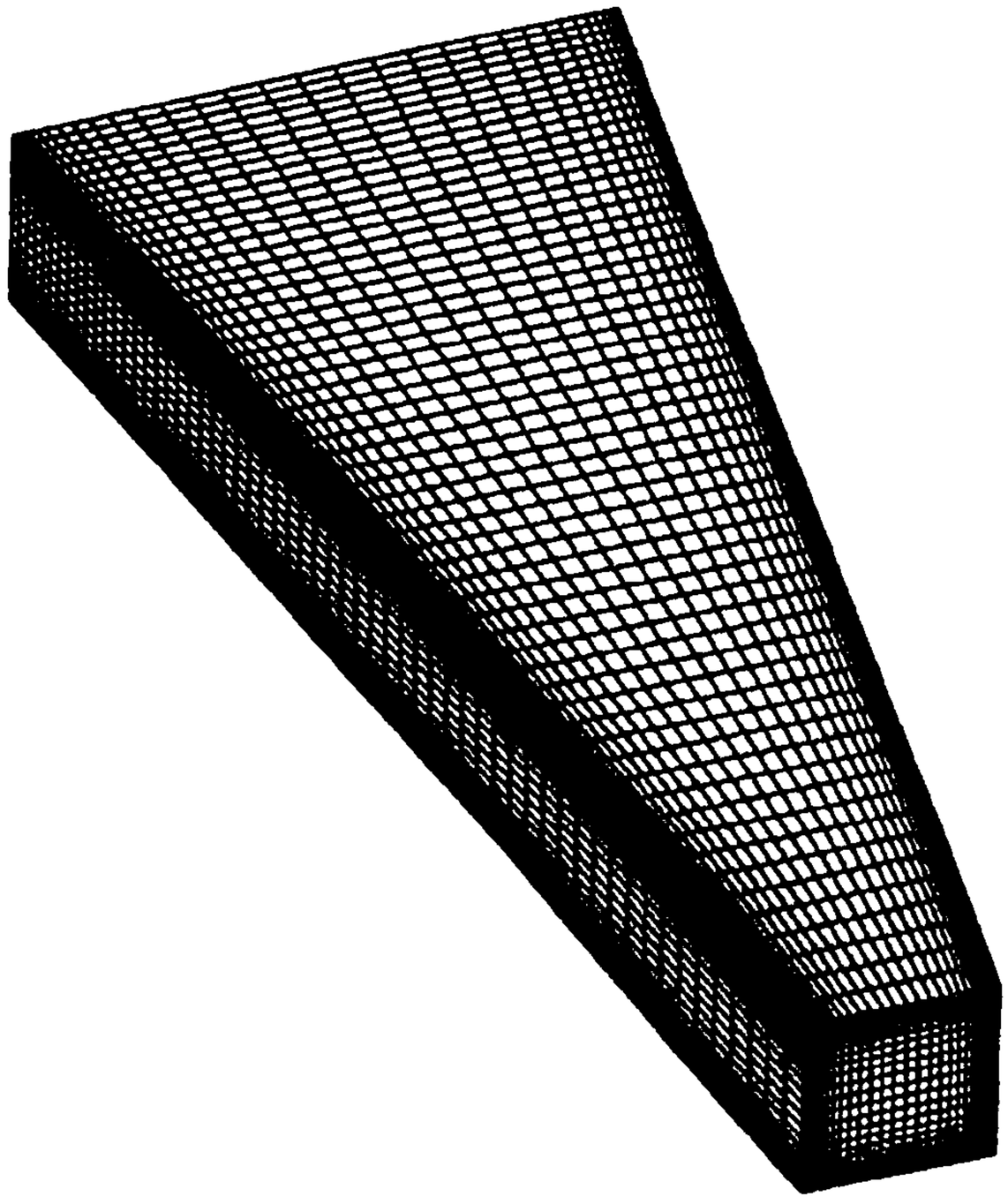

Figure 8.2 - View of the grid.

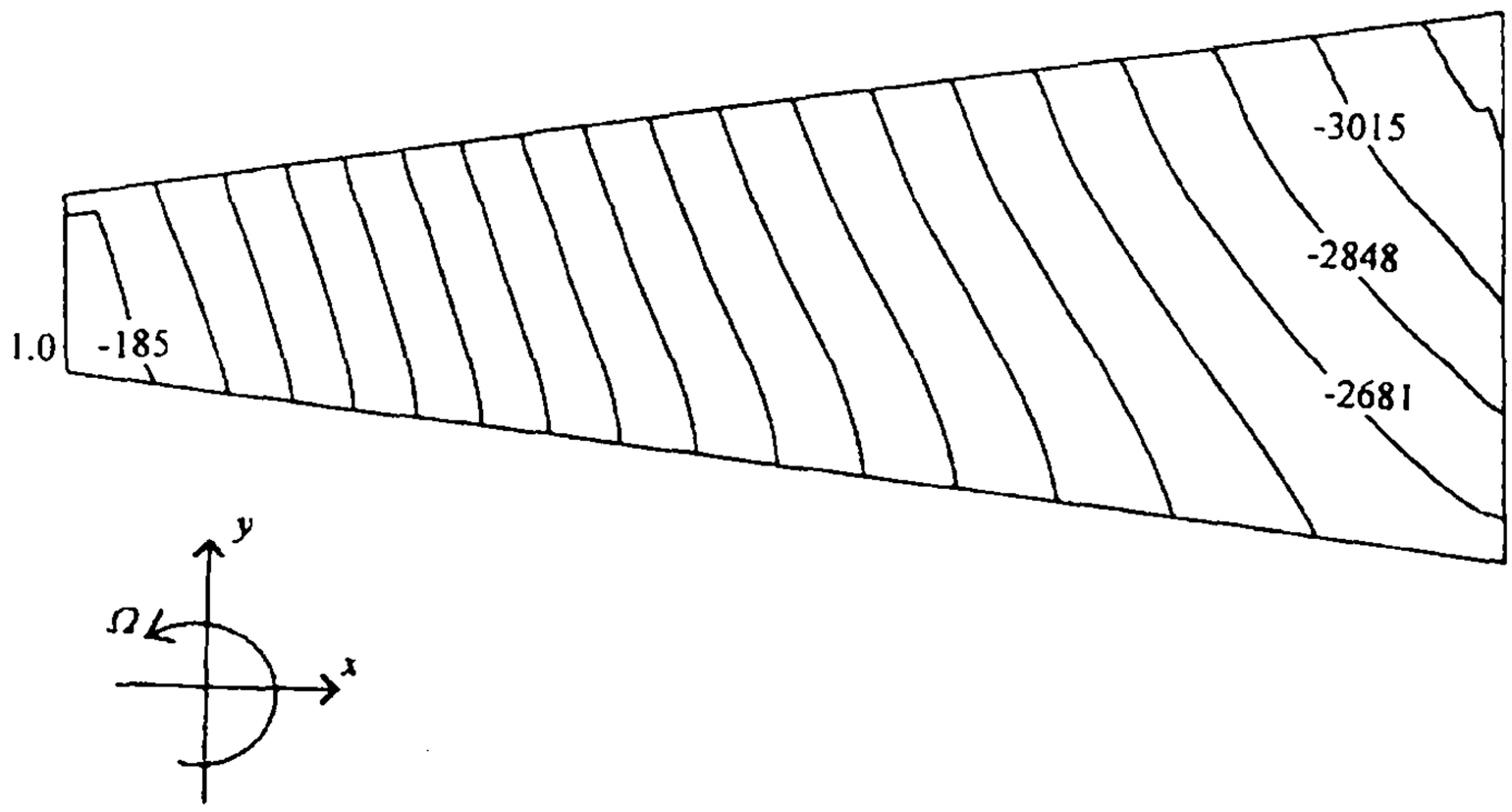

Figure 8.3 - Isovalue lines of the pressure at channel mid-height, using the eddy viscosity formulation, first-order Upwind with $dp / dn = 0$ at the outlet.

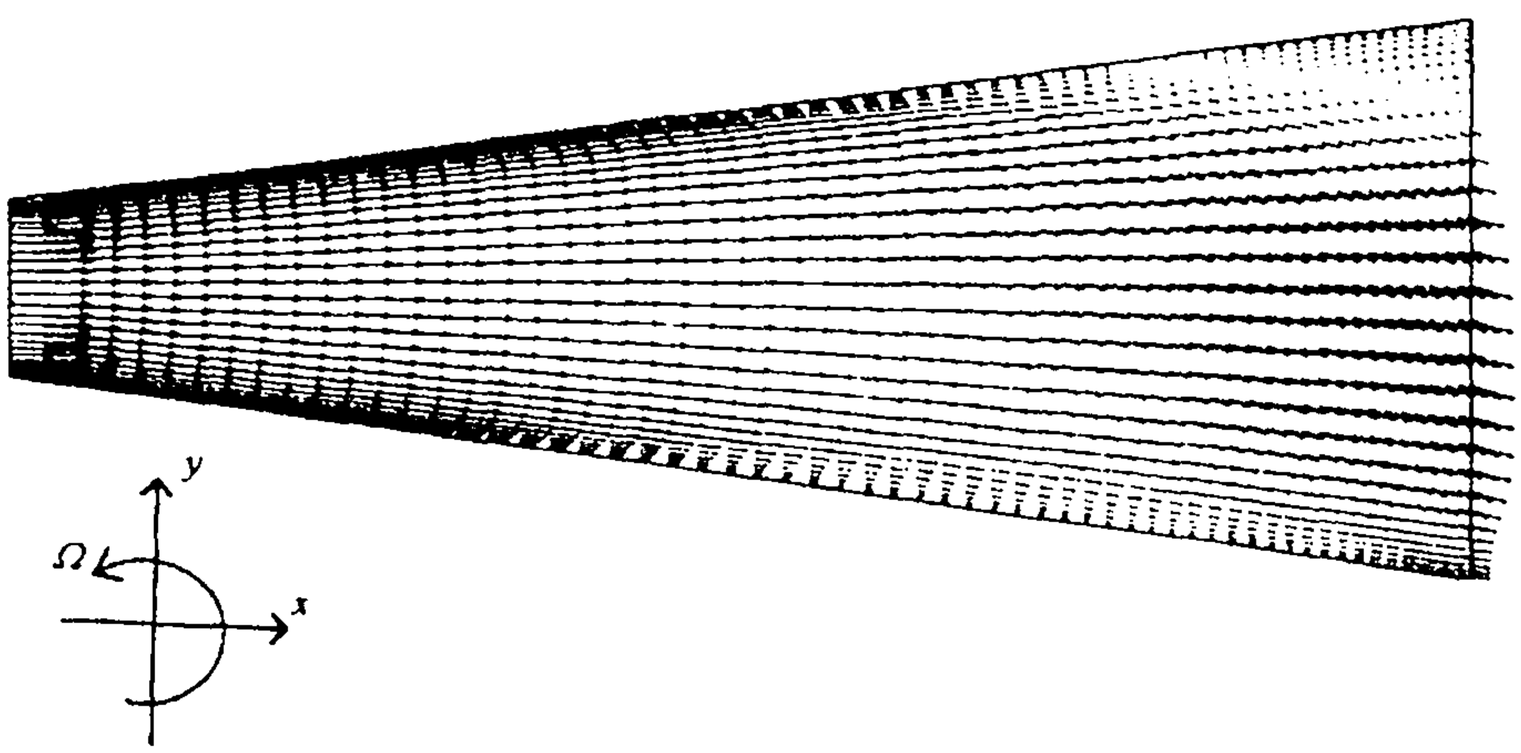

Figure 8.4 - Velocity field at channel mid-height, using the eddy viscosity formulation and first-order Upwind.

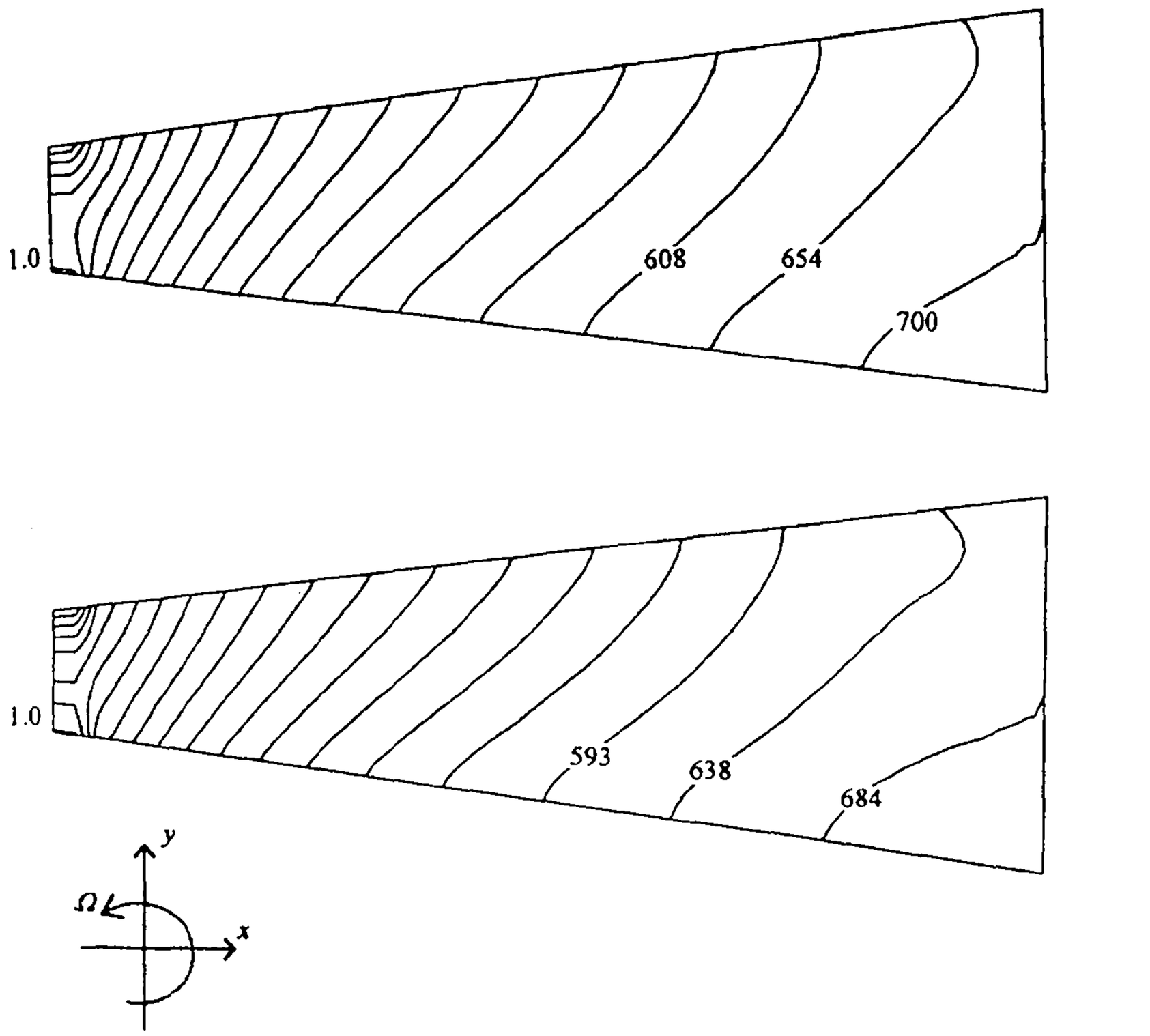

Figure 8.5 - Isovalue lines of the pressure at channel mid-height using the ***eddy viscosity*** *formulation and first-order Upwind (top) and QUICK (bottom).*

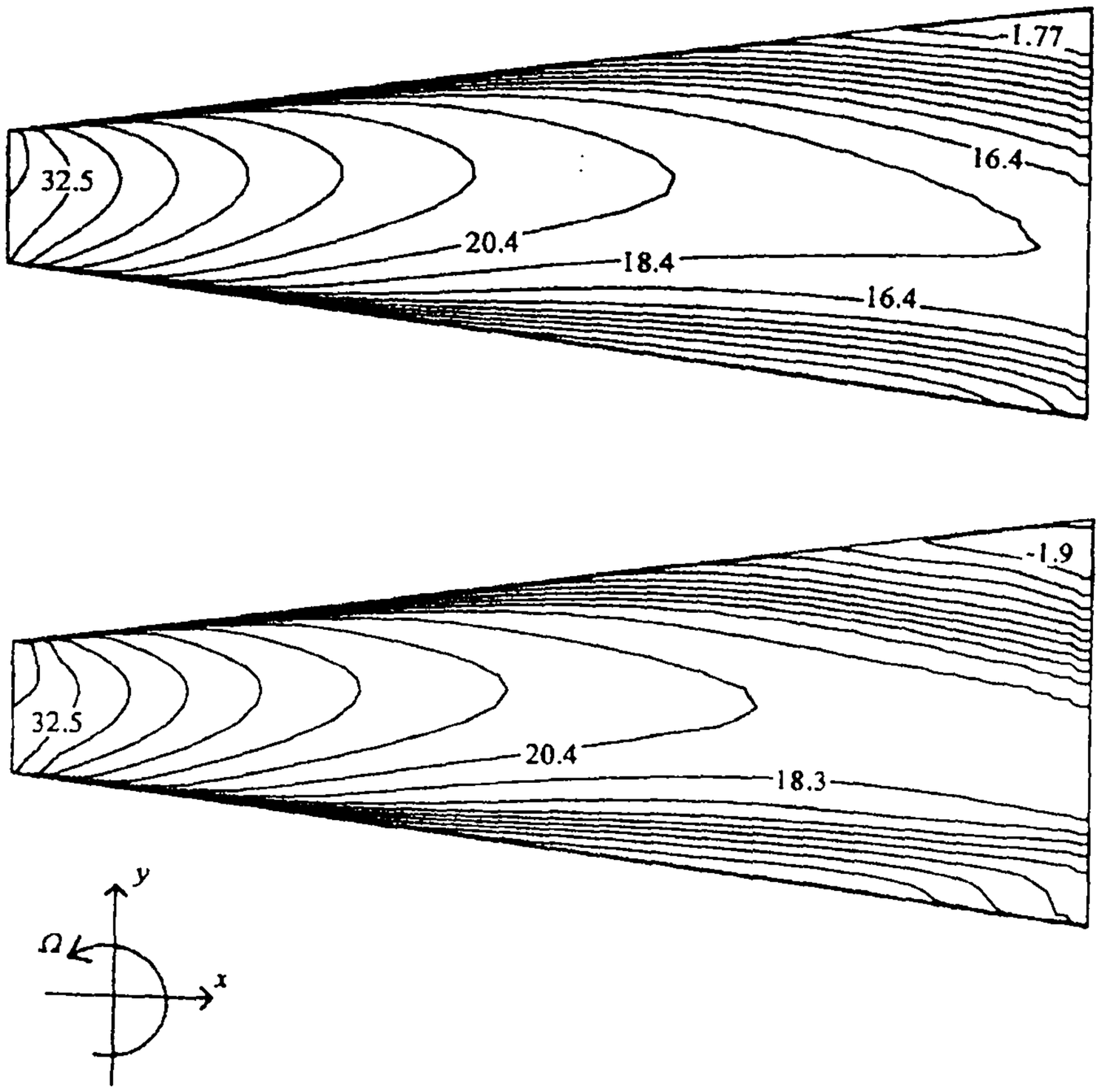

Figure 8.6 - Isovalue lines of the u velocity at channel mid-height using the ***eddy viscosity*** *formulation and first-order Upwind (top) and QUICK (bottom).*

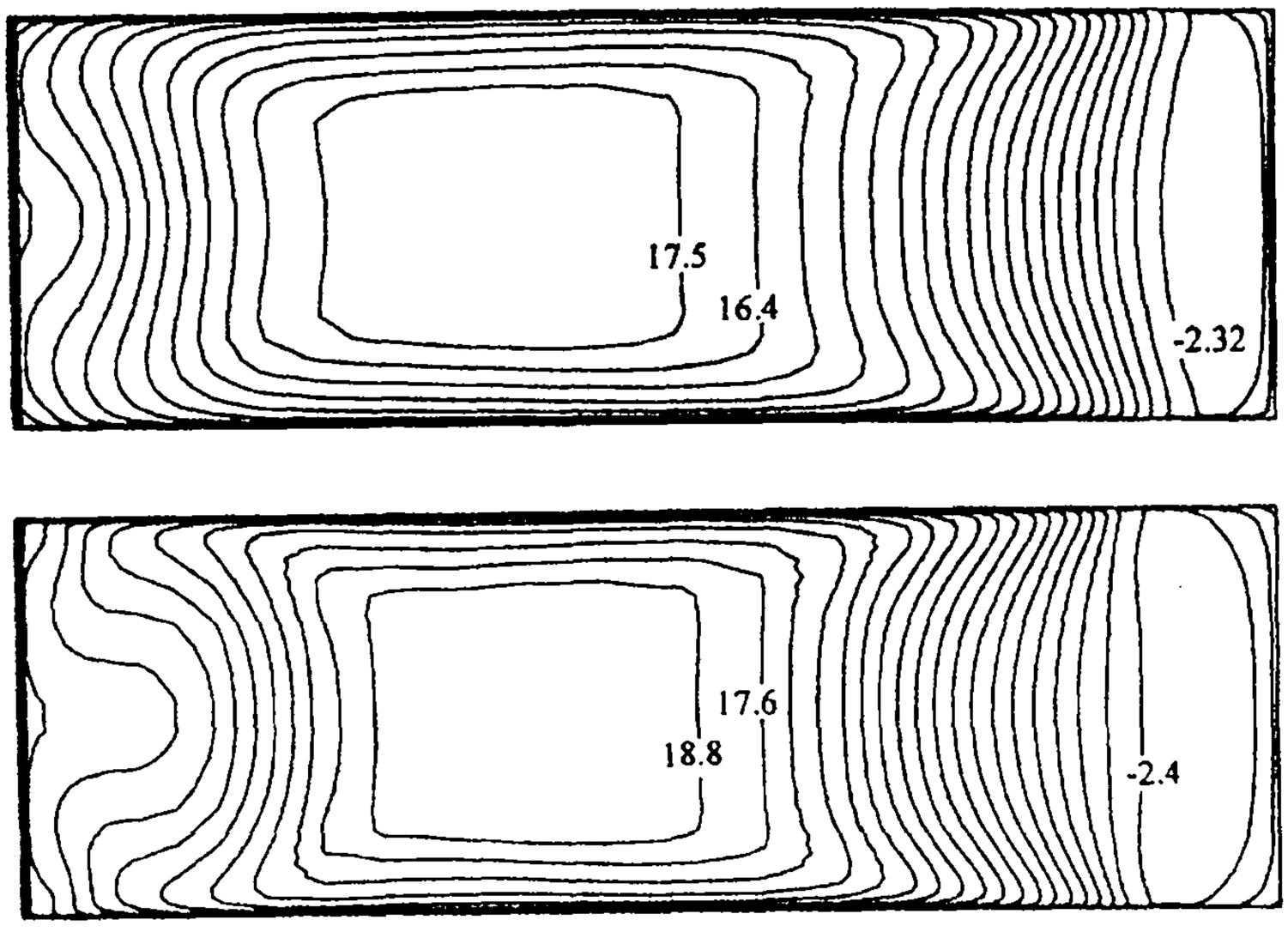

Figure 8.7 - Isovalue lines of the u velocity in reference plane III using the ***eddy viscosity*** *formulation and first-order Upwind (top) and QUICK (bottom).*

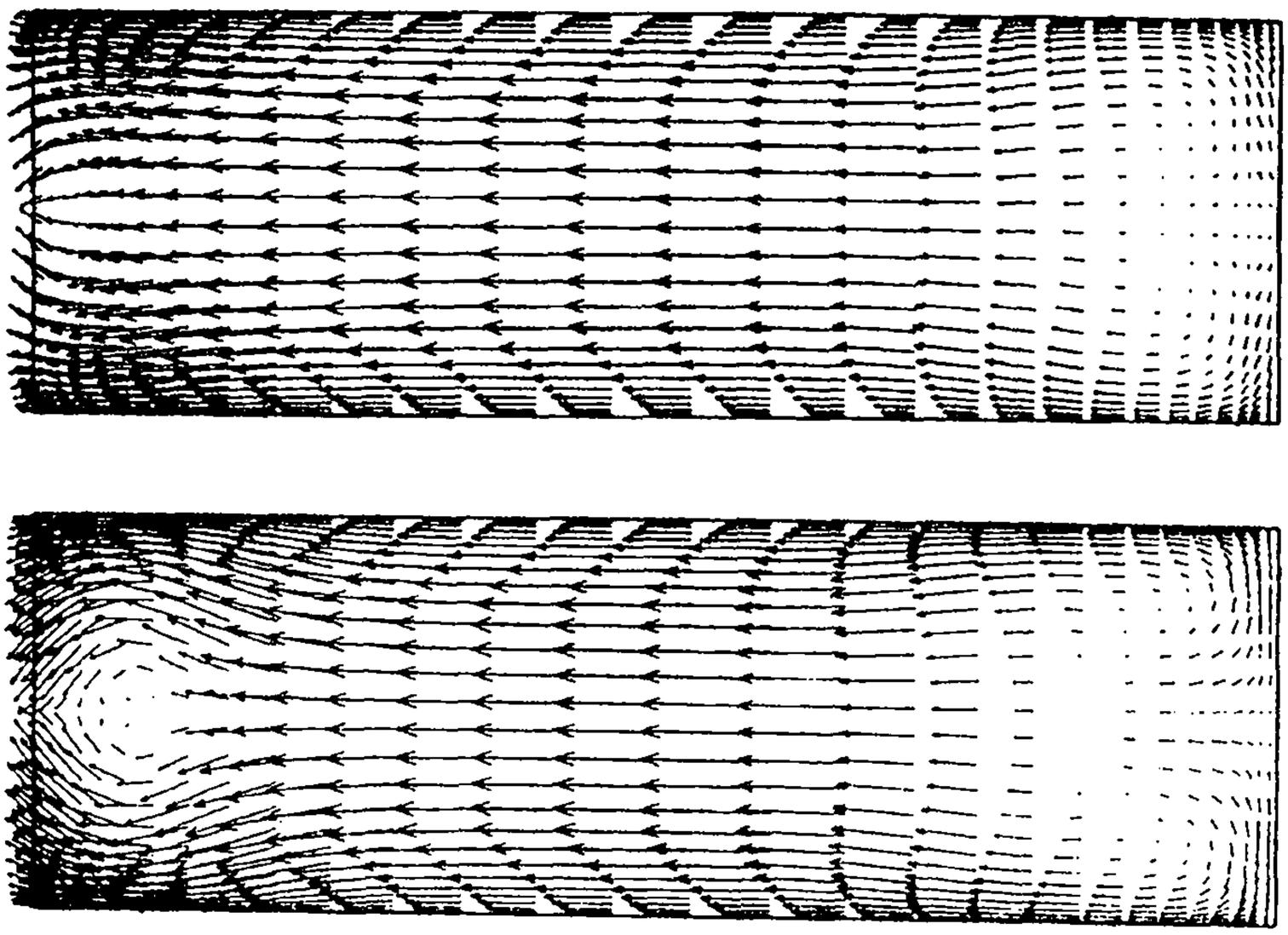

Figure 8.8 - Secondary velocity field in reference plane III using the ***eddy viscosity*** *formulation and first-order Upwind (top) and QUICK (bottom).*

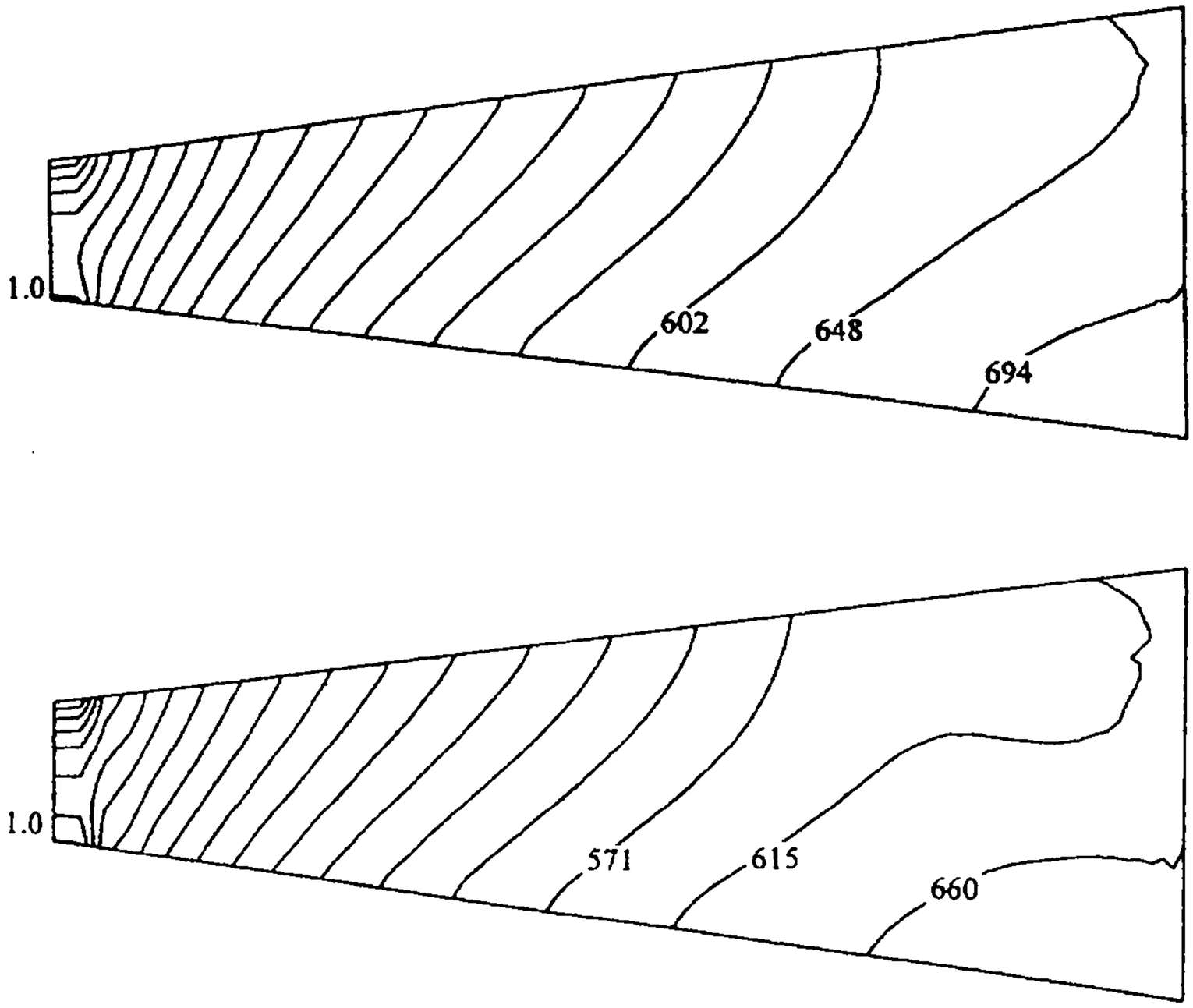

Figure 8.9 - Isovalue lines of the pressure at channel mid-height using the ***modified*** *formulation and first-order Upwind (top) and QUICK (bottom).*

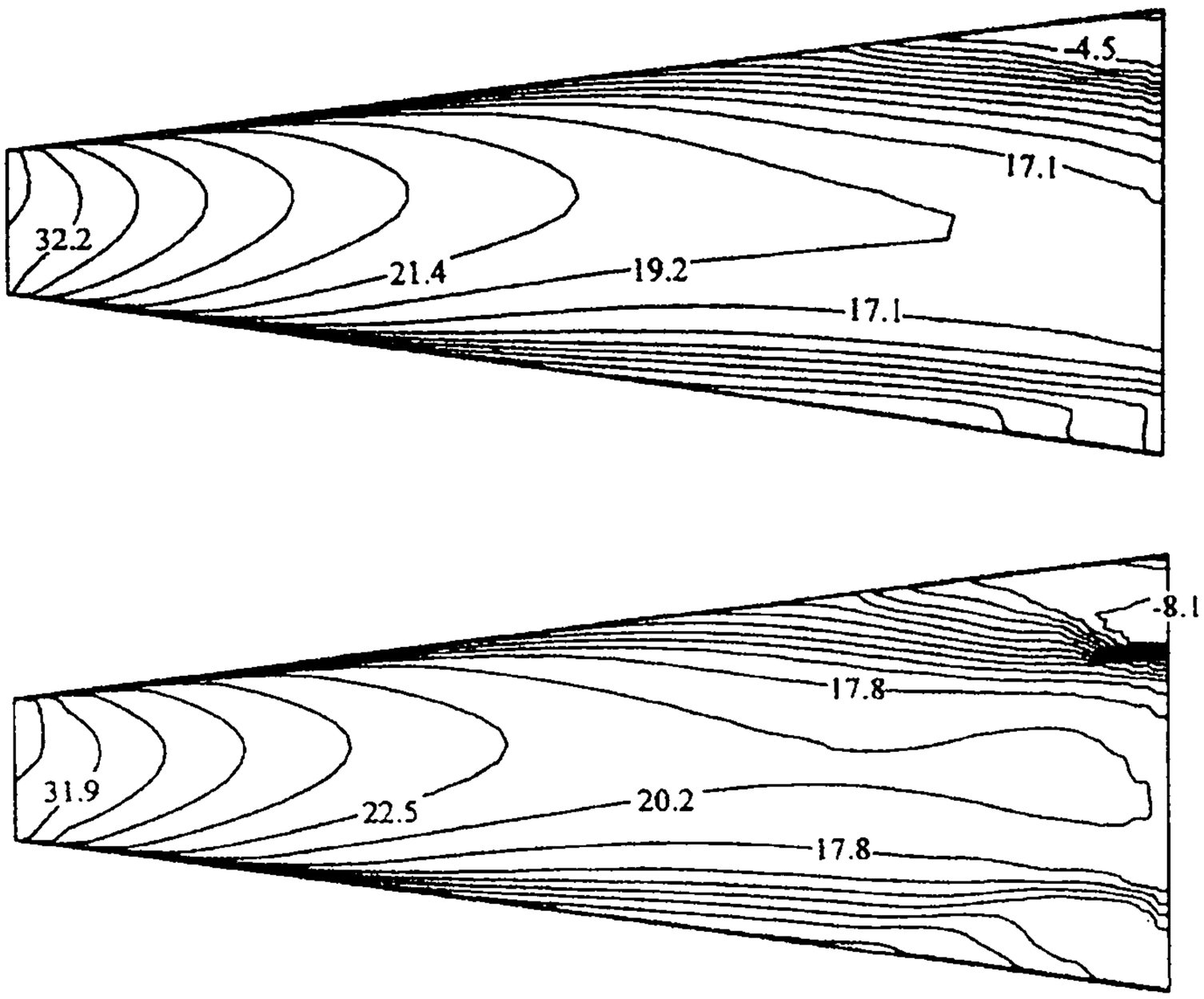

*Figure 8.10 - Isovalue lines of the u-velocity at channel mid-height using the **modified** formulation and first-order Upwind (top) and QUICK (bottom).*

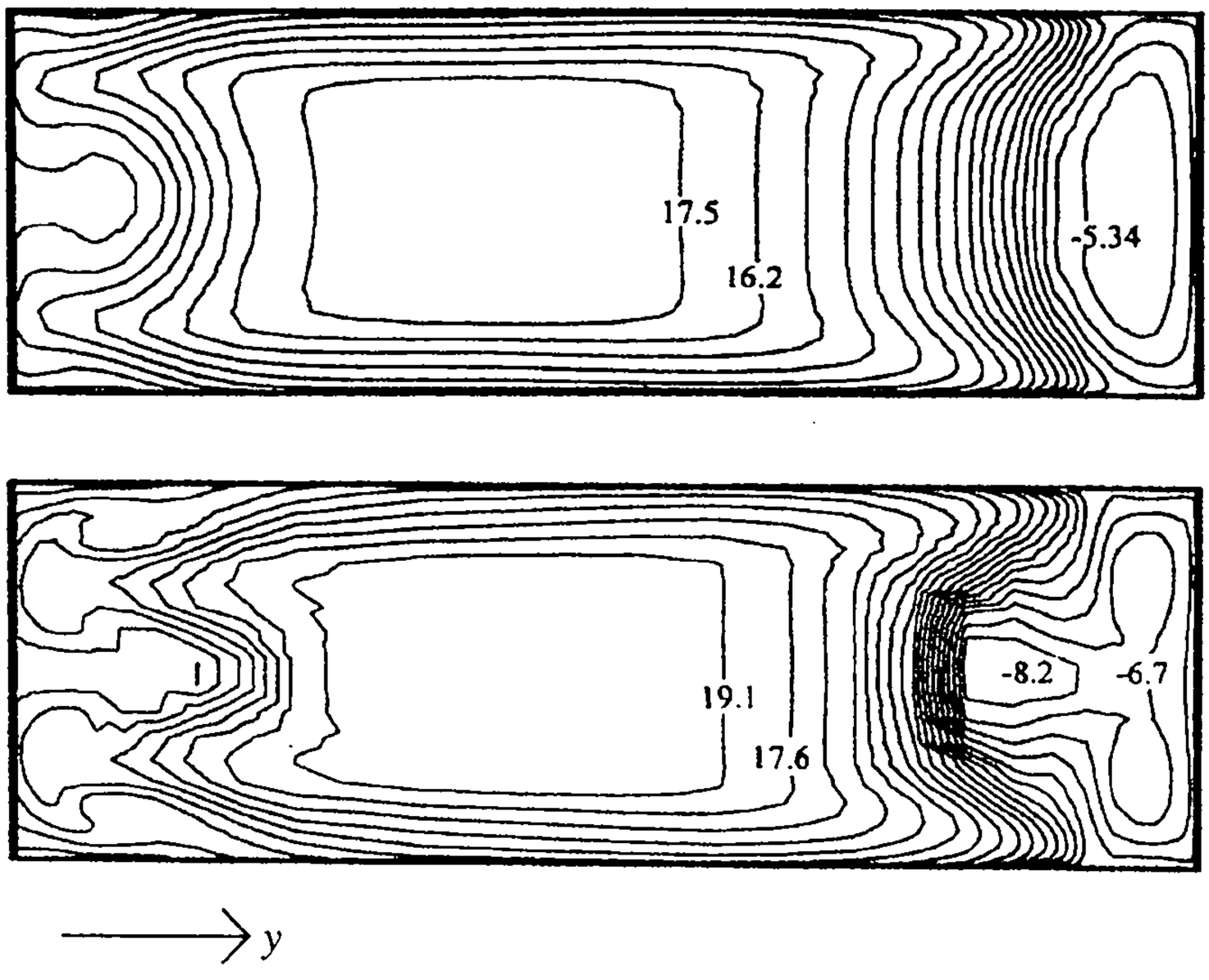

Figure 8.11 - Isovalue lines of the u-velocity in reference plane III using the ***modified*** *formulation and first-order Upwind (top) and QUICK (bottom).*

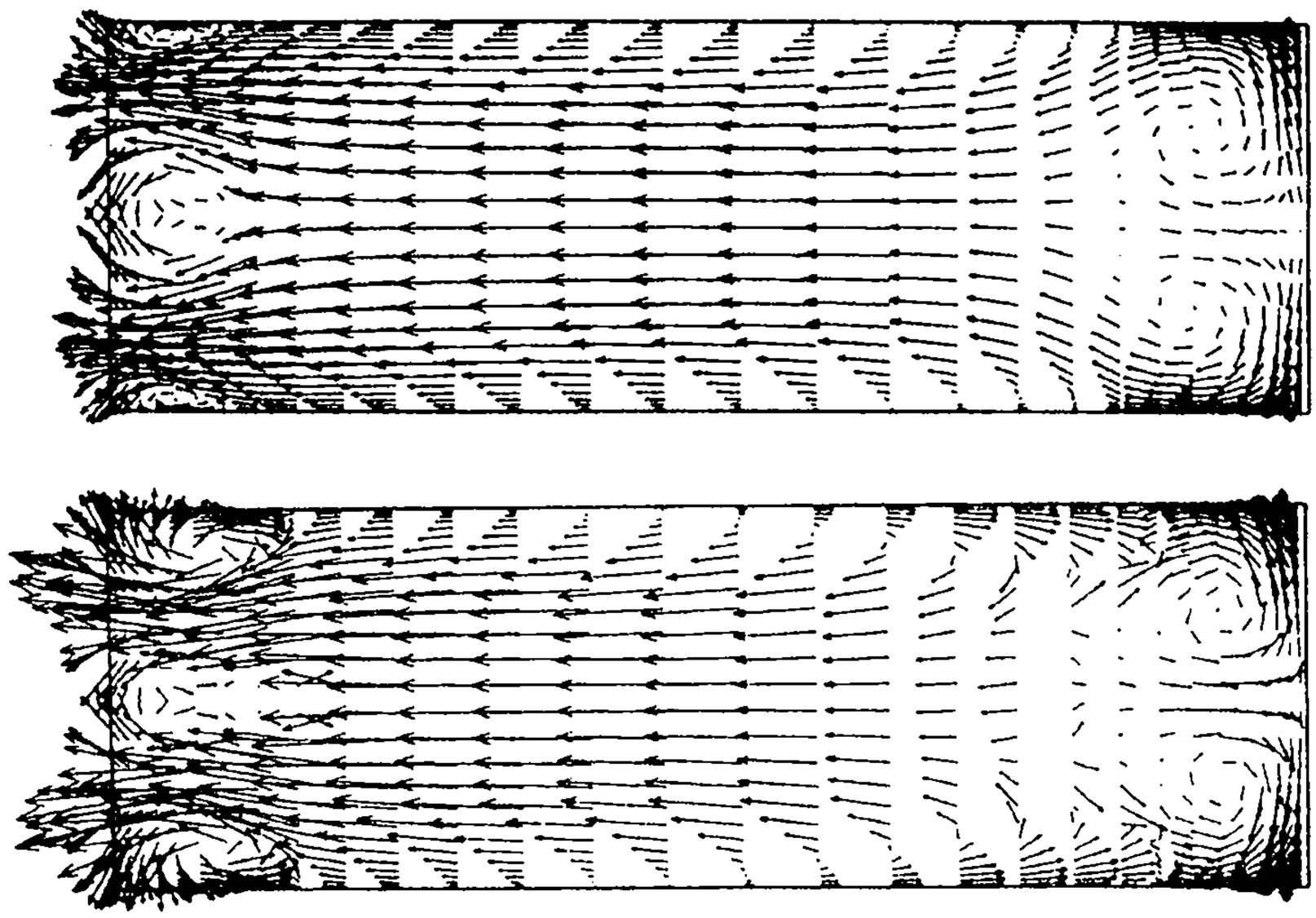

*Figure 8.12 - Secondary velocity field in reference plane III using the **modified** formulation and first-order Upwind (top) and QUICK (bottom)*

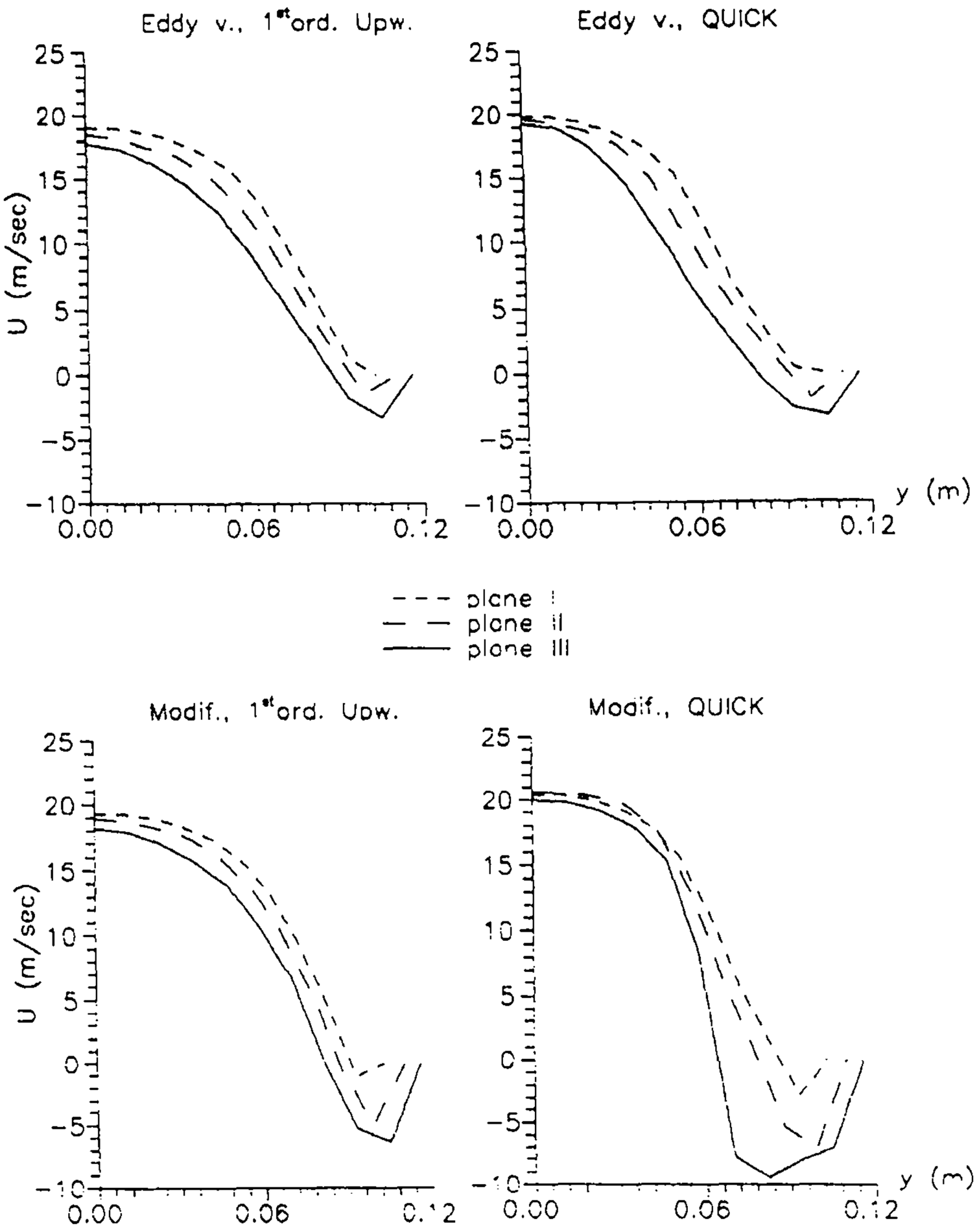

Figure 8.13 - U velocity profiles in the reference planes at channel mid-height, from the center of the duct to the suction side, using the several convection schemes and turbulence formulations.

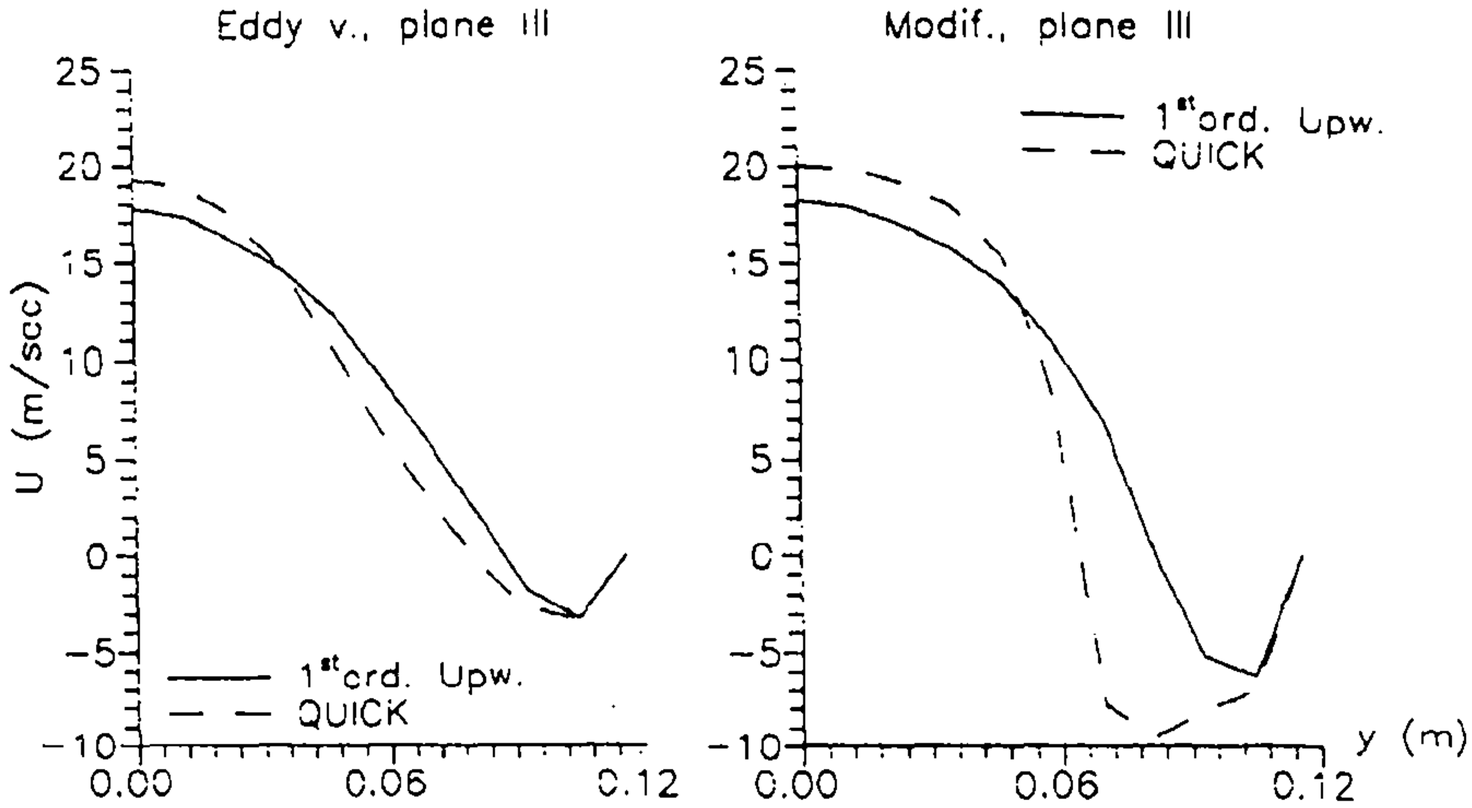

Figure 8.14 - Comparison of the efficacy of the convection schemes in reference plane III for the two formulations.

Chapter 9
Some results on centrifugal machines

9.1 - Introduction.

Before presenting some results obtained on a centrifugal compressor and a centrifugal pump it is necessary to introduce some additional discussion.

The numerical tests on the rotating diffuser presented in the previous chapter have shown that with the formulation adopted in this work it is necessary to assign a pressure distribution at the outlet of a rotating passage, to avoid unphysical pressure distributions, and, as a consequence of the effect of such a boundary condition for the pressure on the solution with GMRES (as seen in the fifth chapter of this thesis), the direct solver has to be used for the solution of the pressure correction equation. The use of the direct solver, while greatly enhancing the robustness of the code and its capability of adopting higher-order convection schemes and the proposed turbulence modelling, imposes a quite strict limit on the number of grid points that can be adopted with the algorithm. In the present case, where only around 40 MegaWords of memory are effectively available, the maximum number of grid points that can be used is 45,000÷ 65,000, greatly dependent on the choice of the number of points on the transversal sections: an increase in the number of points in the blade-to blade and hub-to-shroud directions causes an increase in the width of the band of the matrix, with a consequent sharp increase in the amount of memory required by the direct solver and the necessity of reducing the total number of grid points.

While the use of high-order schemes should reduce the grid dependence and, consequently, the number of grid points required for an accurate description of the flow phenomena, in the case of such a complex flow as the one occurring in a centrifugal compressor or pump it could be rightly argued that it is impossible to obtain a detailed analysis of such a flow with this level of resolution. The results presented, have therefore to be considered as a qualitative description of the flow, providing in any case some useful information both on the use of high-order schemes and on the modified turbulence formulation.

The results presented in the previous chapter have also shown how the use of the modified turbulence modelling has a very striking effect on the secondary flows on a rotating passage. Much more limited differences between the predictions obtained with the two turbulence formulations will instead be seen in the results presented in this chapter: also in this case, it has to be remembered that while in the previous chapter the

grid adopted was possibly capable of an accurate description of the flow phenomena occurring in that simple geometry, for the cases presented in this chapter additional numerical dispersion is certainly being introduced by the coarseness of the grid, in respect to the size of the phenomena that have to be predicted. The results that will be presented give in any case a good indication of the capability of the code and an initial validation for the prediction of the flow centrifugal machines, while additional validation is certainly required.

In this chapter the linear (Boussinesq) modelling of the Reynolds stresses will be adopted, as the study of an appropriate modelling of the Reynolds stresses for turbomachinery flows is beyond the scope of this study, but it has to be underlined that the proposed formulation has as a major advantage the capability of adopting arbitrary modelling of the Reynolds stresses. The value C_2=2.1 has been adopted, as in the previous section.

Finally, in all the cases a constant pressure distribution will be assigned at the outlet, not having better information, imposing an arbitrary constant value and then scaling the pressure field in order to obtain the required value at the inlet.

9.2 - The Eckardt impeller.

The first case that will be presented is the prediction of the flow in a high speed backswept impeller (figure 9.1) for which Eckardt (1980) described detailed measurements. Only one flow passage between two adjacent blades has been considered, with the assumption of periodic conditions upstream and downstream of the impeller blades; the passage has been discretised with a 30×30×50 grid. In the numerical tests the compressor is assumed to operate at rotational speed of 14,000 rpm at its choking conditions at a mass flow of 6.75 kg/s.

The experimental results show the presence of strong secondary flows due to curvature in both the radial and tangential directions which in combination with the boundary layer viscous regions cause the development of the wake flow pattern which appears in the radial part of the impeller. In figure 9.2 a sketch of the basic secondary flow patterns in the radial part of the impeller provided by Eckardt (1976) is presented. A passage vortex occupies the main area of the passage moving anticlockwise towards the hub-pressure side corner, along the pressure side towards the shroud and along the shroud feeding the wake corner region with low-momentum fluid. Close to the suction side of the blade passage there exists a clockwise vortex which moves along the suction side towards the casing. A smaller vortex is generated in the shroud/suction side corner

due to tip leakage flow over the blade tip due to the pressure difference between the blade surfaces.

In the figures 9.3 to 9.9 the calculated flow patterns in some transversal sections before and after the trailing edge are represented, where the vectors represent the projection of the velocity on a plane rectangular section orthogonal to the streamwise direction and having the same area and the same aspect ratio of the effective section. The index k indicates the streamwise position of the plane, the trailing edge of the blade being located between the planes k=38 and k=39. From these figures is possible to notice the effect of both the convection scheme and of the modelling of the turbulent diffusion term on the prediction of the secondary flows; it is interesting, for example, to compare the differences in the prediction of the vortices and the area of low momentum that appears soon before the trailing edge, and how these features subsequently develop after the trailing edge in the main flow. Once again it is important to precise that a much larger variation in the prediction will be obtained if a different modelling of the Reynolds stresses is adopted with the modified formulation.

In figure 9.10 the calculated and measured relative total pressure (as defined by Eckardt, 1980) distributions at rotor discharge are represented; the prediction appears to be quite poor and the use of both higher-order schemes and the modified turbulence formulation does not seem to provide any improvements. In figure 9.11 some of the results obtained by A. Tourlidakis (1992) are also presented; these results have been obtained with a finite volume procedure that is based on a plane-by-plane approach and uses a line solver for the solution of the systems of equations, as has been described in section 3.1. The predicted relative total pressure distribution obtained in this study when using the Upwind scheme (figure 9.10, top) is practically identical to the one obtained by A. Tourlidakis (figure 9.11, bottom).

Finally, in figure 9.12 the calculated streamwise static pressure distribution at midspan of the two side boundaries (the ones containing the lower and upper surface of the blade), obtained using the QUICK scheme and the two turbulence formulation, is represented; very little differences can be noted in the predictions.

Figure 9.1 - Solid model of the Eckardt (1980) backswept impeller

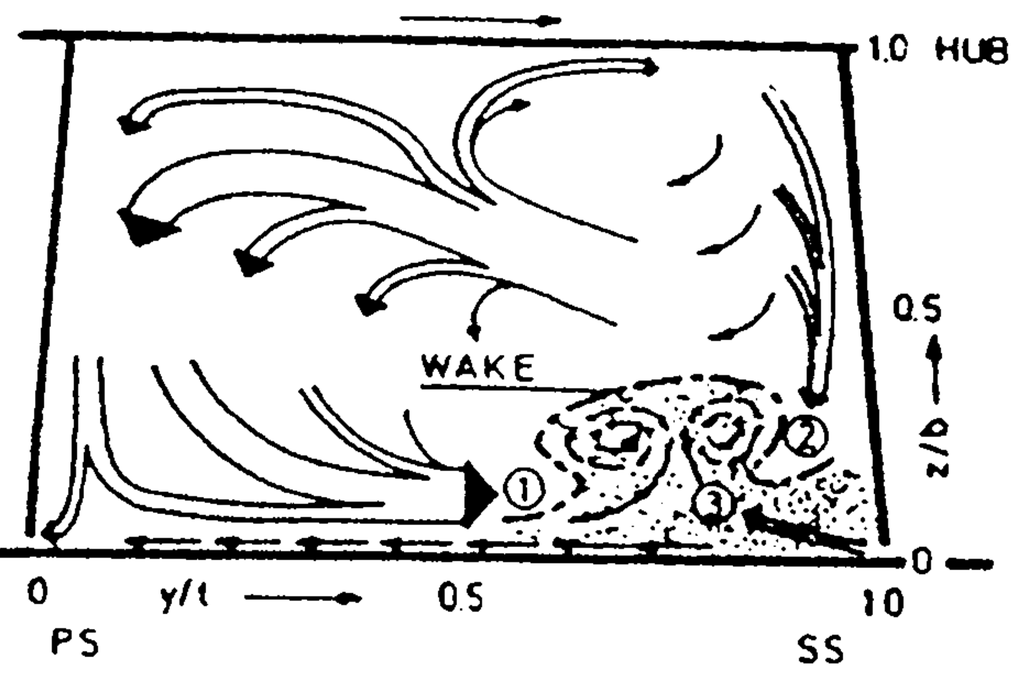

Figure 9.2 - Sketch of the basic secondary flow patterns in the radial part of the impeller (taken from Eckardt, 1976).

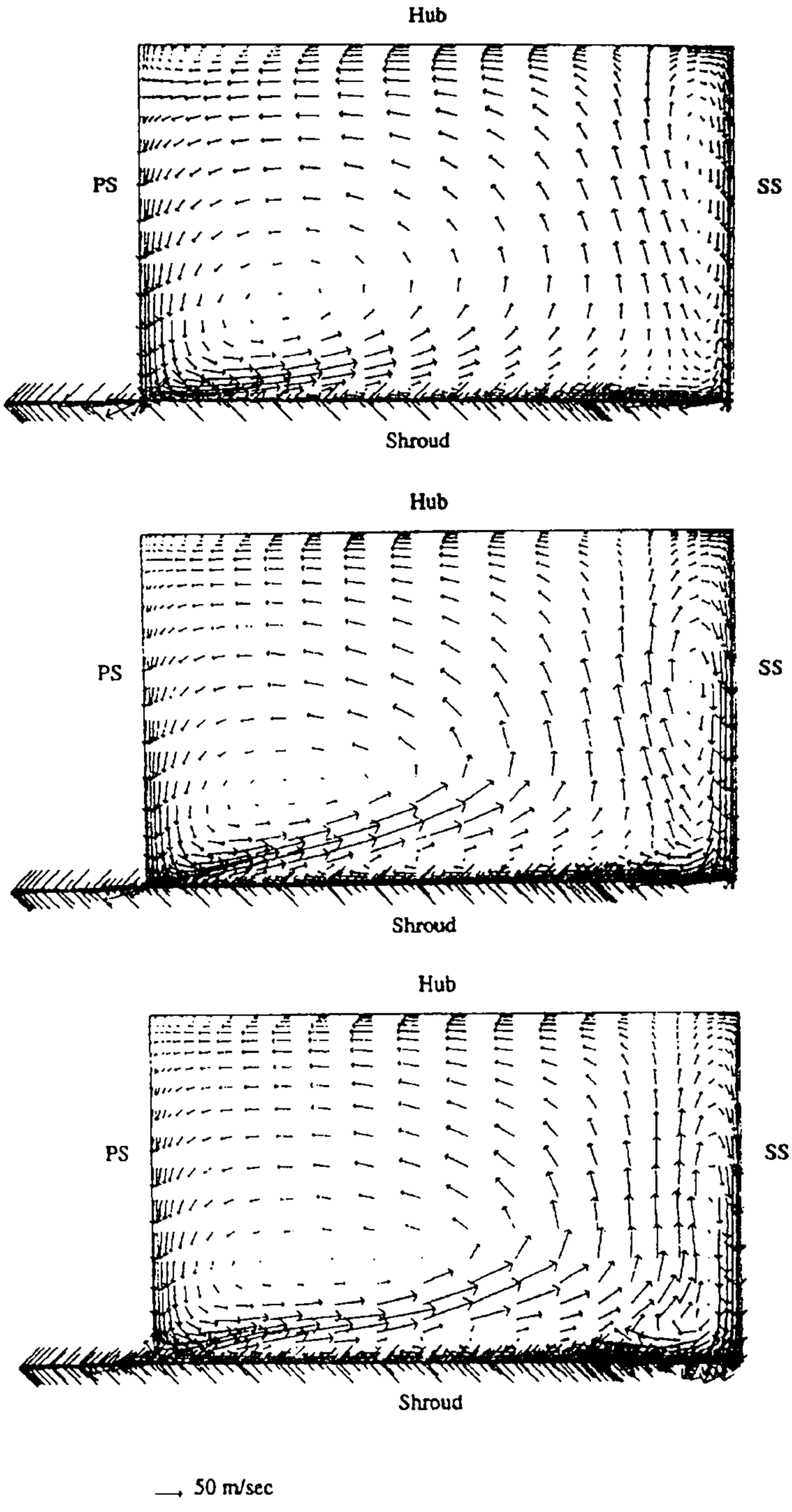

Figure 9.3 - Projection on a transversal plane for k=34 (being k=38 the trailing edge) of the predicted flow patterns, using: first-Upwind and the eddy-viscosity formulation (top), the QUICK scheme and the eddy viscosity formulation (center), the QUICK scheme and the modified formulation (bottom).

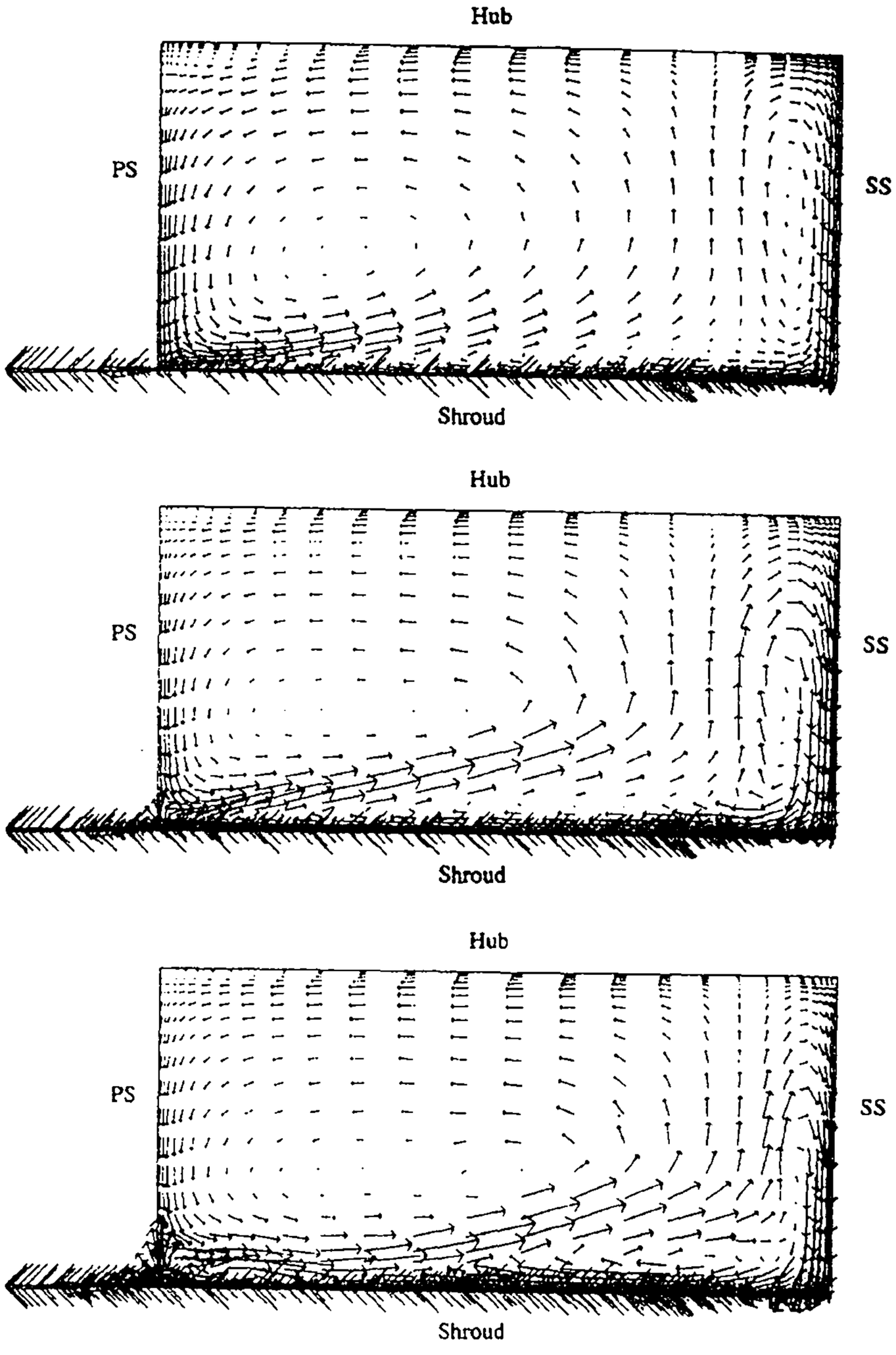

Figure 9.4 - As figure 9.3, for k=36.

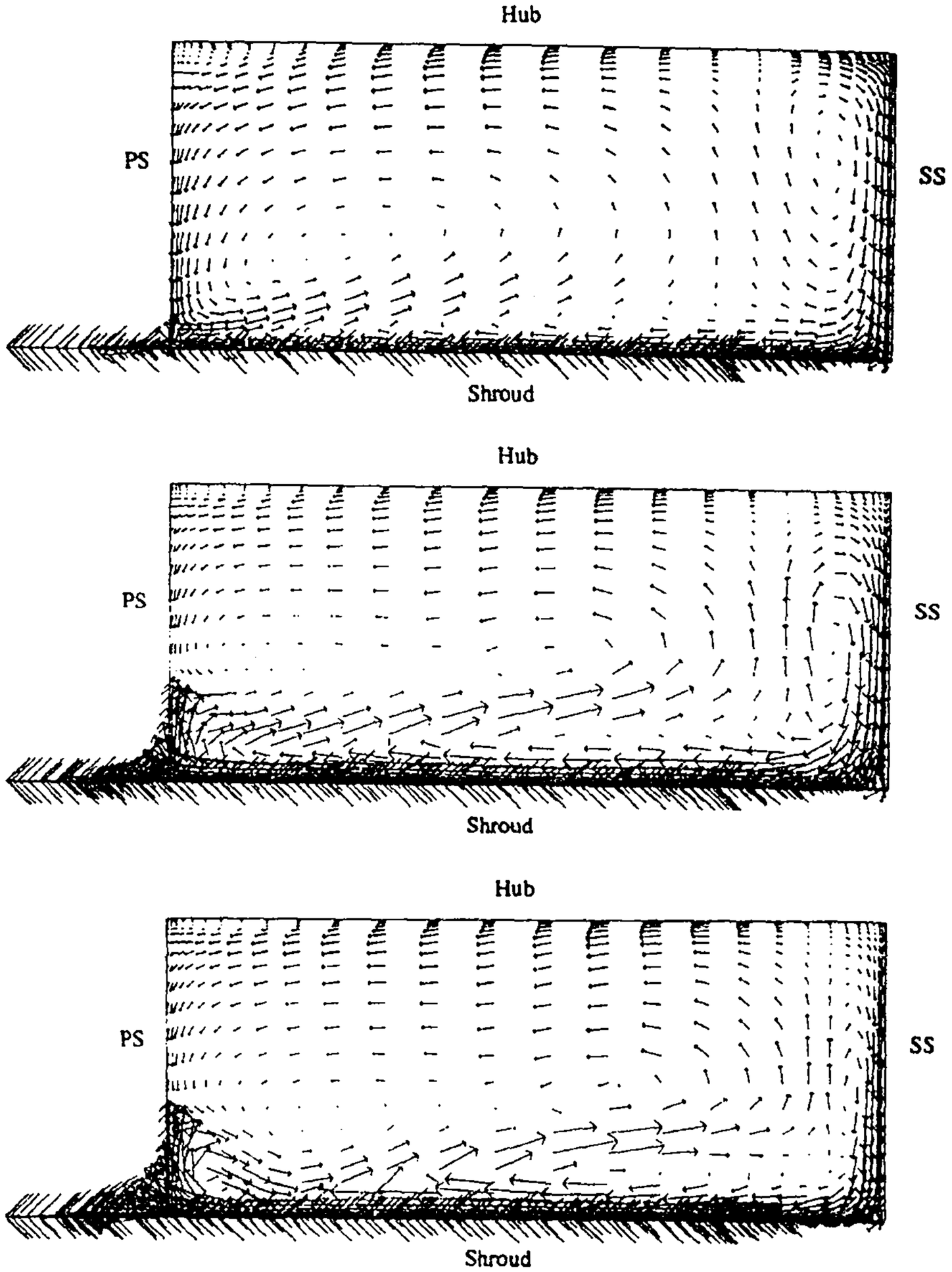

Figure 9.5 - As for figure 9.3, with k=38 (trailing edge).

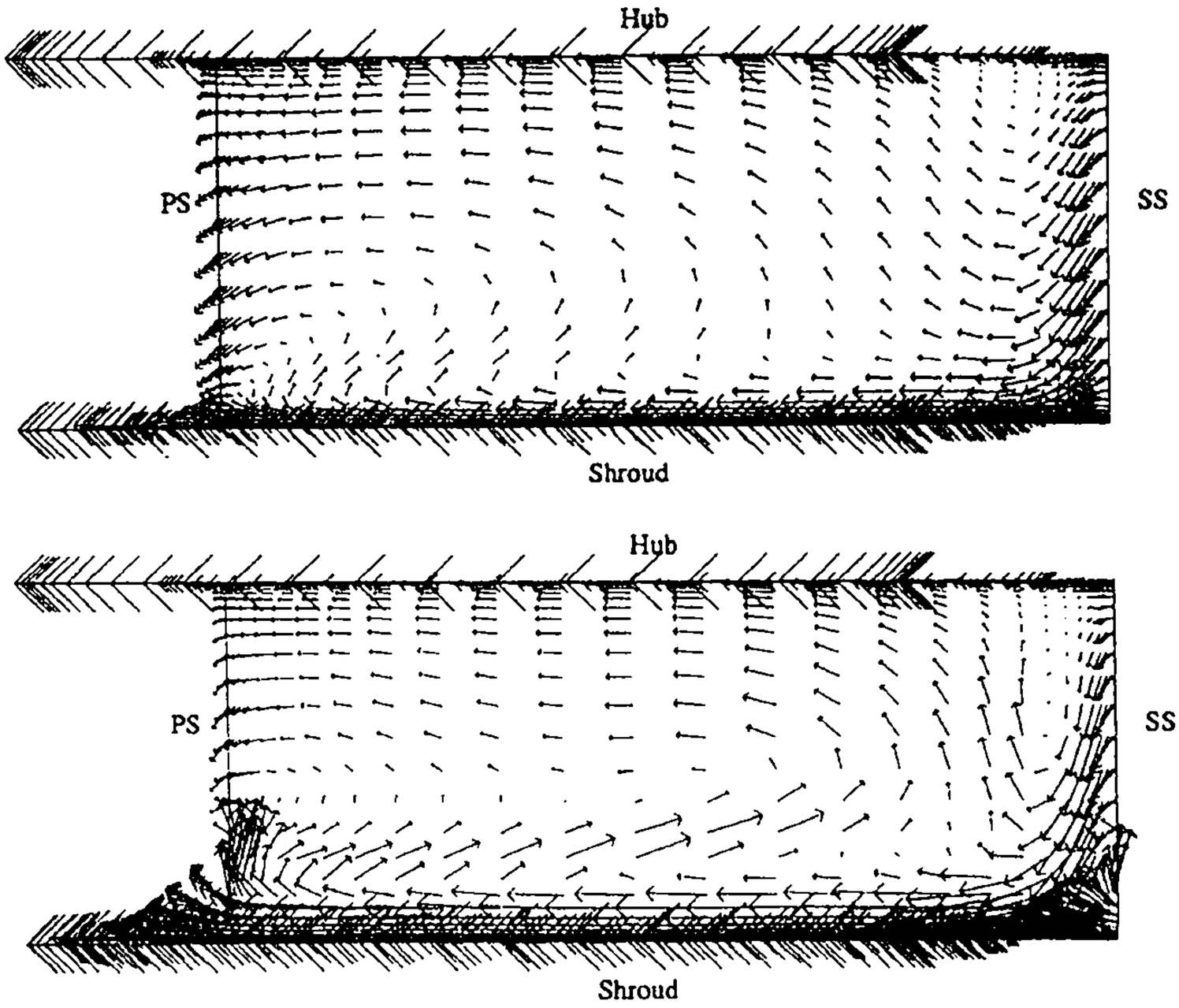

Figure 9.6 - As for figure 9.3, with k=39.

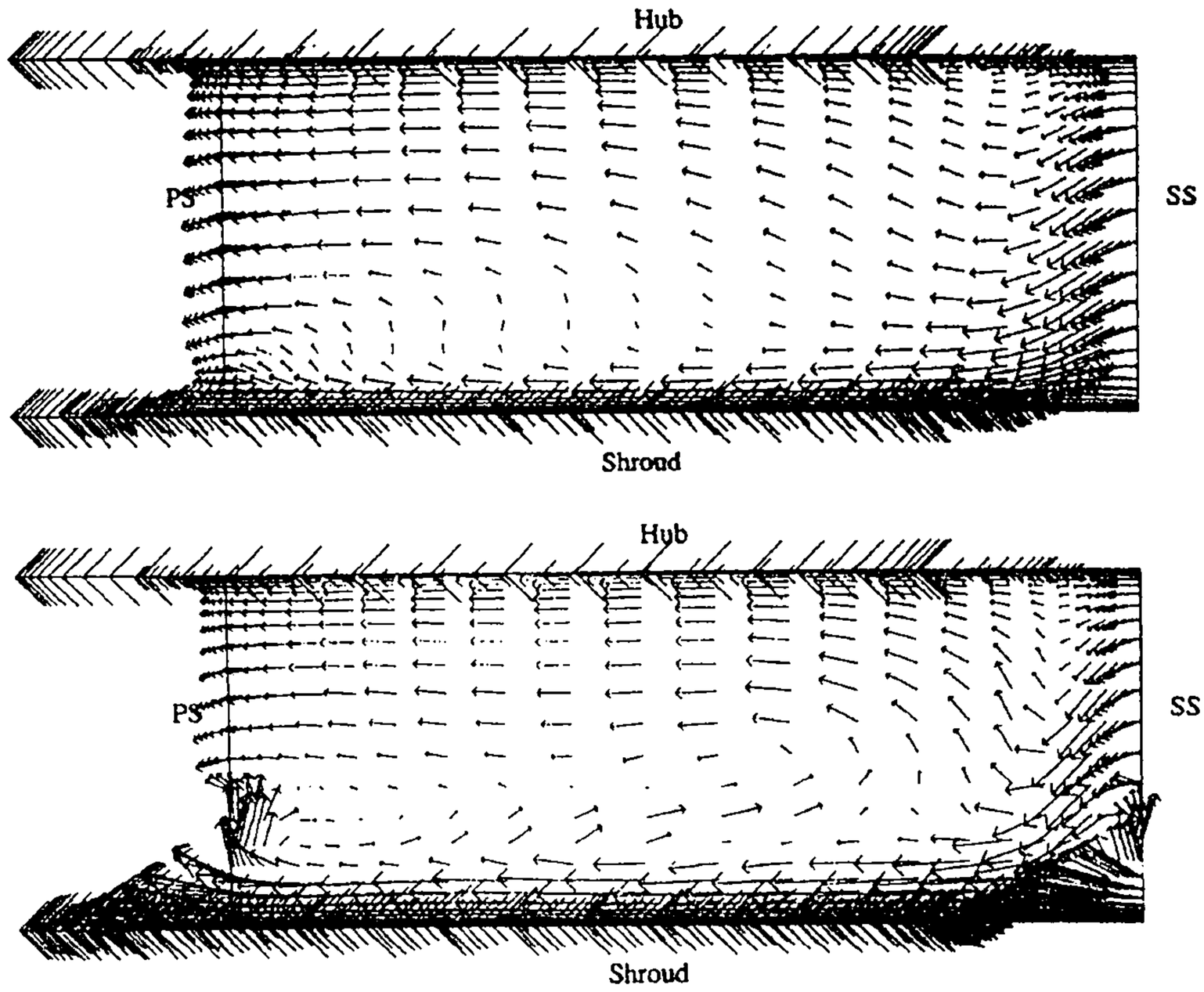

Figure 9.7 - As for figure 9.3, with k=40.

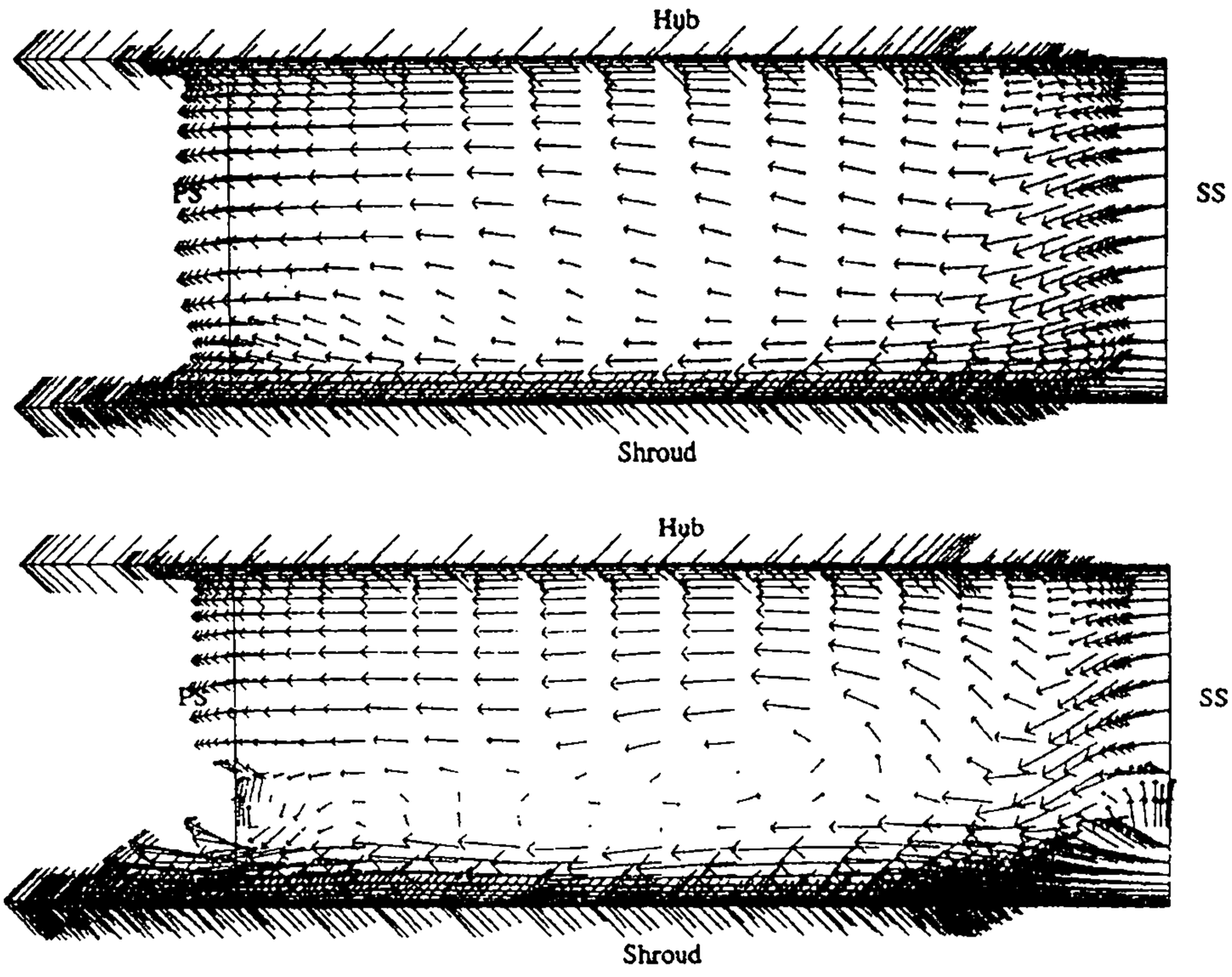

Figure 9.8 - As for figure 9.3, with k=41.

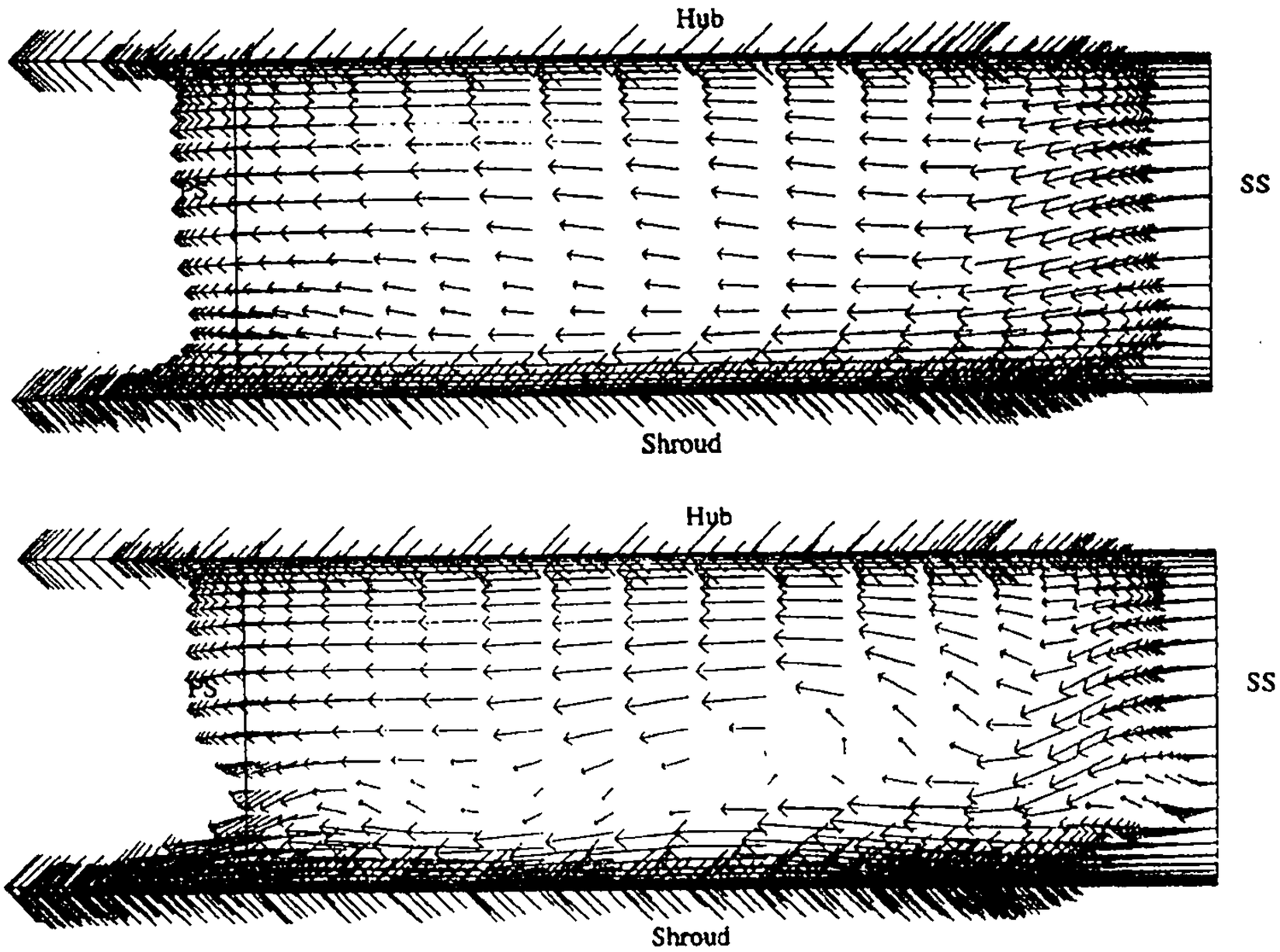

Figure 9.9 - As for figure 9.3, with k=42.

Eddy visc. form., Upwind

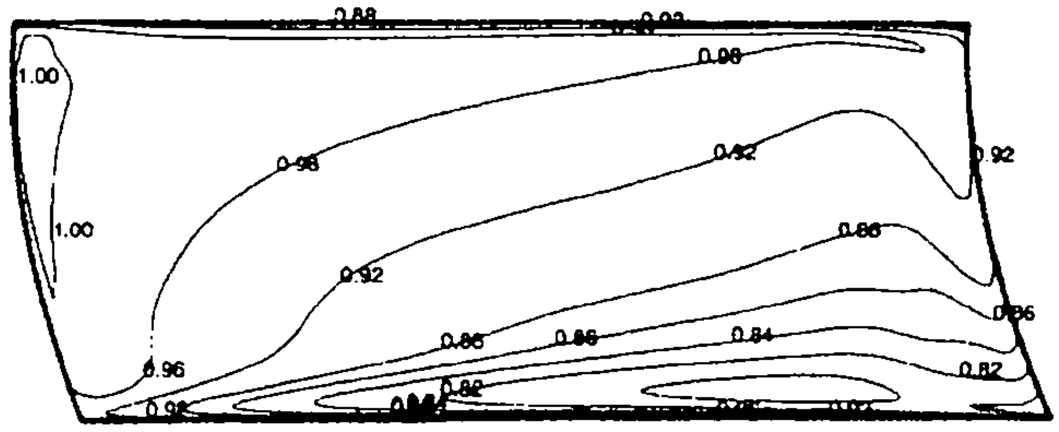

Eddy visc. form., QUICK

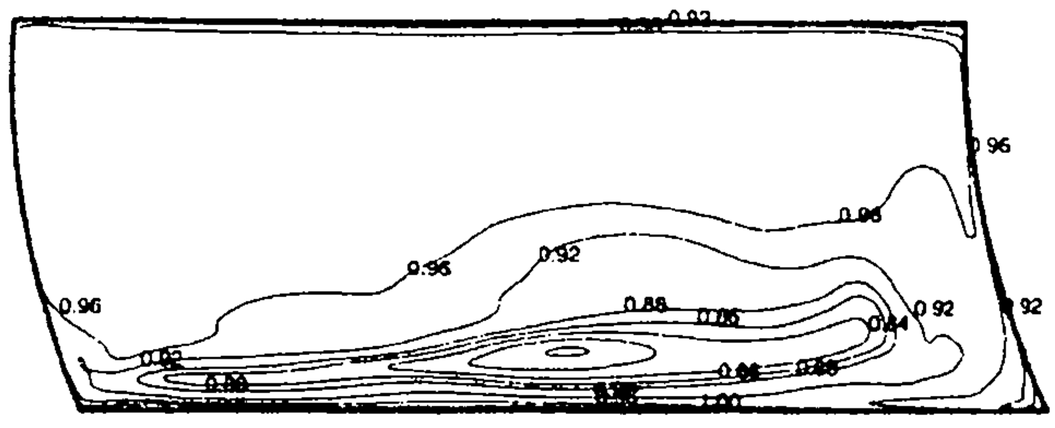

Modified form., QUICK

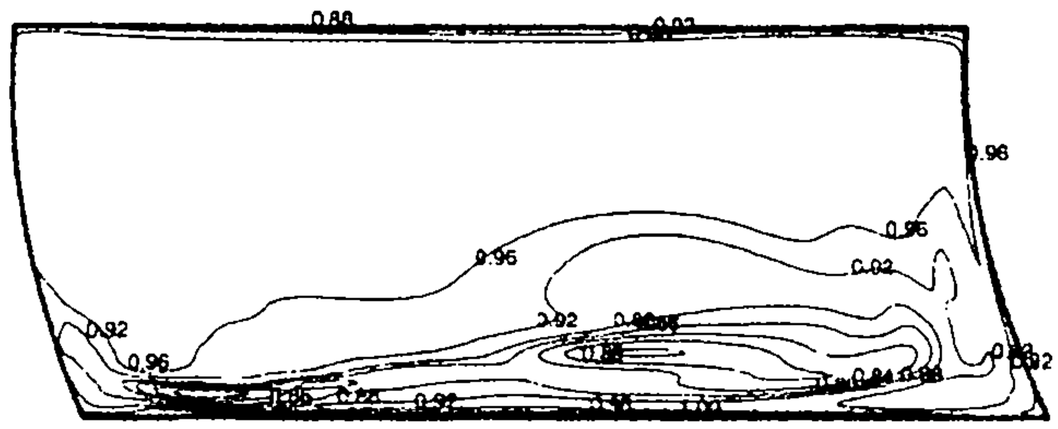

Measured values (Eckardt, 1980)

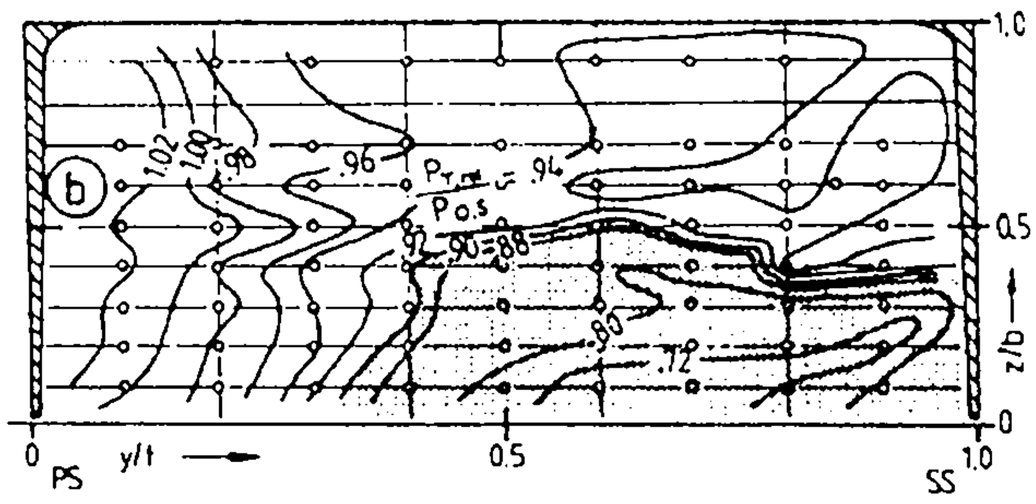

Figure 9.10 - Relative total pressure distribution at rotor discharge.

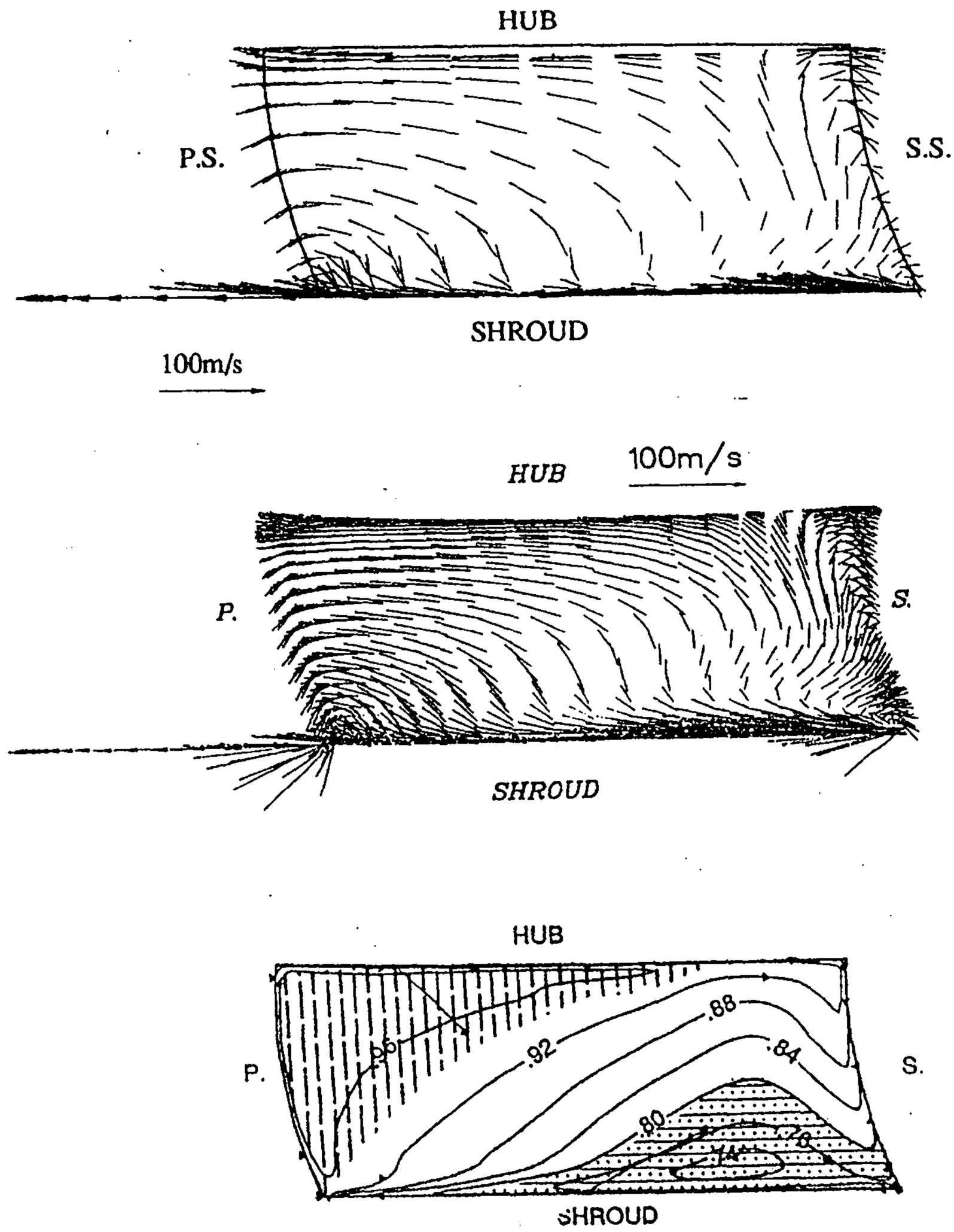

Figure 9.11 – Predicted results at the rotor exit obtained by A. Tourlidakis (1992) using the standard k-ε turbulence model and the first-order Upwind scheme: secondary velocity vectors using a 20×20×50 grid (top) and a 32×32×65 grid (center), and relative total pressure distribution (bottom).

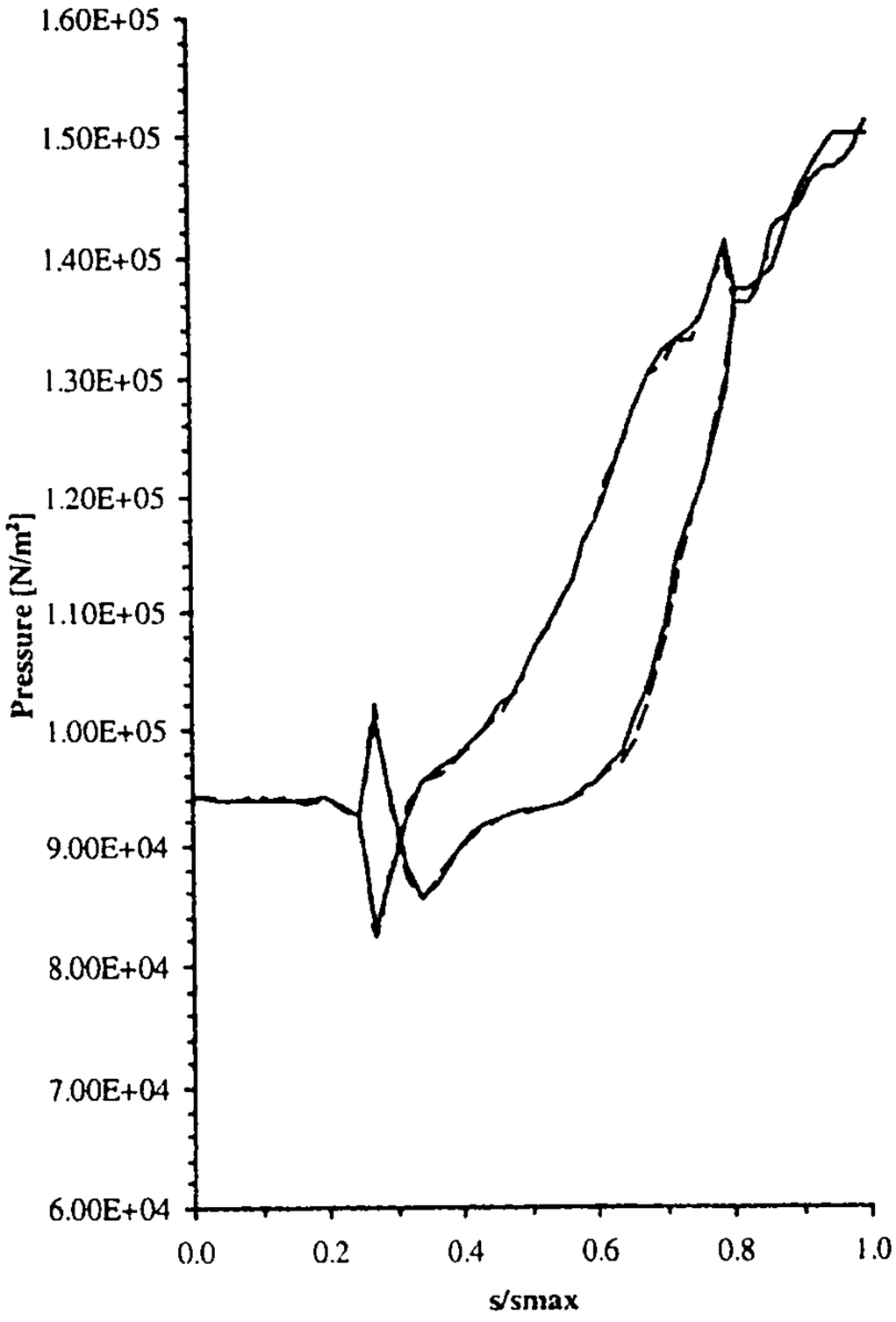

Figure 9.12 - Calculated streamwise pressure distribution, obtained using the QUICK scheme and the two turbulence formulations (solid line = eddy viscosity formulation).

9.3 - The SHF radial pump.

The SHF impeller was designed from the Société Hydrotechnique de France in order to study inlet and outlet recirculations in centrifugal pumps at partial flow rates (Combes and Rieutord, 1992); it is a low specific speed centrifugal impeller, with nominal flow rate of Qn=0.1118 m^3 / s at 1,200 rpm. Experimental investigations show the at a flow rate of 0.6 Qn a large recirculation zone is observed at the shroud ahead of the blades; also the diffuser flow has been shown to be unstable, especially at low flow rate, with zones where the mean radial velocity becomes negative at the shroud for 0.6 Qn; at low flow rate the radial velocity becomes negative in the impeller in the hub region.

In figures 9.13 to 9.16 some flow patterns, obtained on a 29×29×63 grid, are represented, giving a qualitative picture of the flow an nominal and partial flow rate (0.6 Qn) and of the differences between the predictions obtained with the two turbulence formulations.

In figures 9.17 to 9.20 the calculated flow patterns at nominal flow rate in some transversal sections before and after the trailing edge are represented; as seen for the previous cases, it is interesting to observe the effect of the higher-order scheme on the prediction of the flow patterns, and to notice how the use of the modified turbulence formulation seems to enhance such effect.

In figure 9.21 the projection of the velocity on a streamwise surface at the center of the computational domain for partial flow rate and using the QUICK scheme and both the turbulence formulations, is presented. It is interesting to notice the difference in the predictions of the recirculation using the two different turbulence formulations, with the results obtained with the modified formulation showing the backflow of the recirculation extending to the impeller past the trailing edge (notice that the velocity represented is not the radial component of the velocity, but a representative of the streamwise velocity).

In figures 9.22 to 9.27 comparisons of the calculated static pressure with experimental measurements are represented. It is clear from these figures that using the higher-order scheme a closer prediction is obtained, but the two turbulence formulations produce almost identical results. Finally, in figures 9.28 to 9.31 the comparisons of the experimental measurements with the predictions obtained by Muggli (1995) and Hirsch (1996) are represented, where the details on the methods adopted are reported in the figure captions. These results show a closer agreement with the measured data than the predictions obtained in this study; this is most probably due to the use of a better spatial

resolution in these works, confirming the inadequacy in terms of the number of grid points of the grid adopted in this study.

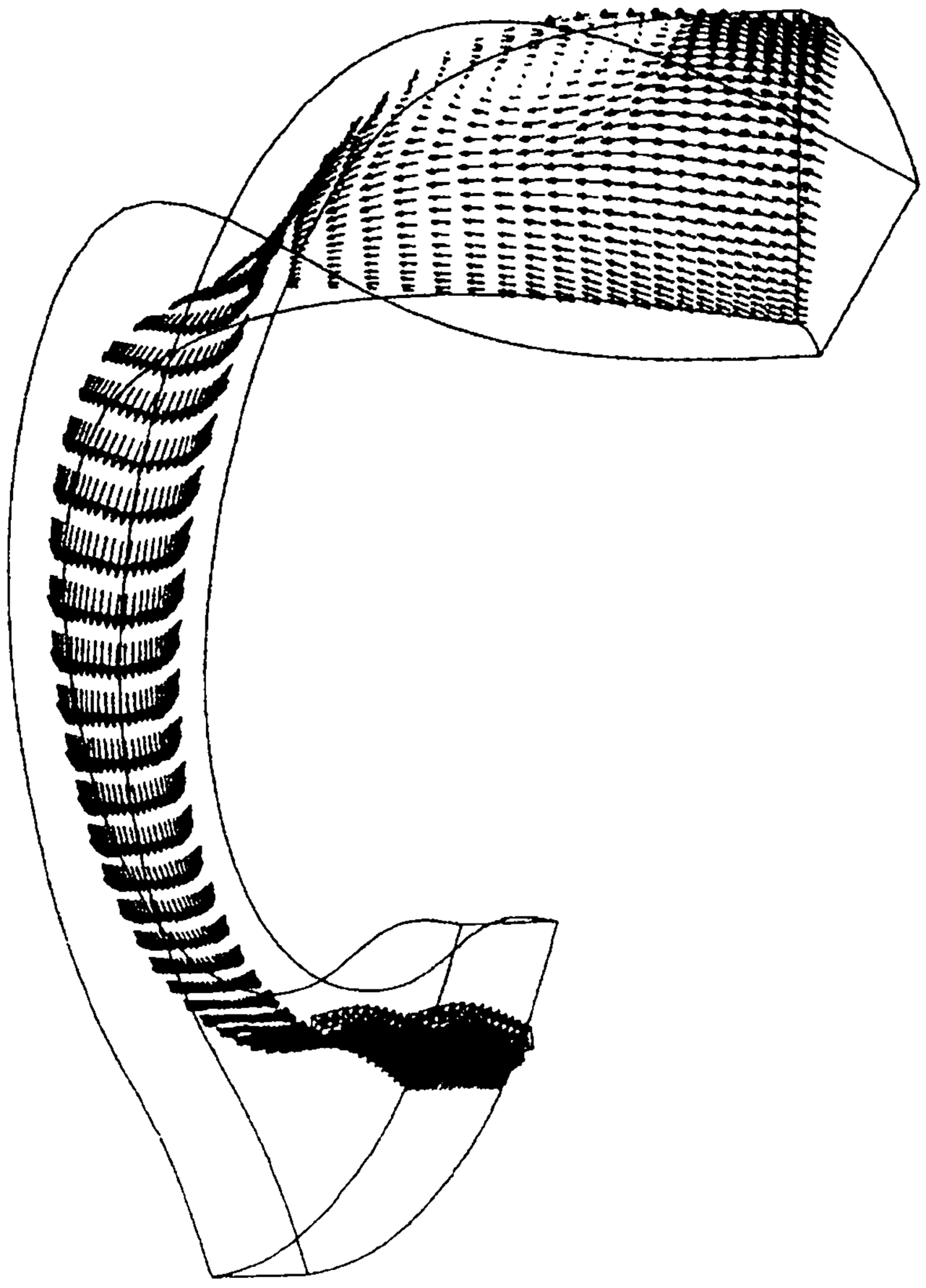

Figure 9.13 - Calculated flow pattern at ***nominal flow rate*** *using the QUICK scheme and the modified turbulence formulation*

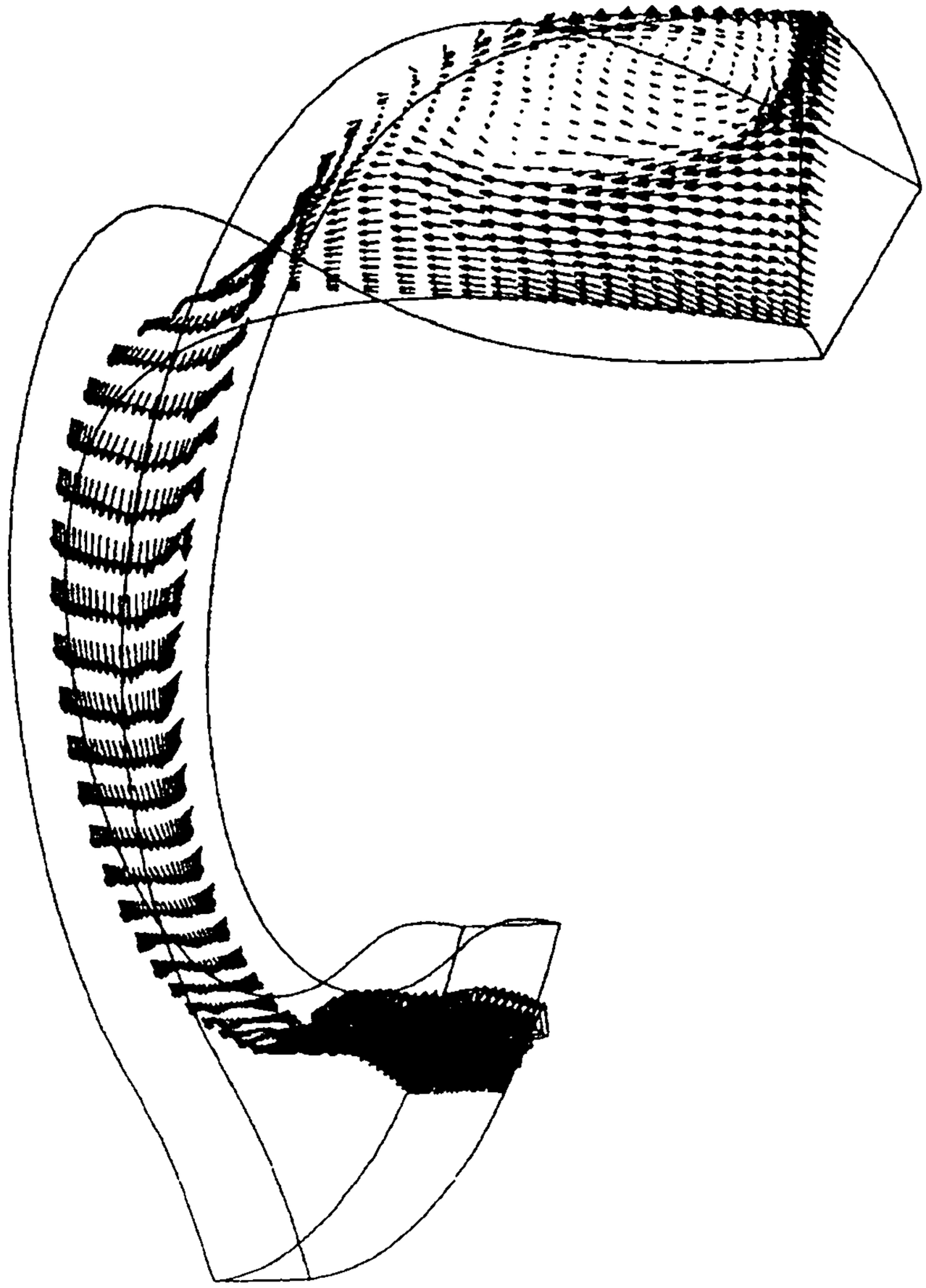

Figure 9.14 - Calculated flow pattern at ***partial flow rate*** *(60%) using the QUICK scheme and the modified turbulence formulation.*

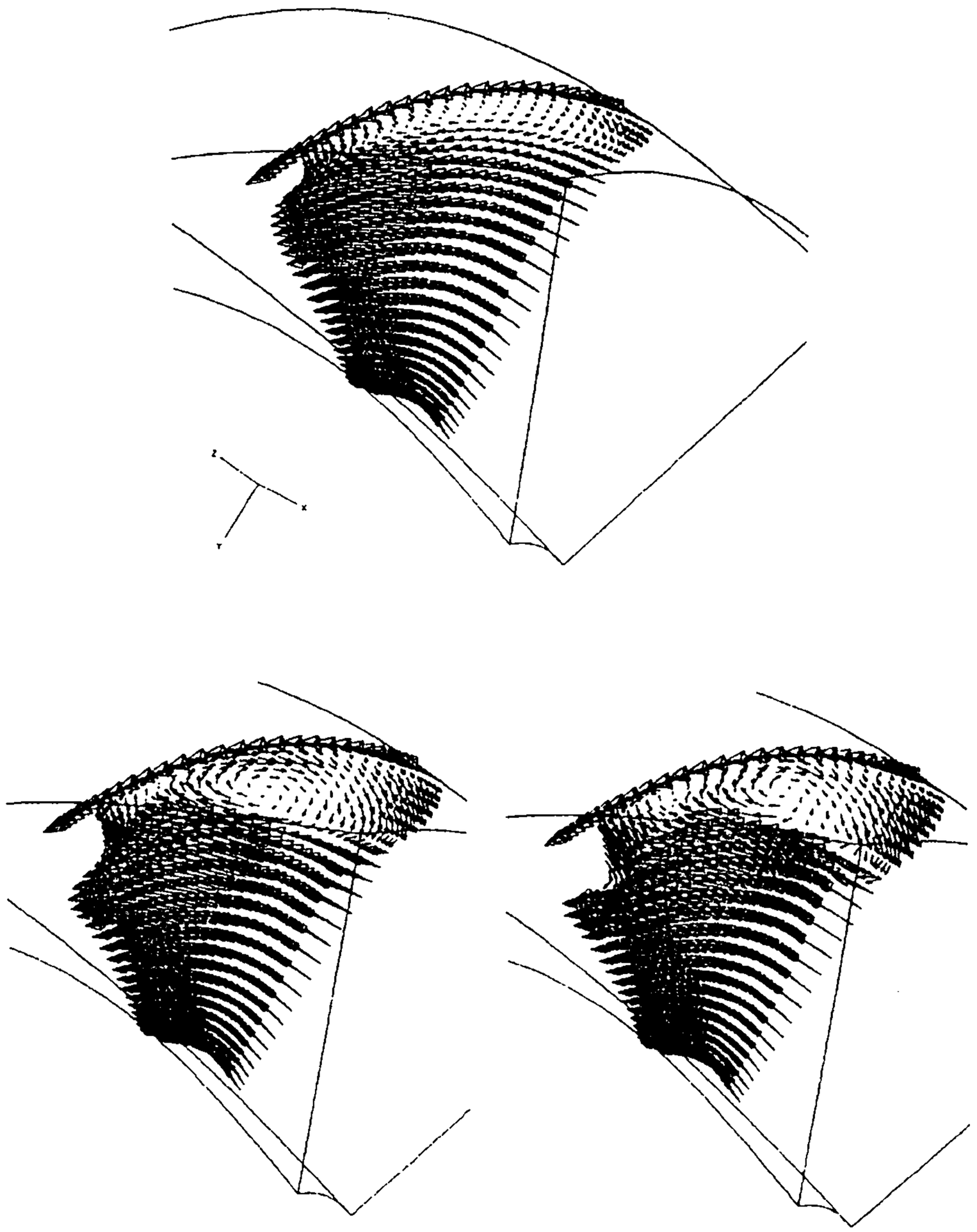

Figure 9.15 - Calculated flow pattern at ***nominal flow rate*** *at k=11 (being k=15 the leading edge) using the first-order Upwind and the eddy-viscosity formulation (top) and the QUICK scheme (bottom) with the eddy-viscosity formulation (left) and the modified formulation (right).*

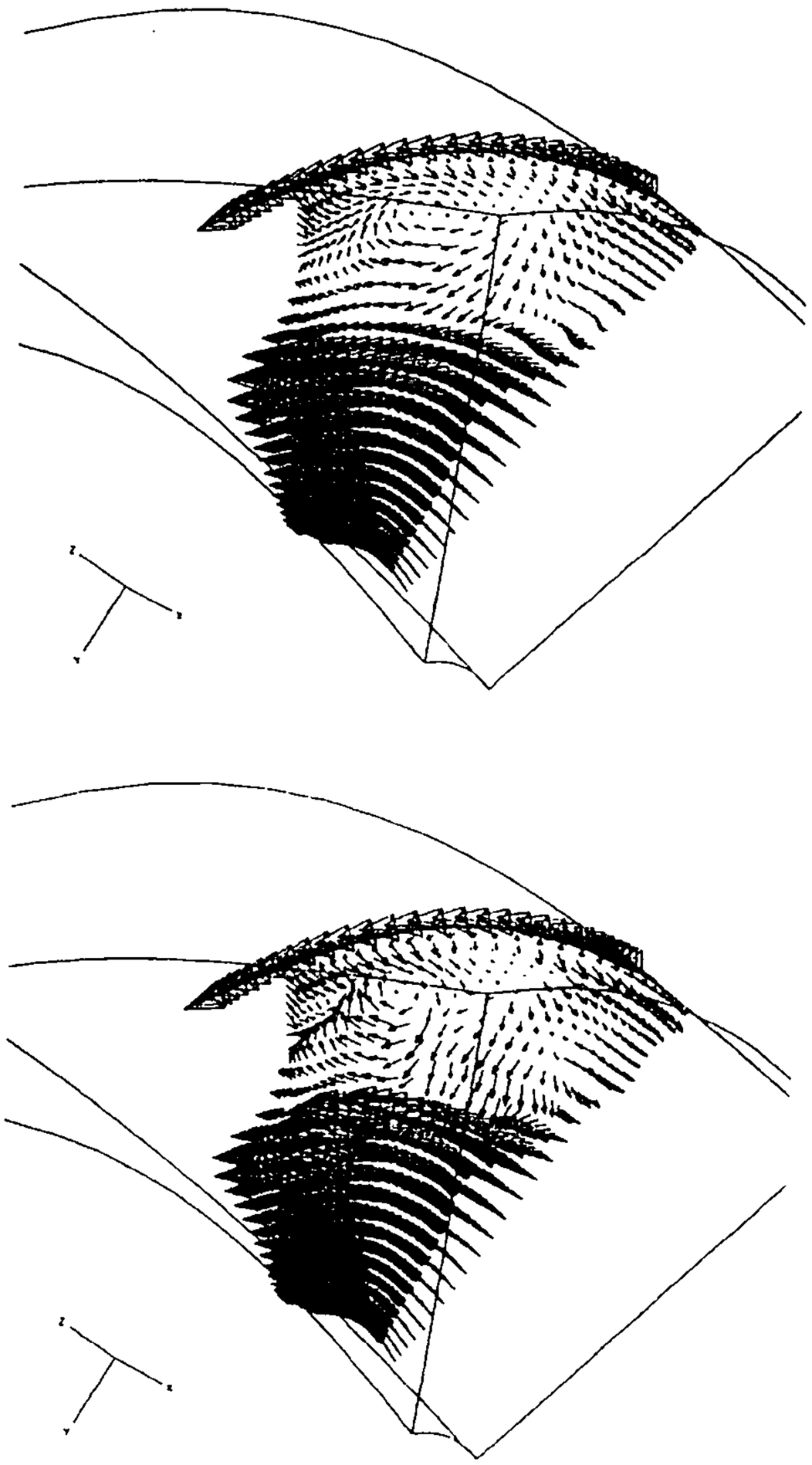

*Figure 9.16 - Calculated flow pattern at **partial flow rate** at k=8 (being k=15 the leading edge) using the QUICK scheme and the eddy viscosity formulation (top) and the modified formulation (bottom).*

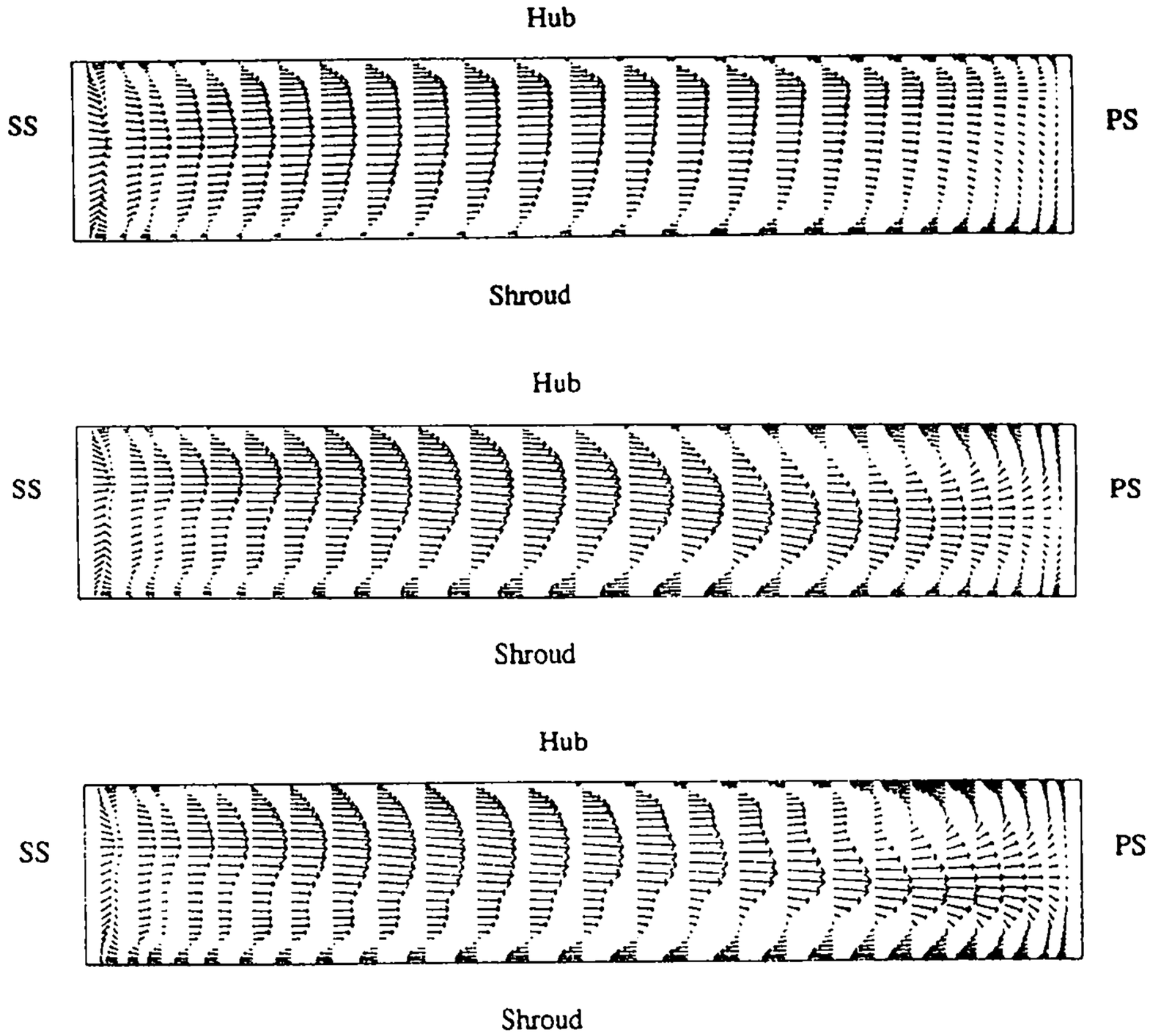

Figure 9.17 - Projection on a transversal plane for k=49 (trailing edge) of the predicted flow patterns, using: first-Upwind and the eddy-viscosity formulation (top), the QUICK scheme and the eddy viscosity formulation (center), the QUICK scheme and the modified formulation (bottom), ***nominal flow rate****.*

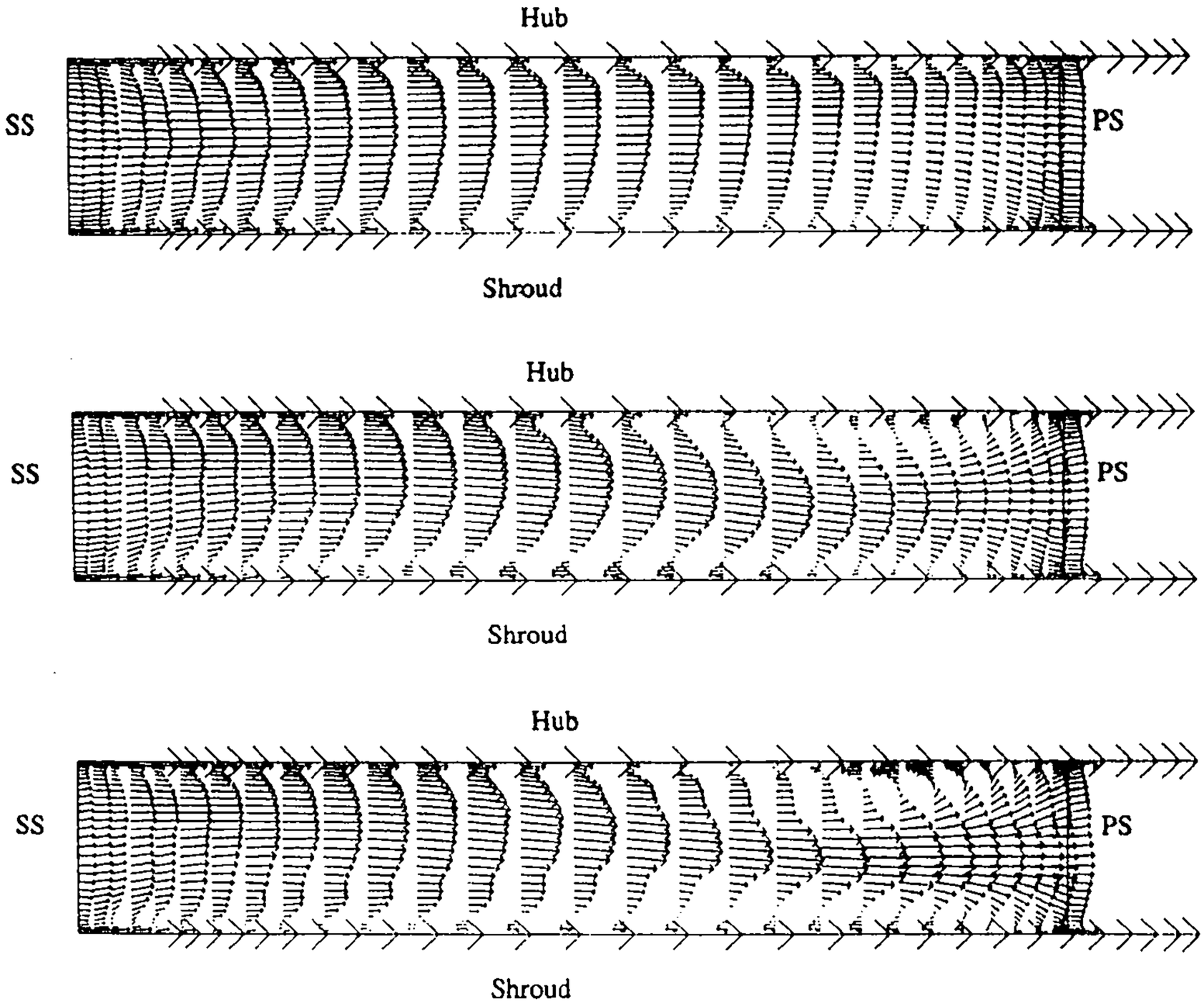

Figure 9.18 - As for figure 9.17, for k=50.

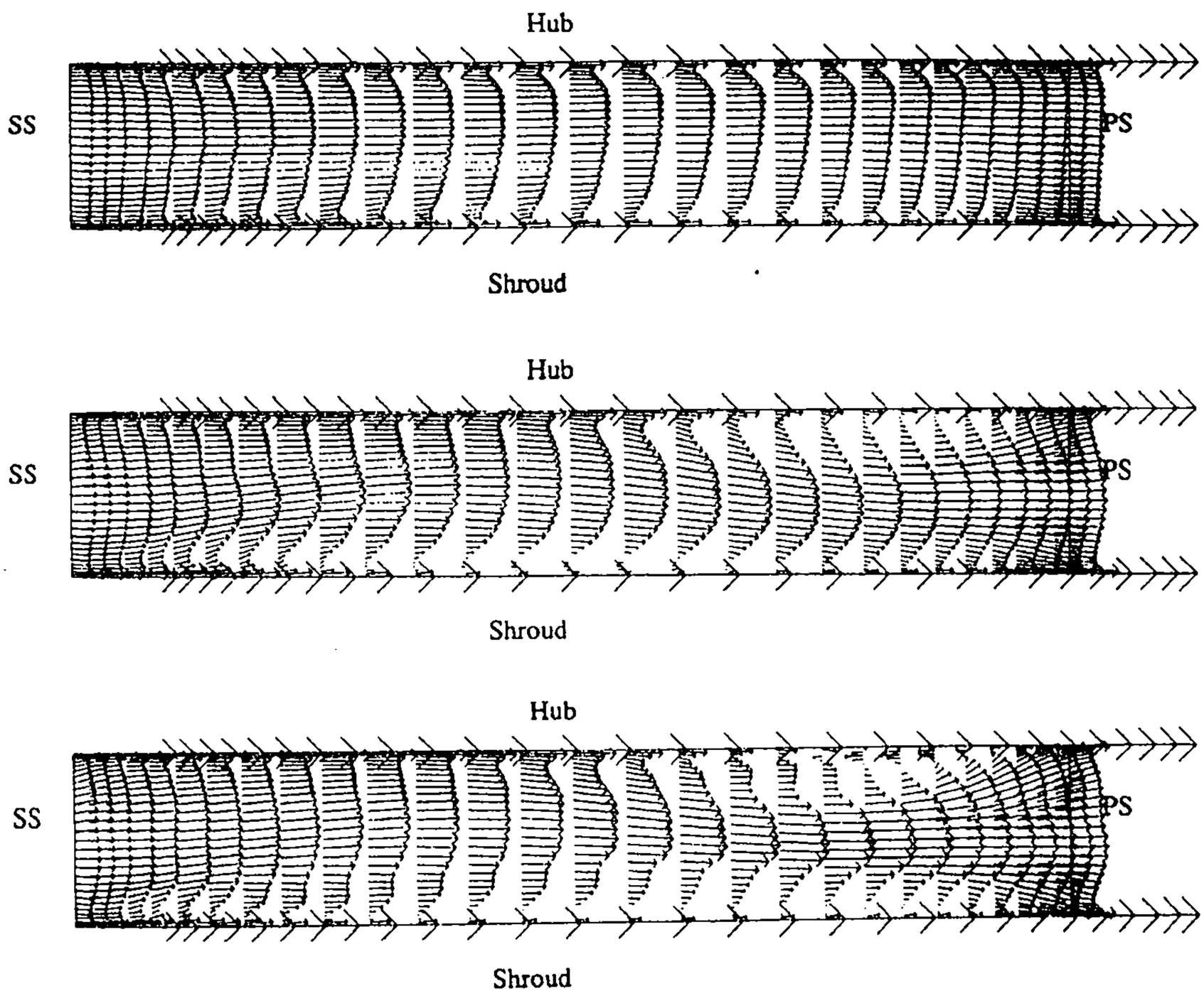

Figure 9.19 - As for figure 9.17, for k=51.

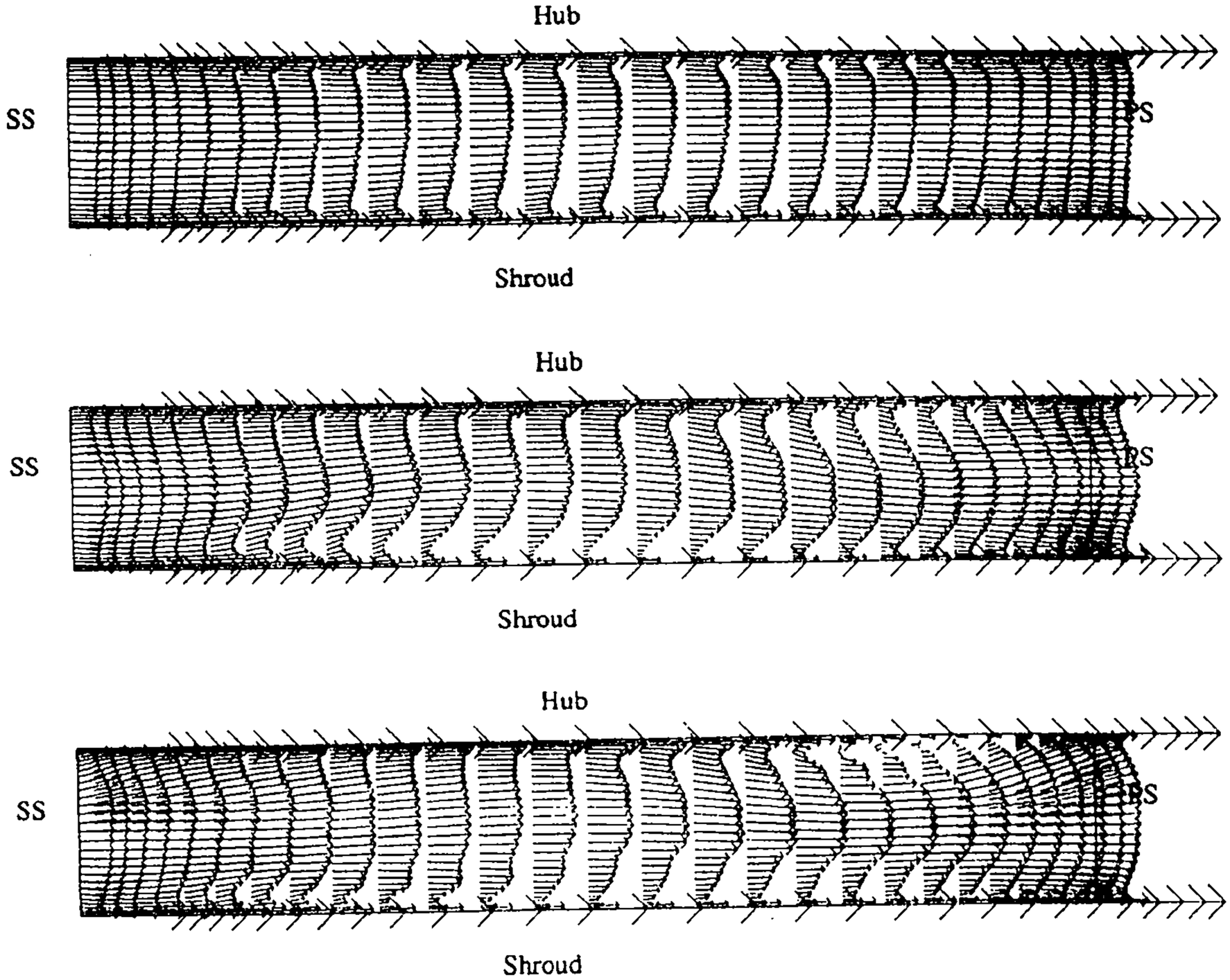

Figure 9.20 - As for figure 9.17, for k=52.

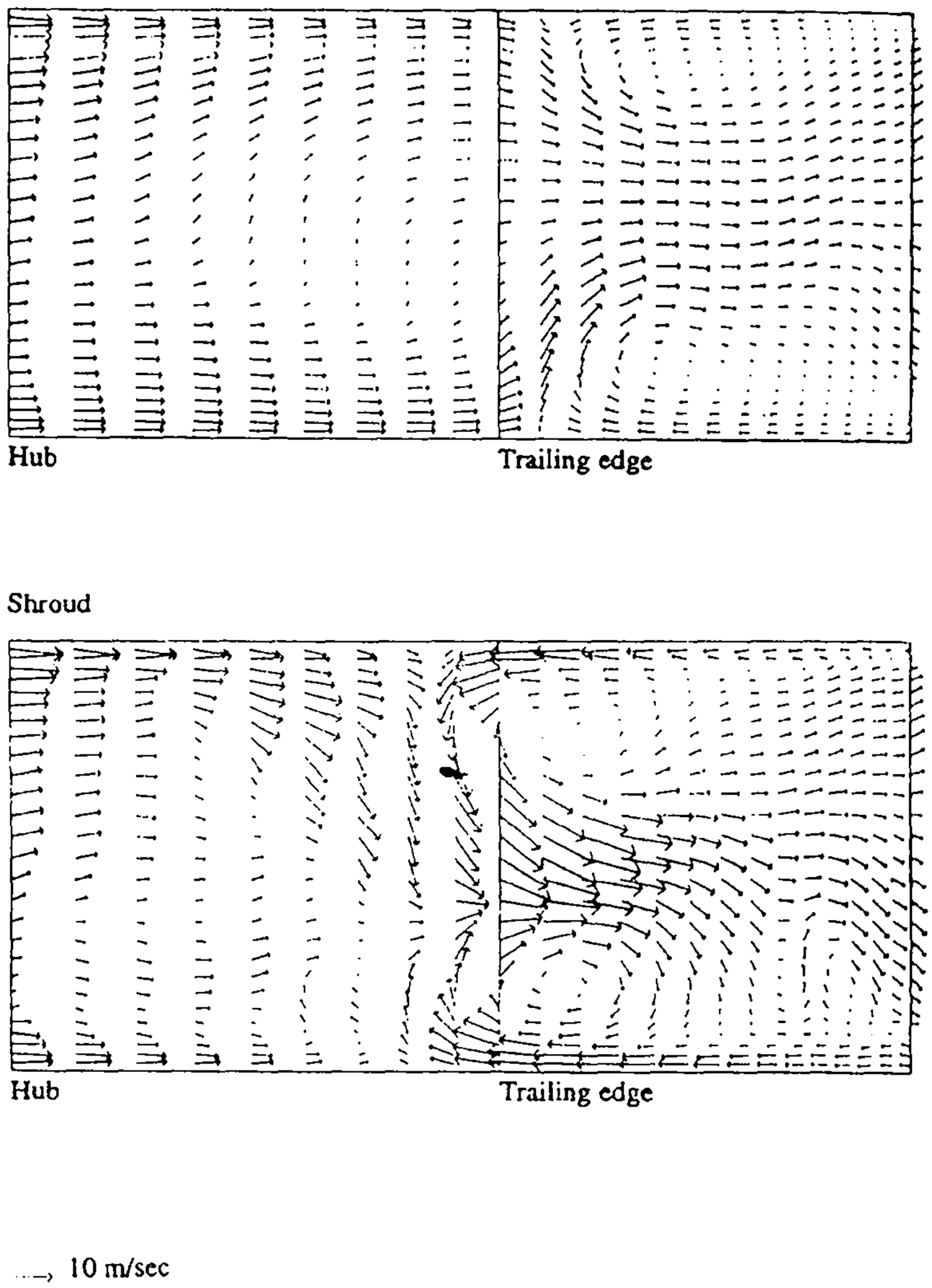

Figure 9.21 - Calculated streamwise velocity at the center of the computational domain, at ***partial flow rate****, using the QUICK scheme and the eddy-viscosity formulation (top) and the modified formulation (bottom).*

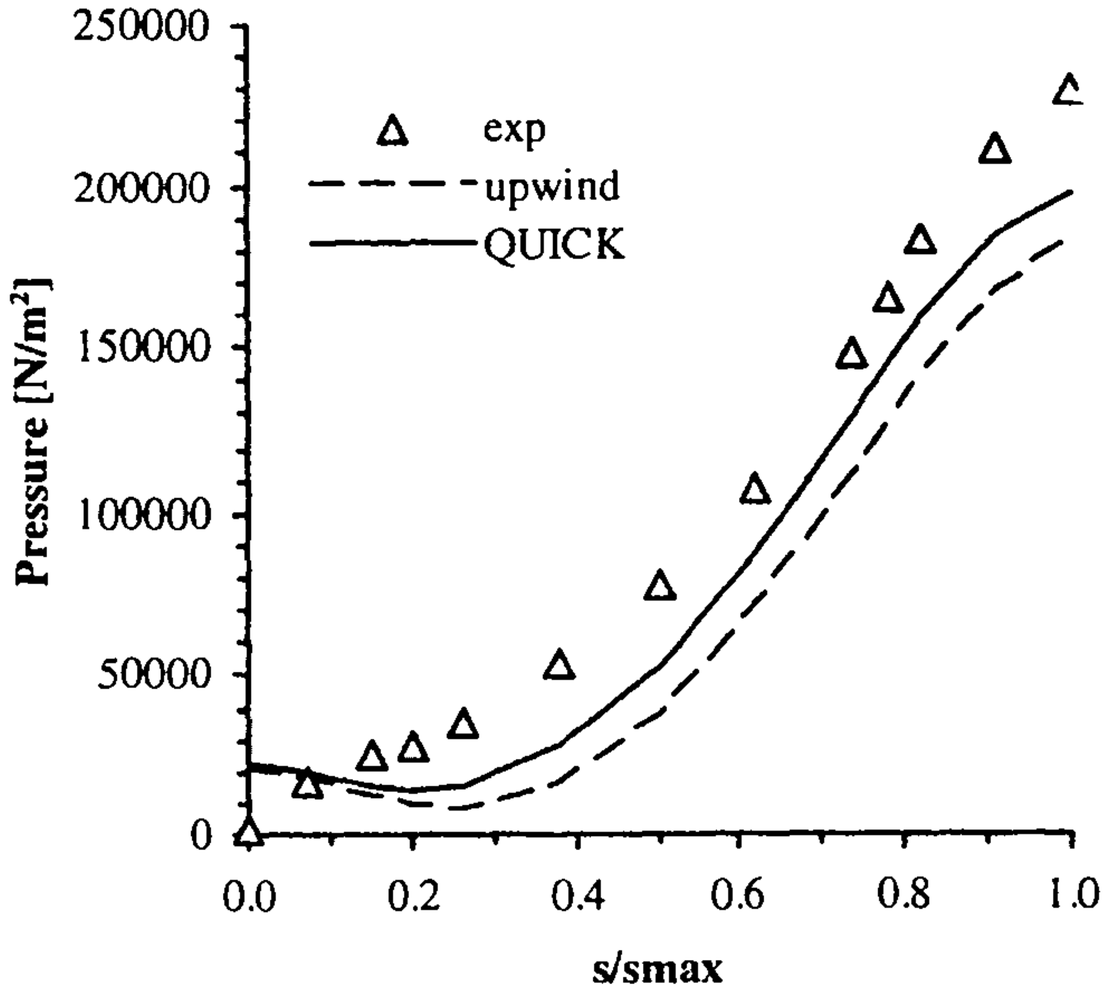

*Figure 9.22 - Static pressure at the **shroud**, comparison between experimental values and values calculated using the **eddy viscosity formulation**, nominal flow rate.*

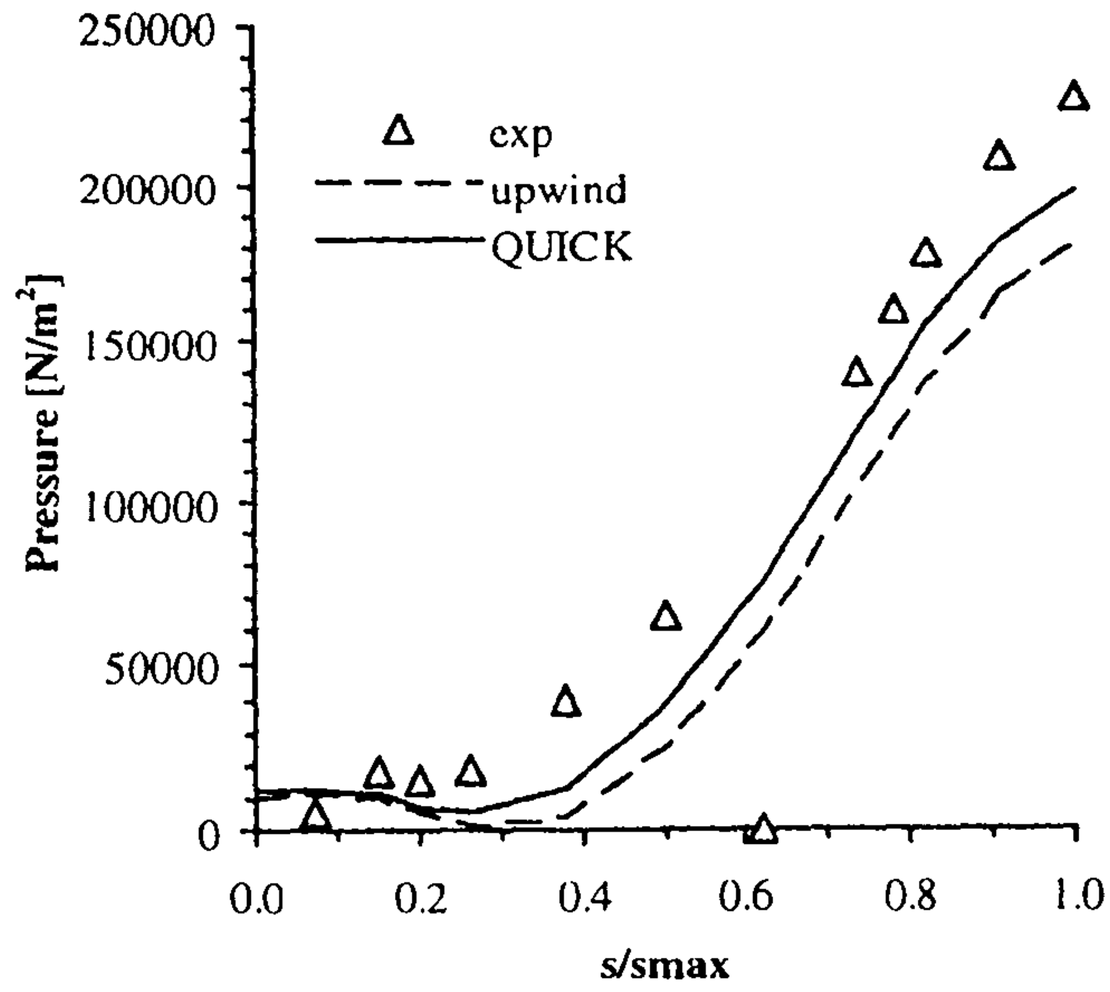

*Figure 9.23 - Static pressure at the **hub**, comparison between experimental values and values calculated using the **eddy viscosity formulation**, nominal flow rate.*

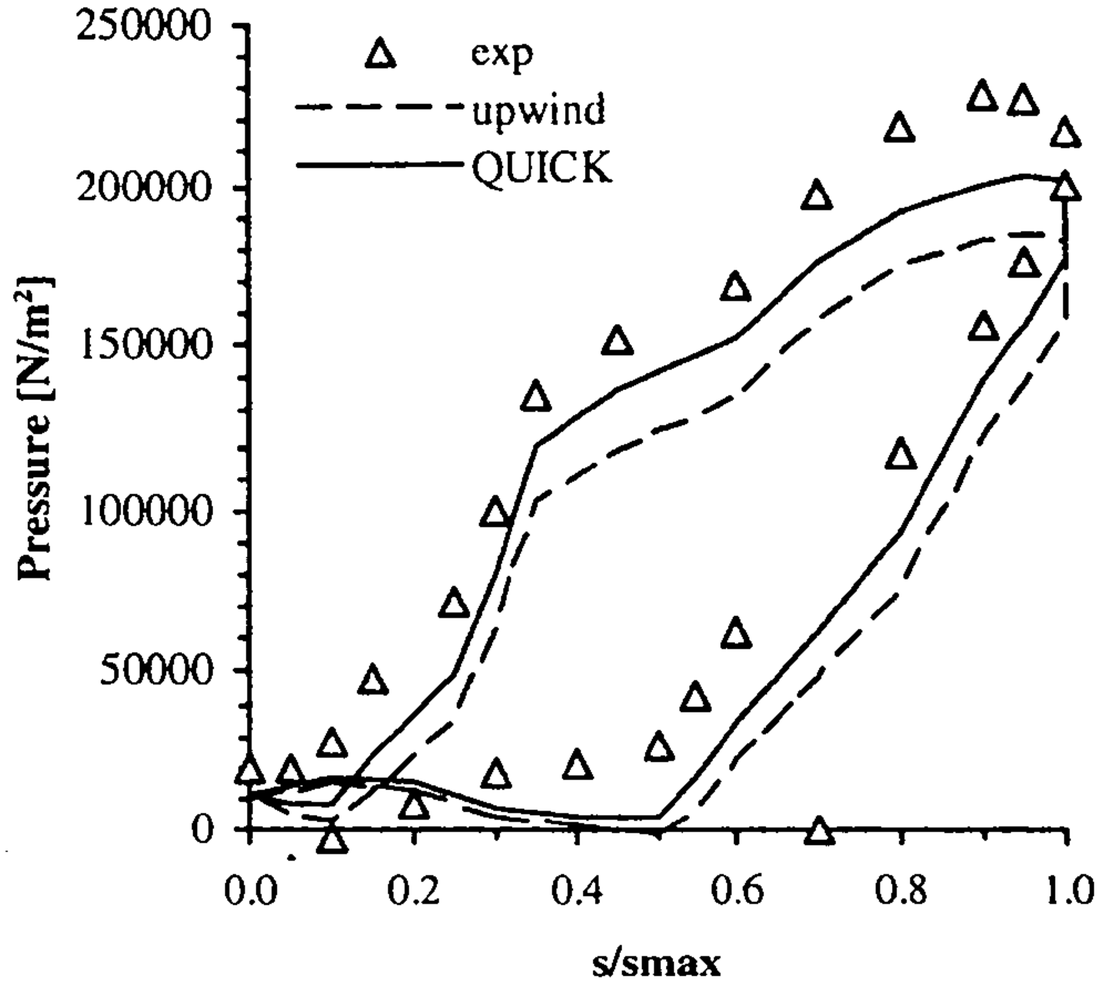

*Figure 9.24 - Static pressure at the **blade**, comparison between experimental values and values calculated using the **eddy viscosity formulation**, nominal flow rate.*

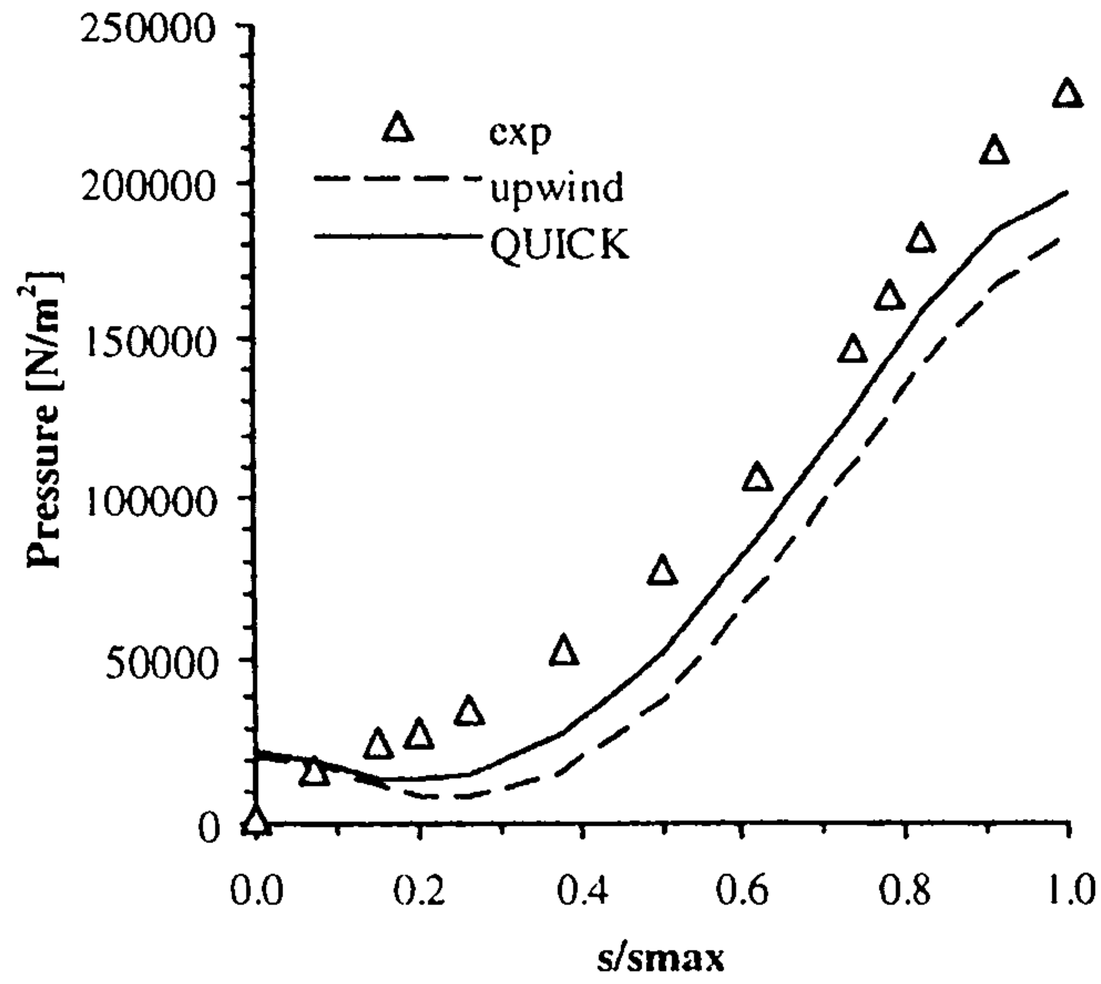

*Figure 9.25 - Static pressure at the **shroud**, comparison between experimental values and values calculated using the **modified formulation**, nominal flow rate.*

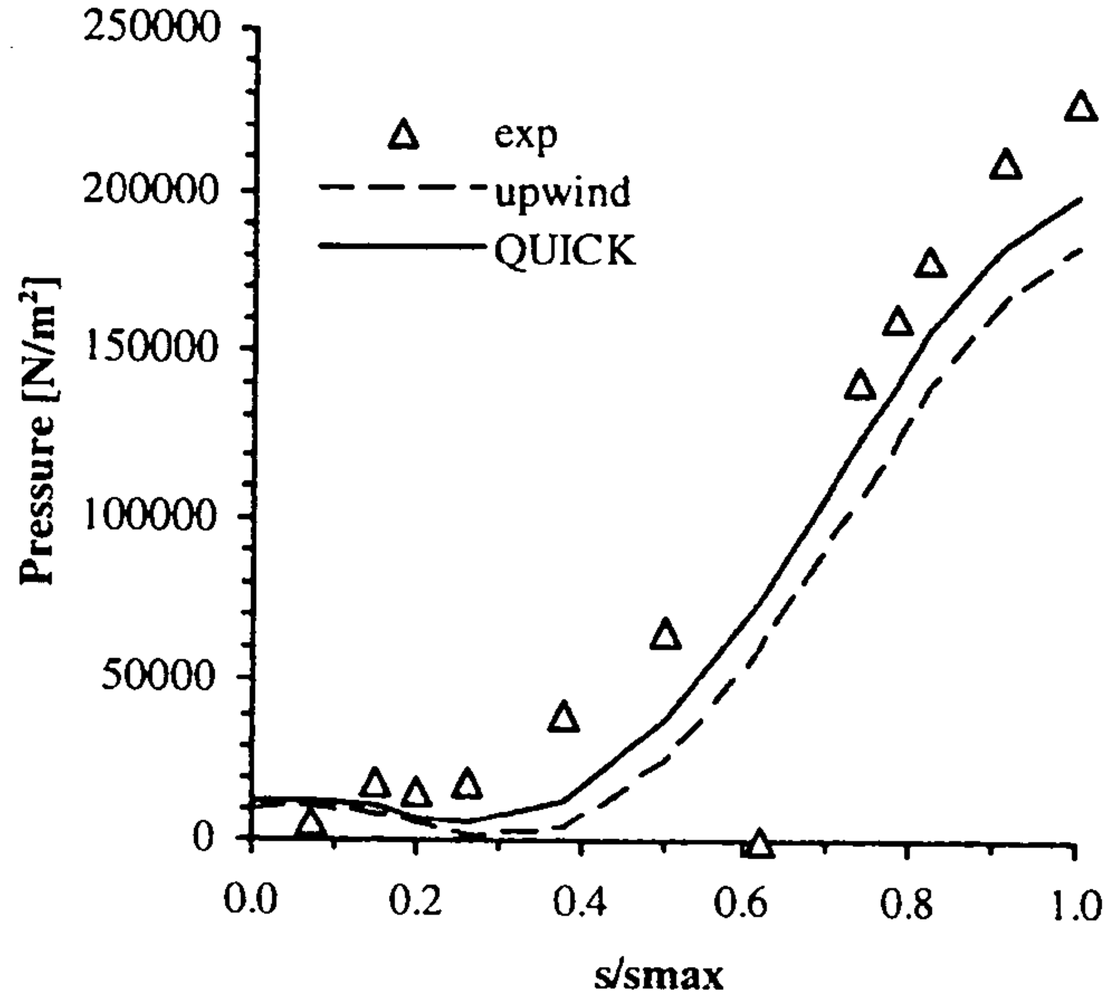

*Figure 9.26 - Static pressure at the **hub**, comparison between experimental values and values calculated using the **modified formulation**, nominal flow rate.*

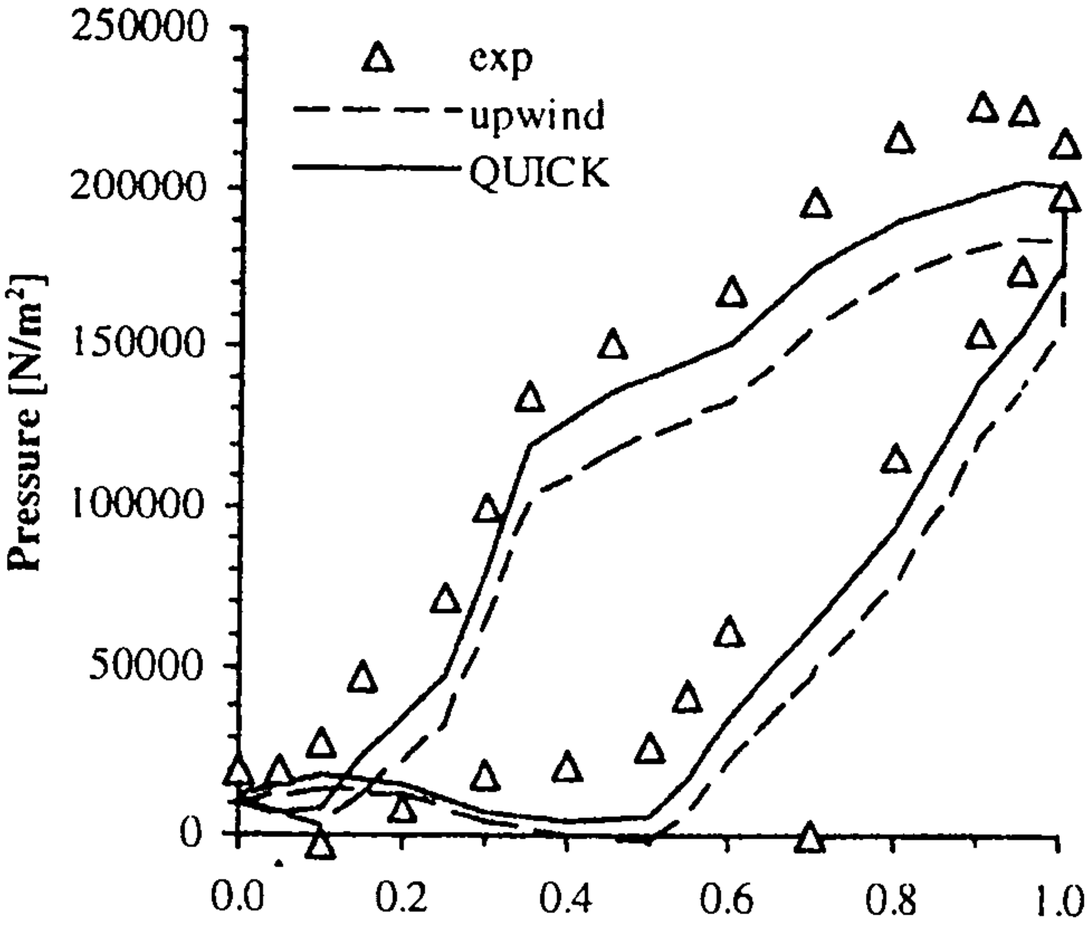

*Figure 9.27 - Static pressure at the **blade**, comparison between experimental values and values calculated using the **modified formulation**, nominal flow rate.*

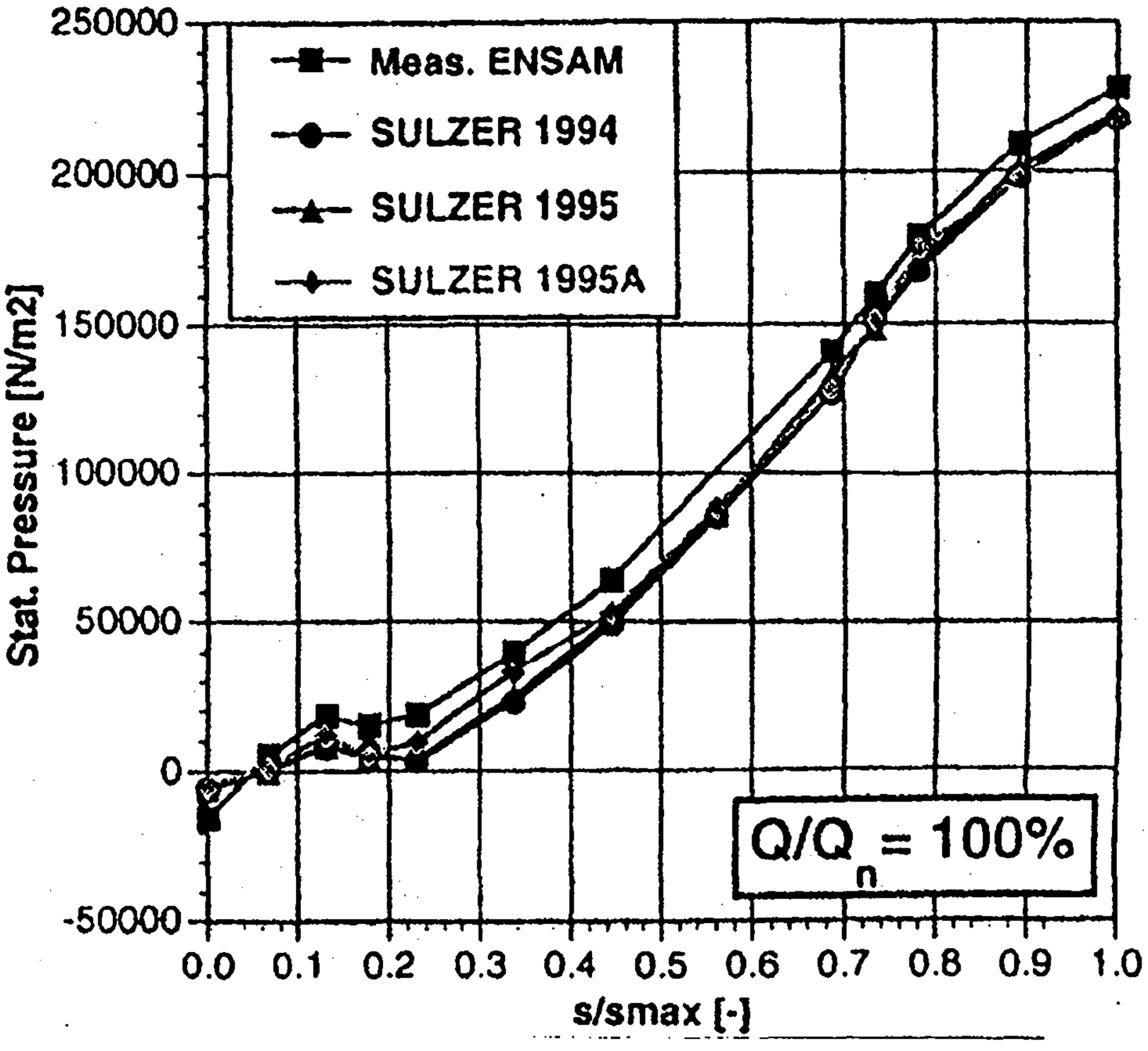

*Figure 9.28 – Static pressure at the **hub**, comparison between the experimental values (in the figure as: 'Meas. ENSAM') and the predictions obtained by F. Muggli (1995), at nominal flow rate, using the TASCflow commercial code and a 29×29×125 grid. The standard k-ε turbulence method was used, while both skewed upwind and the advection correction method where used for the treatment of the convection.*

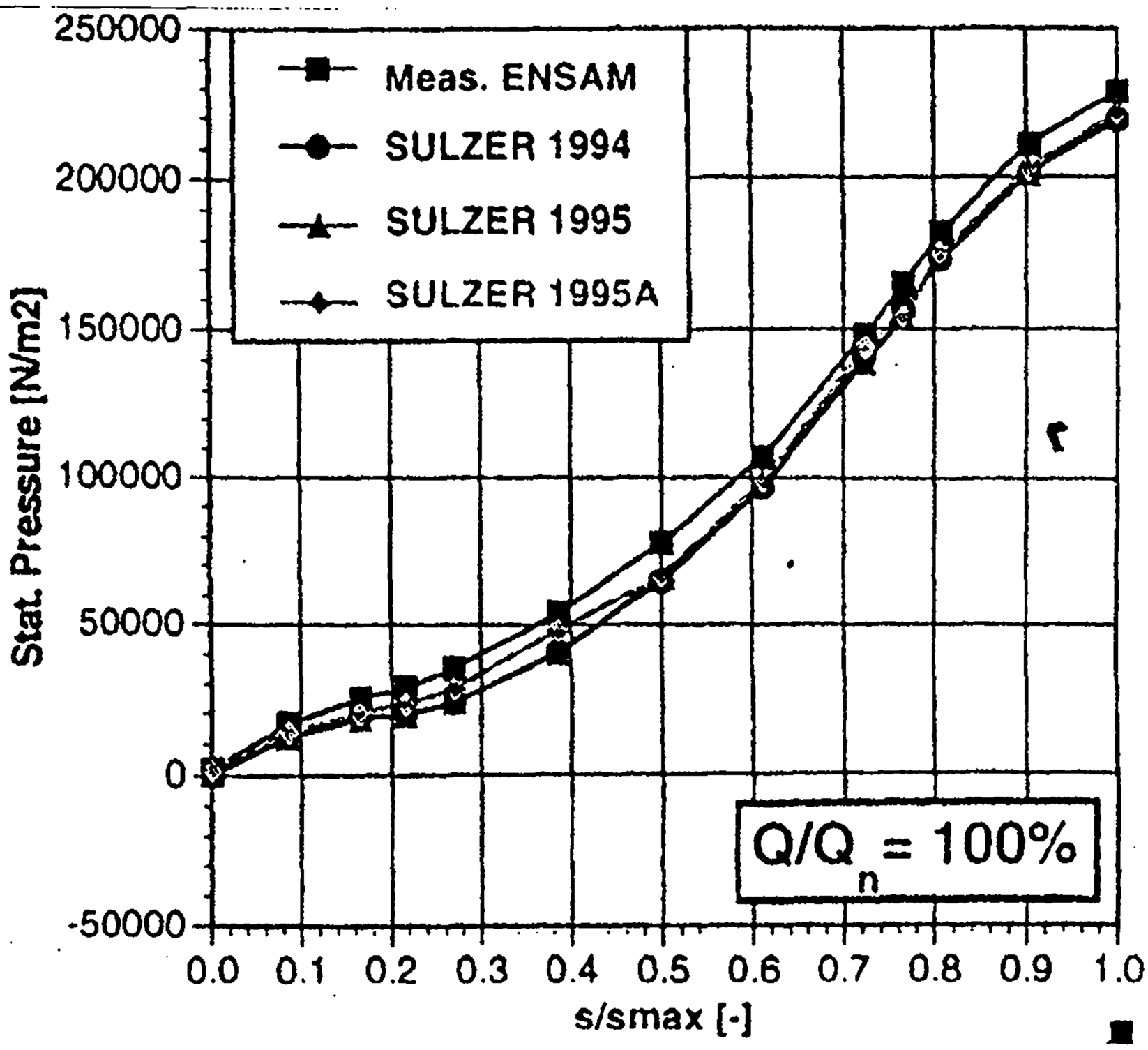

*Figure 9.29 – Static pressure at the **shroud**, comparison between the experimental values (in the figure as: 'Meas. ENSAM') and the predictions obtained by F. Muggli (1995), nominal flow rate.*

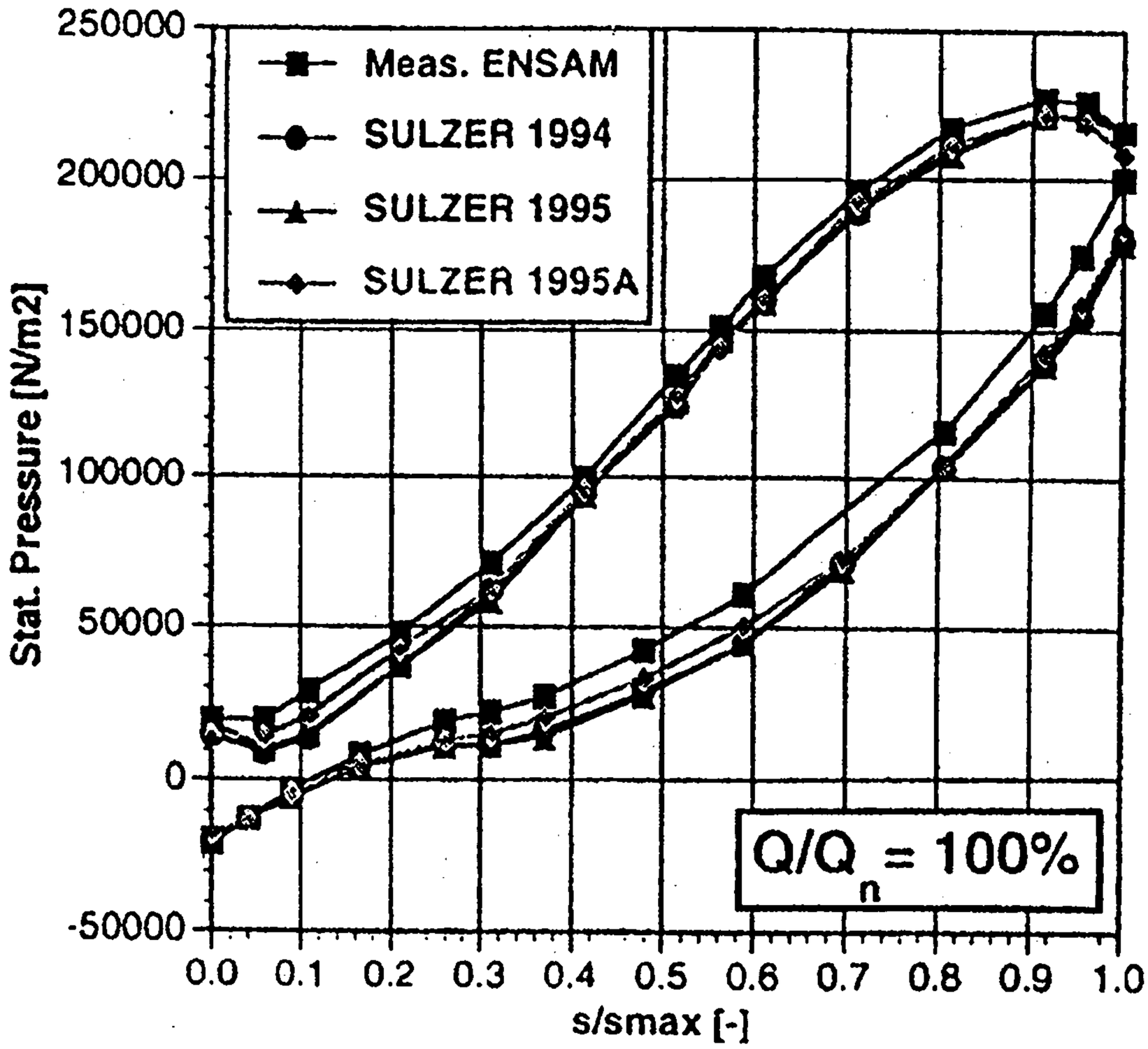

*Figure 9.30 – Static pressure at the **blade**, comparison between the experimental values (in the figure as: 'Meas. ENSAM') and the predictions obtained by F. Muggli (1995), nominal flow rate.*

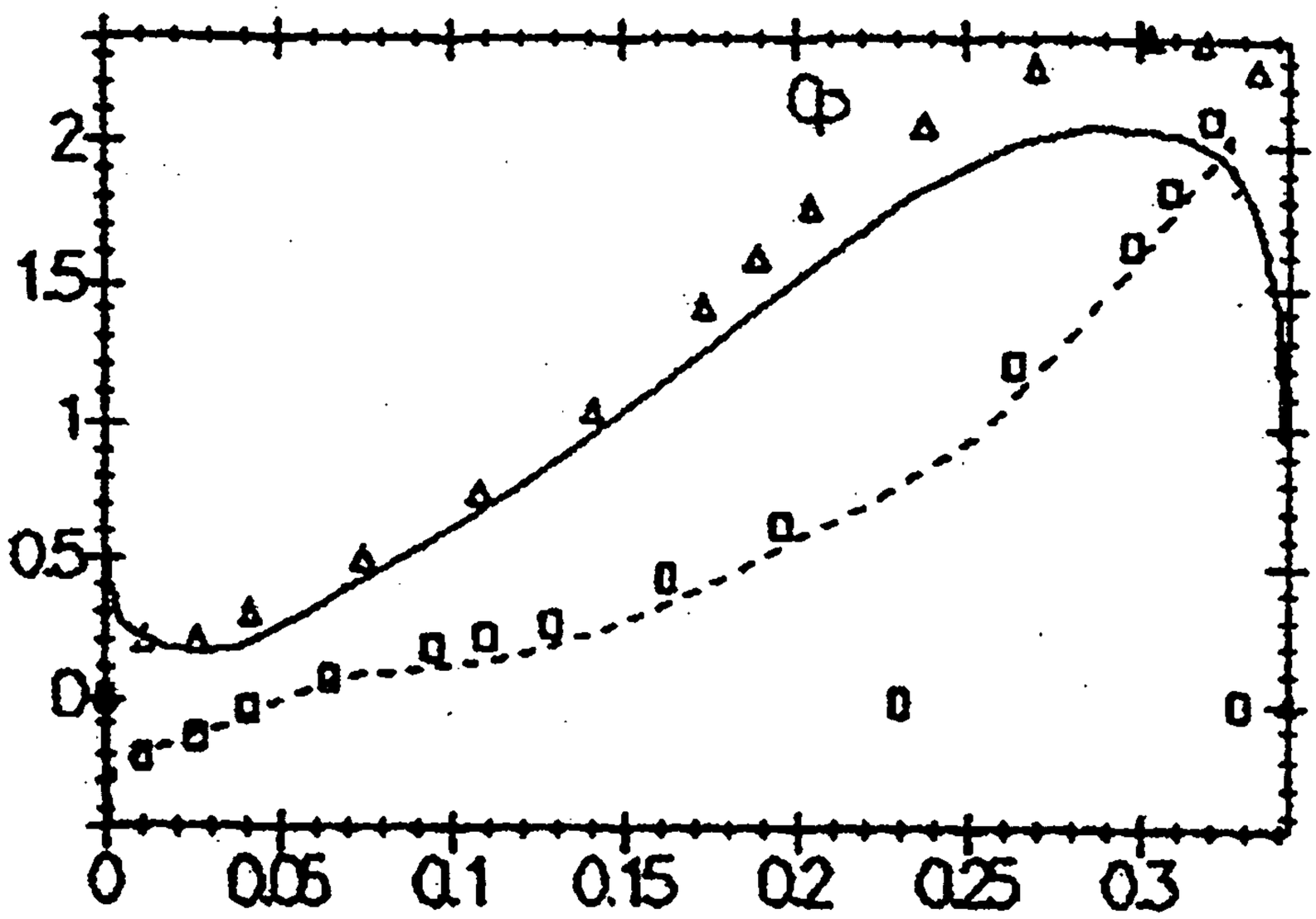

Figure 9.31 – Comparison of the experimental data for the static pressure coefficient along blade surfaces at midspan with the predictions obtained by Hirsch (1996), at nominal flow rate, using the EURANUS/TURBO code and a 65×33×65 grid. The algebraic turbulence model of Baldwin-Lomax has been used, while a second-order centered scheme with second and fourth order artificial dissipation terms was adopted for the treatment of the convection.

Chapter 10
Conclusions and suggestions for future work

In this thesis a new Navier-Stokes solver for three-dimensional geometries, based on a k-ε method with a definition of the turbulent transport diffusion term not based on the eddy-viscosity and capable of adopting arbitrary modelling of the Reynolds stresses, has been presented.

The results of the numerical tests presented show that even the most simple quadratic correction added in the formulation of the Reynolds stresses can produce a drastic improvement in the prediction of flows affected by curvature, and that the proposed algorithm allows a simple and straightforward introduction of any modifications in the Reynolds stresses.

Furthermore, it is evident in all the numerical tests that the modification introduced in the modelling of the turbulent diffusion terms also provides a more accurate value of the physical diffusion and, as a consequence, improves the increase in accuracy obtained with the use of higher-order convection schemes.

On the other hand, the proposed modification also causes a deterioration in the stability of the procedure, and therefore the necessity of lowering the under-relaxation coefficients, with an increase in the computational cost of the code.

It has been shown that with the proposed algorithm it is important to use a direct solver for the solution of the pressure correction equation, especially in the prediction of turbulent flows in rotating passages, where the pressure at the outlet has to be assigned and an iterative solver seems to be unable to produce an acceptable solution.

The adoption of a direct solver is particularly important when using higher-order convection schemes, as has been shown in detail in this thesis, and at the same time it is indispensable to use higher-order schemes when using the proposed modification in the modelling of the turbulent diffusion, but the consequence of this choice of linear solver is

that the algorithm requires a large amount of memory, therefore posing a very strict limit on the number of grid points that can be used.

This limit is certainly the biggest disadvantage of the algorithm, especially for turbomachinery applications, where much more refined grids than the ones adopted for the examples presented in this thesis are required for an accurate description of the flow phenomena. Furthermore, in the case of turbomachinery applications, the adoption of a single H-type block for the computational grid, as in this thesis, appears to create serious problems of both accuracy and stability around the edges of the blades.

For these reasons, it could be argued that the computational procedure that has been presented in this thesis does not appear to be of practical use for applications of engineering interest, and future work should therefore to be directed mainly towards an iterative solver that could overcome the limits of GMRES without requiring large amount of memory, and towards a better description of the edges of the blades, for example through a multi-block approach, as commonly adopted for this kind of applications.

In reality, as the new formulation for the turbulence modelling can be written as a simple correction to the standard eddy viscosity formulation (as in formulae (8.2.1) to (8.2.3)), a more logical continuation of this study would be to introduce the formulae for the turbulent transport as an additional source term in one of the many commercial codes for turbomachinery applications that are on the market, provided that the code can adopt high-order convection schemes that, as has been shown, are indispensable for the use of this particular formulation. In effect many of the existing codes in use in engineering applications have the capability to generate an excellent description of complex geometries through the use of different types of computational grids, often adopt very efficient linear solvers and generally provide the user with the possibility to include external routines in the code.

If the problems of stability and computational cost of the procedure are resolved, the formulation of the turbulent transport diffusion that has been presented in this thesis can certainly become an extremely effective method to introduce non-linear modelling of the

Reynolds stresses in a Navier-Stokes solver, and, at the same time, to provide a more accuarte description of the physical diffusion.

References

D.A. Anderson, J.C. Tannehill and R.H. Pletcher, *Computational Fluid Mechanics and Heat Transfer*, McGrawn-Hill (1984).

A.J. Baker and J.A. Orzechowski, An interaction algorithm for three-dimensional turbulent subsonic aerodynamic juncture region flow, *AIAA Journal* **21**, 524 (1983).

B. Baldwin and H. Lomax, Thin layer approximation and algebraic model for separated flow, *AIAA paper 78-0257* (1978).

R. Barrett, M. Berry, T. Chan, J. Demmel, J. Donato, J. Dongarra, V. Eijkhout, R. Pozo, C. Romine and H. van der Vost, *Templates for the Solution of Linear Systems: Building Blocks for Iterative Methods*, SIAM, netlib, WWW mail (1994).

J. Boussinesq, Theorie de l'ecoulement tourbillant, *Memoires Presentes par Divers Savants Sciences Mathematique at Physiques, Academie des Sciences, Paris,* **23**, 46 (1877).

P. Bradshaw, The effects of streamline curvature on turbulent flow, *AGARDograph* 169 (1973).

A. Brandtl, Multi-level adaptive solutions to boundary-value problems, *Math. Comput.*, **31**, 331 (1977).

W.L. Briggs, *A Multigrid Tutorial*, SIAM, Philadelphia (1987).

W.L. Chen, M.A. Leschziner and F.S. Lien, Non-linear eddy-viscosity modelling for transitional flows pertaining to cascades operating in off-design conditions, in *Latest Advances in the Aerodynamics of Turbomachinery with Special Emphasis upon Unsteady Flows*, IMechE Seminar publication 1996-21 (1996).

J.F. Combes and E. Rieutord, Numerical and experimental analysis of the flow in a centrifugal pump at nominal and partial flow rate, *ASME paper 92-GT-284* (1992).

T.J. Craft, B.E. Launder and K. Suga, Development and application of a cubic eddy-viscosity model of turbulence, *Int. J. Heat and Fluid Flow* **17**, 108 (1996).

T.J. Craft, B.E. Launder and K. Suga, Prediction of turbulent transition phenomena with a nonlinear eddy-viscosity model, *Int. J. Heat and Fluid Flow* **18**, 15 (1997).

Cray Research, Inc., *Scientific Libraries Reference Manual* (SR-2081, 8.2).

W.N. Dawes, Application of a three-dimensional viscous compressible flow solver to a high-speed centrifugal compressor rotor - secondary flow and loss generation, *IMechE paper c261/87* (1987).

R. C. Dean, *On the Unresolved Fluid Dynamics of the Centrifugal Compressor*, Creare Inc., Technical Note Vols. I and II, March 1968.

D. Eckardt, Detailed flow investigations within a high-speed centrifugal compressor impeller, *Transactions of the ASME*, September 1976 (Paper No. 76-FE-13), pp 390-399.

D. Eckardt, Flow field analysis of radial and backswept centrifugal compressor impellers. Pert I: Flow measurements using a laser velocimeter, *ASME CP Performance Prediction of Centrifugal Pumps and Compressors*, pp. 77-86 (1980).

C.A.J. Fletcher, *Computational Techniques for Fluid Dynamics, Vol. I and II*, Springer-Verlag (1988).

P.H. Gaskell and A.K.C. Lau, Curvature-compensated convective transport: SMART, a new boundedness-preserving transport algorithm, *Int. J. Num. Methods in Fluids* **8**, 617 (1988).

G.H. Golub and C.F. Van Loan, *Matrix Computations (second edition)*, Johns Hopkins University Press (1989).

C. Hah, A.C. Bryans, Z. Moussa and M.E. Tomsho, Application of viscous flow computations for the aerodynamic performance of a backswept impeller at various operating conditions, *ASME J. of Turbomachinery* **110,** 330 (1988).

C. Hah and H. Krain, Secondary flows and vortex motion in a high-efficiency backswept impeller at design and off-design conditions, *ASME J. of Turbomachinery* **112**, 7 (1990).

K. Hanjalic and B.E. Launder, A Reynolds-stress model of turbulence and its application to thin shear flows, *J. Fluid Mech.* **52**, 609 (1972).

K. Hanjalic and B.E. Launder, Contribution towards a Reynolds-stress closure for low-Reynolds-number turbulence, *J. Fluid Mech.* **74**, part 4, 593 (1976).

T. Hayase, J.A.C. Humprey and R. Greif, A consistently formulated QUICK scheme for fast and stable convergence using finite-volume iterative calculation procedures, *Journal of Computational Physics* **98**, 108 (1992).

C. Hirsch, *Numerical Computation of Internal and External Flows, Vol. I and II*, John Wiley & Sons (1991).

C. Hirsch, S. Kang and G. Pointel, A numerically supported investigation of the 3D flow in centrifugal impellers. Part I: the validation base, *ASME paper 96-GT-151* (1996).

J.A.C. Humprey, A.M.K. Taylor and J.H. Whitelaw, Laminar flow in a square duct of strong curvature, *J. Fluid Mech.*, **83**, part 3, 509 (1977).

B.R. Hutchinson and G.D. Raithby, A multigrid method based on the additive correction strategy, *Num. Heat Trans.*, **9**, 511 (1986)..

W.P Jones and B.E. Launder, The prediction of laminarization with a 2-equation model of turbulence, *Int. J. Heat & Mass Transfer* **15**, 301 (1972).

K.C. Karki, S.P. Vanka and H.C. Mongia, Fluid flow calculations using a multigrid method and an improved discretization scheme, *Num. Heat Trans, Part B,* **16**, 143 (1989).

K.C. Karki, P.S. Sathyamurthy and S.V. Patankar, Performance of a multigrid method with an improved discretization scheme for three-dimensional fluid flow calculations, *Num. Heat Trans, Part B,* **29**, 275 (1996).

J.R. Kightley and I.P. Jones, A comparison of conjugate gradient preconditionings for three-dimensional problems on a CRAY-1, *Computer Physics Communications,* **37**, 205 (1985).

M. Kobayashi, J.M.C. Pereira and J.C.F. Pereira, A second-order upwind least-squares scheme for incompressible flows on unstructured hybrid grids, *Num. Heat Trans, Part B,* **34**, 39 (1998).

P.L.C. Lage, Modified strong implicit procedure with adaptive optimization of its iteration parameter, *Num. Heat Trans, Part B,* **30**, 255 (1996).

B. Lakshminarayana, Turbulence modelling for complex shear flows, *AIAA Journal* **24**, 1900 (1986).

B. Lakshminarayana, An assessment of computational fluid dynamic techniques in the analysis and design of turbomachinery - The 1990 Freeman Scholar Lecture, *ASME J. of Fluids Engineering* **113**, 315 (1991).

H.P. Langtangen, Conjugate gradients methods and ILU preconditioning on non-symmetric matrix systems with arbitrary sparsity patterns, *Int. J. Numer. Meth. Fluids,* **9**, 213 (1989).

J. Laufer, Investigation of turbulent flow in a two-dimensional channel, *NACA TN* 1053 (1952).

B.E. Launder and D.B. Spalding, *Mathematical Models of Turbulence*, Academic Press, London (1972).

B.E. Launder and D.B. Spalding, The numerical calculation of turbulent flows, *Comput. Methods Appl. Mech. Engrg* **3**, 269 (1974).

B.P. Leonard , A stable and accurate convective modelling procedure based on quadratic upstream interpolation, *Comput. Methods Appl. Mech. Engrg.*, **19**, 59 (1979).

B.P. Leonard, Elliptic Systems: Finite Difference Method IV, in W.J. Minkowycz et al (eds.), *Handbook of Numerical Heat Transfer*, pp 347-378, John Wiley & Sons, (1988).

B.P. Leonard and S Mokhtari, Beyond first-order upwinding: the ULTRA-SHARP alternative for non-oscillatory steady-state simulation of convection, *Int. J. Num. Methods in Engrg.* **30**, 729 (1990).

B.P. Leonard and J.E. Drummond, Why you should not use 'Hybrid', 'Power-Law' or related exponential schemes for convective modelling: there are much better alternatives, *Int. J. Num. Methods in Fluids* **20**, 421 (1995).

F.S. Lien and M.A. Leschziner, A general non-orthogonal collocated finite volume algorithm for turbulent flow at all speed incorporating second-moment turbulence-transport closure, Part 1: Computational implementation, *Comput. Methods Appl. Mech. Engrg.* **114**, 123 (1994a).

F.S. Lien and M.A. Leschziner, Assessment of turbulence-transport models including non-linear RNG eddy-viscosity formulation and second-moment closure for flow over a backward-facing step, *Computers Fluids* **23**, 983 (1994b).

J.W. Liu, Modification of the minimum degree algorithm by multiple elimination, *ACM Transactions of Math. Software* **11**, 141 (1985).

J.W. Liu, The multifrontal method for sparse matrix solution: theory and practice, *SIAM review* **34**, 82 (1992).

J.L. Lumley, Towards a turbulent constitutive relation, *J. Fluid Mech.* **41**, 413 (1970).

J. Luo and B. Lakshminarayana, Three-dimensional Navier-Stokes computation of turbine nozzle flow with advanced turbulence models, *ASME paper 95-GT-302* (1995).

S. Majumdar, Role of underrelaxation in momentum interpolation for calculation of flow with nonstaggered grid, *Num. Heat Trans.* **13**, 125 (1988).

M.W. Markovin, Effects of compressibility on turbulent flows, *The Mechanics of Turbulence*, Gordon and Breach, New York, p. 361 (1961).

A. Melling and J.H. Whitelaw, Turbulent flow in a rectangular duct, *J. Fluid Mech.* **78**, 289 (1976).

J. Moore, A wake and an eddy in a rotating radial-flow passage, Part1: experimental observations, *Journal of Engineering for Power*, July 1973, p. 205.

J. Moore and J.G. Moore, Calculations of three-dimensional viscous flow and wake development in a centrifugal impeller, *ASME CP, Performance Prediction of Centrifugal Pumps and Compressors*, p. 61-67 (1980a)

J. Moore and J.G. Moore, Three-dimensional viscous flow calculations for assessing the termodynamic performance of centrifugal compressors - study of the Eckardt compressor, *AGARD-CP*-282 (1980b).

F. Muggli, Test case 5: SHF radial pump - TASCflow simulation, *ERCOFTAC Seminar and Workshop on 3D Turbomachinery Flow Prediction III* (1995).

H.K. Myong and N. Kasagi, Prediction of anisotropy of the near wall turbulence with an anisotropic low-Reynolds-number k-ε turbulence model, *J. Fluids Eng.* **112**, 521 (1990).

S. Nisizima and A. Yoshizawa, Turbulent channel and Couette flows using an anisotropic k-ε model, *AIAA Journal* **25**, 414 (1987).

S. V. Patankar, *Numerical Heat Transfer and Fluid Flow*, Hemisphere Publishing (1980).

V.C. Patel, W. Rodi and G. Scheurer, Turbulence models for near-wall and low Reynolds number flows: a review, *AIAA Journal* **23**, 1308 (1985).

L. Prandtl, Bericht über Untersuchungen zur a usgebildeten Turbulenz, *ZAMM* **5**, 136 (1925).

L. Prandtl, Über ein neues Formalsystem für die ausgebildete Turbukenz, Nachrichten von de Akad. der Wissenschaft in Gottingen (1945).

C. M. Rhie and W. L. Chow, Numerical study of the turbulent flow past an airfoil with trailing edge separation, *AIAA Journal* **21**, 1525 (1983).

R. Rubinstein and J.M. Barton, Non-linear Reynolds stress models and renormalization group, *Phys. Fluids* A **2**, 1472 (1990).

Y. Saad and M.H. Schoults, GMRES: a generalized minimal residual algorithm for solving non-symmetric linear system, *SIAM J. Sci. Comput.* **7**, 856 (1986).

P.S. Sathyamurthy and S.V. Patankar, Block-correction multigrid method for fluid flow problems, *Num. Heat Trans, Part B*, **25**, 375 (1994).

S. Sheen and J. Wu, Solution of the pressure correction equation by the preconditioned conjugate gradient method, *Num. Heat Trans, Part B*, **32**, 215 (1997).

S. Sheen and J. Wu, Preconditioning techniques for the BiCGSTAB algorithm used in convection-diffusion problems, *Num. Heat Trans, Part B*, **34**, 241 (1998).

T.H. Shih, J. Zhu and J.L. Lumley, A realizable Reynolds stress algebraic equation model, *NASA tech. memo* 105993 (1993).

C.G. Speziale, On turbulent secondary flows in pipes of non-circular cross-section, *Int. J. Engng. Sci.* **20**, 863 (1982).

C.G. Speziale, Closure models for rotating two-dimensional turbulence, *Geophys. Astrophys. Fluid Dyn.* **23**, 69 (1983).

C.G. Speziale, On nonlinear k-l and k-ε models of turbulence, *J. Fluid Mech.* **178**, 459 (1987).

G.E. Schneider and M. Zedan, A modified strongly implicit procedure for the numerical solution of field problems, *Num. Heat Trans.*, **4**, 1 (1981)

H.L. Stone, Iterative solution of implicit approximations of multidimensional partial differential equations, *SIAM, J. Numer. Anal.*, **5**, 530 (1968).

P. Tamamidis and D.N. Assanis, Three-dimensional incompressible flow calculations with alternative discretization schemes, *Num. Heat Transfer, Part B*, **24**, 57 (1993).

A.M.K. Taylor, J.H. Whitelaw and M. Yianneskis, Measurements of laminar and turbulent flow in a curved duct with thin inlet boundary layers, Nasa Contractor Report 3367 (1981).

L.H. Thomas, Elliptic problems in linear difference equations over a network, Watson Sci. Comput. Lab. Report, Columbia University, New York (1949).

A. Tourlidakis, *Numerical Modelling of Viscous Turbomachinery Flows with a Pressure Correction Method*, PhD Thesis, Cranfield Institute of Technology (1992).

A.Tourlidakis and R.L. Elder, Numerical investigation of centrifugal compressor flows with tip leakage using a pressure correction method, *ASME paper 93-GT-109* (1993).

S.P. Vanka, A calcolation procedure for three-dimensional steady, recirculating flows using multigrid methods, *Comp. Meth. Appl. Mech. Eng:*, **55**, 321 (1986a).

S.P. Vanka, Block-implicit calculation of Navier-Stokes equations in primitive variables, *J. Comput. Phys.*, **65**, 138 (1986b).

H.K. Versteeg and W. Malalasekera, *An introduction to computational fluid dynamics – The finite volume method*, Longman Scientific & Technical (1995).

D.C. Wilcox , *Turbulence Modelling for CFD,* DCW Industries Inc. (1993).

D. Young, *Iterative solution of large linear systems,* Academic Press, New York (1971).

J. Zhu and W. Rodi, A low dispersion and bounded convection scheme, *Comput. Methods Appl. Mech. Engrg.* **92**, 87 (1991)

Appendix A
Trilinear interpolation

The data obtained from the code have to be linearly interpolated, in order to obtain the values of the variables in the points of the domain where the flow measures have been taken. The procedure adopted is as follows:

1) given the coordinates (x,y,z), in the absolute frame of reference, of the point where the measure has been taken, the mesh node (i,j,m) having the minimum distance from the given point is found;

2) Using the nodes that precede and follow the node of minimum distance in the three directions, simple tetrahedra are constructed around the node, as shown in figure A.1.

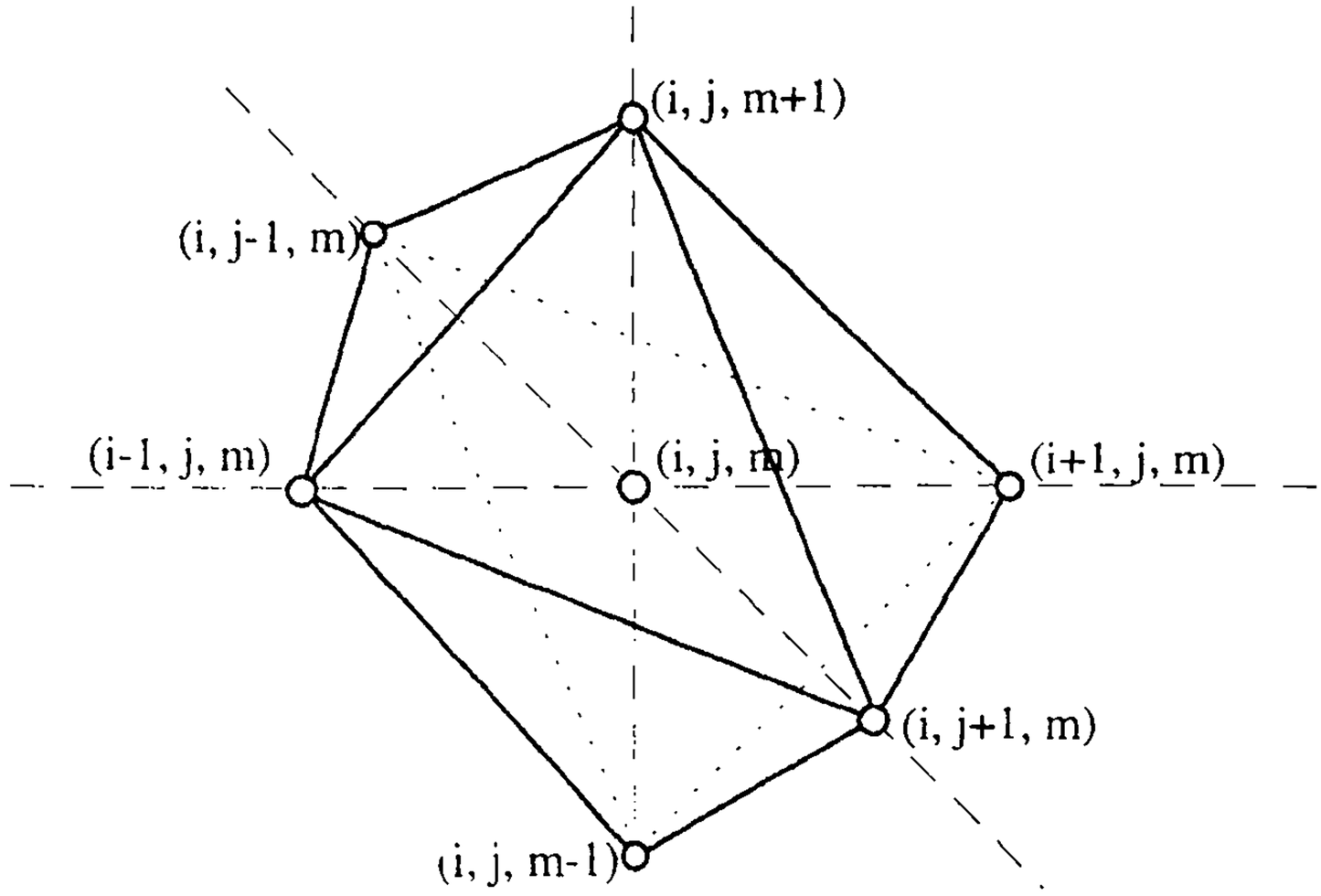

Figure A.1 - Disposition of the tetrahedrons around the node of minimum distance.

3) In each one of the eight tetrahedra a local system of variables(ξ, η, ζ) is introduced, as in figure A.2 and every variable (including the Cartesian coordinates) is described in the tetrahedron with the linear function:

$$\phi(\xi,\eta,\zeta) = a\xi + b\eta + c\zeta + d \tag{A.1}$$

where the four constants can be easily evaluated writing the function (A.1) in the four nodes, where the values of the variables are known; the function (A.1) can therefore be written as:

$$\phi = (\phi_2 - \phi_1)\xi + (\phi_3 - \phi_1)\eta + (\phi_4 - \phi_1)\zeta + \phi_1 \tag{A.2}$$

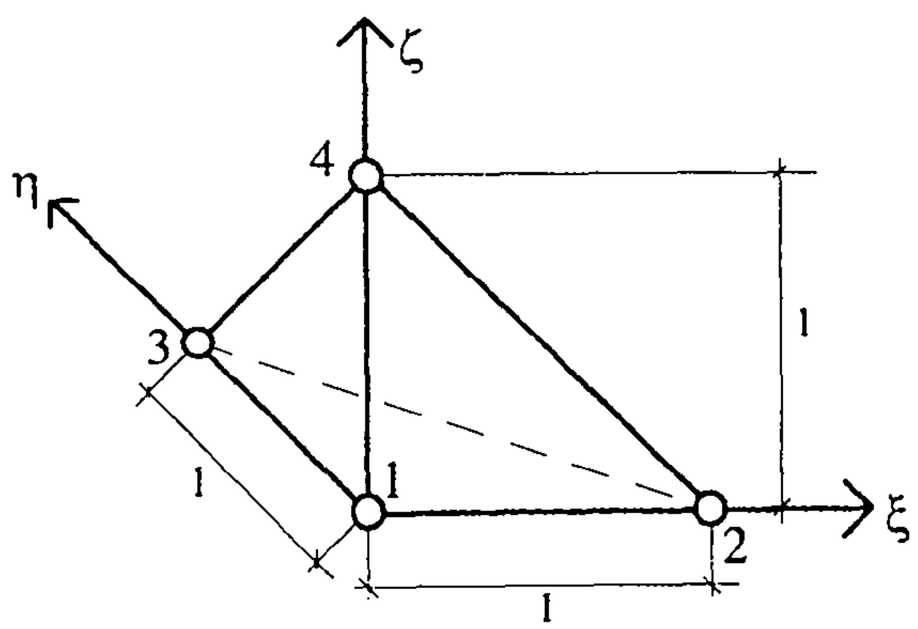

Figure A.2 - Local system of coordinates.

The values of the local variables (ξ,η,ζ) corresponding to the given point (x,y,z) are evaluated solving the system obtained writing equation (A.2) for the Cartesian coordinates:

$$\begin{cases} (x_2 - x_1)\xi + (x_3 - x_1)\eta + (x_4 - x_1)\zeta = x - x_1 \\ (y_2 - y_1)\xi + (y_3 - y_1)\eta + (y_4 - y_1)\zeta = y - y_1 \\ (z_2 - z_1)\xi + (z_3 - z_1)\eta + (z_4 - z_1)\zeta = z - z_1 \end{cases} \tag{A.3}$$

If the point is in the tetrahedron, that is if the corresponding local variables (ξ,η,ζ) satisfy the conditions:

$$\begin{cases} \xi,\eta,\zeta \geq 0 \\ \zeta \leq (1 - \xi - \eta) \end{cases} \tag{A.4}$$

the value of each variable in the point is obtained from the values in the four nodes using formula (A.2).

4) If the point is not in the eight tetrahedra having in common the node of minimum distance, the condition (A.4) is progressively relaxed in order to include the area surrounding the tetrahedra, until the condition is verified: the condition that the coordinates of the given point have to satisfy in order to be associated with one of the tetrahedra (and therefore using formula (A.2) to evaluate the value of a variable in the point) is now:

$$\begin{cases} \xi, \eta, \zeta \geq -\varepsilon \\ \zeta \leq (1 - \xi - \eta) + \varepsilon \end{cases} \qquad (A.5)$$
$$\varepsilon = 0.01, 0.02, \ldots$$

Appendix B
Use of the wall function for complex three-dimensional geometries

The following relations have been obtained for a *two-dimensional flat plate* subject to a *velocity field parallel to its surface*, in the *absence of pressure gradients*; the symbols used are described in figure B.1: defining the non-dimensional variable:

$$y^+ = \frac{\rho C_\mu^{1/4} \sqrt{k}\, \delta_n}{\mu} \tag{B.1}$$

the shear stress in the point P, due to the velocity gradient between the point itself and the wall, is given by:

$$\tau_w = \Lambda_w \left(U_P - u_{wall} \right) \tag{B.2}$$

where u_{wall} is the velocity of the wall and:

$$\Lambda_w = \frac{\mu}{\delta_n} \quad \text{if} \quad y^+ < 11.5 \tag{B.3}$$

corresponding to the case of the point P being in the *laminar* region, and:

$$\Lambda_w = \frac{\mathrm{K} C_\mu^{1/4} \sqrt{k}\, \rho}{\ln\left(E y^+ \right)} \quad \text{if} \quad y^+ > 11.5 \tag{B.4}$$

corresponding to the case of the point P being in the *turbulent* region, where K is the Von Karman's constant (equal to 0.41) and E is a closure coefficient, function of the wall roughness, approximately equal to 9.0 for a smooth wall.

In the wall function method the expressions (B.2)-(B.4) are considered as an *universal function* that gives the stress on the point P due to the wall in function of the normal distance δ_n and the component of the velocity parallel to the wall.

All the links between the point P and the point on the wall S are broken, setting to zero the corresponding coefficient in the transport equation; the only effect of the wall in the solution is the diffusion due to the stress (B.2) that is added in the source term.

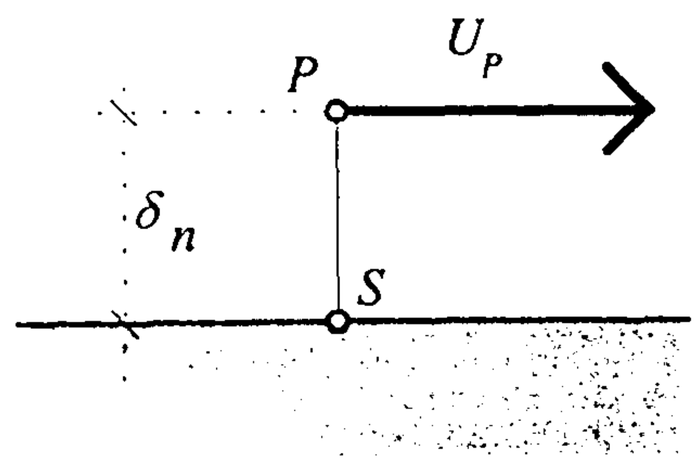

Figure B.1

For a complex three-dimensional geometry, where generalised coordinates are introduced, *differential formulae* are used to define the geometric quantities required, supposing $\delta_n << 1$; at the same time, the generalised coordinates system (ξ, η, ζ) is supposed to be *orthogonal around the point on the wall.* With these hypothesis, supposing for example that the η coordinate is chosen in the direction normal to the wall in the point S, the following expressions can be obtained, where *all the metric coefficients are evaluated in the point on the wall*:

• the normal distance δ_n has components $(0, d\eta, 0)$ in the transformed space (ξ, η, ζ), where:

$$d\eta = \eta(P) - \eta(S) \tag{B.5}$$

• using the differential formulae, the following expressions are obtained for the components of δ_n in the physical space:

$$dx = \frac{\partial x}{\partial \eta} d\eta;\ dy = \frac{\partial y}{\partial \eta} d\eta;\ dz = \frac{\partial z}{\partial \eta} d\eta \tag{B.6}$$

$$\delta_n = d\eta \sqrt{\left(\frac{\partial x}{\partial \eta}\right)^2 + \left(\frac{\partial y}{\partial \eta}\right)^2 + \left(\frac{\partial z}{\partial \eta}\right)^2} \tag{B.7}$$

• defining $\underline{n}$ as the normal direction to the wall in the point S (vector with Unitarian module), and with $\underline{r}$ and $\underline{s}$ the two tangential directions constituting an orthogonal system with the direction $\underline{n}$, their components in the physical space can be obtained supposing that $\underline{r}$ and $\underline{s}$ have been chosen in the direction of other two generalised coordinates ξ and ζ:

$$n_i = \frac{\dfrac{\partial x_i}{\partial \eta}}{\sqrt{\left(\dfrac{\partial x}{\partial \eta}\right)^2 + \left(\dfrac{\partial y}{\partial \eta}\right)^2 + \left(\dfrac{\partial z}{\partial \eta}\right)^2}} \tag{B.8}$$

$$r_i = \frac{\dfrac{\partial x_i}{\partial \xi}}{\sqrt{\left(\dfrac{\partial x}{\partial \xi}\right)^2 + \left(\dfrac{\partial y}{\partial \xi}\right)^2 + \left(\dfrac{\partial z}{\partial \xi}\right)^2}} \tag{B.9}$$

$$s_i = \frac{\dfrac{\partial x_i}{\partial \zeta}}{\sqrt{\left(\dfrac{\partial x}{\partial \zeta}\right)^2 + \left(\dfrac{\partial y}{\partial \zeta}\right)^2 + \left(\dfrac{\partial z}{\partial \zeta}\right)^2}} \tag{B.10}$$

In three-dimensions the velocity in the point P parallel to the wall is a vector and expression (B.2) has to be rewritten as:

$$\underline{\tau}_w = \Lambda_w \left[\underline{U}_P(P) - \underline{V}_{wall} \right] \tag{B.11}$$

where the component of the velocity parallel to the wall in the point P is obtained subtracting to the velocity in the point P the component in the direction of the local normal $\underline{n}$:

$$\underline{U}_P(P) = \underline{V}(P) - \left[\underline{V}(P) \cdot \underline{n} \right] \underline{n} \tag{B.12}$$

and its components in the physical space are:

$$U_{P,i}(P) = u_i(P) - n_i \sum_{j=1}^{3} n_j u_j(P) \tag{B.13}$$

In the **i-th momentum equation** the diffusion term is integrated in the transformed space (ξ, η, ζ), using the Gauss' theorem:

$$\int_{\Theta_P} \frac{1}{J}\frac{\partial}{\partial \xi_r}\left[J(\mu+\mu_t)g^{rs}\frac{\partial u_i}{\partial \xi_s}\right]Jd\Theta = \sum_{r=1}^{6}\pm\int_{A_r}\left[J(\mu+\mu_t)g^{rs}\frac{\partial u_i}{\partial \xi_s}\right]dA \qquad \text{(B.14)}$$

where Θ_P is the volume of the cell centred in P, A_r is the face of the cell with normal $\pm\xi_r$, and the integrals on the right-hand side of equation (B.14) are taken with a positive sign if the *outgoing* normal to the face A_r is directed as ξ_r, with a negative sign in the opposite case.

Supposing, for example, that the *south* face of the control volume is on a solid wall and the η coordinate is directed from *south* to *north*, considering only the normal terms (r=s), being the cross derivatives negligible near a wall, the stress on the wall is written as:

$$\left[(\mu+\mu_t)\frac{\partial u_i}{\partial \eta}\right]_S = \tau_{w,i} = \Lambda_w U_{P,i} \qquad \text{(B.15)}$$

and the *south* integral as:

$$-\int_{A_S} Jg^{22}(\mu+\mu_t)\frac{\partial u_i}{\partial \eta}dA =$$

$$= -J_S \cdot g_S^{22} \cdot \Delta\xi_S \cdot \Delta\zeta_S \cdot \Lambda_w\left\{\left[u_i(P) - n_i\sum_j n_j u_j(P)\right] - u_{wall,i}\right\} \qquad \text{(B.16)}$$

where the pedix S indicates the value on the *south* face.

If the solid walls corresponds to a *north* face, adopting the same definition of η and defining $d\eta$ as (to obtain a positive quantity):

$$d\eta = \eta(N) - \eta(P)$$

where N is the point on the wall, expression (B.15) has to be written as:

$$\left[(\mu+\mu_t)\frac{\partial u_i}{\partial \eta}\right]_N = -\Lambda_w U_{P,i} \qquad \text{(B.17)}$$

and the *north* integral as:

$$\int_{A_N} Jg^{22}(\mu+\mu_t)\frac{\partial u_i}{\partial \eta}\,dA =$$

$$= -J_N \cdot g_N^{22} \cdot \Delta\xi_N \cdot \Delta\zeta_N \cdot \Lambda_w \left\{ \left[u_i(P) - n_i \sum_j n_j u_j(P) \right] - u_{wall,i} \right\} \tag{B.18}$$

In the ***k* equation**, *the diffusion due to the wall is set to zero*; the value of k on the solid walls cannot be prescribed, as the coefficients in the transport equation corresponding to the wall points are also set to zero; a Neumann condition in generally adopted to update the points on the walls:

$$\frac{\partial k}{\partial n} = 0 \tag{B.19}$$

This conditions are referred to as *slip conditions for the turbulence*, as the *no-slip* value $k = 0$ is not imposed on the walls.

The *production* term in the control volumes near the solid walls is written as follows, considering all the velocity variations negligible respect to the one in the direction normal to the wall:

$$G = \tau_{ij}^R \frac{\partial u_i}{\partial \xi_r}\frac{\partial \xi_r}{\partial x_j} \cong \tau_w \frac{|\underline{U}_P|}{\delta_n} = \Lambda_w \frac{|\underline{U}_P|^2}{\delta_n} \tag{B.20}$$

The *dissipation term* in these cells is written as a function of τ_w assuming that the point is in a fully turbulent region, where $\mu_t >> \mu$, so that:

$$\tau_w \cong \mu_t \frac{|\underline{U}_P|}{\delta_n} \tag{B.21}$$

and, using the definition of the eddy viscosity:

$$\varepsilon = \frac{C_\mu \rho k^2}{\mu_t} \cong \frac{C_\mu \rho k^2}{\tau_w}\frac{|\underline{U}_P|}{\delta_n} \tag{B.22}$$

The source term in the control volumes close to the walls is then written as:

$$G - \rho\varepsilon = \Lambda_w \frac{|\underline{U}_P|^2}{\delta_n} - \frac{C_\mu \rho^2 \kappa^2}{\Lambda_w \delta_n} \tag{B.23}$$

In the **ε equation** the value in the points close to the solid walls is prescribed as follows:

$$\varepsilon_P = \frac{k^{3/2} C_\mu^{3/4}}{\mathrm{K}\delta_n} \tag{B.24}$$

The value is assigned setting the coefficients and the source term of the transport equation, in the control volumes close to the walls, as follows:

$$\begin{cases} a_P = 1.0 \\ a_E = a_W = a_N = a_S = a_F = a_B = 0.0 \\ S = \varepsilon_P \end{cases} \tag{B.25}$$

The value of the **Reynolds stresses in function of the stress on the wall** $\underline{\tau}_w$ will be now obtained. What follows refers only to the points close to the solid walls.

From the definition of shear stress, τ_{ij} is the stress in direction i on the volume face with normal in direction j (or vice-versa, being symmetric); the *stresses tensor* $\underline{\underline{\mathrm{T}}}$ can be written in the system $(\underline{n},\underline{r},\underline{s})$ previously introduced, being $\underline{n}$ the direction normal to the wall, noticing that $\underline{\tau}_w$ is the stress on the face of normal $\underline{n}$ and therefore:

$$\begin{cases} \tau_{nn} = \underline{\tau}_w \cdot \underline{n} = \tau_{w,x} n_x + \tau_{w,y} n_y + \tau_{w,z} n_z \\ \tau_{nr} = \underline{\tau}_w \cdot \underline{r} = \tau_{w,x} r_x + \tau_{w,y} r_y + \tau_{w,z} r_z \\ \tau_{ns} = \underline{\tau}_w \cdot \underline{s} = \tau_{w,x} s_x + \tau_{w,y} s_y + \tau_{w,z} s_z \\ \tau_{rr} = 0 \\ \tau_{ss} = 0 \\ \tau_{rs} = 0 \end{cases} \tag{B.26}$$

The components of the stresses tensor in the physical space are then obtained multiplying the tensor by the corresponding directions:

$$\tau_{xy} = \underline{x} \cdot \underline{\underline{T}} \cdot \underline{y} \tag{B.27}$$

or, writing explicitly all the components:

$$\begin{cases} \tau_{xx} = n_x \tau_{nn} n_x + 2 n_x \tau_{nr} r_x + 2 n_x \tau_{ns} s_x \\ \tau_{yy} = n_y \tau_{nn} n_y + 2 n_y \tau_{nr} r_y + 2 n_y \tau_{ns} s_y \\ \tau_{zz} = n_z \tau_{nn} n_z + 2 n_z \tau_{nr} r_z + 2 n_z \tau_{ns} s_z \\ \tau_{xy} = \tau_{yx} = n_x \tau_{nn} n_y + n_x \tau_{nr} r_y + n_x \tau_{ns} s_y + r_x \tau_{nr} n_y + s_x \tau_{ns} n_y \\ \tau_{xz} = \tau_{zx} = n_x \tau_{nn} n_z + n_x \tau_{nr} r_z + n_x \tau_{ns} s_z + r_x \tau_{nr} n_z + s_x \tau_{ns} n_z \\ \tau_{yz} = \tau_{zy} = n_y \tau_{nn} n_z + n_y \tau_{nr} r_z + n_y \tau_{ns} s_z + r_y \tau_{nr} n_z + s_y \tau_{ns} n_z \end{cases} \tag{B.28}$$

Supposing the laminar stresses negligible, the expressions (B.28) are then used for the Reynolds stresses τ_{ij}^{R}.